UNIVERSIDADE ESTADUAL DE PONTA GROSSA
SETOR DE CIÊNCIAS BIOLÓGICAS E DA SAÚDE
PROGRAMA DE PÓS-GRADUAÇÃO EM CIÊNCIAS FARMACÊUTICAS

MARCIA VIVIANE MARCON

MICROPARTÍCULAS POLIMÉRICAS pH-SENSÍVEIS DE CURCUMINA E PIPERINA COM POTENCIAL APLICAÇÃO NA SÍNDROME METABÓLICA

PONTA GROSSA
2026

MARCIA VIVIANE MARCON

MICROPARTÍCULAS POLIMÉRICAS pH-SENSÍVEIS DE CURCUMINA E PIPERINA COM POTENCIAL APLICAÇÃO NA SÍNDROME METABÓLICA

Tese apresentada ao Programa de Pós-Graduação em Ciências Farmacêuticas, Setor de Ciências Biológicas e da Saúde, Universidade Estadual de Ponta Grossa, em associação ampla com a Universidade Estadual do Centro-Oeste, como requisito parcial para obtenção do título de Doutora em Ciências Farmacêuticas.

Orientador: Prof. Dr. Paulo Vitor Farago
Coorientadora: Profa. Dra. Jéssica Mendes Nadal

PONTA GROSSA

2026

Marcon, Marcia Viviane

M32 Micropartículas poliméricas pH-sensíveis de curcumina e piperina com potencial aplicação na síndrome metabólica / Marcia Viviane Marcon. Ponta Grossa, 2026.

165 f.

Tese (Doutorado em Ciências Farmacêuticas - Área de Concentração: Fármacos, Medicamentos e Biociências Aplicadas à Farmácia), Universidade Estadual de Ponta Grossa.

Orientador: Prof. Dr. Paulo Vítor Farago. Coorientadora: Profa. Dra. Jessica Bittencourt Nadal.

1. Síndorme metabólica - Tratamento. 2. Curcumina - Uso terapêutico. 3. Piperina - Uso terapêutico. 4. Microbiota intestinal. 5. Sistemas de liberação de fármacos. I. Farago, Paulo Vítor. II. Nadal, Jessica Bittencourt. III. Universidade Estadual de Ponta Grossa. Fármacos, Medicamentos e Biociências Aplicadas à Farmácia. IV.T.

CDD: 615.19

Ficha catalográfica elaborada por Vera Lucia Braga da Silva- CRB9/1026

MARCIA VIVIANE MARCON

MICROPARTÍCULAS POLIMÉRICAS PH-SENSÍVEIS DE CURCUMINA E PIPERINA COM POTENCIAL APLICAÇÃO NA SÍNDROME METABÓLICA

Tese apresentada para obtenção do grau de Doutor no Programa de Pós-Graduação em Ciências Farmacêuticas, nível Doutorado, Associação Ampla entre a Universidade Estadual de Ponta Grossa (UEPG) e a Universidade do Centro-Oeste (UNICENTRO).

Ponta Grossa, 25 de fevereiro de 2026.

Prof. Dr. PAULO VITOR FARAGO – UEPG – Presidente

Prof. Dr. LEANDRO CAVALCANTE LIPINSKI – UEPG – Membro titular externo

Profa. Dra. JANE MANFRON – UEPG – Membro titular interno

Profa. Dra. FRANCISLAINE APARECIDA DOS REIS – UFPR – Membro titular externo

Profa. Dra. BARBARA JUSTUS – UNICESUMAR – Membro titular externo

UNIVERSIDADE ESTADUAL DE PONTA GROSSA
Programa de Pós-Graduação em Ciências Farmacêuticas - PPGCF
Bloco M Sala 93 B – Campus Universitário – Fone (42) 2102-8937
Av. Carlos Cavalcanti, 4748 – CEP: 84030-900 – PONTA GROSSA – PR – BRASIL

AGRADECIMENTOS

Não existem palavras suficientes para expressar minha gratidão a todos que, direta ou indiretamente, contribuíram para a conclusão desta etapa. Foram muitos os apoios, incentivos e gestos de compreensão ao longo desse percurso, os quais tornaram possível a realização deste trabalho.

Agradeço, primeiramente, à minha família, alicerce fundamental em toda a minha trajetória. Ao meu esposo, Fernando, e ao meu filho, Lucas, pelo amor, parceria, incentivo constante e compreensão nos momentos de ausência, sendo presenças indispensáveis nos desafios diários. À minha mãe, Lurdes, ao meu padrasto, Osni, e à minha irmã, Anaelisa, e sua família, pelo apoio incondicional, paciência e entendimento durante todo esse período, sempre acreditando em mim e respeitando minhas escolhas.

Aos meus amigos, agradeço pelo incentivo, pela torcida sincera e pelas palavras de encorajamento, que tornaram o caminho mais leve mesmo nos momentos mais exigentes. À Mari Ferreira, pelo suporte e auxílio nas demandas do cotidiano, fundamentais para que eu pudesse me dedicar a este trabalho.

Aos colegas do programa de pós-graduação em Ciências Farmacêuticas e do laboratório de pesquisa, Amanda Jansen, Julia Lepinski e Júlia Barbosa, agradeço pela convivência, troca de conhecimentos e parceria ao longo dessa jornada acadêmica.

Ao Vinicius Schaffka, pelo auxílio essencial no processo de validação do método por HPLC, e à Bárbara Justus, pela disponibilidade, apoio constante, parceria e auxílio em todos os momentos.

À equipe do laboratório de pesquisa, em especial à Josemira e Ely, bem como às equipes do Complexo de Laboratórios Multiusuários da UEPG, agradeço pelo suporte técnico e pela colaboração indispensável ao desenvolvimento experimental deste trabalho.

À equipe do Laboratório de Farmacologia Cardiometabólica da UFPR, em especial à Arisa Namie Higashijima, meu sincero agradecimento pelo apoio técnico, dedicação e cuidado com os experimentos.

Agradeço à Profª Mariane de Faria Moss pela amizade, apoio, sugestões, escuta atenta e colaboração nas atividades administrativas da Universidade Estadual de Ponta Grossa, sempre com prontidão e generosidade.

Estendo meus agradecimentos também aos colegas professores do setor de Bioquímica do LUAC pelo apoio durante o período de licença especial, o qual foi de grande importância para o desenvolvimento deste trabalho.

Aos Professores Leandro Lipinski e Celso Luiz Borges, agradeço pelo suporte e orientação nos protocolos experimentais.

Registro minha gratidão à Professora Jessica Mendes Nadal, pela coorientação, dedicação e auxílio no desenvolvimento das atividades, contribuindo de forma significativa para a realização deste trabalho.

À Professora Francislaine Aparecida dos Reis Lívero (UFPR), agradeço pela oportunidade de trabalhar e aprender sob sua orientação, pela dedicação incansável às atividades *in vivo*, pela prestatividade, generosidade e disponibilidade.

Um agradecimento especial ao Professor Paulo Vitor Farago, meu orientador, pelos ensinamentos transmitidos, pela confiança, disponibilidade e dedicação ao longo de todo o processo.

Por fim, agradeço a todos que, de alguma forma, contribuíram para a realização deste trabalho, seja por meio de apoio técnico, científico, emocional ou por palavras de incentivo. A todos, minha sincera e eterna gratidão.

RESUMO

A síndrome metabólica (SM) constitui um importante desafio de saúde pública global, caracterizando-se por um conjunto de alterações metabólicas inter-relacionadas que aumentam significativamente o risco de diabetes mellitus tipo 2, doenças cardiovasculares e mortalidade associada às doenças crônicas não transmissíveis. Entre os compostos bioativos de origem natural investigados para o manejo da SM, a curcumina e a piperina destacam-se por seus efeitos metabólicos, anti-inflamatórios e antioxidantes; entretanto, sua aplicação clínica permanece limitada pela baixa biodisponibilidade oral. Nesse contexto, sistemas farmacotécnicos inovadores, como micropartículas poliméricas pH-sensíveis, emergem como estratégias promissoras para superar limitações relacionadas à solubilidade, estabilidade e absorção intestinal desses compostos bioativos. O presente trabalho teve como objetivo desenvolver micropartículas gastro-resistentes contendo curcumina e piperina, utilizando o polímero Eudragit® S100 e a técnica de spray-drying, bem como avaliar seu desempenho in vitro e in vivo em um modelo experimental pré-clínico de SM de natureza multi-hit, caracterizado pela combinação de hipertensão genética, indução de dislipidemia e consumo crônico de frutose, reproduzindo um quadro metabólico complexo e de evolução prolongada. As micropartículas foram caracterizadas por análises morfológicas, espectroscópicas e térmicas, ensaios de eficiência de encapsulação por cromatografia líquida de alta eficiência (HPLC) e estudos do perfil de dissolução in vitro. A segurança da formulação foi investigada por meio de testes de hemólise e avaliação de toxicidade aguda em ratos Wistar. A atividade biológica da formulação foi investigada em ratos espontaneamente hipertensos submetidos à indução metabólica por dislipidemia e consumo crônico de frutose, considerando parâmetros hemodinâmicos, antropométricos, metabólicos, bioquímicos, inflamatórios e alterações na composição da microbiota intestinal. As micropartículas apresentaram rendimento superior a 50%, tamanho médio submicrométrico homogêneo e potencial zeta negativo, indicativo de estabilidade coloidal. A microscopia eletrônica evidenciou morfologia esférica e ausência de cristais superficiais, enquanto as análises de difração de raios X e calorimetria diferencial de varredura confirmaram a conversão dos bioativos para o estado amorfo, compatível com maior estabilidade térmica e potencial aumento da biodisponibilidade. Os ensaios de dissolução demonstraram perfil de liberação pH-dependente e sustentada por até 24 horas, com melhor ajuste ao modelo cinético de Weibull ($R^2 > 0,99$). Nos estudos in vivo, o tratamento com as micropartículas, particularmente na maior dose avaliada (CP225), promoveu melhora significativa de parâmetros hemodinâmicos, metabólicos e antropométricos, acompanhada por redução da dislipidemia, hiperglicemia e adiposidade visceral. Esses efeitos foram associados à atenuação da inflamação sistêmica, evidenciada pela redução de citocinas pró-inflamatórias, bem como à modulação da microbiota intestinal, caracterizada por aumento da diversidade microbiana e enriquecimento de gêneros produtores de ácidos graxos de cadeia curta, embora sem completa restauração do perfil basal. Os testes de segurança demonstraram baixa toxicidade aguda, sem alterações clínicas, hematológicas, bioquímicas ou histopatológicas relevantes, reforçando o perfil seguro da formulação para administração oral. Em conjunto, os resultados indicam que a encapsulação de curcumina e piperina em micropartículas gastro-resistentes constitui uma estratégia farmacotécnica capaz de potencializar os efeitos sistêmicos desses bioativos, atuando de forma integrada sobre os eixos metabolismo–inflamação–microbiota intestinal em um modelo multi-hit de SM, com relevância tecnológica e biológica para aplicações farmacêuticas, nutracêuticas e funcionais.

Palavras-chave: disfunção metabólica; biodisponibilidade oral; microbiota intestinal; compostos fenólicos; sistemas de liberação modificada.

ABSTRACT

Metabolic syndrome (MetS) constitutes a major global public health challenge and is characterized by a cluster of interrelated metabolic disturbances that significantly increase the risk of type 2 diabetes mellitus (T2DM), cardiovascular diseases, and mortality associated with non-communicable chronic diseases. Among naturally derived bioactive compounds investigated for the management of MetS, curcumin and piperine stand out due to their metabolic, anti-inflammatory, and antioxidant effects; however, their clinical application remains limited by poor oral bioavailability. In this context, innovative pharmacotechnical systems such as pH-sensitive polymeric microparticles have emerged as promising strategies to overcome limitations related to solubility, stability, and intestinal absorption of these bioactive compounds. The present study aimed to develop gastro-resistant microparticles containing curcumin and piperine using the polymer Eudragit® S100 and the spray-drying technique, as well as to evaluate their in vitro and in vivo performance in a preclinical experimental model of MetS. The model followed a multi-hit approach, combining genetic hypertension, dyslipidemia induction, and chronic fructose consumption, thereby reproducing a metabolically complex and long-term pathological condition. The microparticles were characterized through morphological, spectroscopic, and thermal analyses, encapsulation efficiency assays by high-performance liquid chromatography (HPLC), and in vitro dissolution profile studies. Formulation safety was investigated through hemolysis assays and acute toxicity assessment in Wistar rats. The biological activity of the formulation was evaluated in spontaneously hypertensive rats subjected to metabolic induction by dyslipidemia and chronic fructose intake, considering hemodynamic, anthropometric, metabolic, biochemical, inflammatory, and gut microbiota parameters. The microparticles showed yields above 50%, homogeneous submicrometric mean particle size, and negative zeta potential, indicating colloidal stability. Scanning electron microscopy revealed spherical morphology and absence of surface crystals, while X-ray diffraction and differential scanning calorimetry analyses confirmed the conversion of the bioactive compounds to the amorphous state, consistent with improved thermal stability and potential enhancement of bioavailability. Dissolution studies demonstrated a pH-dependent and sustained release profile for up to 24 hours, with the best fit to the Weibull kinetic model ($R^2 > 0.99$). In vivo experiments demonstrated that treatment with the microparticles, particularly at the highest tested dose (CP225), significantly improved hemodynamic, metabolic, and anthropometric parameters, accompanied by reductions in dyslipidemia, hyperglycemia, and visceral adiposity. These effects were associated with attenuation of systemic inflammation, evidenced by reductions in pro-inflammatory cytokines, as well as modulation of gut microbiota composition characterized by increased microbial diversity and enrichment of short-chain fatty acid–producing genera, although without complete restoration of the basal microbial profile. Safety assessments indicated low acute toxicity, with no relevant clinical, hematological, biochemical, or histopathological alterations, reinforcing the safety profile of the formulation for oral administration. Collectively, these findings indicate that encapsulating curcumin and piperine into gastro-resistant microparticles represents a pharmacotechnical strategy capable of enhancing the systemic effects of these bioactive compounds, acting in an integrated manner on the metabolism–inflammation–gut microbiota axis in a multi-hit model of MetS, with technological and biological relevance for pharmaceutical, nutraceutical, and functional applications.

Keywords: metabolic dysfunction; oral bioavailability; gut microbiota; phenolic compounds; modified release systems.

LISTA DE ILUSTRAÇÕES

LISTA DE ABREVIATURAS E SIGLAS

AGL	Ácido graxo livre
Ang II	Angiotensina II
CETP	Proteína de Transferência de Ésteres de Colesterol
CUR	Curcumina
DAMP	Danos teciduais
DCNT	Doenças crônicas não transmissíveis
DMT2	Diabetes mellitus tipo 2
ECA	Enzima Conversora da Angiotensina
ERO	Espécie reativa de oxigênio
GLP-1	Peptídeo semelhante ao glucagon tipo 1
GLUT-4	Transportador de glicose-4
HAS	Hipertensão arterial sistêmica
HDL	Lipoproteína de alta densidade
IDF	Federação Internacional de Diabetes
IL-1β	Interleucina 1 beta
IL-6	Interleucina 6
IL-10	Interleucina 10
LDL	Lipoproteína de baixa densidade
MCP-1	Proteína Quimioatraente de Monócitos 1
NCEP-ATP III	Programa Nacional de Educação sobre Colesterol – Painel de Tratamento de Adultos III

PAMP	Padrões moleculares associados a patógenos
PAD	Pressão arterial diastólica
PAS	Pressão arterial sistólica
PCR	Proteína C reativa
PIP	Piperina
RAS	Sistema renina-angiotensina
SBC	Sociedade Brasileira de Cardiologia
SCFA	Ácido graxo de cadeia curta
SM	Síndrome metabólica
SNP	Polimorfismo de nucleotídeo único
SNS	Sistema nervoso simpático
SRAA	Sistema renina–angiotensina–aldosterona
TG	Triglicerídeos
TNF-α	Fator de necrose tumoral alfa
TLR	Receptor Toll-like
TRL	Lipoproteínas ricas em triglicerídeos
VCAM	Molécula de adesão celular
VLDL	Lipoproteína de densidade muito baixa
WHO	Organização Mundial da Saúde

SUMÁRIO

1 INTRODUÇÃO

A síndrome metabólica (SM) constitui um conjunto de alterações metabólicas inter-relacionadas, incluindo obesidade abdominal, dislipidemia aterogênica, hiperglicemia e hipertensão, que elevam substancialmente o risco de diabetes mellitus tipo 2 e doenças cardiovasculares (Qiu et al., 2023). A prevalência global é estimada em aproximadamente 25% da população adulta (Hosseini et al., 2023), enquanto no Brasil meta-análises recentes indicam prevalências entre 29% e 34%, ultrapassando 40% entre idosos. Esses números refletem a forte influência do sedentarismo e do aumento da obesidade, consolidando a SM como um problema de saúde pública de grande magnitude (Valadares et al., 2022). Além das repercussões cardiometabólicas, a SM associa-se também ao aumento da incidência de neoplasias e ao maior risco de mortalidade por doenças crônicas não transmissíveis (Qiu et al., 2023).

Nesse contexto, cresce o interesse por compostos bioativos de origem natural capazes de modular vias inflamatórias, oxidativas e metabólicas envolvidas na fisiopatologia da SM. Entre esses compostos, a curcumina, um polifenol extraído do rizoma de Curcuma longa L., destaca-se por suas propriedades anti-inflamatórias, antioxidantes e hipolipemiantes, com efeitos documentados sobre glicemia de jejum, triglicerídeos e HDL-C (Nurcahyanti et al., 2022; Qiu et al., 2023). Entretanto, apesar do amplo potencial terapêutico, sua aplicação clínica é limitada por baixa solubilidade aquosa, instabilidade química e extenso metabolismo de primeira passagem, resultando em biodisponibilidade oral reduzida (Hamed et al., 2024; Wang, Gong, Zhou, 2025).

A piperina, alcaloide presente em Piper nigrum L., além de apresentar atividades metabólicas próprias, atua como bioativador farmacocinético ao inibir enzimas metabolizadoras e a P-glicoproteína, aumentando significativamente a biodisponibilidade da curcumina em humanos (Hosseini et al., 2023; Preza-Rodríguez et al., 2024). Ensaios clínicos recentes reforçam a relevância dessa combinação, demonstrando melhora significativa de parâmetros lipídicos e de componentes associados à SM (Preza-Rodríguez et al., 2024). Esses achados sustentam o potencial terapêutico da associação curcumina–piperina, embora as limitações farmacocinéticas da curcumina ainda representem um desafio importante.

Diante dessas limitações, tecnologias farmacotécnicas de liberação modificada têm sido investigadas. Micropartículas poliméricas gastro-resistentes, especialmente aquelas formuladas com Eudragit S100, apresentam solubilidade seletiva em pH $\geq$ 7, permitindo proteger compostos sensíveis da degradação ácida e direcionar sua liberação ao intestino, região de

maior absorção e intensa interação com a microbiota (Heikal et al., 2023; Evonik Health Care, 2025). Evidências recentes indicam que sistemas pH-sensíveis contendo curcumina podem aumentar a estabilidade do composto e favorecer sua dissolução in vitro (Hamed et al., 2024). Paralelamente, estudos clínicos com formulações de curcumina demonstram melhorias em parâmetros inflamatórios, oxidativos e metabólicos (Asghari et al., 2024).

Apesar dos avanços observados tanto na elucidação dos efeitos clínicos da curcumina associada à piperina quanto no desenvolvimento de sistemas farmacotécnicos destinados a superar barreiras de solubilidade, estabilidade e metabolismo de primeira passagem, ainda são escassos os estudos que combinem essas abordagens em uma mesma formulação. A combinação desses compostos incorporada em micropartículas poliméricas gastro-resistentes pode representar uma estratégia particularmente promissora, uma vez que tais sistemas são capazes de proteger os bioativos da degradação ácida, modular sua liberação no trato gastrointestinal e favorecer a absorção em regiões de maior permeabilidade e relevância metabólica. A avaliação dessa abordagem integrada permite avançar da compreensão mecanística para aplicações com potencial clínico mais robusto, contribuindo para o desenvolvimento de alternativas terapêuticas adjuvantes seguras e com maior potencial translacional para o manejo da SM.

Esta tese está apresentada em formato alternativo, estruturada em artigos, conforme as diretrizes do Programa de Pós-Graduação em Ciências Farmacêuticas da Universidade Estadual de Ponta Grossa (UEPG) e da Universidade Estadual do Centro-Oeste (UNICENTRO). O trabalho está organizado em: introdução, revisão de literatura, objetivos (geral e específicos), três artigos científicos derivados do projeto de pesquisa, seguidos das conclusões e das respectivas referências.

2 REVISÃO DE LITERATURA

2.1 DOENÇAS CRÔNICAS NÃO TRANSMISSÍVEIS

As doenças crônicas não transmissíveis (DCNT) permanecem como o principal desafio de saúde pública mundial, sendo responsáveis por aproximadamente 75% de todos os óbitos registrados em 2021. Dentre esses, destacam-se 18 milhões de mortes prematuras, ocorridas antes dos 70 anos, das quais a grande maioria (82%) foi registrada em países de baixa e média renda, onde os sistemas de saúde apresentam maiores fragilidades (WHO, 2023). No Brasil, a situação acompanha a tendência global: em 2019, as DCNT responderam por 76% das mortes, e cerca de dois terços desses óbitos (66%) ocorreram em adultos entre 30 e 69 anos, idade considerada produtiva, reforçando não apenas o impacto epidemiológico, mas também as implicações sociais e econômicas associadas (Lima et al., 2024).

A etiologia das DCNT é multifatorial e resulta da interação entre condições não modificáveis, como a predisposição genética e os antecedentes familiares, e fatores modificáveis, diretamente relacionados ao estilo de vida. Nesse grupo, destacam-se o tabagismo, o sedentarismo, o consumo nocivo de álcool, padrões alimentares inadequados e o excesso de peso ou obesidade, reconhecidos pela OMS e pela OPAS como determinantes críticos na evolução dessas doenças (WHO, 2023; PAHO, 2023). A presença desses fatores não apenas favorece o surgimento das DCNT, como também intensifica o risco de complicações cardiovasculares, metabólicas e neoplásicas, reforçando a necessidade de estratégias preventivas voltadas à identificação precoce e ao controle desses elementos de risco (WHO, 2023).

Paralelamente, observa-se uma transição epidemiológica global, marcada pela redução relativa das doenças infecciosas e pelo aumento de distúrbios metabólicos. Entre 1990 e 2021, registrou-se um incremento de 49,4% na ocorrência dessas desordens, reforçando a centralidade dos fatores metabólicos no perfil de saúde contemporâneo (Mettananda; Mettananda, 2024). Esse deslocamento no perfil de saúde populacional tem repercussões diretas na carga global das DCNT, impondo novos desafios para os sistemas de saúde, sobretudo na implementação de políticas públicas integradas de prevenção e manejo clínico. Nesse contexto, destaca-se a síndrome metabólica como uma condição de grande relevância por reunir, em um mesmo quadro, fatores de risco e alterações associadas às principais DCNT.

2.2 SÍNDROME METABÓLICA

2.2.1 Definição e complicações

A SM representa uma condição clínica de grande relevância no espectro das DCNT. Sua origem é multifatorial e caracteriza-se pela agregação de fatores de risco cardiometabólico, incluindo hipertensão arterial sistêmica, resistência à insulina, obesidade abdominal e dislipidemia (Madan et al., 2023; Prone-Olazabal et al., 2023).

A presença da SM está fortemente associada ao aumento da probabilidade de desfechos clínicos graves. Evidências indicam que indivíduos acometidos apresentam risco cinco vezes maior de desenvolver diabetes mellitus tipo 2, duplicação da probabilidade de ocorrência de doenças cardiovasculares em até 10 anos (Lopez-Candales, 2017) e incremento no risco de acidente vascular cerebral e infarto agudo do miocárdio, além da duplicação da mortalidade associada a esses eventos. Também está associada a maior risco de infecções, internações prolongadas e necessidade de cuidados intensivos (Reyes; Pak; Moon, 2020).

2.2.2 Prevalência e critérios de diagnóstico

A SM constitui um relevante problema global de saúde pública, associado ao avanço da urbanização, às mudanças no padrão alimentar e ao envelhecimento populacional (Lee et al., 2023). A prevalência internacional varia entre 12,5% e 31,4%, dependendo dos critérios utilizados (Noubiap et al., 2022), enquanto, no Brasil, estima-se que alcance aproximadamente 29 a 34% da população adulta (de Siqueira Valadares, 2022).

Apesar das variações entre definições, as diretrizes convergem em quatro eixos fundamentais: obesidade central, dislipidemia, hipertensão arterial e intolerância à glicose. Entre os principais sistemas diagnósticos, destacam-se: WHO (1999), que exige resistência insulínica ou diabetes associada a dois componentes adicionais; NCEP-ATP III (2005), baseado na presença de três entre cinco alterações metabólicas (obesidade abdominal, triglicerídeos, HDL, pressão arterial, glicemia); e IDF (2006), que utiliza a obesidade central como critério obrigatório, associada a dois fatores adicionais.

Em resposta a essas discrepâncias, um consórcio internacional liderado por entidades como a Federação Internacional de Diabetes e a Associação Americana do Coração publicou, em 2009, a Joint Interim Statement (JIS), visando harmonizar os critérios diagnósticos. Estudos recentes demonstram que os critérios clássicos permanecem eficazes na predição de risco cardiovascular (DCV) e diabetes mellitus tipo 2 (DM2), e o NCEP/JIS continua sendo amplamente adotado em pesquisas e diretrizes devido à sua consistência na associação com eventos cardiovasculares (Yousefzadeh et al., 2024). Ainda que os critérios diagnósticos estejam relativamente consolidados, compreender os determinantes associados ao desenvolvimento e à progressão da SM é essencial para contextualizar sua complexidade clínica.

2.2.3 Fatores de risco

O desenvolvimento da SM resulta de uma interação complexa entre predisposição genética, hábitos de vida e processo de envelhecimento (Codazzi et al., 2024; Lin et al., 2021). Do ponto de vista genético, alterações como variantes no gene FTO, conhecido como “gene da obesidade”, aumentam a susceptibilidade e a progressão da SM, em razão de sua participação no metabolismo de ácidos graxos (Mizuno, 2018; Nagrani et al., 2020), enquanto mecanismos epigenéticos, como a hipometilação de genes circadianos, também têm sido implicados na elevação do risco (Rana et al., 2022).

No âmbito comportamental, destaca-se a influência da alimentação, em que dietas caracterizadas pelo alto consumo de ultraprocessados e pela baixa ingestão de fibras e micronutrientes estão associadas ao aumento do risco de obesidade, hipertensão e diabetes (Rauber et al., 2018; Mambrini et al., 2023). Além disso, padrões alimentares inadequados, como a omissão do café da manhã ou a ingestão excessiva de calorias no período noturno, demonstram correlação direta com a maior prevalência de SM (Alkhulaif; Darkoh, 2022).

A falta de exercício físico também constitui fator determinante, pois reduz a expressão do transportador de glicose GLUT-4 e compromete a captação muscular de glicose, favorecendo a resistência insulínica (Chomiuk et al., 2024). Mesmo períodos relativamente curtos de sedentarismo prolongado são capazes de anular os benefícios obtidos por práticas regulares de exercício (Wu et al., 2022).

Por fim, o envelhecimento exerce papel relevante ao intensificar mecanismos de estresse oxidativo e reduzir a capacidade antioxidante do organismo (Dziegielewska-Gesiak, 2021). Alterações associadas, como encurtamento dos telômeros (Devrajani et al., 2023), obesidade sarcopênica (Nishikawa et al., 2021), resistência à insulina e disfunções do ciclo circadiano (Dominguez; Barbagallo, 2016), além de mudanças hormonais, como menopausa (Nair; Pillai; Nair, 2021) e andropausa (Blaya et al., 2017), ampliam a vulnerabilidade do idoso às complicações da SM. Esse conjunto de mecanismos ajuda a explicar por que intervenções voltadas a apenas um componente tendem a ter impacto limitado, reforçando a importância de estratégias terapêuticas que considerem múltiplos processos simultaneamente.

Esse conjunto de fatores evidencia que a síndrome metabólica resulta da interação de múltiplos processos biológicos interdependentes, nos quais alterações metabólicas, inflamatórias e hormonais se reforçam mutuamente. Nesse contexto, mecanismos integradores capazes de conectar estímulos ambientais, metabolismo energético e resposta imune têm sido progressivamente investigados.

Entre esses mecanismos, destaca-se o papel do trato gastrointestinal, particularmente da microbiota intestinal, como um importante mediador entre fatores ambientais, como dieta, estilo de vida e envelhecimento, e o desenvolvimento das alterações cardiometabólicas características da SM. Assim, a abordagem intestinal surge como um componente essencial para a compreensão mais abrangente dessa condição.

2.2.4 Abordagem intestinal: microbiota e barreira intestinal na síndrome metabólica

Nos últimos anos, evidências crescentes indicam que o intestino desempenha papel central na fisiopatologia da síndrome metabólica (SM). Além de atuar na digestão e absorção de nutrientes, o trato gastrointestinal abriga trilhões de microrganismos que compõem a microbiota intestinal, considerada um importante modulador do metabolismo energético, da imunidade e da homeostase sistêmica. Alterações nesse ecossistema microbiano, processo conhecido como disbiose, têm sido associadas ao desenvolvimento de obesidade, resistência à insulina, dislipidemia e hipertensão arterial, componentes característicos da SM (Wang et al., 2020; Boulangé et al., 2016).

A microbiota intestinal participa de diversas funções metabólicas relevantes, incluindo a fermentação de fibras alimentares e a produção de metabólitos bioativos, como os ácidos graxos de cadeia curta (short-chain fatty acids – SCFAs), que influenciam diretamente a sensibilidade à insulina, o metabolismo lipídico e a regulação da inflamação sistêmica. Esses metabólitos atuam em receptores acoplados à proteína G e em vias metabólicas que modulam o armazenamento energético, a resposta inflamatória e a comunicação entre o intestino e órgãos periféricos (Boulangé et al., 2016).

A disbiose intestinal tem sido descrita em diferentes condições metabólicas. Em indivíduos com obesidade ou síndrome metabólica, observam-se frequentemente alterações na composição e na diversidade da microbiota, incluindo modificações na razão Firmicutes/Bacteroidetes e redução de bactérias produtoras de SCFAs, como Faecalibacterium e Roseburia. Essas alterações podem favorecer o armazenamento energético, promover inflamação metabólica de baixo grau e contribuir para a progressão das alterações metabólicas associadas à SM (Wang et al., 2020).

Além das alterações na composição microbiana, a integridade da barreira intestinal também desempenha papel fundamental nesse processo. A barreira intestinal é composta por uma complexa estrutura formada pela camada de muco, células epiteliais e junções intercelulares, que atuam como sistema de defesa contra a translocação de microrganismos e toxinas. A disfunção dessa barreira, frequentemente descrita como aumento da permeabilidade intestinal, permite a passagem de endotoxinas bacterianas, como lipopolissacarídeos (LPS), para a circulação sistêmica, desencadeando respostas inflamatórias que contribuem para o desenvolvimento de doenças cardiometabólicas (Xiao et al., 2024).

Esse fenômeno, denominado endotoxemia metabólica, tem sido relacionado ao aumento da inflamação sistêmica de baixo grau, um dos principais mecanismos envolvidos na resistência à insulina e na progressão da síndrome metabólica. A ativação de vias inflamatórias mediadas por receptores toll-like (TLRs) e citocinas pró-inflamatórias promove alterações no metabolismo da glicose e dos lipídios, contribuindo para o desenvolvimento de obesidade, diabetes tipo 2 e dislipidemia (Boulangé et al., 2016; Gurung et al., 2020).

Além disso, estudos recentes demonstram que a microbiota intestinal também pode influenciar a regulação da pressão arterial por meio de mecanismos envolvendo o sistema nervoso simpático, a produção de metabólitos microbianos e a modulação da inflamação sistêmica. Modelos experimentais indicam que alterações na microbiota estão associadas à redução da diversidade bacteriana e ao aumento da razão Firmicutes/Bacteroidetes em modelos

de hipertensão, sugerindo que a disbiose intestinal pode contribuir para a manutenção da pressão arterial elevada (Yang et al., 2015; Toral et al., 2019; Ge et al., 2024).

Dessa forma, o intestino configura-se como um eixo central na regulação da homeostase metabólica, integrando sinais nutricionais, metabólicos e imunológicos por meio de interações dinâmicas entre microbiota, barreira intestinal e hospedeiro. Alterações nesse sistema contribuem simultaneamente para inflamação sistêmica, resistência à insulina, dislipidemia e hipertensão, reforçando o caráter multifatorial e interconectado da síndrome metabólica. Nesse sentido, a compreensão dos mecanismos fisiopatológicos envolvidos na SM exige a análise integrada desses diferentes eixos — metabólico, inflamatório, neuroendócrino e intestinal —, os quais serão abordados de forma detalhada na seção a seguir.

2.2.5 Fisiopatologia da síndrome metabólica

A fisiopatologia da SM resulta de um conjunto de processos interligados que convergem para a desregulação metabólica característica da síndrome (Fathi, 2018; Fahed et al., 2022). Apesar de persistir o debate sobre a natureza independente ou integrada de seus componentes, há consenso quanto ao papel central da obesidade visceral e da resistência insulínica na sustentação do quadro (Alberti et al., 2009; Matsuzawa; Funahashi; Nakamura, 2011; Pekgor et al., 2019). A partir desses eixos, instauram-se alterações como inflamação crônica, hipertensão arterial e dislipidemias, que, em conjunto, impulsionam a progressão da SM em direção ao diabetes mellitus tipo 2 (DM2) e às doenças cardiovasculares (DCVs) (Patial et al., 2024; Nilsson; Tuomilehto; Rydén, 2019). Nesta seção, serão abordados os principais elementos presentes na fisiopatologia da SM, também resumidos na Figura 1.

2.2.5.1 Aumento da gordura visceral

A obesidade visceral, caracterizada pelo acúmulo de gordura na cavidade abdominal, constitui a comorbidade mais prevalente e determinante na fisiopatologia da SM (Hagberg; Spalding, 2024). O excesso desse tecido adiposo está diretamente associado à progressão para

o diabetes mellitus tipo 2 (DM2) e ao desenvolvimento de doenças cardiorrenais (Guo et al., 2023).

Além de atuar como reservatório energético, o tecido adiposo visceral exerce função endócrina, secretando adipocinas e hormônios que regulam processos metabólicos (Fahed et al., 2022). O acúmulo excessivo leva à hipertrofia dos adipócitos, alterações na adipogênese, resistência à ação inibitória da insulina sobre a lipólise, alterações na matriz extracelular e infiltração de células imunológicas (Tchernof; Després, 2013; Rosendo-Silva et al., 2024).

FIGURA 1 – Descrição gráfica do processo fisiopatológico da síndrome metabólica. ERO, espécie reativa de oxigênio; HDL, lipoproteína de alta densidade; IL-6, interleucina-6; PCR, proteína C reativa; TGs, triglicerídeos; TNF-α, fator de necrose tumoral alfa.

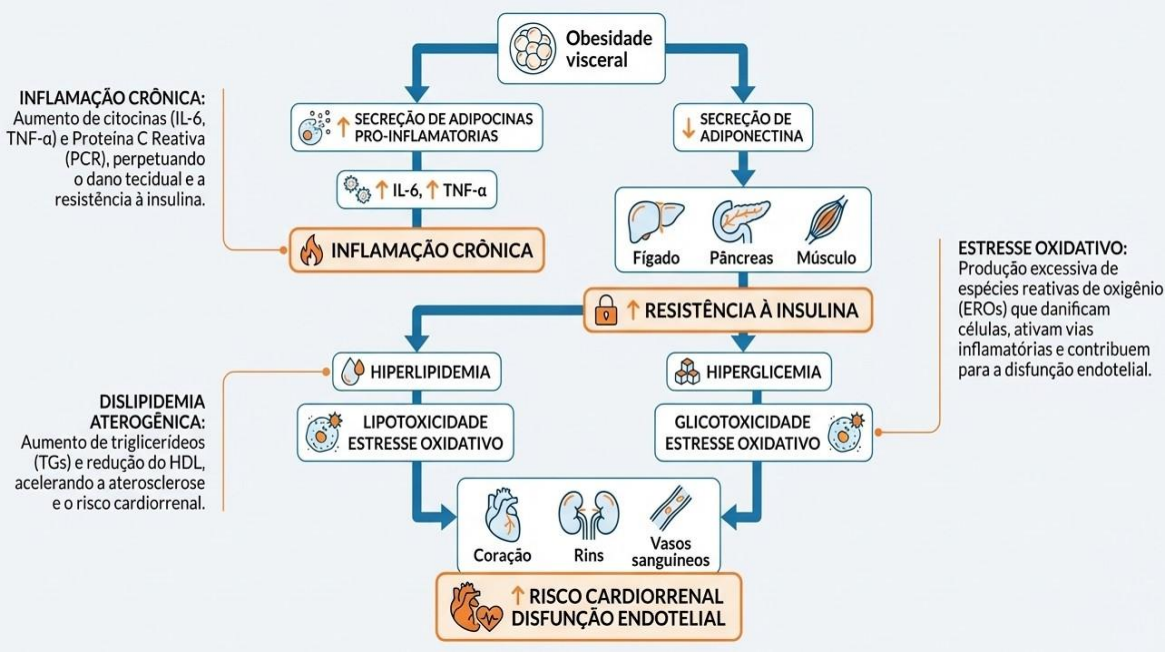

Fonte: A autora

Esse desequilíbrio secretor resulta em aumento da produção de leptina, frequentemente associado ao desenvolvimento de resistência à leptina e à redução de seus efeitos metabólicos, concomitantemente à diminuição da adiponectina, uma adipocina de ação anti-inflamatória que favorece a sensibilidade à insulina e exerce efeito protetor contra a aterosclerose e o diabetes (Neeland et al., 2024; Yadav et al., 2025).

Paralelamente, o tecido adiposo visceral também contribui para a ativação do sistema renina-angiotensina-aldosterona (SRAA) por meio do aumento da síntese local de angiotensinogênio, favorecendo a maior geração de angiotensina II (Ang II). Esse processo promove retenção de sódio, vasoconstrição e ativação de vias oxidativas, criando um ambiente

propício ao desenvolvimento de disfunções cardiovasculares (Saiki et al., 2009; Rajagopalan et al., 1996; Lassegue et al., 2001).

2.2.5.2 Resistência à insulina

A resistência insulínica constitui um dos pilares centrais da SM, estando diretamente associada à hiperglicemia e à hiperinsulinemia compensatória. Quando os tecidos periféricos, principalmente músculo esquelético, fígado e tecido adiposo, tornam-se menos responsivos à ação da insulina, a utilização da glicose é prejudicada, o que leva à necessidade de secreção aumentada do hormônio pelo pâncreas (Hudish; Reusch; Sussel, 2019).

Essa condição favorece a lipólise aumentada no tecido adiposo e eleva a liberação de ácidos graxos livres na circulação. O fígado passa a captar esse excedente, contribuindo para a deposição lipídica hepática e para o desenvolvimento de esteatose hepática. Além disso, a resistência insulínica altera o metabolismo lipídico hepático de modo a promover o surgimento de um perfil dislipidêmico aterogênico (Barbalho, 2015).

2.2.5.3 Inflamação crônica e estresse oxidativo

A SM está associada a um estado pró-inflamatório e de estresse oxidativo sustentado, resultante da interação de múltiplos mecanismos moleculares e celulares que amplificam o dano metabólico e tecidual (Ghosh et al., 2017; Masenga et al., 2023). A hiperativação de enzimas como a NADPH oxidase e as disfunções mitocondriais aumentam a produção de espécies reativas de oxigênio (EROs), que promovem peroxidação lipídica, danos irreversíveis em proteínas e DNA, além de ativar fatores de transcrição, como NF-κB, que regula genes pró-inflamatórios, e HIF-1α, que afeta a angiogênese, desencadeando inflamação e o remodelamento tecidual (Denisenko et al., 2020).

Entre os principais biomarcadores inflamatórios elevados na SM destacam-se a interleucina-6 (IL-6), o fator de necrose tumoral alfa (TNF-α), a proteína C-reativa (CRP), o fibrinogênio e a leptina, enquanto a adiponectina e a interleucina-10 (IL-10) apresentam níveis reduzidos (Quadro 1) (Kopp et al., 2003). A IL-6, secretada por macrófagos e adipócitos, está

aumentada na resistência à insulina e obesidade, regulando o metabolismo da glicose e lipídeos, estimulando a produção hepática de reagentes de fase aguda (PCR, fibrinogênio) e contribuindo para aterogênese por meio da ativação do sistema renina-angiotensina (RAS) e da expressão de moléculas de adesão celular (VCAMs). Em especial, a elevação de PCR apresenta forte correlação com risco de diabetes tipo 2 e eventos cardiovasculares (Fahed et al., 2022; Hotamisligil, 2006).

QUADRO 1 – Alterações na expressão de adipocinas e marcadores inflamatórios em diferentes condições metabólicas

Expressão Aumentada (↑)	Expressão Reduzida (↓)
Leptina, PAI-1, quemerina	Adiponectina, omentina
IL-1, IL-6, IL-8, MCP-1, TNF-α	IL-10
CRP de alta sensibilidade, fibrinogênio	
TLR2 e TLR4 monocíticos	

Fonte: A autora

O TNF-α, produzido principalmente no tecido adiposo, correlaciona-se diretamente com a massa adiposa e com a resistência insulínica. Essa citocina prejudica a sinalização da insulina ao inativar receptores e moléculas intracelulares, além de estimular lipólise hepática e aumentar a concentração de ácidos graxos livres na circulação (Zhang et al., 2002).

Outro eixo relevante envolve os receptores Toll-like (TLRs), especialmente TLR2 e TLR4. Esses receptores reconhecem tanto padrões moleculares associados a patógenos (PAMPs), como o lipopolissacarídeo (LPS), quanto padrões de dano endógeno (DAMPs), incluindo ácidos graxos saturados, lipoproteína de baixa densidade (LDL) oxidada e produtos finais de glicação avançada. A ativação dos TLRs leva à produção de citocinas pró-inflamatórias (IL-1β, IL-6, TNF-α, MCP-1), sustentando o processo inflamatório. Modelos animais demonstram que a ausência de TLR2 ou TLR4 reduz adiposidade, resistência insulínica e inflamação tecidual (Himes; Smith, 2010). Em humanos, sua superexpressão em monócitos está associada ao aumento da permeabilidade intestinal e à endotoxemia, fatores que intensificam a inflamação na SM (Fahed et al., 2022).

Além disso, as EROs interagem com o sistema renina-angiotensina e com o receptor LOX-1, estabelecendo um ciclo de retroalimentação que perpetua a disfunção endotelial, a inflamação e a proliferação celular. Esse processo favorece a progressão da dislipidemia, do diabetes tipo 2, da hipertensão arterial e de outras complicações cardiovasculares (Mehta; Griendling, 2007; Fahed et al., 2022).

Assim, a inflamação crônica e o estresse oxidativo representam eixos centrais na fisiopatologia da SM, sustentando a interação entre obesidade visceral, resistência insulínica e disfunção endotelial. Esses processos configuram alvos terapêuticos prioritários para reduzir complicações metabólicas e cardiovasculares. Além disso, alterações no equilíbrio da microbiota e na barreira intestinal têm sido relacionadas a esse estado inflamatório persistente, ampliando a compreensão dos mecanismos envolvidos na SM (Gurung et al., 2020; Scazzocchio et al., 2020; Xiao et al., 2024).

2.2.5.4 Hipertensão arterial sistêmica

A hipertensão arterial sistêmica (HAS) é uma condição crônica, multifatorial e não transmissível, definida pela elevação sustentada da pressão arterial sistólica (≥ 140 mm Hg) e/ou da pressão arterial diastólica (≥ 90 mm Hg), aferidas em dois momentos distintos e com técnica adequada (Brandão et al., 2025). No contexto da SM, a elevação da pressão arterial está majoritariamente associada à ativação disfuncional do sistema renina-angiotensina-aldosterona (SRAA). A obesidade visceral induz os adipócitos a produzirem quantidades excessivas de angiotensinogênio, estimulando o SRAA e promovendo vasoconstrição, retenção de sódio e água, bem como hipertensão (Lin et al., 2022). Além disso, o desequilíbrio na secreção de adipocinas, particularmente a hiperleptinemia associada à obesidade visceral, pode estimular centros hipotalâmicos e aumentar a atividade do sistema nervoso simpático, contribuindo para a elevação da pressão arterial (Verhaar et al., 2020). Como consequência, indivíduos com HAS associada à SM apresentam maior prevalência de alterações cardiovasculares e renais subclínicas, incluindo hipertrofia ventricular esquerda, aterosclerose precoce da carótida, redução da elasticidade aórtica, retinopatia hipertensiva e microalbuminúria. Tais alterações elevam significativamente o risco de evolução para doenças cardiovasculares graves (Mulè et al., 2014).

2.2.5.5 Dislipidemia

As dislipidemias correspondem a alterações quantitativas ou qualitativas nas lipoproteínas plasmáticas, podendo manifestar-se como elevação do colesterol da lipoproteína de baixa densidade (LDL-c), aumento dos triglicerídeos ou de lipoproteínas ricas em triglicerídeos, redução do colesterol da lipoproteína de alta densidade (HDL-c) ou combinações dessas alterações. Essas alterações podem ocorrer de forma isolada ou combinada e estão diretamente associadas ao aumento do risco de doença cardiovascular aterosclerótica (Rached et al., 2025). Na SM, predomina um padrão de dislipidemia aterogênica caracterizado por hipertrigliceridemia, redução de HDL-c e elevação de lipoproteínas ricas em triglicerídeos e colesterol não-HDL, frequentemente relacionado à resistência à insulina e ao excesso de adiposidade visceral (Martiniakova; Mondockova; Kovacova, 2024; Rached et al., 2025).

O principal mecanismo subjacente é a resistência à insulina, que compromete a ação do hormônio no tecido adiposo, aumentando a lipólise e a liberação de ácidos graxos livres. Esses ácidos graxos são captados pelo fígado e estimulam a produção excessiva de lipoproteína de muito baixa densidade (VLDL), resultando em hipertrigliceridemia (Fu et al., 2024). Simultaneamente, a resistência à insulina reduz a atividade da lipoproteína lipase, enzima fundamental para a hidrólise de triglicerídeos, intensificando a anormalidade lipídica (Shang et al., 2024).

Outro aspecto relevante é o papel das adipocinas, cujo desequilíbrio observado na SM intensifica o estado inflamatório já descrito. A redução da adiponectina, aliada ao predomínio de mediadores pró-inflamatórios, compromete a sensibilidade insulínica e contribui para a manutenção da resistência à insulina, favorecendo, consequentemente, o agravamento da dislipidemia (Satish; Saxena; Agrawal, 2019).

A predisposição genética também influencia significativamente, já que variantes em genes relacionados ao metabolismo lipídico, como aqueles que regulam apolipoproteínas e enzimas, incluindo a lipase hepática, podem alterar os perfis lipídicos e aumentar a susceptibilidade à dislipidemia (Moon et al., 2024).

Além disso, fatores ambientais exercem papel decisivo. Dietas ricas em gorduras saturadas e açúcares favorecem a progressão da dislipidemia, enquanto a prática regular de exercício físico contribui para melhorar a sensibilidade à insulina e facilitar a depuração de triglicerídeos (Ambroseli et al., 2023). Por fim, o estresse

oxidativo, frequentemente intensificado na SM, tem sido implicado como mecanismo que exacerba as irregularidades lipídicas e amplia o risco de complicações (Satish; Saxena; Agrawal, 2019).

Dessa forma, a SM configura-se como uma condição sistêmica, em que alterações metabólicas, inflamatórias e vasculares coexistem e se reforçam mutuamente. Esse

entendimento não apenas justifica sua associação com diabetes mellitus tipo 2, doenças cardiovasculares e maior mortalidade, mas também evidencia a necessidade de estratégias terapêuticas integradas que abordem simultaneamente seus múltiplos mecanismos fisiopatológicos. A compreensão integrada desses mecanismos fisiopatológicos reforça a necessidade de abordagens terapêuticas que atuem simultaneamente sobre múltiplos eixos metabólicos, inflamatórios e regulatórios.

2.3 ESTRATÉGIAS DE TRATAMENTO DA SÍNDROME METABÓLICA

2.3.1 Estratégias farmacológicas

Até o momento, não existe um fármaco único aprovado para o tratamento específico da SM. O manejo farmacológico, portanto, visa o controle individual de cada componente da condição clínica (Figura 2) (Grundy, 2016).

No manejo da resistência insulínica, destacam-se os sensibilizadores da insulina, como a metformina e as glitazonas (rosiglitazona, pioglitazona), conforme recomendado pelas diretrizes oficiais para o tratamento do diabetes mellitus tipo 2 (Lyra et al., 2025; SOCIEDADE BRASILEIRA DE DIABETES, 2025). Para o tratamento das dislipidemias, as estatinas permanecem como primeira escolha, podendo ser associadas à ezetimiba, sequestrantes de sais biliares ou, em casos de hipertrigliceridemia predominante, à administração de fibratos ou à suplementação com ácidos graxos ômega-3, de acordo com as diretrizes brasileiras de dislipidemias e prevenção da aterosclerose (Rached et al., 2025).

Já a hipertensão arterial pode ser tratada com inibidores da enzima conversora

de angiotensina (ex.: enalapril), antagonistas do receptor AT1 da angiotensina II (ex.: losartana), antagonistas dos canais de cálcio (ex.: anlodipina), diuréticos (ex.: hidroclorotiazida) e betabloqueadores (ex.: propranolol), utilizados em monoterapia ou em associação, conforme o perfil clínico do paciente. Essas estratégias terapêuticas estão alinhadas às diretrizes nacionais vigentes, como a Diretriz Brasileira de Hipertensão Arterial – 2025 (Brandão et al., 2025), além de evidências da literatura internacional (Lim; Eckel, 2014; Dobrowolski et al., 2022).

Apesar de sua eficácia, o tratamento farmacológico tradicional apresenta limitações, incluindo efeitos adversos, custos elevados e baixa adesão associada à necessidade de múltiplos

medicamentos (Lim; Eckel, 2014). Além disso, tais abordagens não atuam de forma integrada sobre os múltiplos mecanismos fisiopatológicos da SM.

FIGURA 2. Fluxograma do tratamento farmacológico da síndrome metabólica.

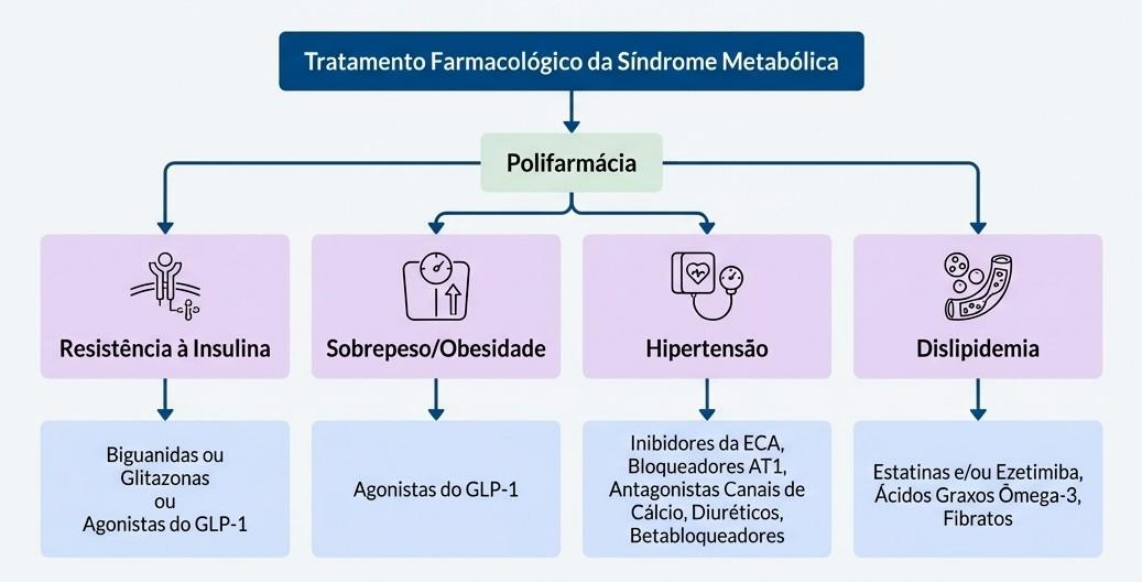

Fonte: A autora

Diante dessas limitações, os agonistas do receptor do peptídeo semelhante ao glucagon tipo 1 (GLP-1) e os coagonistas GIP/GLP-1 têm emergido como alternativas terapêuticas promissoras, com atuação mais abrangente sobre o risco cardiometabólico. Inicialmente desenvolvidas para o tratamento do diabetes mellitus tipo 2, essas terapias passaram a demonstrar benefícios adicionais, incluindo perda ponderal significativa, melhora da resistência à insulina e impacto favorável sobre

diversos componentes da síndrome metabólica (McGowan et al., 2025).

Os agonistas de GLP-1, como a semaglutida, exercem seus efeitos por meio do aumento da secreção de insulina dependente da glicose, redução da secreção de glucagon, retardo do esvaziamento gástrico e ação central na regulação da saciedade. Evidências clínicas robustas indicam que sua utilização promove não apenas melhora glicêmica, mas também redução de eventos cardiovasculares maiores em indivíduos com sobrepeso ou obesidade e doença cardiovascular estabelecida, independentemente da presença de diabetes (Lincoff et al., 2023; Deanfield et al., 2025). Ademais, benefícios renais têm sido consistentemente descritos, incluindo redução da progressão da doença renal crônica e da mortalidade cardiovascular em populações de alto risco (Perkovic et al., 2024; Colhoun et al., 2024).

No mesmo espectro terapêutico, os coagonistas de GIP/GLP-1, como a tirzepatida, apresentam efeitos ainda mais expressivos sobre o peso corporal e os parâmetros metabólicos. A ativação simultânea dos receptores de GLP-1 e GIP resulta em maior potencial insulinotrópico e efeitos amplificados sobre o balanço energético. Ensaios clínicos têm demonstrado reduções substanciais de peso, melhora do perfil lipídico, redução da pressão arterial e diminuição da circunferência abdominal (Jastreboff et al., 2025; Sattar et al., 2025).

No contexto específico da síndrome metabólica, análises derivadas de ensaios clínicos indicam que a tirzepatida reduz significativamente a prevalência da SM e melhora simultaneamente seus componentes, sugerindo uma abordagem mais integrada em comparação às terapias convencionais (Nicholls et al., 2024). Além disso, evidências recentes apontam benefícios em condições frequentemente associadas à SM, como a doença hepática gordurosa associada à disfunção metabólica, com resolução histológica da esteato-hepatite sem progressão da fibrose (Loomba et al., 2024).

Diretrizes recentes reforçam o papel dessas terapias no manejo da obesidade e de suas complicações cardiometabólicas, recomendando sua utilização como parte de uma abordagem contínua e integrada a intervenções no estilo de vida (Celletti et al., 2025). Entretanto, ressalta- se que a manutenção dos benefícios depende da continuidade do tratamento, uma vez que a sua interrupção pode resultar em recuperação ponderal e piora dos parâmetros metabólicos.

2.3.2 Estratégias não farmacológicas

As modificações do estilo de vida constituem a primeira linha de intervenção na SM, especialmente por meio de uma dieta equilibrada e da prática regular de exercício físico, complementadas quando necessário por intervenções farmacológicas individualizadas para cada comorbidade (Denisenko et al., 2020; Nilsson; Tuomilehto; Rydén, 2019). No âmbito da nutrição, intervenções dietéticas bem planejadas podem estabilizar ou até reverter o quadro sindrômico. Clifton (2019) destaca que a substituição de carboidratos por gorduras poli- insaturadas reduz triglicerídeos, eleva HDL e contribui para o controle da pressão arterial. As dietas mediterrâneas demonstram benefícios adicionais, incluindo perda de peso, regulação glicêmica e lipídica, efeito anti-inflamatório e redução da pressão arterial (Dayi; Ozgoren, 2022). De forma semelhante, as dietas à base de plantas, ricas em polifenóis, exercem ação antioxidante, promovem redução ponderal e diminuem marcadores inflamatórios (Thomas; Calle; Fernandez, 2023; Ambroselli et al., 2023).

Em relação à atividade física, a combinação de exercícios aeróbicos e de resistência apresenta efeitos pleiotrópicos sobre o metabolismo, refletidos na redução do peso corporal, da circunferência abdominal e da pressão arterial, além da melhora dos perfis glicêmico, lipídico e inflamatório (Ostman et al., 2017; Lemos; Torrinhas; Waitzberg, 2023). A cessação do tabagismo também desempenha papel essencial, contribuindo para a melhora global desses parâmetros (SBC, 2017).

Embora mudanças de estilo de vida e fármacos sintéticos constituam a base do tratamento, estudos recentes têm destacado o potencial de substâncias naturais como alternativas ou estratégias terapêuticas complementares, especialmente pela capacidade de atuar sobre múltiplos alvos fisiopatológicos de forma integrada (Abdulghani et al., 2024; Ullah et al., 2025).

2.4 FITOFÁRMACOS

De acordo com a Agência Nacional de Vigilância Sanitária (ANVISA, 2025),

fitofármacos são substâncias químicas purificadas e isoladas a partir de matéria-prima vegetal, com estrutura química definida e atividade farmacológica responsável pelos efeitos terapêuticos. Diversas espécies vegetais vêm sendo reconhecidas como fontes de fitofármacos e outros compostos bioativos com potencial no tratamento da SM, seja pela capacidade de potencializar a eficácia de terapias convencionais, seja pela redução de efeitos adversos associados ao uso prolongado de medicamentos sintéticos. Além disso, esses compostos podem permitir o uso de doses menores dos fármacos convencionais, potencialmente aumentando a segurança do tratamento e contribuindo para a prevenção de doenças crônicas não transmissíveis (DCNTs) (Taghadosi et al., 2024). Nesse contexto, fitofármacos como a curcumina (CUR) e a piperina (PIP) têm despertado especial interesse, reunindo evidências consistentes de efeitos antioxidantes, anti-inflamatórios, metabólicos e moduladores da microbiota intestinal (Tagde et al., 2021; Gupta et al., 2020). Apesar dos efeitos promissores descritos, a eficácia clínica desses compostos ainda depende de estratégias que superem limitações relacionadas à estabilidade, absorção e biodisponibilidade. Suas propriedades serão discutidas individualmente nos tópicos seguintes.

2.4.1 Curcumina

A curcumina [(1E,6E)-1,7-bis(4-hydroxy-3-methoxyphenyl)-1,6-heptadiene-3,5-dione] é um composto fenólico natural extraído dos rizomas de Curcuma longa L., do qual vem sendo isolada desde o século XIX (Figura 3). No Brasil, C. longa é amplamente conhecida como açafrão-da-terra e utilizada na culinária como tempero e corante, em razão de sua coloração intensa, além de ser tradicionalmente associada a propriedades terapêuticas e dietéticas. O uso medicinal dessa espécie, entretanto, é muito mais antigo e remonta a séculos, especialmente na medicina tradicional indiana (Naksuriya et al., 2014).

FIGURA 3. *Curcuma longa L.* - Espécie vegetal (A), Rizoma (B) e produto do rizoma desidratado e pulverizado (C).

Fonte: Adaptado de PLANTS OF THE WORLD ONLINE. Disponível em: http://plantsoftheworldonline.org/. Acesso em: 02 set. 2025.

A partir do rizoma desidratado e moído, obtém-se o pó dourado conhecido como turmérico, caracterizado por sua elevada concentração de curcuminoides. O teor total desses compostos em C. longa varia geralmente entre 1 e 5% do peso seco do rizoma (Dei Cas; Ghidoni, 2019), sendo composto majoritariamente por curcumina (77%), seguida por demetoxicurcumina (17%) e bisdemetoxicurcumina (6%). As diferenças estruturais entre esses análogos resultam principalmente da presença ou ausência de grupos metoxila nos anéis aromáticos, mantendo-se o esqueleto β-dicetona central, conforme ilustrado na Figura 4 (Naksuriya et al., 2014). Esses compostos apresentam baixa solubilidade em água e éter, embora sejam solúveis em etanol, acetona, dimetilsulfóxido e outros solventes orgânicos (Santiago et al., 2015).

FIGURA 4. Estrutura química de curcuminoides extraídos de *Curcuma longa L.*:

Curcumina (A), Desmetoxicurmina (B) e Bisdesmetoxicurcumina (C).

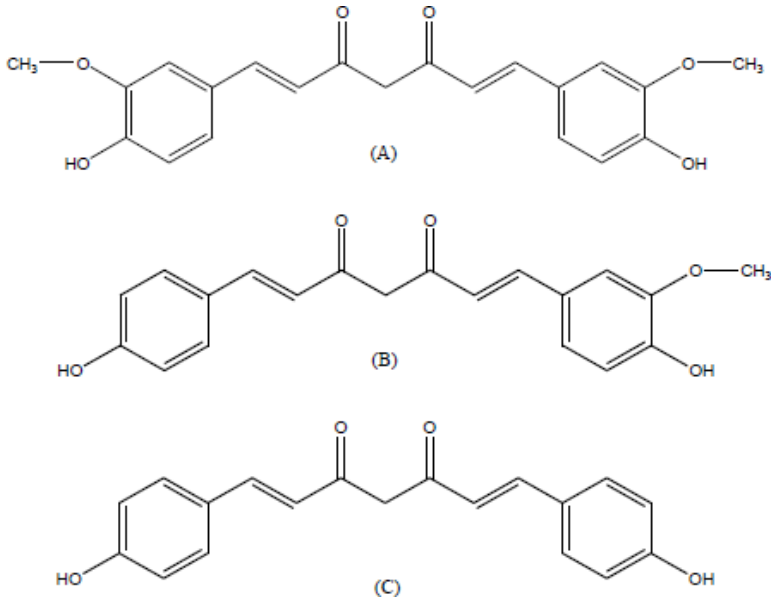

Fonte: Naksuriya et al., 2014.

A curcumina apresenta um perfil farmacológico pleiotrópico, com capacidade de modular simultaneamente múltiplas vias de sinalização celular, o que explica a diversidade de suas ações biológicas (Tagde et al., 2021). Entre seus efeitos mais bem documentados destacam-se as propriedades antioxidantes e anti-inflamatórias, associadas à modulação de mediadores como NF-κB, COX-2 e citocinas pró-inflamatórias (Aggarwal; Harikumar, 2009). Além disso, diversos estudos descrevem atividades antidiabéticas, antimicrobianas (bacterianas e fúngicas), antiproliferativas, anticancerígenas e hepatoprotetoras atribuídas à curcumina (Aggarwal; Sung, 2009; Gupta et al., 2020). Evidências mais recentes também indicam efeitos neuroprotetores e impacto positivo sobre funções cognitivas, além de potenciais benefícios no controle da obesidade e do diabetes tipo 2, condições frequentemente associadas à síndrome metabólica (Soleimani; Sahebkar; Hosseinzadeh, 2018).Estudos recentes confirmam que os grupos fenólicos e metoxila presentes na estrutura da curcumina são cruciais para suas múltiplas atividades biológicas, atuando como doadores de elétrons e moduladores de vias de sinalização celular. Esses grupos funcionais conferem à molécula uma expressiva capacidade antioxidante, mediada tanto pela neutralização de espécies reativas quanto pela ativação de vias protetoras, como Nrf2/ARE. Além disso, têm sido associados a efeitos antitumorais, incluindo indução de apoptose, inibição da

proliferação celular e supressão da angiogênese em diferentes linhagens tumorais (Tagde et al., 2021; Taghadosi et al., 2024). Dessa forma, o estudo das atividades biológicas da curcumina e a elucidação detalhada de seus mecanismos de ação continuam despertando crescente interesse na comunidade científica, especialmente devido ao seu potencial translacional em doenças crônicas multifatoriais.

No contexto antioxidante, a curcumina não apenas contribui para a neutralização de espécies reativas de oxigênio, mas também modula a atividade de enzimas antioxidantes endógenas, como superóxido dismutase (SOD), catalase (CAT) e glutationa peroxidase (GPx), reduzindo a peroxidação lipídica e os danos celulares associados ao estresse oxidativo. Esse efeito adquire particular relevância na síndrome metabólica, condição em que o excesso de radicais livres favorece a disfunção metabólica e vascular (Gupta et al., 2020).

Em relação à resposta inflamatória, a curcumina inibe a ativação do fator nuclear kappa B (NF-κB) e reduz a expressão de citocinas pró-inflamatórias, como TNF-α e IL-6, além de suprimir enzimas como a ciclooxigenase-2 (COX-2) e as lipoxigenases (LOX). Essa modulação atenua a inflamação crônica de baixo grau, característica da SM, além de exercer efeito protetor contra complicações cardiovasculares associadas (Jyotirmayee et al., 2023; Ghoran et al., 2022; Tagde et al., 2021).

Do ponto de vista metabólico, a curcumina favorece a sensibilidade insulínica, auxilia no controle glicêmico e melhora o perfil lipídico. Investigações clínicas e pré-clínicas sugerem que a curcumina apresenta efeitos sobre vias metabólicas relacionadas ao metabolismo do colesterol, modulando a absorção intestinal de colesterol, a remoção hepatocelular de LDL e o transporte reverso de colesterol. Comparativamente, a curcumina tem mostrado maior eficácia na redução de triglicerídeos, enquanto as estatinas permanecem mais efetivas na redução do LDL-c (Hegde et al., 2023; Panahi et al., 2018). Ensaios clínicos recentes também corroboram reduções significativas nos níveis de colesterol total e LDL em indivíduos suplementados com curcumina em doses de 500–1000 mg/dia, fortalecendo seu potencial no manejo de dislipidemias (Tagde et al., 2021; Yuan et al., 2016).

No contexto antimicrobiano, a curcumina demonstra atividade direta contra bactérias e fungos por meio da desestabilização de membranas celulares e indução de estresse oxidativo. Mais recentemente, evidências apontam para o papel modulador da curcumina sobre a microbiota intestinal, aumentando a diversidade microbiana e favorecendo o crescimento de gêneros benéficos, como Lactobacillus e Bifidobacterium, ao mesmo tempo em que reduz populações potencialmente patogênicas. Essa modulação pode contribuir para a restauração da barreira intestinal, redução da inflamação sistêmica e melhora do metabolismo de glicose e lipídios, sendo um mecanismo adicional de interesse para o manejo da SM (Gupta et al., 2020; Zam et al., 2018).

Apesar do amplo potencial, a eficácia da curcumina é limitada por sua baixa solubilidade aquosa, instabilidade química e metabolismo de primeira passagem, fatores que limitam sua biodisponibilidade oral (Ozawa et al., 2017). Para superar essas limitações farmacocinéticas, estratégias de encapsulação em nano e micropartículas poliméricas e o uso de adjuvantes têm se mostrado alternativas promissoras. Esses sistemas favorecem maior penetração através de membranas biológicas, permitem redução da dose administrada, minimizam potenciais efeitos tóxicos e atuam como transportadores eficientes de compostos bioativos (Tagde et al., 2021), reforçando seu potencial terapêutico. Du Preez et al. (2019) demonstraram que nanopartículas de curcumina em baixas doses produzem efeitos equivalentes a doses convencionais muito mais elevadas. Esse achado sustenta o uso de sistemas micro e nanoparticulados em condições crônicas, como a SM, nas quais perfis de exposição mais estáveis podem resultar em maior eficácia clínica e melhor adesão ao tratamento (Hegde et al., 2023).

2.4.2 Piperina

A piperina é um alcaloide piperídico presente nos frutos de Piper nigrum L. e Piper longum L., responsável pelo sabor picante característico da pimenta-preta (Figura 5).

No Brasil, é popularmente conhecida como pimenta-preta ou pimenta-do-reino. Piper nigrum, planta trepadeira da família Piperaceae originária da Índia, foi inicialmente

utilizada na medicina, mas consolidou-se como condimento de sabor picante e amargo, de ampla circulação comercial e grande relevância econômica para regiões produtoras (Oliveira, Alencar-Filho, Vasconcellos et al., 2014; Ahmad et al., 2012).

FIGURA 5. *Piper nigrum* - Espécie vegetal (A) e Frutos secos inteiros e pulverizados (B).

Fonte: Adaptado de PLANTS OF THE WORLD ONLINE. Disponível em: http://plantsoftheworldonline.org/. Acesso em: 02 set. 2025.

Quimicamente, a piperina é classificada como uma amida (1-piperolpiperidina), sendo o composto majoritário presente nos frutos (Figura 6). No organismo, sofre biotransformação, originando ácido pipérico e piperidina (Roger, 1998). Trata-se de uma substância cristalina, incolor ou esbranquiçada, com ponto de fusão entre 128 e 132 °C. É solúvel em gasolina, clorofórmio, etanol, ácido acético e benzeno, levemente solúvel em éter etílico e insolúvel em água (Almeida, 2017; Roger, 1998).

Evidências provenientes principalmente de estudos pré-clínicos, conduzidos em modelos celulares e animais, indicam que a piperina exerce múltiplas atividades farmacológicas, incluindo efeitos anti-inflamatórios, antioxidantes,

imunomoduladores, neuroprotetores, antidepressivos, antiproliferativos e antitumorais (Octavia et al., 2024; Zaini et al., 2020). Em modelos experimentais, a piperina demonstrou reduzir marcadores de inflamação e estresse oxidativo, bem como atenuar danos teciduais associados a processos inflamatórios sistêmicos (Mohammadi et al., 2019). Além disso, estudos pré-clínicos indicam que o composto pode modular o metabolismo lipídico por meio da inibição da adipogênese e da redução dos níveis plasmáticos de triglicerídeos e colesterol (Mhaske; Sreedharan; Mahadik, 2018). No âmbito clínico, a principal aplicação investigada da piperina relaciona-se ao seu papel como bioativador natural, capaz de aumentar a biodisponibilidade de nutrientes e fármacos por mecanismos que envolvem a inibição de enzimas metabolizadoras — como citocromos P450 e UDP-glicuronosiltransferases — e o bloqueio da P-glicoproteína intestinal, favorecendo a absorção sistêmica de compostos bioativos (Tagde et al., 2021; Shoba et al., 1998).

Além de seu valor culinário, a planta é rica em vitaminas A e C, ferro e potássio. Também contém diversos metabólitos secundários, como amidas e alcaloides, propenilfenois, lignanas, neolignanas, terpenos, flavonas, cumarina, pironas, flavonoides, neogliganano, sarmentina e sarmentosina, entre outros (Ahmad et al., 2012).

FIGURA 6: Estrutura química de piperina.

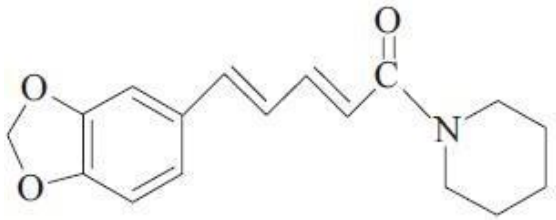

Fonte: Adaptado de Ahmad e colaboradores (2012).

No âmbito industrial, a piperina também encontra aplicação em formulações cosméticas, pela capacidade de estimular a proliferação de melanócitos e atuar na pigmentação cutânea, e em formulações agroquímicas, aproveitando-se de sua toxicidade natural para o controle de pragas (Gupta et al., 2020).

Embora apresente ampla gama de benefícios farmacológicos, em doses elevadas a piperina pode causar efeitos adversos gastrointestinais, incluindo irritação

gástrica e agravamento de quadros de gastrite, úlcera péptica, pancreatite e hemorroidas, além de estar associada a potenciais riscos em indivíduos hipertensos (Octavia et al., 2024). Esses achados reforçam a necessidade de avaliar cuidadosamente a dose e a forma farmacotécnica de administração.

Por outro lado, uma das propriedades mais relevantes da piperina em aplicações farmacêuticas e nutracêuticas é sua atuação como bioativador natural. A molécula, devido ao seu caráter lipofílico, é capaz de inibir processos de metabolização como a glucuronidação hepática e intestinal, além de atuar sobre isoformas do citocromo P450 e a bomba de efluxo P-glicoproteína (Mhaske; Sreedharan; Mahadik, 2018). Esses mecanismos explicam o aumento da biodisponibilidade de diversos nutrientes e fármacos, incluindo a curcumina, o que justifica seu uso crescente em formulações combinadas e sistemas de liberação controlada (Tagde et al., 2021).

2.4.3 Associação curcumina–piperina

A combinação CUR/PIP é uma das estratégias mais eficazes para potencializar a ação da curcumina. A piperina aumenta expressivamente sua absorção, podendo elevar as concentrações plasmáticas em até 20 vezes por meio da inibição de transportadores de efluxo intestinal e da redução do metabolismo de primeira passagem, decorrente da inibição de enzimas de biotransformação hepática e intestinal (Shobha et al., 1998; Dewi; Setyaningsih, 2023). Além disso, há evidências de sinergia funcional, uma vez que ambas modulam vias inflamatórias, oxidativas e metabólicas relevantes à SM.

A associação também exerce efeitos complementares na microbiota intestinal, promovendo equilíbrio microbiano e reduzindo marcadores inflamatórios sistêmicos (Zam, 2018; Gupta et al., 2020). Entretanto, apesar da eficácia, a combinação ainda enfrenta desafios relacionados à estabilidade, solubilidade e degradação acelerada no trato gastrointestinal (Alam et al., 2024). Por isso, estratégias farmacotécnicas vêm sendo exploradas para proteção, direcionamento e liberação controlada dos compostos.

Abordagens como derivatização molecular, complexação com polímeros, nanoencapsulação e microencapsulação têm sido propostas para superar limitações físico- químicas e ampliar a eficácia terapêutica (Racz et al., 2022; Azad et al., 2024).

Em especial, sistemas pH-sensíveis obtidos por spray drying apresentam vantagens ao proteger CUR e PIP em ambiente gástrico e liberar os compostos de forma direcionada no intestino, região de maior absorção. Nesse cenário, sistemas de liberação modificada surgem como alternativa para proteger os compostos e modular sua disponibilidade no trato gastrointestinal.

2.5 SISTEMAS DE LIBERAÇÃO MODIFICADA DE FÁRMACOS

Os sistemas de liberação controlada constituem estratégias farmacotecnológicas desenvolvidas para modular a taxa, o local e a duração da liberação de fármacos no organismo. No contexto da SM, esses sistemas assumem importância crescente por proporcionarem maior estabilidade plasmática, redução da frequência de administração, melhor adesão ao tratamento e menor ocorrência de efeitos adversos. Tais avanços são especialmente relevantes para compostos bioativos de origem natural, como a curcumina e a piperina, cuja aplicação clínica é limitada por barreiras farmacocinéticas (Tagde et al., 2021; Racz et al., 2022).

Um dos principais desafios no desenvolvimento de formulações farmacêuticas é a baixa solubilidade aquosa, estimada em cerca de 40% das substâncias ativas utilizadas pela indústria, característica que compromete a absorção gastrointestinal e o desempenho terapêutico (Schafroth et al., 2012). Muitas dessas moléculas se enquadram na Classe II do Sistema de Classificação Biofarmacêutica (SCB), caracterizada por baixa solubilidade e alta permeabilidade. O SCB, amplamente utilizado por agências regulatórias como FDA e EMA, fornece parâmetros essenciais para orientar o desenvolvimento de formulações (Zhang et al., 2018).

Para superar essas limitações, diferentes estratégias farmacotécnicas têm sido estudadas com o objetivo de modificar propriedades físico-químicas e otimizar o perfil de liberação. A tecnologia de liberação modificada apresenta vantagens significativas em relação às formas convencionais, incluindo maior estabilidade química, menor flutuação plasmática, redução da toxicidade e melhor adesão ao tratamento (Restani et al., 2010; Patra et al., 2018; Ghoran et al., 2022).

A escolha da formulação ideal deve considerar fatores como natureza, estabilidade, solubilidade e toxicidade do fármaco, além do perfil de liberação

desejado, do alvo terapêutico e dos métodos de síntese ou de modificação estrutural necessários para obtenção de partículas poliméricas (Quodbach, 2025; Adepu; Ramakrishna, 2021). Entre os sistemas mais utilizados destacam-se nanopartículas, lipossomas e micropartículas, que oferecem vantagens específicas, como proteção do ativo, controle da taxa de liberação e possibilidade de direcionamento terapêutico (Adepu; Ramakrishna, 2021).

As nanopartículas poliméricas (<1 μm) constituem um dos sistemas de liberação mais estudados para fármacos hidrofóbicos, como a curcumina e a piperina. Podem ser classificadas em nanocápsulas, caracterizadas por um núcleo líquido envolto por invólucro polimérico, e nanoesferas, estruturas sólidas nas quais o fármaco se encontra disperso na matriz. Suas principais vantagens incluem maior capacidade de carga, proteção contra degradação, aumento da absorção intestinal e potencial de direcionamento sítio-específico (Adepu; Ramakrishna, 2021; Shivani, 2015).

Os lipossomas são vesículas esféricas constituídas por uma ou mais bicamadas fosfolipídicas, capazes de encapsular simultaneamente compostos hidrofílicos (no compartimento aquoso) e lipofílicos (na membrana). Graças à sua biocompatibilidade, biodegradabilidade e baixo risco imunogênico, essa tecnologia já tem aplicações clínicas consolidadas e algumas formulações aprovadas por agências regulatórias internacionais. Entre os principais benefícios destaca-se a melhoria da solubilidade de fármacos lipofílicos, a redução de sua toxicidade sistêmica e a viabilização de liberação controlada. Especificamente para a curcumina, estudos recentes mostraram que a encapsulação em lipossomas aumenta sua estabilidade em fluidos biológicos e amplia sua biodisponibilidade oral em comparação com formulações convencionais (Chen et al., 2024; Radha et al., 2024).

As micropartículas (1–1000 μm) apresentam-se como sistemas de liberação de medicamentos altamente versáteis, podendo ser organizadas como microesferas, em que o ativo está distribuído na matriz polimérica, ou como microcápsulas, nas quais o fármaco está confinado em um reservatório interno, seja sólido ou líquido (da Silva et al., 2023). Esses sistemas são particularmente adequados para compostos hidrofóbicos, pois permitem modular o perfil de liberação — seja sustentada, retardada ou dirigida a sítios específicos —, além de proteger moléculas sensíveis contra degradação. Para esse propósito, são empregados polímeros biodegradáveis como poliésteres (por exemplo, PLGA, PCL) e polímeros metacrílicos (como Eudragit® RS ou S-100), que oferecem flexibilidade ao design do sistema (Kállai-Szabó et al., 2024). A seleção

adequada do solvente utilizado no processo (água, etanol, acetato de etila etc.) é essencial para garantir a estabilidade, segurança e características desejadas da partícula final, incluindo toxicidade mínima e eficiência de remoção adequada (Rodrigues et al., 2020).

Entre os sistemas discutidos, as micropartículas apresentam particular interesse para compostos bioativos hidrofóbicos, pois permitem modular o perfil de dissolução e proteger moléculas instáveis. Para que esses benefícios se traduzam em formulações seguras e eficazes, a escolha da técnica de obtenção torna-se decisiva. Nesse cenário, o método de spray drying destaca-se como uma das abordagens mais promissoras, sendo amplamente explorado para a produção de micropartículas de curcumina e piperina.

2.5.1 Obtenção de nano/micropartículas pelo método de spray drying

Entre as estratégias utilizadas para aumentar a solubilidade e otimizar o perfil de liberação de fármacos, as dispersões sólidas se destacam pelos bons resultados. Essas podem ser obtidas por métodos de fusão, como a extrusão a quente, ou por evaporação de solventes, entre os quais o spray drying é amplamente aplicado (Ashour et al., 2016).

O spray drying apresenta vantagens relevantes para a indústria farmacêutica e de alimentos: é escalonável, versátil, de baixo custo e permite operação contínua. Em comparação com técnicas como liofilização ou secagem a vácuo, possibilita a obtenção de partículas esféricas, homogêneas e com baixa umidade, além de custo significativamente reduzido (Shishir; Chen, 2017; Yupanqui et al., 2024). Também oferece benefícios adicionais, como proteção de compostos bioativos, melhoria de propriedades organolépticas e de estabilidade, resultando em partículas de alta qualidade e fácil aplicação industrial (Sosnik; Seremeta, 2015). Para curcuminoides, o spray drying tem se mostrado particularmente promissor em relação a outras técnicas, como nanoprecipitação, hidratação de filme fino, coacervação e gelificação iônica. O método permite gerar partículas em escala submicrométrica ou nanométrica, com conversão parcial para o estado amorfo e controle de morfologia, características que favorecem a taxa de dissolução e a estabilidade (Ghoran et al., 2022).

O processo é rápido e envolve a dissolução, suspensão ou emulsificação do fármaco com o polímero em solvente aquoso ou orgânico. Essa mistura é alimentada no equipamento por bomba peristáltica e atomizada em bico de pequeno diâmetro, entrando em contato imediato com ar aquecido. As gotículas formadas sofrem evaporação instantânea dentro da câmara de secagem, originando partículas finas que são separadas em ciclone e coletadas em recipiente apropriado (Engel et al., 2017; Shivani, 2015).

2.5.2 Polímeros e sistemas pH-dependentes

Os polímeros são macromoléculas naturais ou sintéticas, constituídas por unidades químicas repetidas (meros) ligadas por ligações covalentes. Suas propriedades derivam do tamanho, da estrutura química e das interações intra e intermoleculares (Mano; Mendes, 2004).

Excipientes poliméricos incluem compostos naturais, como gelatina, quitosana e celulose; semissintéticos, como derivados de celulose, polietilenoglicóis e poliamidas; além de produtos de fermentação, como a goma xantana. Esses materiais são amplamente empregados em formas farmacêuticas administradas por diferentes vias — oral, parenteral ou inalatória (Karolewicz, 2016).

Além de funções básicas, os polímeros podem apresentar propriedades adicionais relevantes para sistemas inteligentes de liberação de fármacos, como sensibilidade a estímulos, mucoadesão, inibição de enzimas, aumento da penetração intestinal, mascaramento de sabores, efeito tampão, inibição de bombas de efluxo e até atividades farmacológicas próprias (Karolewicz, 2016).

Entre os polímeros sintéticos, os derivados metacrílicos, conhecidos comercialmente como Eudragit®, têm ampla aplicação na tecnologia farmacêutica. São copolímeros derivados do ácido acrílico e metacrílico, cuja solubilidade é dependente do pH do meio gastrointestinal. Essa característica permite tanto a liberação direcionada de fármacos — por dissolução em meios ácidos ou alcalinos — quanto a liberação controlada no tempo, por inchamento de polímeros insolúveis e permeáveis (Patra et al., 2018).

O Eudragit® S100 (Figura 7) tem se destacado por sua solubilidade seletiva em

pH ≥ 7, o que direciona a liberação ao intestino, região de maior absorção da curcumina e da piperina (Yusuf et al., 2021; Purnamasari et al., 2023). Trata-se de um copolímero aniônico de ácido metacrílico e metacrilato de metila, insolúvel em meio ácido, mas solúvel em meio intestinal, conferindo gastrorresistência e uso preferencial em formulações de liberação colônica (Patra et al., 2018; Informe Técnico, 2018).

FIGURA 7. Estrutura química do Eudragit® S100

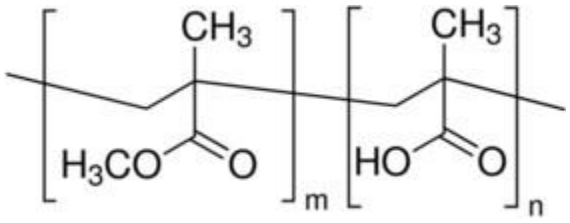

Fonte: A autora

O desenvolvimento de dispersões sólidas obtidas por spray drying utilizando Eudragit® S100 tem mostrado eficácia em aumentar a solubilidade aquosa de fármacos pouco solúveis. Além disso, as micropartículas obtidas oferecem vantagens adicionais: proteção de substâncias instáveis contra degradação (oxidação e hidrólise), mascaramento de odor ou sabor desagradável, aumento da validade do produto, encapsulação de líquidos ou substâncias

incompatíveis e possibilidade de modular a liberação de forma prolongada, retardada, sítio- específica ou sustentada (Biscaia et al., 2023; Farago, 2007).

2.6 SISTEMAS DE LIBERAÇÃO MODIFICADA CONTENDO CUR E PIP

No caso de compostos bioativos como a curcumina e a piperina, o spray drying associado a polímeros funcionais, como os metacrílicos, tem demonstrado vantagens relevantes: proteção contra degradação térmica ou ácida, conversão do estado cristalino para amorfo, aumento da solubilidade aparente e modulação do perfil de liberação no trato gastrointestinal (Yusuf et al., 2021; Lu et al., 2021). Esses atributos

tornam a microencapsulação uma estratégia atrativa não apenas para superar limitações farmacocinéticas, mas também para ampliar a aplicabilidade dessas moléculas em formulações farmacêuticas, nutracêuticas e alimentos funcionais.

Para a curcumina, Yupanqui et al. (2024) reportaram que micropartículas de extrato de cúrcuma obtidas por spray drying apresentaram aumento de solubilidade, estabilidade térmica e redução da toxicidade aguda, reforçando a viabilidade da técnica em sistemas funcionais. De forma semelhante, Lu et al. (2021) observaram que a escolha dos materiais de parede impactou a eficiência da microencapsulação, resultando na conversão para o estado amorfo e em maior estabilidade. Complementarmente, Taghadosi et al. (2024) demonstraram que a encapsulação da curcumina em goma persa, também por spray drying, conferiu elevada estabilidade química em matrizes lácteas, apontando potencial para o setor de alimentos funcionais.

No caso da associação curcumina–piperina, Purnamasari et al. (2023) mostraram que micropartículas obtidas por spray drying apresentaram liberação sustentada, ajustando-se a modelos cinéticos de dissolução. Em estudo complementar, Biscaia (2018) encapsulou piperina em micropartículas poliméricas de Eudragit® S100 e RS30D, também por spray drying, e verificou efeitos significativos no tratamento da obesidade em ratos alimentados com dieta hiperlipídica, sugerindo potencial translacional no manejo de distúrbios metabólicos.

Ensaios clínicos clássicos e recentes confirmam que a coadministração de curcumina e piperina pode elevar em até 20 vezes as concentrações plasmáticas da curcumina (Dewi; Setyaningsih, 2023). Além da ação farmacocinética, há evidências de que a combinação exerce efeitos sinérgicos sobre a microbiota intestinal. A curcumina atua em múltiplos mecanismos já descritos, enquanto a piperina apresenta propriedades antimicrobianas que podem contribuir para o reequilíbrio microbiano. Essa interação sugere um efeito aditivo ou sinérgico, em que a piperina não apenas amplia a exposição sistêmica da curcumina, mas também participa da modulação do microbioma (Zam et al., 2018).

Essa sinergia farmacocinética e microbiológica confere ao par curcumina–piperina um perfil de alta relevância translacional, especialmente no contexto da SM. Ao mesmo tempo em que ampliam a biodisponibilidade da curcumina, esses compostos modulam processos-chave associados à fisiopatologia da síndrome, como inflamação de baixo grau, estresse oxidativo, resistência à insulina e disbiose intestinal. Nesse sentido, micropartículas poliméricas pH- sensíveis obtidas por spray

drying despontam como alternativa para proteger e liberar controladamente essa combinação em sítios intestinais de absorção, maximizando seus efeitos funcionais e terapêuticos (Ghoran et al., 2022; Racz et al., 2022).

Em síntese, embora terapias convencionais tenham eficácia limitada frente à complexidade da SM, compostos naturais como a curcumina e a piperina emergem como alternativas promissoras. Contudo, sua aplicação clínica ainda é restringida pela baixa biodisponibilidade e instabilidade. Esse entrave tem impulsionado o desenvolvimento de sistemas farmacotécnicos inovadores, entre os quais as micropartículas pH-sensíveis obtidas por spray drying se destacam como estratégia viável. Embora avanços importantes tenham sido alcançados, ainda são limitados os estudos que avaliam de forma integrada a associação curcumina–piperina em sistemas pH-sensíveis voltados à SM. Diante dessa lacuna, o presente estudo se propõe como passo necessário na continuidade do debate acadêmico, contribuindo para o avanço científico e para o desenvolvimento de novas alternativas terapêuticas.

3 OBJETIVOS

3.1 OBJETIVO GERAL

Desenvolver micropartículas pH-sensíveis contendo curcumina e piperina, obtidas por spray drying, e avaliar sua segurança e desempenho in vitro e in vivo em modelo animal de síndrome metabólica.

3.2 OBJETIVOS ESPECÍFICOS

- Obter micropartículas gastro-resistentes de curcumina e piperina, empregando Eudragit® S100 por spray drying, e caracterizá-las quanto à morfologia, propriedades espectroscópicas, térmicas e eficiência de encapsulação.
- Desenvolver e validar método analítico por HPLC para quantificação de curcumina e piperina nos sistemas poliméricos.
- Avaliar a liberação e a segurança das micropartículas por meio de ensaios in vitro (perfil de dissolução, hemólise) e in vivo (toxicidade aguda em ratos Wistar).
- Investigar a eficácia biológica das micropartículas em modelo experimental de síndrome metabólica induzida em ratos SHR, analisando parâmetros clínicos e metabólicos (peso corporal, pressão arterial, perfil glicídico e lipídico).
- Examinar os efeitos do tratamento em biomarcadores bioquímicos séricos e inflamatórios (IL-6, TNF-α).
- Avaliar o impacto das micropartículas no microbioma intestinal, considerando sua potencial contribuição para os efeitos metabólicos observados.

4 ARTIGO CIENTÍFICO 1

Co-Quantification of Curcumin and Piperine by RP-HPLC/DAD in Spray-Dried Microparticles for Quality Control

3.2.1.1 Marcia Viviane Marcon[1]*
https://orcid.org/0000-0003-1657-9152
3.2.1.2 Vinícius Monteiro Schafka[2]
https://orcid.org/0000-0001-7780-1728

3.2.1.3 Barbara Justus[3]
https://orcid.org/0000-0003-3943-9304

3.2.1.4 Jessica Mendes Nadal[3]
https://orcid.org/0000-0002-2419-2110

3.2.1.5 Cyntia Maria Schnekenberg[4]
https://orcid.org/0000-0002-8812-1952

3.2.1.6 Jaqueline de Bortoli Shirabayashi[5]
https://orcid.org/0000-0002-4775-4585

3.2.1.7 Francislaine Aparecida dos Reis Lívero[6]
https://orcid.org/0000-0001-6533-0850

3.2.1.8 Paulo Vitor Farago[1,4]
https://orcid.org/0000-0002-9934-4027

[1] Graduate Program in Pharmaceutical Sciences, State University of Ponta Grossa, Paraná, Brazil
[2] Graduate Program in Chemistry, State University of Ponta Grossa, Paraná, Brazil
[3] State University of Ponta Grossa, Paraná, Brazil
[4] Graduate Program in Dentistry, State University of Ponta Grossa, Paraná, Brazil
[5] Laboratory of Preclinical Research of Natural Products, Paranaense University (UNIPAR), Umuarama, Paraná, Brazil
[6] Laboratory of Cardiometabolic Pharmacology, Federal University of Paraná, and Laboratory of Preclinical Research of Natural Products, UNIPAR, Brazil

*Correspondence: mmarcon@uepg.br; Tel.: +55-42-999033709

HIGHLIGHTS

- Microparticles were successfully produced using the solid dispersion technique.
- A fast and simple RP-HPLC method was validated for CUR and PIP quantification.

Abstract: Curcumin has limited oral bioavailability, while piperine can act as a bioenhancer. Reliable simultaneous quantification is essential for quality control. This study aimed to develop and validate a simple, precise, and robust RP-HPLC/DAD method for the simultaneous determination of curcumin (CUR) and piperine (PIP) in spray-dried microparticles. Microparticles were produced by spray drying with Eudragit® S100, and the analytical method was validated according to ICH Q2 and ANVISA RDC 166/2017. Specificity, linearity, precision, accuracy, robustness, and encapsulation efficiency (EE) were assessed. Linearity was demonstrated within 200–500 $\mu g \cdot mL^{-1}$ (CUR) and 8–20 $\mu g \cdot mL^{-1}$ (PIP) with $r>0.996$. Recoveries were ~100% (CUR 100.18%; PIP 99.56%) with CV<5%. Encapsulation efficiency was ≥99% for both analytes. Conclusion: the method is accurate, robust, and appropriate for routine quality control of microparticulate formulations containing CUR and PIP.

Keywords: curcumin; piperine; microparticles; RP-HPLC; method validation; spray drying.

INTRODUCTION

Curcumin—the principal curcuminoid from *Curcuma longa* L.—has been extensively investigated for its interaction with multiple cellular signaling pathways and its broad spectrum of biological activities, including antioxidant, anti-inflammatory, antidiabetic, antibacterial, antifungal, antiproliferative, anticancer, and hepatoprotective effects [1,2]. Despite encouraging *in vitro* and *in vivo* findings, clinical trials have not conclusively demonstrated therapeutic efficacy, largely because of curcumin's poor oral bioavailability [3–5]. Encapsulation in nano- or microparticulate systems has therefore been proposed to improve stability and absorption [6]. Co-administration with piperine, an alkaloid from *Piper nigrum*, is a particularly promising strategy, as piperine markedly enhances curcumin bioavailability [7,8]. To advance such formulations toward translational use, robust analytical methods are needed to accurately quantify the bioactive compounds and to support regulatory compliance, reproducibility, and quality assurance [9].

Although numerous methods quantify curcumin and piperine individually, reports of their simultaneous HPLC quantification are relatively scarce, particularly in solid formulations such as spray-dried microparticles, whose importance is increasing in pharmaceutical development, functional foods, and biotechnology. Among the few exceptions are an isocratic HPLC–UV/DAD method validated to ICH standards in CUR+PIP microparticles [9], RP-HPLC procedures applied to formulations/nanoparticles [10,11,12], and a classical RP-HPLC–PDA application in Eudragit® nanoparticles [13]. This landscape supports the use of HPLC–UV/DAD for quality control (QC), as it combines short run times, low solvent consumption, and cost-effectiveness/transferability, whereas LC–MS/MS remains more appropriate for trace-level bioanalysis.

In this context, this study aimed to develop and validate, in accordance with the International Conference on Harmonisation (ICH) [14] and Brazilian ANVISA Resolution RDC No. 166/2017, an isocratic RP-HPLC/DAD method for the simultaneous quantification of curcumin and piperine in spray-dried microparticles. In addition, we evaluated process yield, encapsulation efficiency, mean particle diameter, zeta potential, and morphology to demonstrate the method's applicability to assay testing and routine quality control. By providing a precise, reproducible, and time-efficient analytical tool, this work supports the quality control of pharmaceutical and nutraceutical formulations and establishes a translational foundation for broader biotechnological applications in health, environmental sustainability, and functional foods**.**

MATERIAL AND METHODS

3.2.1.9 Reagents and Solvents

Curcumin (95.2% curcuminoids: 74.2% curcumin, 15.5% demethoxycurcumin, 5.5% bisdemethoxycurcumin) was supplied by Tianxu Natural Pigment (China). Piperine (95.69% purity) was obtained from Xi'an Tian Ben Bio-engineering (China). Eudragit® S100 was donated by Evonik Brasil Ltda. Methanol and acetonitrile (HPLC grade, Merck, Germany) were used, and ultrapure water was prepared using a Millipore® system.

3.2.1.10 Preparation of Polymeric Microparticles Containing Curcumin and Piperine

Microparticles containing curcumin (CUR) and piperine (PIP) were prepared by spray drying with Eudragit® S100 (MSCP). The theoretical formulation (10 g) comprised 500 mg CUR and 20 mg PIP (20% w/w active load). The solvent system consisted of ethanol:water (60:40, v/v). Table 1 summarizes the composition of the active and blank formulations.

CUR and PIP were dissolved in ethanol under magnetic stirring (800 rpm, FISATOM model 754, Brazil). Eudragit® S100 was then added under the same stirring conditions. Distilled water was gradually added, and the mixture was maintained under continuous stirring for 12 h. The resulting dispersion was dried by spray drying (LABMAQ, model MSD 0.5) using the following parameters: atomizer diameter 0.82 mm, atomization pressure 3 $kgf \cdot cm^{-2}$, drying air flow 25 $L \cdot min^{-1}$, feed rate 0.40 $L \cdot h^{-1}$, inlet temperature 135 ± 5 °C, and outlet temperature 60 ± 5 °C.

Table 1 – Composition of the polymeric microparticle formulation containing CUR and PIP.

Formulation	CUR (g)	PIP (g)	Eudragit® S100 (g)	Ultrapure H_2O (mL)	Ethanol (mL)
MPES100	—	—	10.0	480	720
MPCP	1.924	0.076	8.0	480	720

MPES100 (negative control); MPCP (Eudragit® S100 microparticles with CUR and PIP).

3.2.1.11 Particle Size and Zeta Potential

Were measured by dynamic light scattering (Zetasizer Nano ZS90, Malvern). Samples were diluted in ultrapure water (1:500, v/v), sonicated for 15 min, and analyzed in triplicate.

3.2.1.12 Morphology

Morphology was evaluated using field-emission scanning electron microscopy (FE-SEM; Tescan Mira 3). Microparticles, pure drug substances, the polymer, and the physical mixture were sputter-coated with gold (Shimadzu IC-50) prior to analysis and examined at an accelerating voltage of 15 kV.

3.2.1.13 Chromatographic Conditions

Chromatographic analyses were conducted on a Shimadzu Nexera-i LC2040C HPLC system equipped with a DAD detector and a Shim-pack C18 reversed-phase column (150 × 4.6 mm, 5 µm). The mobile phase consisted of acetonitrile:methanol:water with 0.1% formic acid (55:5:40, v/v/v) at a flow rate of 1.0 $mL \cdot min^{-1}$ in isocratic mode at 25 °C. The injection volume was 10 µL, with detection at 410 nm (CUR) and 341 nm (PIP). The total runtime was 15 min.

3.2.1.14 Standard Solutions

Stock solutions of CUR and PIP (500 $\mu g \cdot mL^{-1}$) were prepared in methanol and diluted to yield working standards (200–500 $\mu g \cdot mL^{-1}$ for CUR; 8–20 $\mu g \cdot mL^{-1}$ for PIP). All solutions were filtered through PTFE membranes (0.22 µm, Macherey-Nagel, Germany) prior to analysis.

3.2.1.15 Method Validation for Simultaneous Quantification of Curcumin and Piperine

Method validation was conducted in accordance with the International Conference on Harmonisation (ICH) guidelines [14] and the Brazilian ANVISA Resolution RDC No. 166/2017 [15]. The parameters evaluated included specificity, linearity, limits of detection (LOD) and quantification (LOQ), precision, accuracy, and robustness.

Specificity was confirmed by comparing chromatograms of microparticles containing CUR and PIP with those of blank formulations, demonstrating the absence of interfering peaks.

Linearity was assessed from three independent calibration curves, each constructed with six concentrations: CUR (200–500 $\mu g \cdot mL^{-1}$) and PIP (8–20 $\mu g \cdot mL^{-1}$). Regression equations and correlation coefficients (R) were obtained from mean values.

Sensitivity was determined by calculating LOD and LOQ according to ICH guidelines, using the standard deviation (SD) of the response and the slope (S) of the calibration curve (Equations 1–2):

Equation 1 and 2

$$LOD = \frac{3{,}3 \times SD}{S} \quad (1) \qquad LOQ = \frac{10 \times SD}{S} \quad (2)$$

Precision was evaluated at two levels: repeatability (intra-day) and intermediate precision (inter-day). Triplicate analyses were performed at three concentration levels for each analyte. Results were expressed as %CV.

Accuracy was assessed by recovery, with nine determinations per analyte at three concentration levels low (200 $\mu g \cdot mL^{-1}$ CUR; 8.0 $\mu g \cdot mL^{-1}$ PIP); medium (300 $\mu g \cdot mL^{-1}$ CUR; 12.0 $\mu g \cdot mL^{-1}$ PIP); and high (500 $\mu g \cdot mL^{-1}$ CUR; 20.0 $\mu g \cdot mL^{-1}$ PIP). Acceptable recoveries were defined between 95% and 105% (Equation 3).

Equation 3

$$\%\ accuracy = \frac{experimental}{theoretical} \times 100$$

Robustness was examined at 300 $\mu g \cdot mL^{-1}$ for CUR and 12 $\mu g \cdot mL^{-1}$ for PIP under deliberate variations in mobile phase composition (55:5:40, 54:5:41, and 56:5:39, v/v/v) and column temperature (22 °C and 28 °C). Effects were evaluated using ANOVA followed by Tukey's test.

Resolution between peaks was calculated according to Equation 4, based on retention times (tR1, tR2) and peak widths at half-height (Wh1, Wh2):

Equation 4

$$R_S = \frac{1.18(t_{R2} - t_{R1})}{W_{h1} + W_{h2}} \qquad (t_{R2} > t_{R1})$$

- t_{R1}, t_{R2} = retention times of the peaks
- W_{h1}, W_{h2} = peak widths at half-height

3.2.1.16 Encapsulation Efficiency (EE%)

Was determined as described in Equation 5 [16]. Microparticles were weighed into 10 mL volumetric flasks, dispersed in 8 mL methanol, stirred at 1,000 rpm for 12 h, diluted to volume, and filtered through PTFE membranes (0.22 µm).

Equation 5 $$EE\ (\%) = \frac{\text{drug mass in micropartical}}{\text{Initial theoretical drug mass}} \times 100$$

Theoretical drug concentrations were 288.48 µg·mL⁻¹ for CUR and 11.52 µg·mL⁻¹ for PIP. All assays were performed in triplicate using the validated method, with detection at 410 nm (CUR) and 341 nm (PIP).

3.2.1.17 Statistical Analysis

Results are expressed as mean ± standard deviation. Statistical significance between groups was evaluated using one-way ANOVA, with $\alpha = 0.05$.

RESULTS

3.2.1.18 Microparticle Production

Spray drying of Eudragit® S100 dispersions yielded free-flowing powders with distinct coloration. Blank microparticles (MPES100) were white, whereas curcumin–piperine microparticles (MPCP) were orange, consistent with the characteristic hue of curcumin. The average production yields were 56.27% for MP ES100 and 53.34% for MP CP.

3.2.1.19 Particle Size and Zeta Potential

CUR–PIP microparticles showed a mean diameter of 680 ± 18 nm, with unimodal distribution and polydispersity index < 0.3. Blank microparticles presented a larger mean diameter of 1506 ± 198 nm. The zeta potential of CUR–PIP microparticles was −40.53 mV.

3.2.1.20 Morphology

FEG-SEM analysis showed crystalline morphology for CUR and heterogeneous crystalline structure for PIP. Eudragit® S100 presented spherical particles with low size variation (Figure 1). CUR–PIP microparticles displayed spherical morphology with smooth surfaces and slight irregularities, without crystalline deposits (Figure 2). Microscopy diameters were consistent with DLS measurements.

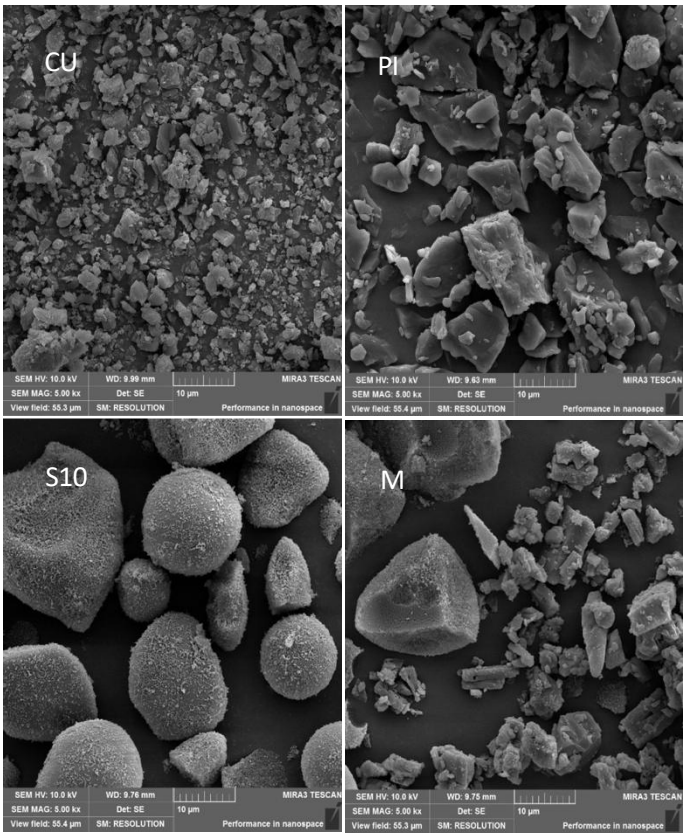

FIGURE 1. FEG-SEM micrographs of pure drugs—curcumin (CUR) and piperine (PIP)—of the polymer Eudragit® S100 (S100) and of the physical mixture, 5k× magnification.

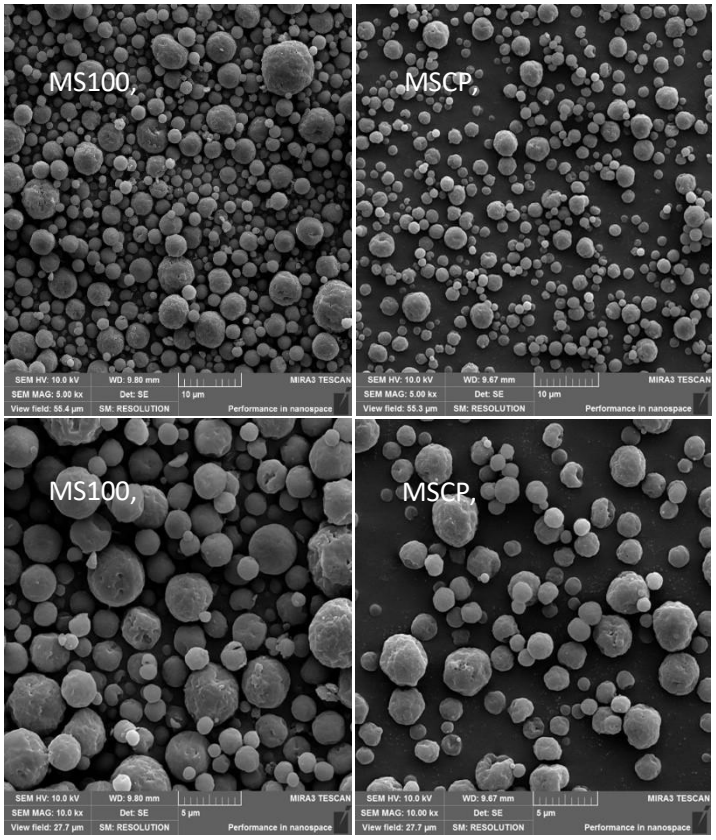

FIGURE 2. FEG-SEM micrographs of microparticles prepared from Eudragit® S100 with and without curcumin and piperine: MS100 and MSCP, at 5k× and 10k× magnifications.

3.2.1.21 Chromatographic Method Validation Specificity and Retention Times

The optimized mobile phase (acetonitrile:methanol:water with 0.1% formic acid, 55:5:40, v/v/v) enabled complete separation within 15 min at a flow rate of 1.0 mL·min⁻¹. Retention times were 4.55 min for CUR and 4.88 min for PIP. Chromatograms of blank microparticles showed no interfering peaks, confirming specificity (Figure 3).

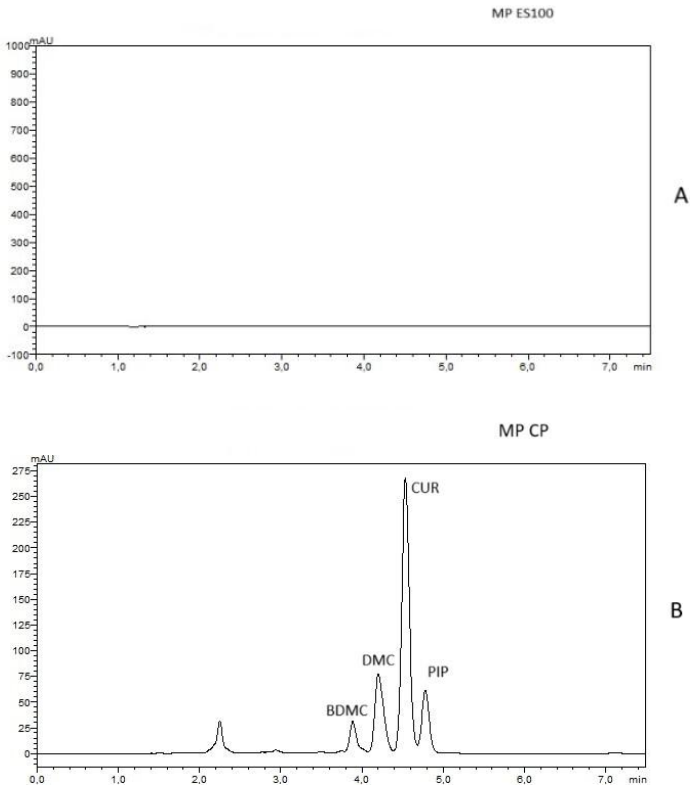

Figure 3. Chromatograms of unloaded microparticles (MP ES100) (A) and microparticles containing curcumin (CUR), piperine (PIP), demethoxycurcumin (DMC), and bisdemethoxycurcumin (BDMC) (MP CP) (B), obtained by HPLC.

3.2.1.22 Linearity

Calibration curves for CUR (200–500 µg·mL⁻¹) and PIP (8–20 µg·mL⁻¹) were linear, with regression coefficients of r = 0.9965 and r = 0.9971, respectively (Figure 4). ANOVA indicated a significant model fit without evidence of lack of fit (α = 0.05) (Table 2).

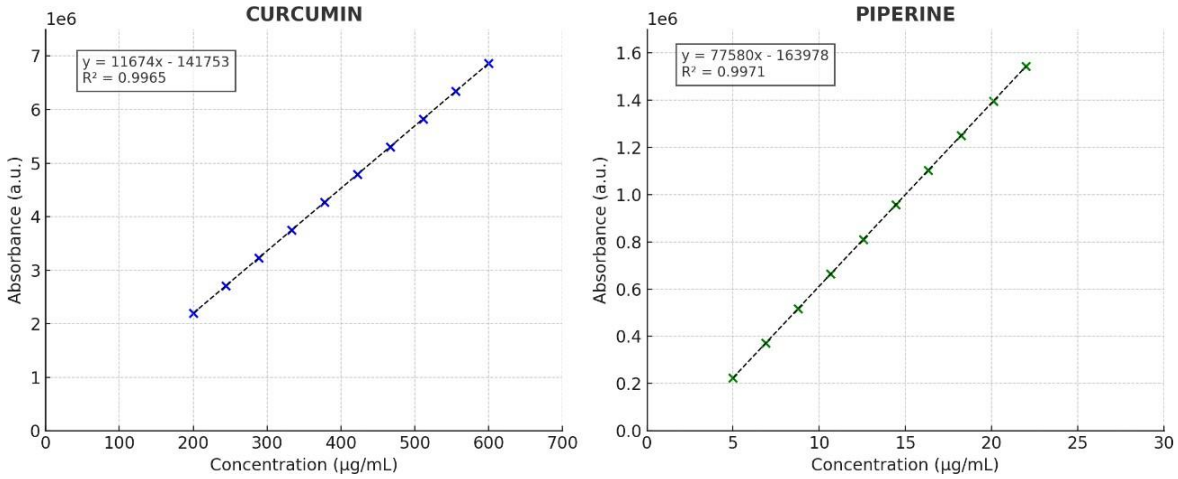

Figure 4. Average calibration curves for CUR and PIP with acetonitrile:methanol:water + 0.1% formic acid (55:5:40, v/v/v).

Table 2. ANOVA results for linearity of the analytical method for CUR and PIP (summary).

	SS	DF	MS	*F*	*F* tab
CUR					
Model	2,1012 x 10^{13}	1	2,1012 x10^{13}	15216,8	4,49
Residual	2,2099 x 10^{10}	16	1,3812 x 10^{9}		
				Linear	
Lack of fit	9,4160 x 10^{9}	4	2,3540 x 10^{9}	2,227	3,26
Pure error	1,2683 x 10^{10}	12	2,3540 x 10^{9}		
				No lack of fit	
PIP					
Model	8.994396 x 10^{9}	1	8.9943963 x 10^{9}	2997,81	4,49
Residual	8.994396 x 10^{9}	16			
				Linear	
Lack of fit	4.8732098 x 10^{9}	4	1.218302 x 10^{9}	3,25	3,26
Pure error	4.1211866 x 10^{9}	12	343.43 x 10^{6}		
				No lack of fit	

Note: Where SS = sum of squares; DF = degrees of freedom; MS = mean square; F = F test value; F tab = tabulated F value.

3.2.1.23 Sensitivity

Limits of detection (LOD) were 21.24 µg·mL^{-1} (CUR) and 0.90 µg·mL^{-1} (PIP), while limits of quantification (LOQ) were 64.37 µg·mL^{-1} (CUR) and 2.73 µg·mL^{-1} (PIP).

3.2.1.24 Precision

Intermediate precision was evaluated considering intra-day, inter-day, and inter-analyst variation. The results for precision, expressed as repeatability and intermediate precision, are presented in Table 3 for curcumin (CUR) and piperine (PIP).

Table 3. Intra-day and inter-day precision for CUR and PIP (found vs. nominal; %CV).

Set	Nominal CUR (µg/mL)	Found CUR (µg/mL)	CV% (CUR)	Nominal PIP (µg/mL)	Found PIP (µg/mL)	CV% (PIP)
Intra-day #1	500	504.11	0.405	20	20.17	0.072
Intra-day #2	300	305.51	0.078	12	11.99	0.433
Intra-day #3	200	202.46	0.313	8	8.31	0.054
Inter-day #1	500	474.95	2.397	20	18.38	1.978
Inter-day #2	300	274.71	2.895	12	12.30	2.111
Inter-day #3	200	177.30	1.212	8	6.55	4.909

3.2.1.25 Accuracy

Accuracy values were within 99–104%, with recoveries falling within the predefined acceptance range of 95–105% (Table 4).

Table 4. Accuracy at three concentration levels for CUR and PIP.

Analyte	Theoretical (µg/mL)	Experimental (µg/mL)	Recovery (%)	CV (%)
CUR	200	202.46	101.23	0.51
CUR	300	305.51	101.84	0.51
CUR	500	504.11	100.82	0.51
PIP	8	8.31	103.92	2.06
PIP	12	11.99	99.91	2.06
PIP	20	20.17	100.86	2.06

3.2.1.26 Robustness

Deliberate variations in mobile phase composition (±1%) and column temperature (22–28 °C) did not

significantly alter quantification. Coefficients of variation remained below 2%, and recoveries were consistently between 95% and 105% (Table 5).

Table 5. Robustness at 300 µg/mL CUR and 12 µg/mL PIP under temperature and mobile phase variations.

Analyte / Condition	Condition	CV (%)	Recovery (%)
CUR – Mobile phase	54/5/41 (v/v/v)	0.11	95.29
CUR – Mobile phase	56/5/39 (v/v/v)	1.46	95.33
CUR – Temperature	22 °C	0.35	95.02
CUR – Temperature	28 °C	1.79	95.06
PIP – Mobile phase	54/5/41 (v/v/v)	0.77	101.49
PIP – Mobile phase	56/5/39 (v/v/v)	0.65	103.56
PIP – Temperature	22 °C	0.48	99.02
PIP – Temperature	28 °C	0.04	102.43

3.2.1.27 Resolution and Peak Purity

The USP resolution between CUR and PIP was 1.50. Peak purity indices determined by DAD were 1.00 for CUR and 0.99 for PIP, exceeding the established thresholds and confirming the absence of impurities (Figure 5).

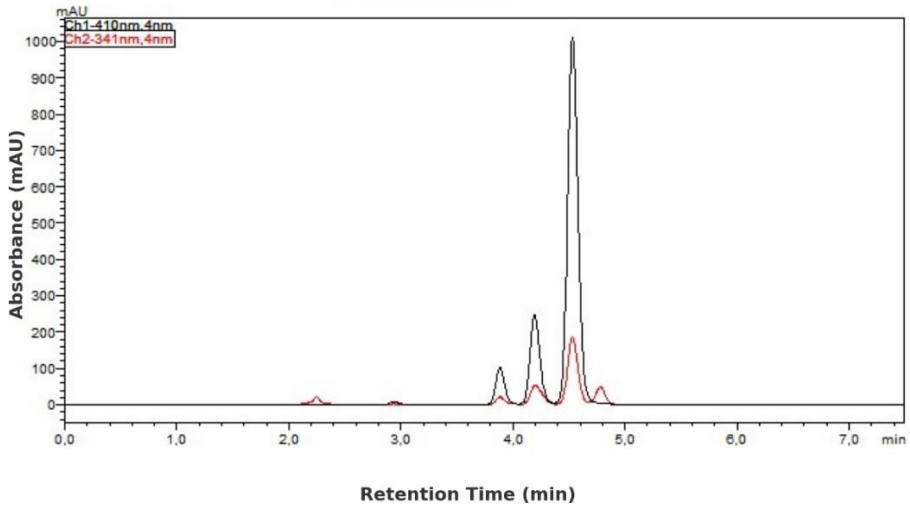

Figure 5. Chromatography in 410 nm e 341 nm with acetonitrile:methanol:water + 0.1% formic acid (55:5:40, v/v/v).

3.2.1.28 Encapsulation Efficiency

The curcumin and piperine (CUR/PIP) microparticles, prepared in ethanol:water (60:40, v/v), exhibited high encapsulation efficiencies, calculated by the indirect method, with values of 100.18% for curcumin

and 99.56% for piperine (Table 6). These results, obtained from triplicate samples, demonstrate excellent incorporation of both compounds into the microparticulate system.

Table 6. Encapsulation efficiency (%EE) of CUR and PIP in microparticles.

Formulation	Theoretical CUR (µg/mL)	Theoretical PIP (µg/mL)	Incorporated CUR (µg/mL±SD)	Incorporated PIP (µg/mL±SD)	%EE (CUR)	%EE (PIP)
MPCP	288.48	11.52	289.01 ± 6.97	11.47 ± 0.24	100.18	99.56

DISCUSSION

Curcumin (CUR) and piperine (PIP) microparticles produced by *spray drying* were successfully obtained. Yields of 53–56% fall within the range commonly reported for polymeric matrices. Losses largely arise from inherent process inefficiencies, notably powder adhesion to the chamber and cone surfaces and partial retention in the cyclone. Comparable outcomes have been described for Eudragit® S100/RS30D microparticles loaded with piperine (≈40–57% yield, 66–90% encapsulation efficiency), in which stickiness and interfacial phenomena—such as polymer migration to the droplet air–water interface and film formation—limit recovery [17]. Consistent trends are observed across recent systems: Yupanqui et al. [18] reported 31.7% for chitosan/mannitol formulations; Tabare et al. [19] noted a decrease from ~90% to ~45% with increasing Eudragit® FS content, with an intermediate condition (F4) of ~70% in the presence of trehalose/L-isoleucine; and Mankan et al. (2025) [20] achieved 70–86% for curcumin–lecithin complexes using maltodextrin as a carrier, alongside improvements in powder flowability and apparent solubility.

Dynamic light scattering (DLS) indicated a mean hydrodynamic diameter of 680 ± 18 nm for CUR–PIP microparticles, with a unimodal size distribution and low PDI (<0.30). Drug-free microparticles were significantly larger (1506 ± 198 nm), suggesting that the actives favored the formation of smaller and more uniform particles [21,22]. According to ISO/TS 80004-2, nanoparticles measure 1–100 nm and microparticles 1–1000 µm; thus, the microparticles obtained are submicrometric, likely reflecting aggregation or coalescence of primary nanoparticles during drying [23]. This dimensional range is advantageous for oral delivery of hydrophobic compounds and is consistent with the generation, by spray drying with Eudragit® S100, of systems intended for intestinal release [21,24]. The observed diameters are smaller than those commonly reported for analogous spray-dried formulations [21,25,26].

The zeta potential was −40.53 mV, consistent with the anionic character conferred by the ionizable carboxylic groups of Eudragit® S100, which are deprotonated at pH > 7. Absolute values exceeding ±30 mV indicate effective electrostatic stabilization [27], supporting colloidal stability and minimizing aggregation.

With respect to morphology, the microparticles displayed predominantly spherical shapes, smooth surfaces with slight irregularities, and no smaller adhered structures, indicating the absence of surface drug accumulation and corroborating encapsulation efficiency. The mean diameter observed was consistent with the values obtained by DLS. These findings agree with previous studies employing comparable methodology and the Eudragit® S100 polymer [17].

Regarding validation of the simultaneous quantification method for CUR and PIP, the main focus of this work, the procedure ICH and ANVISA requirements, demonstrating specificity, precision, robustness, and reliability. Although the calibration range for CUR (200–500 µg·mL^{-1}) could be extended to lower concentrations to broaden applicability to bioavailability and pharmacokinetic studies [28,29], the current choice is fit-for-purpose for quality control of pharmaceutical and nutraceutical

formulations, in accordance with ICH Q2 and ANVISA RDC 166/2017. In finished products, HPLC–DAD/UHPLC methods typically operate in the $\mu g \cdot mL^{-1}$ range with emphasis on assay, content uniformity, and stability, as illustrated by simultaneous CUR+PIP determination [9], multi-laboratory studies of curcuminoids in supplements [30] and stability-indicating approaches for extracts, tablets, and capsules [31]. Moreover, aligning encapsulated levels with clinically relevant doses, such as 500 mg CUR with 5–10 mg PIP [32,33], strengthens the translational character of the study by bringing analytical metrics closer to the therapeutic context; by contrast, trace-level quantification in the ng–$\mu g \cdot mL^{-1}$ range, characteristic of bioanalysis, requires compliance with ICH M10 [1] and lies outside the present scope.

Additionally, when comparing the chromatographic performance of the present method with the literature ([9], [10], [11]), CUR and PIP eluted rapidly (4.55 and 4.88 min, respectively) with baseline separation under isocratic conditions (ACN:MeOH:water + 0.1% formic acid) and differential DAD detection at 410 nm (CUR) and 341 nm (PIP), with a total run time of 15 min. Across published methods, both retention times and detection wavelengths vary widely owing to differences in stationary phase, column dimensions/particle size, organic proportion, pH/acidification, flow rate, temperature, and matrix. For instance, single-wavelength approaches around 360–353 nm tend to yield longer retention (CUR/PIP ≈ 7.2/8.5 min in [11] and 7.91/5.58 min in [9]), whereas ultrafast methods (<3.5 min for both; [10]: 2.43/3.09 min) detect at 282 nm, a band far from CUR's absorption maximum, potentially trading specificity/sensitivity for speed. Regarding total run time, [9] and [10] report 10 min, while [11] uses 15 min, consistent with ours and preserving a window for resolution and robustness in complex matrices. In terms of recovery (accuracy), our values (~100% for both analytes – Table 5) align with the reported ranges: [11] CUR 98.7–102.93% and PIP 97.8–100.97%; [10] CUR 98–100.6% and PIP 99.4–100%. Moreover, the separation fulfilled system-suitability requirements, with a USP resolution of 1.50 between CUR and PIP (DAD peak-purity indices of 1.00 for CUR and 0.99 for PIP), corroborating the absence of co-eluting interferences. Thus, employing analyte-specific wavelengths together with retention times below 5 min and a 15-min run balances speed with sensitivity/selectivity, delivering recovery performance comparable to reference methods [9-11].

Encapsulation efficiencies were high, 100.18% for CUR and 99.56% for PIP. These triplicate values indicate excellent incorporation and are consistent with the literature, albeit higher than previously reported [18,9,21,17]. This performance likely reflects strong drug–polymer affinity and an optimized solvent system that promoted the formation of stable solid dispersions and reduced drying losses. Nevertheless, an efficiency exceeding 100% for CUR may reflect systematic bias rather than true recovery, arising from analytical variability, baseline integration, or weighing errors [34]; additionally, matrix effects may amplify the signal given curcumin's strong absorbance and fluorescence [35]. To mitigate these factors and confirm the findings, orthogonal verification using methods such as LC–MS/MS is recommended [28,36].

In summary, the method proved specific, precise, and robust for the simultaneous quantification of CUR and PIP within the evaluated ranges; orthogonal confirmation and an expanded linear range are natural next steps to extend its applicability to more demanding translational contexts.

CONCLUSION

The proposed RP-HPLC method demonstrated specificity, linearity, accuracy, precision, and robustness within the evaluated conditions, confirming its reliability for routine application. With a short runtime, conventional solvents, and simple isocratic conditions, the assay reduces analytical complexity and facilitates cost-effective implementation in both research and quality-control laboratories. Its reproducibility across analysts and facilities enables confident batch release, stability-indicating studies, formulation screening, and process monitoring. In summary, the method is simple, sensitive, and transferable, providing a practical analytical tool that links experimental formulation development to regulated workflows and supports scale-up and technology maturation.

Funding

This research received no external funding.

Conflict of Interest

The authors declare no conflict of interest.

Acknowledgments

The authors thank UEPG and UNIPAR for technical support.

Data Availability

The datasets generated are available from the corresponding author upon request.

REFERENCES

1. Soleimani V, Sahebkar A, Hosseinzadeh H. Turmeric (*Curcuma longa*) and its major constituent (curcumin) as nontoxic and safe substances: review. *Phytother Res*. 2018;32(6):985-95. doi:10.1002/ptr.6054.
2. Tagde P, Tagde P, Islam F, et al. The multifaceted role of curcumin in advanced nanocurcumin form in the treatment and management of chronic disorders. *Molecules*. 2021;26(23):7109. doi:10.3390/molecules26237109.
3. Gupta T, et al. Enhancing bioavailability and stability of curcumin using solid lipid nanoparticles (CLEN). *Front Bioeng Biotechnol*. 2020;8:879. doi:10.3389/fbioe.2020.00879.
4. Wang YJ, Pan MH, Cheng AL, et al. Stability of curcumin in buffer solutions and characterization of its degradation products. *J Pharm Biomed Anal*. 1997;15(12):1867-76.
5. Hegde M, Girisa S, Chetty BB, et al. Curcumin formulations for better bioavailability: what we learned from clinical trials thus far? *ACS Omega*. 2023;8:10713-46.
6. Evans AC, Martin KA, Saxena M, et al. Curcumin nanodiscs improve solubility and serve as radiological protectants. *Nanomaterials (Basel)*. 2022;12(20):3619.
7. Baspinar Y, Üstündas M, Bayraktar O, Sezgin C. Curcumin and piperine loaded zein-chitosan nanoparticles: development and in-vitro characterisation. *Saudi Pharm J*. 2018;26(3):323-34.
8. Mhaske DB, Sreedharan S, Mahadik KR, et al. Role of piperine as an effective bioenhancer in drug absorption. *Pharm Anal Acta*. 2018;9(7):1-10. doi:10.4172/2153-2435.1000591.
9. Setyaningsih D, Santoso YA, Hartini YS, et al. Isocratic HPLC for simultaneous quantification of curcumin and piperine in a microparticle formulation. *Heliyon*. 2021;7(3):e06541.
10. Kuber RB. Method development and validation for estimation of curcumin and piperine by RP-HPLC. *Int J Appl Pharm*. 2019;11(1):1-12.
11. Khismatrao A, Bhairy S, Hirlekar R. Development and validation of RP-HPLC method for simultaneous estimation of curcumin and piperine. *Int J Appl Pharm*. 2018;10(5):1-15.
12. Shaikh S, Jain V. Development and validation of an RP-HPLC method for the simultaneous determination of curcumin, piperine and camphor in an Ayurvedic formulation. *Int J Pharm Pharm Sci*. 2018;10(4):1-10.
13. Moorthi C, et al. Application of validated RP-HPLC-PDA method for simultaneous estimation of curcumin and piperine in Eudragit E 100 nanoparticles. *J Pharm Res*. 2013;6(4):488-95.
14. International Conference on Harmonisation (ICH). Validation of analytical procedures: text and methodology Q2(R1). Geneva: ICH; 2005.
15. Agência Nacional de Vigilância Sanitária (ANVISA). Resolution RDC No. 166, July 24, 2017. Criteria for validation of analytical methods.

16. Li M, Rouaud O, Poncelet D. Microencapsulation by solvent evaporation: state of the art for process engineering approaches. *Int J Pharm*. 2008;363(1-2):26-39.
17. Biscaia PB, et al. Meth(acrylic) microparticles containing piperine: RP-UHPLC-DAD method for drug-loading and *in vitro* release. *Lat Am J Pharm*. 2023;42(9).
18. Yupanqui CT, Suksanga A, Ardhanwanich S, Ungphaiboon S. Spray-dried microparticles of turmeric extract for improved delivery and low toxicity. *Pharmacia.* 2024;71:e126108. doi:10.3897/pharmacia.71.e126108.
19. Tabare E, Dauchot T, Cochez C, Glonti T, Antoine C, Laforêt F, *et al.* Eudragit® FS microparticles containing bacteriophages, prepared by spray-drying for oral administration. *Pharmaceutics.* 2023;15(6):1602. doi:10.3390/pharmaceutics15061602.
20. Mankan E, Sagdic O, Karadag A. Development and characterization of spray-dried curcumin–lecithin complexes with improved solubility and *in vitro* digestive and thermal stability. *Foods.* 2025;14(18):3157. doi:10.3390/foods14183157.
21. Schneider AC, Brener CES, Daudt NF, Cruz L, Silva CB. Development of microparticles and microparticulated tablets containing piperine. *Braz J Pharm Sci.* 2023. doi:10.1590/s2175-97902023e21265.
22. Umerska A, Paluch KJ, Inkielewicz-Stepniak I, Tajber L. Exploring the release mechanisms of curcumin from polymeric carriers—a Weibull model approach. *Eur J Pharm Biopharm.* 2018;132:180–190. doi:10.1016/j.ejpb.2018.09.001.
23. Al Khatib AO, Yousfan A, Abed A, El-Tanani M, Al-Obaidi H. Development of pimozide spray dried lipid nanoparticles with enhanced targeting of non-small cell lung cancer. *J Drug Deliv Sci Technol.* 2025;106969:1–25.
24. Hassan AS, El-Mahdy MM, El-Badry M, El-Gindy GE-DA. Different approaches for enhancement of curcumin aqueous solubility and dissolution rate. *J Adv Biomed Pharm Sci.* 2019;2:152–361. Available from: http://jabps.journals.ekb.eg
25. Mohylyuk V, Simões S, Veiga F, Cabral-Marques H. Wurster fluidized bed coating of microparticles: towards scalable production of oral sustained-release liquid medicines for patients with swallowing difficulties. *AAPS PharmSciTech.* 2020;21(3).
26. Mithu SH, Rani R, Dhingra D, Kumar S, Dilbaghi N. Evaluation of the surface chemistry and drug–polymer interaction of semi-crystalline microparticles for the development of controlled release formulations. *Mater Sci Eng C.* 2017;76:559–567.
27. Neves AR, Lucena C, Lima F, et al. Novel resveratrol nanodelivery systems based on lipid nanoparticles to enhance its oral bioavailability. *Int J Nanomedicine.* 2013;8:177–187.
28. Peters FT, Drummer OH, Musshoff F. Validation of new methods. *Forensic Sci Int*. 2007;165(2-3):216-24.
29. Heath DD, Pruitt MA, Brenner DE, Rock CL. Curcumin in plasma and urine: quantitation by high-performance liquid chromatography. *J Chromatogr B*. 2003;783(1):287-95.
30. Mudge EM, Brown PN, Rimmer CA, Phillips MM. Determination of curcuminoids in turmeric dietary supplements by HPLC-DAD: multi-laboratory study through the NIH-ODS/NIST quality assurance program. *J AOAC Int*. 2020 Nov 1;103(6):1625–1632. doi:10.1093/jaoacint/qsaa069
31. Mohammed HA, Alsahabi DS, Hegazy AM, et al. Analytical purity determinations of *Curcuma longa* through a QbD validated HPLC approach. *Foods*. 2023;12:1010.
32. Shoba G, Joy D, Joseph T, Majeed M, Rajendran R, Srinivas PS. Influence of piperine on the pharmacokinetics of curcumin in animals and human volunteers. *Planta Med*. 1998;64(4):353-56.
33. Lao CD, et al. Dose escalation of a curcuminoid formulation. *BMC Complement Altern Med*. 2006;6:10
34. EURACHEM/CITAC. *Quantifying uncertainty in analytical measurement*. 3rd ed. 2012.
35. Niessen WMA. *Liquid Chromatography–Mass Spectrometry*. 3rd ed. Boca Raton: CRC Press; 2006.
36. González O, Blanco ME, Iriarte G, Bartolomé L, Maguregui MI, Alonso RM. Bioanalytical chromatographic method validation according to current regulations, with a special focus on LOQ, robustness and matrix effect. *J Chromatogr A*. 2014;1353:10-27.

37. International Council for Harmonisation (ICH). M10: Bioanalytical method validation. Geneva: ICH; 2022. Available from: https://www.ich.org/page/m10-bioanalytical-method-validation
38. International Organization for Standardization (ISO). ISO/TS 80004-2:2015. Nanotechnologies — Vocabulary — Part 2: Nano-objects. Geneva: ISO; 2015. [2]
39. International Council for Harmonisation (ICH). M10: Bioanalytical method validation. Geneva: ICH; 2022. Available from: https://www.ich.org/page/m10-bioanalytical-method-validation
40. International Organization for Standardization (ISO). ISO/TS 80004-2:2015. Nanotechnologies — Vocabulary — Part 2: Nano-objects. Geneva: ISO; 2015. [2]

5 ARTIGO CIENTÍFICO 2

pH-Sensitive Submicrometric Polymeric Particles Prepared by Drying for Co-Delivery of Curcumin and Piperine: *In Vitro* Dissolution and *In vivo* Acute Toxicity

Marcia V. Marcon[1]

Rivair Gonçalves Junior[2]

Vinícius M. Schaffka[3]

Jessica Mendes Nadal[1]

Arisa Namie Higashijima[4]

Rafaela Caroline Santa Clara[4]

Jaqueline de Bortoli Shirabayashi[5]

Barbara Justus[1]

Mackelly Simionatto[1]

Jane Manfron[1,2]

Francislaine Aparecida dos Reis Lívero[4,5]

Paulo Vitor Farago[1,2]*

[1] State University of Ponta Grossa (UEPG), Graduate Program in Pharmaceutical Sciences, Ponta Grossa, Paraná, Brazil; [2] State University of Ponta Grossa (UEPG), Graduate Program in Health Sciences, Ponta Grossa, Paraná, Brazil; [3] State University of Ponta Grossa (UEPG), Graduate Program in Chemistry, Ponta Grossa, Paraná, Brazil; [4] Federal University of Paraná (UFPR), Graduate Program in Pharmacology, Curitiba, Paraná, Brazil. [5] Paranaense University (UNIPAR), Graduate Program in Animal Science, Umuarama, Paraná, Brazil.

*Correspondence: pvfarago@uepg.br; Tel.: +55-42-3220-3120 (P.V.F.

Graphical Abstract

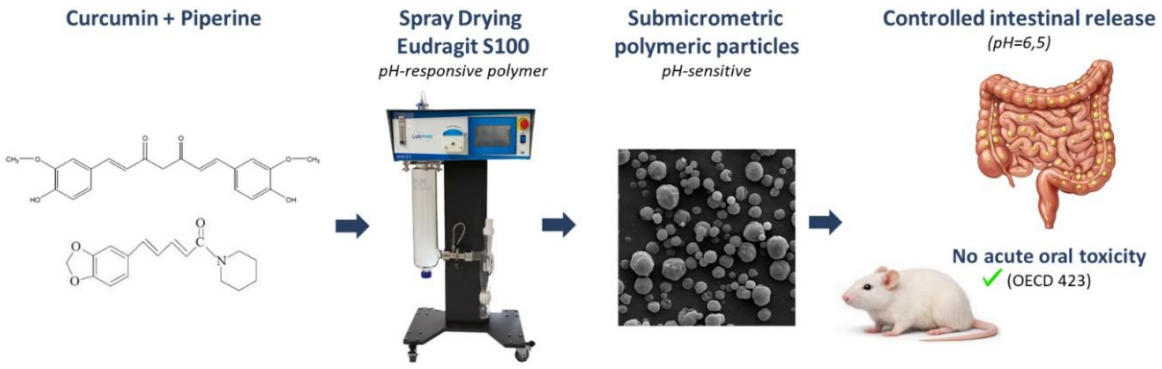

pH-sensitive submicrometric polymeric particles modulate intestinal release of curcumin and piperine with preliminary safety for functional food applications.

ABSTRACT

Curcumin (CUR) and piperine (PIP) exhibit several biological activities of nutraceutical interest. However, their use is limited by low aqueous solubility and bioavailability. Encapsulation into pH-sensitive polymeric systems represents a promising strategy to optimize sustained release and safety of these compounds, expanding their translational potential in nutraceutical formulations and functional foods. In this study, submicrometric polymeric particles containing CUR and PIP were obtained by spray drying using Eudragit S100. The formulations were characterized by yield, encapsulation efficiency, morphology (FE-SEM), physicochemical properties (zeta potential, size distribution), crystallinity (XRD) and *in vitro* dissolution profile. An *in vitro* erythrocyte hemolysis assay was also performed as a safety screening. Acute toxicity was investigated in Wistar rats exposed to single oral doses of the formulation at 300 or 2000 mg/kg. The submicrometric polymeric particles showed yields above 50% and high encapsulation efficiencies close to 100%. Particle size analysis indicated homogeneous submicrometric polymeric particles, with negative zeta potential, suggesting colloidal stability. FE-SEM confirmed spherical morphology and absence of surface crystals. XRD analyses demonstrated conversion of CUR and PIP to the amorphous state, which was associated with increased thermal stability by TGA. *In vitro* dissolution assays revealed sustained release for up to 24 h, with the best fit to the Weibull model ($R^2 > 0.99$). The hemolysis assay indicated low hemolytic activity, consistent with suitable hemocompatibility. The acute toxicity assay showed no evidence of adverse effects under the tested conditions. Taken together, encapsulation of CUR and PIP using Eudragit S100 enabled sustained release and maintained an adequate safety profile in acute and *in vitro* exposure models, supporting the technological suitability of this system for further application in nutraceutical and functional food formulations.

Keywords: Bioactive Delivery Systems; Functional Foods; Polymeric System; Polymethacrylates; Toxicity Tests.

3.2.1.29 Highlights:

- High encapsulation, narrow size with negative zeta potential and spherical amorphous morphology were observed for pH-sensitive submicrometric Eudragit S100 particles co-loading curcumin and piperine
- pH-sensitive submicrometric polymeric particles enable sustained co-release of curcumin and piperine
- No signs of acute oral toxicity in Wistar rats under the tested conditions (OECD 423 guideline)

1. INTRODUCTION

Curcumin, a polyphenolic compound derived from *Curcuma longa* L., has been widely studied for its health-promoting properties and potential applications in nutraceutical products and functional foods (Taghadosi et al., 2024; Tagde et al., 2021). However, its practical use is considerably constrained by low aqueous solubility, rapid degradation, and poor gastrointestinal absorption, which together result in limited systemic bioavailability (Hegde et al., 2023; Yusuf et al., 2021; Purnamasari et al., 2023; Gupta et al., 2020).

Piperine, the major alkaloid of black pepper (*Piper nigrum* L.), has been recognized not only for its antioxidant and anti-inflammatory activities but also as a natural bioenhancer capable of inhibiting metabolic enzymes and promoting intestinal absorption (Chopra et al., 2017). Co-administration of piperine with curcumin can markedly increase plasma concentrations of curcumin, yet piperine itself suffers from low aqueous solubility and limited bioavailability (Gupta et al., 2020; Octavia et al., 2024). Therefore, effective delivery systems are required to fully exploit the synergistic potential of the curcumin–piperine combination.

Encapsulation technologies have emerged as promising strategies to overcome these limitations. Systems such as liposomes, nanoemulsions, protein carriers, and polymeric nanoparticles have been investigated to improve solubility and stability and may contribute to enhanced bioavailability of curcumin and piperine (Yusuf et al., 2021; Patra et al., 2018). More recently, co-encapsulation approaches have demonstrated improved dispersibility, stability, and biological activity compared with the free compounds (Goëlo et al., 2020; Lu et al., 2021).

Among the available strategies, pH-responsive polymers such as Eudragit S100 [methacrylic acid–methyl methacrylate copolymer (1:2)] are particularly advantageous, as they remain largely intact under gastric conditions and dissolve at intestinal pH, ensuring delayed release. Spray drying with this polymer converts crystalline curcumin and piperine into amorphous dispersions, increases dissolution, and protects them from degradation. In addition, the polymeric matrix also enables changes in the release profile and may improve bioavailability (Yusuf et al., 2021; Purnamasari et al., 2023). To the best of our knowledge, no

prior study has reported pH-triggered submicrometric particles co-loading curcumin and piperine in Eudragit S100 produced by spray drying for this specific purpose, which underscores the novelty of the present study.

Beyond efficacy, safety is a fundamental requirement for nutraceutical formulations. Although curcumin and piperine are generally recognized as safe at conventional doses, new delivery systems require rigorous toxicological evaluation. Methacrylate-based polymers, such as those employed in advanced adhesive and coating systems, have demonstrated excellent biocompatibility and chemical stability, supporting their suitability for biomedical and food-related applications (Pupo et al., 2013). Recent studies have shown that spray dried microparticles containing turmeric extract not only improve the delivery of bioactives but also exhibit low acute toxicity, reinforcing the translational applicability of such systems (Yupangui et al., 2024). However, toxicological data for submicrometric, dual-loaded systems containing curcumin and piperine remain limited; a comprehensive safety assessment is still lacking, and a dedicated investigation is therefore required.

In this context, the present study aimed to determine whether the co-encapsulation of curcumin and piperine in an Eudragit S100 matrix could enhance their physicochemical stability and promote controlled intestinal release without inducing acute oral toxicity. To this end, the formulation was comprehensively evaluated through physicochemical characterization, *in vitro* dissolution assays, complementary erythrocyte hemolysis testing, and acute oral toxicity testing in rodents, thereby consolidating its potential application in functional foods and nutraceutical products.

2. MATERIAL AND METHODS

2.1 Reagents and solvents

Curcuma longa L. extract with 95.2% curcuminoids was supplied by Tianxu Natural Pigment (China). *Piper nigrum* L. extract was supplied by Xi'an Tian Ben Bio-engineering (China). The polymer poly(methacrylic acid-*co*-methyl methacrylate) 1:2 (Eudragit S100) was kindly donated by Evonik (Brazil). Ethanol 96%, sodium phosphate monobasic monohydrate (ACS), sodium phosphate dibasic heptahydrate (ACS) and sorbitan monooleate ethoxylate (Tween 80) were acquired from Synth (Brazil).

2.2. Methods

2.2.1. Preparation of curcumin and piperine submicrometric polymeric particles

Submicrometric polymeric particles (SPPs) were obtained from poly(methacrylic acid-*co*-methyl methacrylate) (Eudragit S100, ES100), curcumin (CUR) and piperine (PIP), yielding a 10 g batch with a 20% (w/w) total bioactive compound load (500 mg CUR and 20 mg PIP). Ethanol:water (60:40, v/v) was used as solvent. CUR and PIP were dissolved in 720 mL of ethanol under magnetic stirring (800 rpm; Fisatom 754, Brazil), followed by addition of the polymer under the same conditions. After complete dissolution, 480 mL of distilled water were gradually added, maintaining stirring for 12 h. A bioactive-free formulation (SPP ES100) was also prepared using the same procedure. The formulations were spray dried (Labmaq MSD 0.5, Brazil) under the following conditions: atomizer nozzle diameter 0.82 mm, pressure 3 kgf·cm^{-2}, air flow 25 L·min^{-1}, feed rate 0.40 L·h^{-1}, inlet temperature 135 ± 5 °C and outlet temperature 60 ± 5 °C (Marcon et al., 2025).

2.2.2. Physical mixture

Homogeneous physical mixtures (PM) were prepared with ES100, CUR and PIP in a 1:1:1 mass ratio. Components were weighed individually and manually homogenized with a spatula, mortar and pestle until uniform mixing was obtained.

2.2.3. Formulation yield

The yield (R) of spray dried SPPs was determined in triplicate and calculated as the ratio between the final mass and the sum of the initial masses of polymer and bioactive compounds, as per Equation 1.

$$R(\%) = \frac{particle\ 5ei6ht}{initial\ 5ei6ht\ (polymer<bioactives)} x100 \text{ (Equation 1)}$$

2.2.4. Encapsulation efficiency assessment

2.2.4.1. Equipment and chromatographic conditions

Analyses were performed on a Shimadzu Nexera-i LC2040C HPLC system (Japan) equipped with diode-array detector (DAD), pump, degasser (DGU), autosampler (SIL-Autosampler) and column oven. A C18 reverse-phase Shim-pack column (150 × 4.6 mm; 5 µm) was used. Wavelengths were determined by UV–Vis scanning (190–400 nm), selecting 410 nm for CUR

and 341 nm for PIP. The previously validated method (Marcon *et al.,* 2025) was run isocratically at 25 °C with a mobile phase of acetonitrile:methanol:water (55:5:45, v/v/v), flow rate 1.00 mL·min⁻¹, injection volume 10.0 µL and total run time 15.0 min.

2.2.4.2. Encapsulation efficiency

Encapsulation efficiency (EE, %) was determined according to Li, Rouaud and Poncelet (2008), using Equation 2.

$$EE(\%) = \frac{dru6\ 5ei6ht\ in\ particles}{initial\ 5ei6ht\ \ (theoretical)} x100 \qquad \text{(Equation 2)}$$

SPPs were weighed into 10.0 mL volumetric flasks, then 8.00 mL of methanol were added and the suspension was kept under magnetic stirring at 1000 rpm for 12 h. Volume was brought to 10.0 mL and solutions were filtered through PTFE membranes (0.22 µm). The theoretical concentration obtained was 300.00 µg·mL⁻¹ (288.48 µg·mL⁻¹ CUR and 11.52 µg·mL⁻¹ PIP). Determinations were performed in triplicate using a validated method for analytical ranges of 200.0–500.0 µg·mL⁻¹ (CUR) and 8.00–20.00 µg·mL⁻¹ (PIP) with detection at 410 nm and 341 nm, respectively.

2.2.5. Characterization of submicrometric polymeric particles

2.2.5.1. Determination of mean diameter and zeta potential

Mean diameter and zeta potential were determined using a Zetasizer Nano ZS90 (Malvern Instruments v8.02, UK) (Marcon et al., 2025). Samples were diluted in ultrapure water (1:500, v/v) and sonicated for 15 min (Ultrasonic Cleaner 1440DA, Brazil) at room temperature. Each sample was analyzed in triplicate with three independent dilutions (n = 3), using water as dispersant and refractive index 1.33.

2.2.5.2. Morphological and surface analysis by field-emission scanning electron microscopy (FE-SEM)

Morphology and surface were assessed by field-emission SEM (Tescan Mira 3, Czech Republic). Submicrometric polymeric particles, bioactives, polymer and physical mixture were analyzed. Samples were gold-coated using a Shimadzu IC-50 Ion Coater (Kyoto, Japan) and observed at 15 kV (Marcon et al., 2025). Micrographs were recorded with Electron Optical Design software.

2.2.5.3. Fourier-transform infrared spectroscopy (FTIR)

Bioactive–polymer interactions were evaluated by FTIR (Shimadzu IR-Prestige-21, Japan) in the 4000–400 cm^{-1} range, resolution 4 cm^{-1}, 32 scans·min^{-1}. Samples were prepared as KBr pellets (2% w/w), containing 4.00 mg of sample and 196.00 mg of KBr (Ribeiro et al., 2023).

2.2.5.4. X-ray diffraction (XRD)

Material crystallinity was analyzed by XRD (Rigaku Ultima IV diffractometer, Japan), using CuKα radiation (λ = 1.5418 Å), at 40 mA and 30 kV, scanning at 2.00°·min^{-1} over 2θ 5.00°–80.00° (Camargo et al., 2023). Pure bioactives and polymer, physical mixture and submicrometric polymeric particles were analyzed.

2.2.5.5. Thermal analysis (TGA)

Thermal stability was evaluated by thermogravimetry (STA 6000, PerkinElmer, USA), previously calibrated for temperature using indium as the reference standard (m.p. 156.6 °C). Samples were heated from 20.0 to 600.0 °C at 10.0 °C·min^{-1} under N_2 flow (50 mL·min^{-1}) (da Silva, 2024)..

2.2.6. *In vitro* dissolution test

For the comparative dissolution study, two pellet were produced under identical processing conditions at the same CUR/PIP dose per unit: (i) SPP pellet, prepared by blending the bioactive-loaded submicrometric polymeric particles with lactose and (ii) Free-bioactive mixture (FM) pellets, prepared by mixing the CUR+PIP powder (25:1, CUR:PIP) with lactose. This design isolates the effect of encapsulation on release kinetics. A Shimadzu SSP-10A hydraulic press (Japan) was used at 60 N for 1 min to obtain 600 mg units. The SPP pellets contained 200 mg of particles (38.5 mg CUR and 1.5 mg PIP) and 400 mg lactose; the PM

pellets contained 40 mg of FM (38.5 mg CUR and 1.5 mg PIP) and 560 mg lactose. Tests were conducted in a USP dissolution tester (Ethik Technology, Brazil) with apparatus 1 (basket) at 37 ± 0.5 °C and 75 rpm, containing 450 mL of 20 mM phosphate buffer (pH 6.5) with 2.0% Tween 80 for providing the sink conditions. Each formulation was tested in sextuplicate, using one pellet per replicate. Samples (5 mL) were collected at predetermined time intervals (1, 3, 5, 7, 10, 15, 20, 30, 45, 60, 90, 120, 150, 180, 240, 300, 360, 720 and 1440 min), with medium replacement. After filtration (0.22 µm), CUR and PIP release was quantified by HPLC-DAD as per the validated method (Marcon *et al*., 2025) at 410 and 341 nm, respectively. Percent dissolution was corrected by the cumulative dilution factor. Dissolution efficiency was determined as the ratio between the area under the dissolution curve and the area corresponding to 100% dissolution over the same time interval (Equation 3).

$$DE(t) = \frac{\int_0^t y\,dt}{y_{100}\,t} x100\% \qquad \text{(Equation 3)}$$

In addition, the time required to reach 50% (t_{50}%) and 80% (t_{80}%) cumulative release was determined directly from the dissolution curves for each formulation. Dissolution profile similarity between the free-bioactive mixture (FM) and the submicrometric polymeric particles (SPP CP) was further assessed using the similarity factor (f_2), calculated according to regulatory recommendations, with values between 50 and 100 indicating similar profiles and values below 50 indicating dissimilar release behavior (Lu et al., 2021).

In vitro dissolution data were also fitted to the mathematical release models of zero-order, first-order, Higuchi, Hopfenberger, Gompertz, Korsmeyer-Peppas, Baker-Londsale, and Weibull using standard formulas in Microsoft Excel 365, as per Costa & Sousa Lobo (2001). Model fit was assessed using the adjusted coefficient of determination (adjusted R^2), the Akaike Information Criterion (AIC) and the Model Selection Criterion (MSC).

2.2.7. In-vitro erythrocyte membrane-integrity assay

An in-vitro, cell-based hemocompatibility assay was employed as an early-phase screening tool to detect potential membrane-disruptive effects, rather than to simulate direct systemic exposure (Ferreira et al., 2020). The erythrocyte hemolysis test was conducted using defibrinated sheep erythrocytes (Laborclin, Brazil). These erythrocytes were suspended in 0.01 M phosphate buffer (pH 7.4; 4 °C) adjusted to 5% hematocrit. Samples were prepared by

adding 10 µL of an ethanolic co-stock of CUR/PIP (CUR 100 µg/mL; PIP 4.0 µg/mL; 25:1, w/w) or dose-equivalent SPP dispersions to 490 µL of erythrocyte suspension (final volume 500 µL), yielding final concentrations of 2.0 µg/mL CUR and 0.08 µg/mL PIP. SPP doses were calculated to deliver the same CUR and PIP amounts based on the measured bioactive load (20% w/w total actives; 25:1 CUR:PIP). After 24 h incubation at 120 rpm, suspensions were centrifuged (4000 rpm, 5 min) and supernatant absorbance was read at 540 nm. Erythrocytes in buffer and with water served as negative and positive controls, respectively. Percent hemolysis was determined in triplicate according to Equation 4.

$$\text{Hemolysis}(\%) = \frac{(A_{sample} - A_{blank}) - A_{neg}}{(A_{pos} - A_{neg})} \times 100 \qquad \text{(Equation 4)}$$

where A_{sample} is the absorbance of the treated erythrocyte suspension, A_{blank} is the absorbance of the corresponding sample blank, A_{neg} is the absorbance of the negative control (buffer) and A_{pos} is the absorbance of the positive control (complete lysis).

2.2.8. Acute toxicity evaluation

2.2.8.1. Animals

Male Wistar rats (200–250 g) supplied by the State University of Ponta Grossa (UEPG, Brazil) were used to investigate the acute toxicity of CUR-PIP SPPs. Animals were kept at the Cardiometabolic Pharmacology Laboratory of the Federal University of Paraná (UFPR) under standardized housing conditions, with free access to commercial chow and filtered water. Environmental variables were carefully monitored, maintaining ambient temperature at 22 ± 2°C, relative humidity at 50 ± 10% and a 12h light/dark cycle. To ensure animal welfare, environmental enrichment was routinely provided. All procedures followed the ethical principles for animal experimentation established by the Brazilian National Council for the Control of Animal Experimentation (CONCEA) and complied with the ARRIVE guidelines for reporting animal studies (Percie du Sert et al., 2020). The experimental protocol was approved by the UFPR Animal Use Ethics Committee (CEUA/UFPR no. 1656).

2.2.7.2. Experimental design

The acute oral toxicity assay was performed according to OECD guideline 423 (2001). Male Wistar rats (n = 6) were fasted for 8 h before single-dose gavage administration of curcumin–piperine particles. As no prior toxicological data were available for this formulation, dose selection followed OECD 423. The initial dose was 300 mg/kg of SPPs, equivalent to 60 mg/kg total actives (57.7 mg/kg CUR; 2.3 mg/kg PIP). If no toxicity signs were observed at this level, the subsequent dose was 2000 mg/kg of SPPs, equivalent to 400 mg/kg total actives (384.6 mg/kg CUR; 15.4 mg/kg PIP). Conversely, if toxic manifestations occurred, the dose would be reduced to 50 mg/kg of SPPs, equivalent to 10 mg/kg total actives (9.6 mg/kg CUR; 0.38 mg/kg PIP). Stepwise progression continued until one of the following outcomes was reached: (i) appearance of significant toxic signs; (ii) occurrence of mortality; (iii) absence of adverse responses at the highest dose tested; or (iv) death at the lowest tested dose. A control group (n = 6) received only vehicle (filtered water) under identical conditions.

2.2.7.3. Assessment of clinical signs

Following oral administration of curcumin–piperine particles, the animals were observed intensively during the first 30 min and subsequently at 1, 2, 3 and 4 h post-dosing. Clinical and behavioral parameters recorded included grooming, piloerection, respiratory pattern, abdominal contractions, diarrhea, lethargy, motor incoordination, sedation, coma, and mortality. At the end of the 4 h observation period, rats had free access to chow and water. Thereafter, animals were monitored daily for 14 consecutive days to identify possible late toxic effects or deaths (Silva et al., 2022).

2.2.7.4. Euthanasia, sample collection and analyses

On day 15, after a 12 h fasting period, the animals were humanely euthanized by anesthetic overdose with 20% isoflurane in a closed chamber. Blood samples were obtained by decapitation and subsequently processed for hematological and biochemical evaluations. Serum glucose levels were determined using a portable glucometer (Accu-Chek Active, Roche, Germany). Hematological analyses comprised red blood cell counts and total and differential leukocyte counts. Biochemical parameters, including total cholesterol, triglycerides, aspartate aminotransferase (AST), alanine aminotransferase (ALT), urea and creatinine were quantified using a semi-automated analyzer with commercial diagnostic kits. The liver, kidneys, heart and spleen were dissected, rinsed in physiological saline and weighed on an analytical balance. Relative organ weight was expressed as the percentage ratio of organ weight to body weight. Representative tissue samples were fixed in 10% buffered formalin, routinely processed for histopathology, embedded in paraffin, sectioned and stained with hematoxylin

and eosin (H&E). Slides were examined under a Leica DM 2500 light microscope (Germany) by a veterinary pathologist to detect possible morphological changes related to treatment.

3. RESULTS AND DISCUSSION

3.1. Preparation and yield of curcumin and piperine submicrometric polymeric particles

Submicrometric polymeric Eudragit S100 particles were obtained by spray drying, yielding a free-flowing powder with characteristic color. Bioactive-free submicrometric polymeric particles (SPP ES100) were white, while those containing curcumin and piperine (SPP CP) were orange, consistent with pure CUR. Yields were expressed as mean ± standard deviation (n = 3), calculated by Equation 1. SPP ES100 and SPP CP formulations showed average values of 56.27 ± 0.85% and 53.34 ± 0.71%, respectively.

3.1.2. Encapsulation efficiency (EE)

CUR and PIP-loaded SSPs prepared in ethanol:water (60:40, v/v) exhibited high encapsulation efficiencies by the indirect method, with encapsulation efficiencies close to 100% for CUR and PIP. These results, obtained in triplicate from a total theoretical concentration of 300 $\mu g \cdot mL^{-1}$ (288.48 $\mu g \cdot mL^{-1}$ CUR and 11.52 $\mu g \cdot mL^{-1}$ PIP), demonstrate suitable bioactive incorporation into the submicrometric polymeric system.

Experimental data agreed with previous studies, although with higher encapsulation efficiency values than those previously reported (Yupangui et al., 2024; Setyaningsih et al., 2021). Piperine (PIP) also exhibited high encapsulation efficiency, exceeding literature values (Schneider et al., 2023; Biscaia et al., 2023). These results may be attributed to strong interactions between the actives and the polymeric matrix, favored by the ethanol-water ratio (60:40, v/v), which promoted the formation of stable solid dispersions and reduced bioactive losses during drying. In addition, as the submicrometric polymeric particles were produced by spray drying, partial deposition of Eudragit S100 on the chamber walls may have occurred, effectively reducing the recovered polymer mass and leading to an apparently high encapsulation efficiency close to quantitative incorporation (Sundararajan et al., 2023).

Thus, these results support the suitability of Eudragit S100 and spray drying as an effective technological approach for incorporating poorly soluble bioactives into submicrometric polymeric systems.

3.2. Characterization of submicrometric polymeric particles

3.2.1. Particle-size analysis and zeta potential

CUR–PIP submicrometric polymeric particles presented an average of 680 ± 18 nm, with unimodal distribution and low polydispersity indices, indicating homogeneity. Bioactive-free submicrometric polymeric particles showed a larger diameter (1506 ± 198 nm), suggesting that the presence of the bioactive compouds favored formation of smaller and more uniform particles (Schneider et al., 2023; Umerska et al., 2018).

According to ISO/TS 80004-2, nanoparticles measure 1-100 nm and microparticles 1-1000 µm. The particles obtained were classified as submicrometric. This size range is attributed to the stability of the feed solution and to the atomization and solvent-evaporation dynamics of the spray drying process, which favored the formation of uniformly small polymeric particles rather than aggregation or fusion of nanoparticles during drying (Al Khatib et al., 2025). The submicrometric dimension favors oral bioavailability of hydrophobic compounds (Schneider et al., 2023; Hassan et al., 2019; Kawabata et al., 2011) and confirms the efficiency of spray drying with Eudragit S100 in obtaining stable intestinal-release systems. The diameters obtained were smaller than those reported in other spray drying studies (Schneider et al., 2023; Mohylyuk et al., 2021; Mithu et al., 2017; Biscaia, et al., 2023; Porras-Saavedra et al., 2015).

Zeta potential, determined by electrophoretic analysis in aqueous medium, was −40.53 mV. This negative value reflects the high anionic charge conferred by the ionizable carboxylic groups of Eudragit S100, which dissociate at pH above 7.0. Magnitudes greater than ±30 mV indicate appropriate colloidal stability (Neves et al., 2013), promoting electrostatic repulsion between particles and minimizing aggregation. Such stability is essential for oral sustained-release formulations, ensuring microparticle integrity up to the intestine and selective bioactive release.

3.2.2. Field-emission scanning electron microscopy (FE-SEM)

Morphological and surface characteristics of bioactive compounds, polymer, and submicrometric polymeric particles were evaluated by FE-SEM. CUR exhibited crystalline morphology, while PIP showed a crystalline structure with heterogeneous size distribution. Eudragit S100 showed predominantly spherical particles with low size variation, typical of polymeric powders (Figure 1).

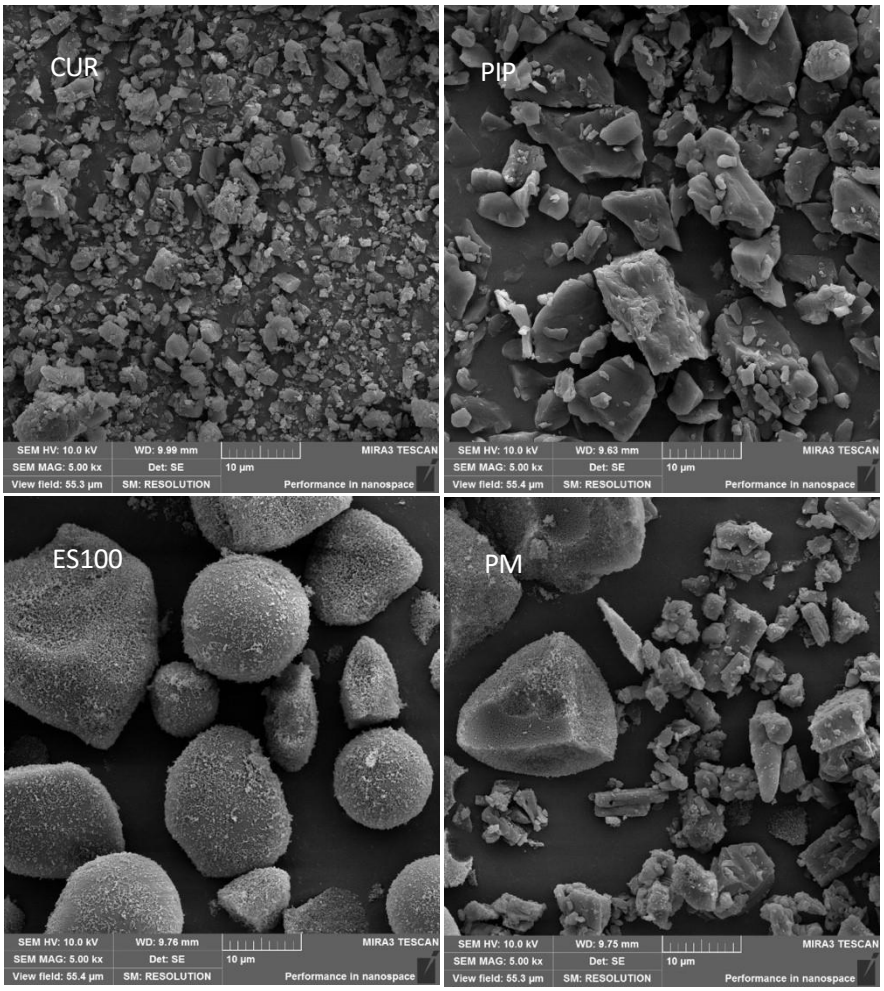

FIGURE 1. FE-SEM micrographs of the pure bioactives curcumin (CUR) and piperine (PIP), the polymer Eudragit S100 (ES100), and the physical mixture (PM), at 5k× magnification.

Submicrometric polymeric particles (Figure 2) exhibited a predominantly spherical morphology, with smooth surfaces showing slight irregularities and no smaller adhered structures, indicating the absence of surface bioactive accumulation. The observed mean diameter was consistent with the values obtained by particle-size analysis. These results are in agree with previous studies using Eudragit S100 polymer (Biscaia et al., 2023; Cruz et al., 2010). Although most submicrometric polymeric particles displayed a predominantly spherical morphology with only minor surface irregularities. Comparable surface have been described in other spray dried botanical microparticles (Bobek et al., 2016), confirming that such features are often related to the rapid solvent evaporation and shell formation process. This morphology can arise during spray drying when surface moisture evaporation leads to the formation of a rigid shell, followed by partial collapse of the internal structure. The extent of this deformation depends on process parameters such as inlet temperature, feed rate and drying air humidity, as well as on the

physicochemical properties of the feed suspension (e.g., polymer composition, viscosity and surface tension). In the present study, only minor erythrocyte-like features were observed, attributable to solvent evaporation dynamics during spray drying rather than representing a dominant morphological characteristic of the system. Similar mechanisms have been reported for spray dried powders exhibiting partial structural collapse or vacuolated surfaces (Sundararajan et al., 2023; Barańska-Dołomisiewicz et al., 2025).

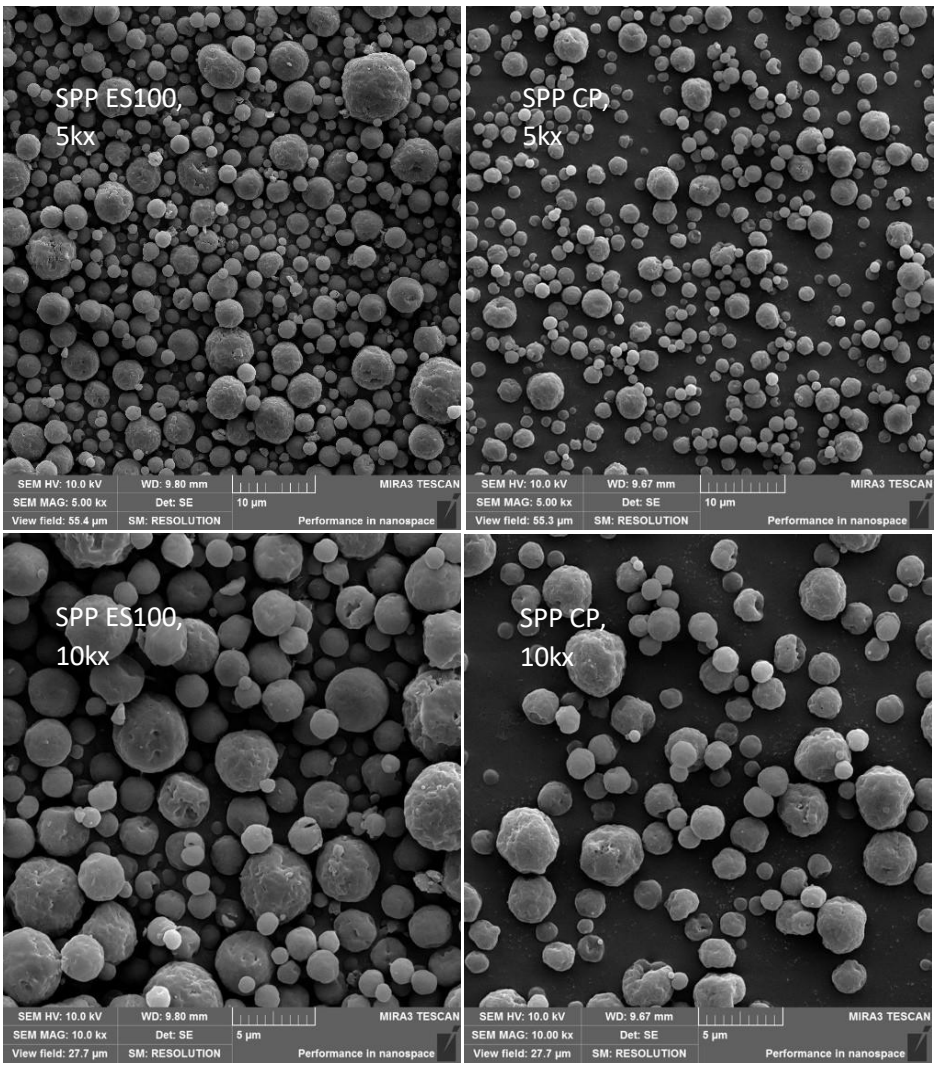

FIGURE 2. FE-SEM micrographs of submicrometric polymeric particles prepared from Eudragit S100 without (SPP ES100) and with curcumin and piperine (SPP CP) at 5k× and 10k× magnifications

3.2.3 Fourier-transform infrared spectroscopy (FTIR)

Infrared spectroscopy was employed to analyze the submicrometric polymeric particles, the physical mixture, and the raw materials used as reference standards, allowing the identification of changes in functional groups through comparison with their respective reference spectra.

The spectrum of curcumin (CUR) showed a band at 3508 cm^{-1} (O–H), 1625 cm^{-1} (C=O of conjugated ketone), 1510 and 1427 cm^{-1} (aromatic and aliphatic C=C), 1276 cm^{-1} (C–O), 1023 cm^{-1} (C–O–C ether) and bands at 961, 819 and 712 cm^{-1} attributed to C–H vibrations of alkenes, in agreement with the literature (Yupangui et al., 2024; Azkia et al., 2020; Sharma & Pathak, 2016).

The spectrum of piperine (PIP) showed aromatic C–H stretching at 3012 cm^{-1}, aliphatic C–H at 2939 cm^{-1}, carbonyl (CO–N) at 1638 cm^{-1}, aromatic C=C at 1585 cm^{-1}, as well as peaks at 1484 cm^{-1} (CH_2 bending), 1252 cm^{-1} (asymmetric =C–O–C), 936 cm^{-1} (C–O) and 847, 830 and 810 cm^{-1} (out-of-plane C–H), as described previously (Octavia et al., 2024; Zaini et al., 2020; Schneider et al., 2023; Dahiya et al., 2018).

Eudragit S100 showed a broad band at ~3500 cm^{-1} (O–H and adsorbed water), C–H stretching between 2900–3000 cm^{-1}, absorptions at 1387, 1450 and 1484 cm^{-1} (methyl groups), bands at 2990 and 2950 cm^{-1} (methylene C–H) and 1732 cm^{-1} (aliphatic ester C=O), in agreement with the literature (Bunhak et al., 2015).

Comparison of the FTIR spectra (Figure 3A) showed that the physical mixture retained the main absorption bands of the individual components, whereas in the CUR–PIP submicrometric polymeric particles (SPP CP) the characteristic, sharp O–H stretching band of curcumin, associated with intramolecularly hydrogen-bonded hydroxyl groups in the crystalline state, was no longer observed in the 3200–3600 cm^{-1} region. The disappearance of this band indicates the involvement of CUR hydroxyl groups in intermolecular hydrogen-bond interactions with the polymeric matrix, supporting effective molecular-level encapsulation (Yupangui et al., 2024; Azkia et al., 2020). Importantly, no new absorption bands were detected in the SPP CP spectrum, confirming that the encapsulation process did not involve the formation of new chemical bonds but rather non-covalent interactions between the bioactives and the polymer.

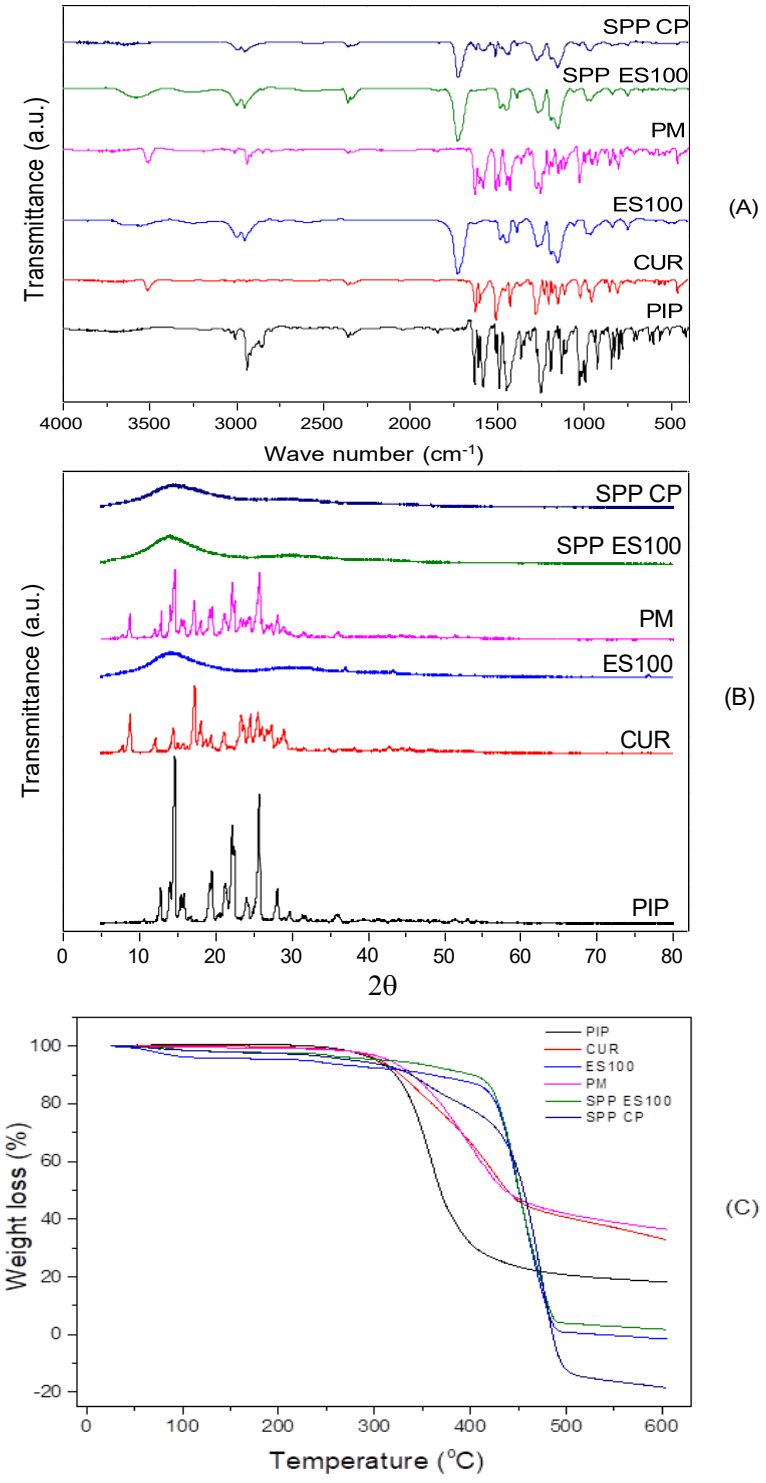

FIGURE 3. FT-IR spectra (A), diffractograms (B) and thermogravimetric curves (C) of Eudragit S100 (ES100), the bioactives CUR and PIP, the physical mixture (PM) and the submicrometric polymeric particles (SPP ES100 and SPP CP).

3.2.4. X-ray diffraction (XRD)

XRD is essential to assess solid-state properties such as crystalline phases, degree of amorphization and reactive behavior, which directly influence bioactive dissolution and solubility.

Diffractograms (Figure 3B) showed marked differences between submicrometric polymeric particles, physical mixture and pure components. Crystalline patterns exhibited intense, defined peaks, while amorphous forms presented characteristic halos. The higher solubility of amorphous solids arises from the disordered molecular arrangement, which reduces the energy required to separate molecules (Octavia et al., 2024; Kawabata et al., 2011; Patel et al., 2015).

Curcumin (CUR) displayed characteristic peaks at 2θ of 8.89°, 14.31°, 17.20°, 23.30°, 24.70°, 25.50° and 28.80°, confirming its reported crystalline nature (Ozawa et al., 2017; Porras-Saavedra et al., 2015). Piperine (PIP) showed well-defined peaks at 2θ of 14.68°, 15.58°, 19.60°, 22.20°, 25.70°, 28.30° and 31.70°, also indicating a crystalline solid (Octavia et al., 2024; Zaini et al., 2020). The polymer lacked defined peaks, corroborating its amorphous character (Mithu et al., 2017; Higashi et al., 2015).

In the submicrometric polymeric particles, a remarkable reduction in CUR and PIP crystalline peaks was observed, indicating that the encapsulation process promoted bioactive amorphization (Ansari et al., 2011).

3.2.5 Thermal analysis (TGA)

TGA assesses component stability by mass variation as a function of temperature or time, reflecting physical or chemical transformations (Oliveira, Yoshida & Gomes, 2011).

Results (Figure 3C) showed thermal behavior similar to that described in the literature. Eudragit S100 remained stable up to 300 °C, with substantial loss between 350-460 °C, a typical decomposition range for the polymer matrix (Bunhak et al., 2015). Curcumin (CUR) presented two degradation events at ~200 and ~400 °C, corresponding to its melting and oxidative degradation. Piperine (PIP) exhibited initial decomposition near 250 °C, consistent with reported 230-330 °C (Octavia et al., 2025; Zaini et al., 2020; Dahiya et al., 2018; Alshehri, Haq & Shakeel, 2018).

The physical mixture presented overlapping events of the bioactives and the polymer, confirming the presence of all components and suggesting no major interaction.

Submicrometric polymeric particles containing CUR and PIP (SPP CP) showed shifts of mass-loss events to higher temperatures, indicating increased thermal stability. Bioactive-free submicrometric polymeric particles (SPP ES100) presented a profile similar to the pure polymer.

In addition, the melting events of CUR and PIP were not observed in the SPP CP thermogram, also indicating their conversion to the amorphous state. This behavior demonstrates that the encapsulation process successfully enhanced the thermal stability, protecting the bioactive compounds from early degradation. These findings corroborate the XRD results, which showed suppression of crystalline peaks. Thus, encapsulation in Eudragit S100 increased thermal stability and formed a stable amorphous system, confirming the efficiency of spraydrying and suggesting potential increases in solubility.

3.3. *In vitro* assays

3.3.1. Dissolution assay

The dissolution profiles showed that the free-bioactive mixture (FM) exhibited a faster initial release, whereas the submicrometric polymeric particles (SPP) promoted a slower and more sustained release over time, with both systems reaching nearly complete dissolution after 24 h for curcumin (Figure 4A) and piperine (Figure 4B). As the data were not normally distributed ($p < 0.05$), comparisons were performed using the Mann-Whitney test, which did not reveal statistically significant differences between FM and SPP when considering the overall dissolution period for CUR ($p = 0.161$) or PIP ($p = 0.448$). Despite the lack of global statistical significance, the distinct release kinetics observed, particularly at early time points, indicate a clear modulation of the dissolution rate by the polymeric system.

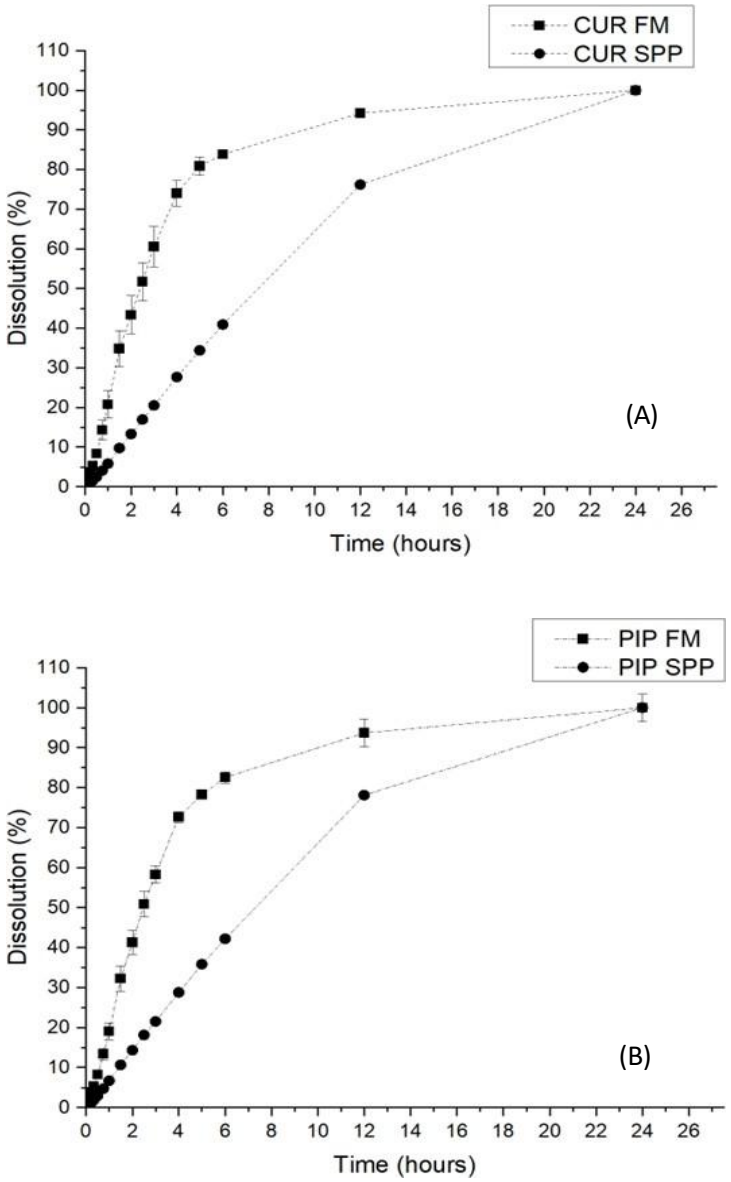

FIGURE 4. Dissolution profiles of curcumin (A) and piperine (B) from free-bioactive mixtures (FM) and Eudragit S100 solid polymeric particles (SPP) in phosphate buffer (pH 6.5) at 37 ± 0.5 °C.

Dissolution was also assessed by the area under the curve (AUC) and by dissolution efficiency (DE) at 120 min (Figure 5A). The free-bioactive mixture (FM) released 44.9% for CUR and 42.8% for PIP, while the submicrometric polymeric particles showed 13.7% and 14.8%, respectively. These results confirm that submicrometric polymeric particles reduced the dissolution rate compared with the pure bioactives. Similar data were reported by Dewi & Setyaningsih, who observed 13.49% dissolution at 120 min for PVA solid dispersions containing CUR and PIP.

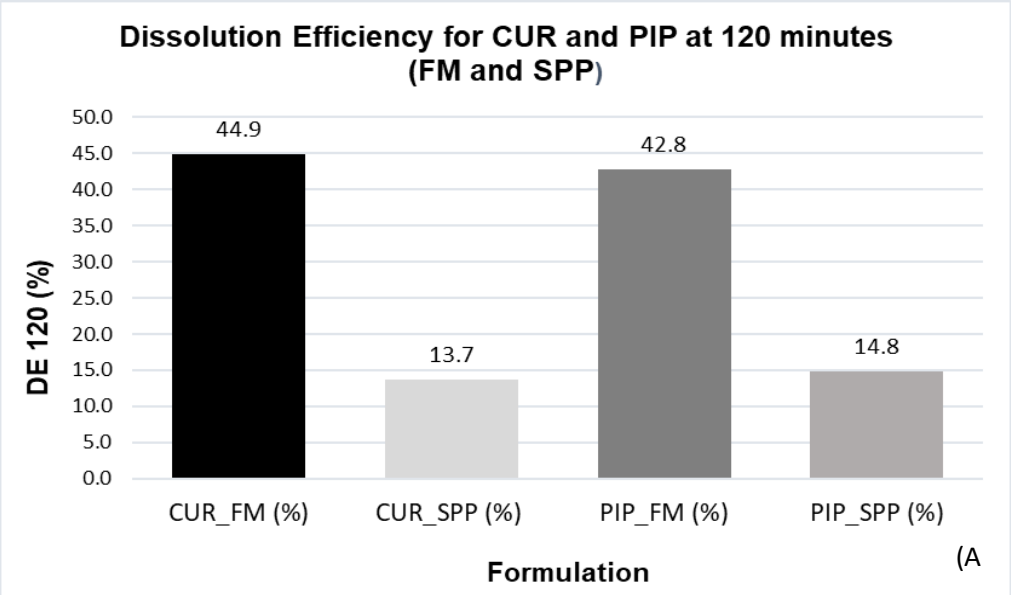

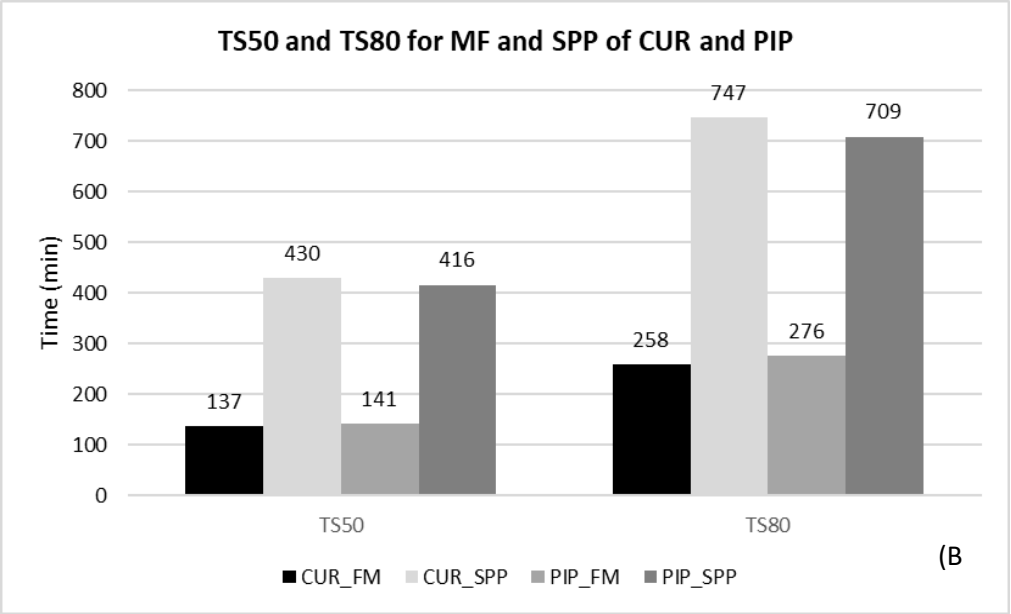

FIGURE 5. Dissolution efficiency (DE_{120}) and release kinetics of curcumin and piperine from free bioactive mixtures (FM) and Eudragit S100 submicrometric polymeric particles (SPP) containing curcumin (CUR) and piperine (PIP).

(A) Dissolution efficiency (DE_{120}) of FM and SPP CP formulations. (B) Time required for 50% (t_{50}%) and 80% (t_{80}%) release of CUR and PIP from FM and SPP CP formulations.

The 50% (TS50) and 80% (TS80) release times of the bioactives in the free bioactives mixtures (FM) and in the submicrometric polymeric particles (SPP CP) were determined (Figure 5B). FM showed TS50 between 137–141 min, whereas in SPP CP this interval increased to 416–

430 min. The 80% release in SPP CP exceeded 700 min. Significant differences were observed between formulations for TS50 ($p = 0.02$) and TS80 ($p = 0.04$).

The similarity factor (f_2) confirmed that the dissolution profiles of FM and SPP CP were dissimilar, with values of 30.01 for t_{50}% and 31.82 for t_{80}%. According to Azad et al. (2024), high dissolution efficiency values are characteristic of immediate-release formulations. Therefore, the reduced dissolution efficiency observed for the polymeric system indicates effective modulation of CUR and PIP release, supporting its suitability as a modified-release delivery strategy (van Duong & van der Mooter, 2016). This behavior is consistent with previous reports demonstrating that polymer selection critically governs release behavior. Umerska et al. (2018) reported rapid curcumin release from Eudragit RLPO nanoparticles (91 ± 5% within 1 h), whereas PLGA- and PCL-based systems exhibited markedly slower release, reaching 47 ± 2% and 55 ± 2% after 24 h, respectively. Similarly, Biscaia et al. (2023) showed that Eudragit S100 microparticles released 80% of piperine in 670 min, while Eudragit RS30D formulations reached only 68.7% after 24 h. Comparable sustained-release behavior was also observed by Schneider et al. (2023) for ethylcellulose-based particles, which released approximately 81% of piperine over 24 h. Collectively, these findings highlight the decisive role of polymer composition in controlling release pattern and corroborate the present results, aligning with recent reviews that emphasize polymer-based delivery systems as effective strategies to modify the dissolution, solubility and bioavailability of CUR and related bioactives (Azad et al., 2024).

Kinetic models are relevant tools to predict transport mechanisms involved in in vivo dissolution (van Duong & van der Mooter, 2015/2016). In this study, dissolution profiles of the CUR–PIP combination, both as free-bioactive mixture (FM) and as spray-dried submicrometric polymeric particles (SPP), were analyzed using different kinetic models. Data were fitted by nonlinear regression, allowing representation of the released fraction as a function of time and evaluation of fit quality by adjusted R^2, AIC and MSC (Dewi & Setyaningsih, 2023; Zhang et al., 2010).

Results (Table S1) showed that dissolution profiles of curcumin and piperine, for both SPP and FM systems, fitted preferentially to the Weibull model, with high adjusted R^2 values. Adjusted R^2 represents the proportion of variance explained by the model; AIC balances goodness-of-fit and model parsimony (lower values indicate better performance); and MSC reflects model precision, with values above 2 considered satisfactory (van Duong & van der Mooter, 2016; Abdul, Mohammed & Salem, 2021). Accordingly, the Weibull model was considered the most appropriate overall, presenting lower AIC and higher MSC values across formulations.

The Weibull model (Equation 4), an empirical function capable of describing a wide range of release profiles, adequately distinguished the formulations, evidencing faster release for FM

and prolonged release for SPP systems. For SPP, the parameter β > 1.3 indicated a sigmoidal release profile consistent with combined diffusion and erosion mechanisms, suggesting a modified-release behavior favorable for maintaining stable plasma concentrations (Siepmann & Peppas, 2001).

$$\frac{M_t}{M_\infty} = 1 - \exp\left(-\left(\frac{t - T_i}{\alpha}\right)^{\beta}\right) \qquad \text{(Equation 4)}$$

Although the Weibull model provided the best overall performance, the biexponential model showed superior statistical fitting for microparticle formulations (CUR-SPP and PIP-SPP), as evidenced by higher adjusted R^2 values and lower AIC values. However, its increased complexity and higher number of parameters may be associated with potential overfitting, particularly considering the marginal improvement relative to simpler models and the behavior observed in residual distributions.

The improved performance of the biexponential model in SPP systems can be attributed to the biphasic release behavior, characterized by an initial burst release of drug molecules weakly bound or adsorbed on the particle surface, followed by a sustained release phase governed by diffusion through the polymeric matrix and/or particle erosion. This dual-release mechanism is consistent with the structural characteristics of Eudragit S100-based systems and explains the enhanced flexibility of the biexponential model in capturing the release kinetics of microparticles. Nevertheless, while this model better describes mechanistic complexity, its flexibility may also increase sensitivity to experimental variability.

In contrast, the Weibull model, despite its empirical nature, provided a more parsimonious and stable description of the dissolution profiles, with consistently high adjusted R^2 values and favorable AIC and MSC parameters across all formulations. Therefore, the Weibull model was selected as the most appropriate for comparative purposes, whereas the biexponential model proved particularly useful for mechanistic interpretation of the biphasic release behavior observed in microparticle systems.

Consistent with these findings, previous studies have reported different kinetic behaviors depending on formulation characteristics. For instance, Yupangui et al. (2024) observed that chitosan–mannitol microparticles released approximately 80% of curcuminoids within 6 h in simulated gastric fluid (acidic pH), with the Korsmeyer–Peppas model providing the best fit (R^2 = 0.9598). In contrast, the submicrometric polymeric particles developed in the present study, evaluated at pH 6.5, exhibited slower and sustained release with excellent fitting to the Weibull model (R^2 > 0.99; β > 1.3). These findings highlight the influence of both the polymer matrix and dissolution medium on release kinetics.

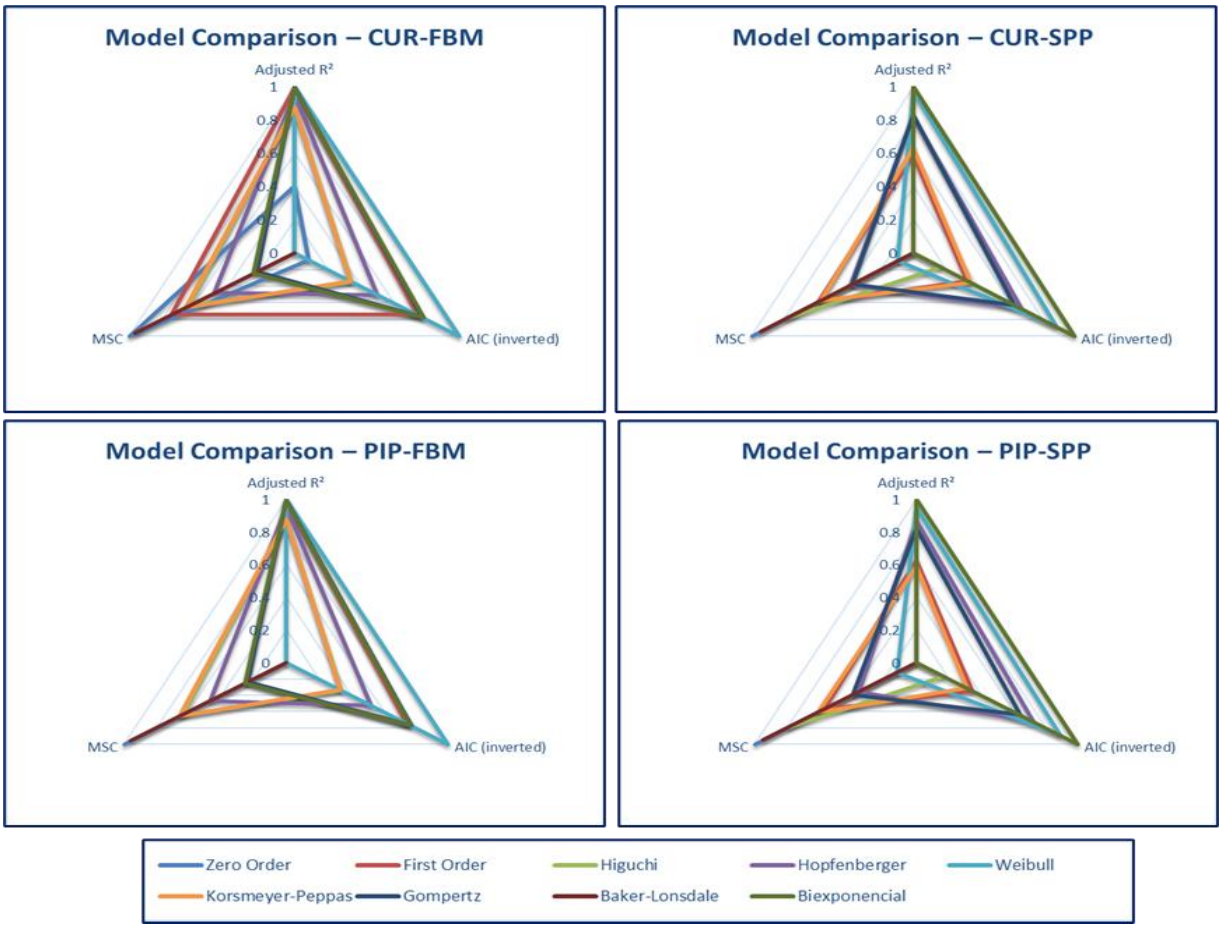

Figure 6. Comparison of adjusted R², AIC and MSC to describe curcumin and piperine release from Eudragit S100 submicrometric polymeric particles (SPP) and free-bioactive mixture (FM).

Similar diffusion–erosion-controlled release profiles have been reported for polymeric nanocapsule systems, in which drug release is governed by polymer degradation and matrix porosity (Chassot et al., 2015; Justus et al., 2019). Additionally, previous work from our group demonstrated limited release of piperine (~16% after 2 h) from Eudragit S100 microparticles in simulated gastric fluid (pH 1.2), confirming the gastro-resistant behavior of the system (Biscaia et al., 2023). In agreement with these findings, no visible structural changes were observed in the pellets after 2 h at pH 1.2 in the present study, further supporting the stability of the formulation under gastric conditions and its suitability for targeted intestinal delivery.

Oral absorption involves multiple sequential processes, including disintegration, dissolution, chemical degradation, gastric emptying, intestinal transit, mucosal permeation, and first-pass metabolism, and is strongly influenced by both formulation characteristics and gastrointestinal physiology (Dewi & Setyaningsih, 2023; Huang, Lee & Yu, 2009). Although kinetic modeling provides valuable insights into drug release mechanisms, it does not fully capture the complexity of in vivo performance. Therefore, additional in vivo and clinical studies are required

to more accurately assess the impact of the formulation on oral bioavailability and therapeutic response.

While sustained release is attractive for protecting bioactives from gastric degradation and prolonging GI residence time, its effects on absorption must be considered. Curcumin bioavailability still depends strongly on the rate and site of intestinal absorption, even when solubility is increased (Hegde et al., 2023). pH-sensitive matrices such as Eudragit S100 favor intestinal release, where absorption is more efficient (Yusuf et al., 2021), but a slower release profile may result in lower plasma peak concentrations relevant for certain biological effects. Moreover, processing parameters, such as drying temperature, directly influence release kinetics and consequently absorption potential (Purnamasari et al., 2023). Therefore, despite the in vitro benefits, only in vivo absorption studies can confirm whether the sustained profile observed results in greater systemic bioavailability and functional efficacy, as highlighted in reviews on nano- and microstructured delivery systems for bioactives (Patra et al., 2018).

Sustained release, while reducing the initial dissolution rate, provides the advantage of maintaining more stable intestinal concentrations of curcumin and piperine over time, which is favorable for absorption and may reduce the need for high or frequent dosing. The submicrometric polymeric particles developed in this study showed prolonged release, as confirmed by kinetic modeling with the Weibull equation ($R^2 > 0.99$), indicating a sigmoidal profile associated with combined diffusion and erosion mechanisms. This behavior aligns with previous reports on polymeric carriers (Biscaia et al., 2023; Schneider et al., 2023; Umerska et al., 2018) and underscores the translational potential of enteric polymer–based microparticles as modified-release systems.

Notably, even though the total release at 24 hours was comparable to that of the free-bioactive mixture, the markedly slower release during the initial hours may prevent high local concentration peaks and sustain intestinal exposure, which is advantageous for the absorption of low-permeability compounds (Tabanelli et al., 2021). Moreover, the Weibull model parameters ($\beta > 1.3$) indicate a sigmoidal dissolution profile arising from heterogeneous bioactive dispersion and a combined diffusion–erosion release mechanism, characteristic of polymeric matrices (Heredia et al., 2022; Martín-Camacho et al., 2023). This controlled-release behavior is expected to moderate the release rate, may enhance effective absorption and minimizing dosing frequency.

From a regulatory standpoint, methacrylate copolymers analogous to Eudragit S100 (anionic methacrylate copolymer) have been evaluated by the European Food Safety Authority (EFSA) and considered not of safety concern when used as coating or glazing agents in solid food supplements, with corresponding specifications incorporated into European Union additive

legislation (EFSA, 2010a, 2010b; European Commission, 2013). In the United States, basic methacrylate copolymer has been notified as Generally Recognized as Safe (GRAS) for intended uses in dietary supplements and related acrylate/methacrylate copolymers are listed for indirect food-contact applications under 21 CFR Part 177 (Food and Drug Administration [FDA], 2017, 2021). Collectively, these frameworks support the use of enteric methacrylate coatings in solid supplement dosage forms, aligning with the translational route envisioned here; however, they do not imply authorization for broad use in conventional foods, which would require separate evaluation and regulatory approval.

3.3.2. Hemolysis assay

The hemolysis degree obtained was 2.63 ± 0.53%, confirming the low interaction of Eudragit S100 with the erythrocyte membrane due to the negative charge present on the erythrocyte surface (Technical Report, 2018). Submicrometric polymeric particles containing curcumin (CUR) and piperine (PIP) showed hemolytic behavior similar to unloaded submicrometric polymeric particles (2.48 ± 0.05%), indicating low hemolysis rates compared with positive (100.0%) and negative (1.73 ± 0.18) controls. According to ASTM F756-17 and ISO 10993-4 standards, hemolysis values below 5% are considered non-hemolytic or clinically insignificant (ASTM INTERNATIONAL, 2017; INTERNATIONAL ORGANIZATION FOR STANDARDIZATION, 2017); therefore, the results obtained demonstrate that the formulation did not induce hemolysis, evidencing its safety upon contact with erythrocytes. These findings indicate a low potential for membrane-disruptive effects in this *in vitro* model, supporting the preliminary safety profile of the formulation.

3.4. Acute toxicity evaluation

3.4.1. Assessment of clinical signs, relative organs and body weight in rats

Animals receiving a single oral administration of curcumin–piperine submicrometric polymeric particles at 300 mg/kg and 2000 mg/kg presented no clinical or behavioral changes during the observation period—from the first 30 min post-treatment up to 14 days—compared with controls (Table S2).

Body-weight and organ-weight data for all experimental groups are summarized in Table 1. During the 14 days of monitoring, all rats showed progressive body-weight gain. At the end, mean body weight was 328.60 ± 13.57 g in controls, 347.30 ± 10.80 g in the 300 mg/kg group and 321.01 ± 9.16 g in the 2000 mg/kg group. Weight-gain trajectories were similar across

groups, indicating that microparticle administration did not impair physiological growth. Furthermore, no statistically significant differences were observed in body-weight progression or in relative organ weights (liver, spleen, heart and kidneys) between treated animals and controls.

These findings agree with Yupangui (2023), who also reported low toxicity for turmeric microparticles encapsulated with chitosan and mannitol administered as a single 2000 mg/kg dose, with no toxic symptoms, mortality, or alterations in internal organs. The similarity of results reinforces that both micro- and nanoencapsulation of curcumin derivatives present comparable safety profiles, supporting these formulations as safe alternatives for oral administration in experimental models.

Table 1. Body weight and relative organ weight of Wistar rats treated orally with vehicle or submicrometric polymeric particles CUR/PIP (SPP CP) (300 or 2000 mg/kg) after a 14-day experimental period.

3.2.1.30 Basal		SPP CP	
		300 mg/kg	**2000 mg/kg**
		Body weight (g)	
14-day	328.60 ± 13.57	347.30 ± 10.80	321.01 ± 9.16
		Relative organ weight (%)	
Liver	3.31 ± 0.09	3.19 ± 0.18	3.33 ± 0.11
Spleen	0.18 ± 0.01	0.17 ± 0.01	0.19 ± 0.01
Heart	0.36 ± 0.009	0.36 ± 0.01	0.34 ± 0.01
Kidneys	0.77 ± 0.032	0.70 ± 0.03	0.74 ± 0.01

Values are expressed as mean ± S.E.M., *n* = 5-6. Data are presented as mean ± S.E.M., *n* = 5-6. Statistical analysis was performed using one-way ANOVA followed by Tukey's post hoc test.

3.4.2. Serum biochemical parameters in Wistar rats treated with curcumin–piperine submicrometric polymeric particles

Biochemical analysis of serum markers in Wistar rats exposed to curcumin–piperine submicrometric polymeric particles showed no significant changes among experimental groups (Figure 7). Total cholesterol concentrations were 47.60 ± 6.03 mg/dL in controls, 55.67 ± 4.07 mg/dL in the 300 mg/kg group and 54.07 ± 2.22 mg/dL in the 2000 mg/kg group (Figure 7A). Triglycerides remained consistent, averaging 54.20 ± 3.14 mg/dL, 63.03 ± 0.86 mg/dL and 57.68 ± 5.47 mg/dL in the basal, 300 mg/kg and 2000 mg/kg groups, respectively (Figure 7B). Hepatic enzymes were also unaffected: ALT activity was 66.23 ± 2.59 U/L (basal), 60.67 ± 3.55 U/L (300 mg/kg) and 61.53 ± 4.90 U/L (2000 mg/kg) (Figure 7C), while AST averaged 130.9 ± 14.74 U/L, 103.80 ± 4.88 U/L and 112.90 ± 13.20 U/L, respectively (Figure 7D). Serum urea ranged from 31.10 ± 0.87 mg/dL (basal) to 30.60 ± 2.15 mg/dL and 29.60 ± 2.41 mg/dL (300 and 2000 mg/kg groups) (Figure 7E). In contrast, serum creatinine levels were significantly reduced in animals treated with curcumin–piperine submicrometric polymeric particles compared with the control group. As creatinine is eliminated predominantly by glomerular filtration with negligible tubular reabsorption, decreases in this marker, in the absence of concomitant increases in serum urea or renal histopathological alterations, are generally interpreted as indicative of preserved renal function (Stevens & Levin, 2019; Junqueira et al., 2021). This finding is consistent with recent evidence describing curcumin and piperine as compounds with a favorable renal safety profile, capable of attenuating oxidative stress and inflammation and preventing elevations in serum creatinine in different experimental models (Trujillo et al., 2021; El-Saadony et al., 2023). Therefore, the reduction in creatinine observed in the present study together with unchanged biochemical parameters and preserved renal histoarchitecture, reinforces the renal safety of the evaluated formulation.

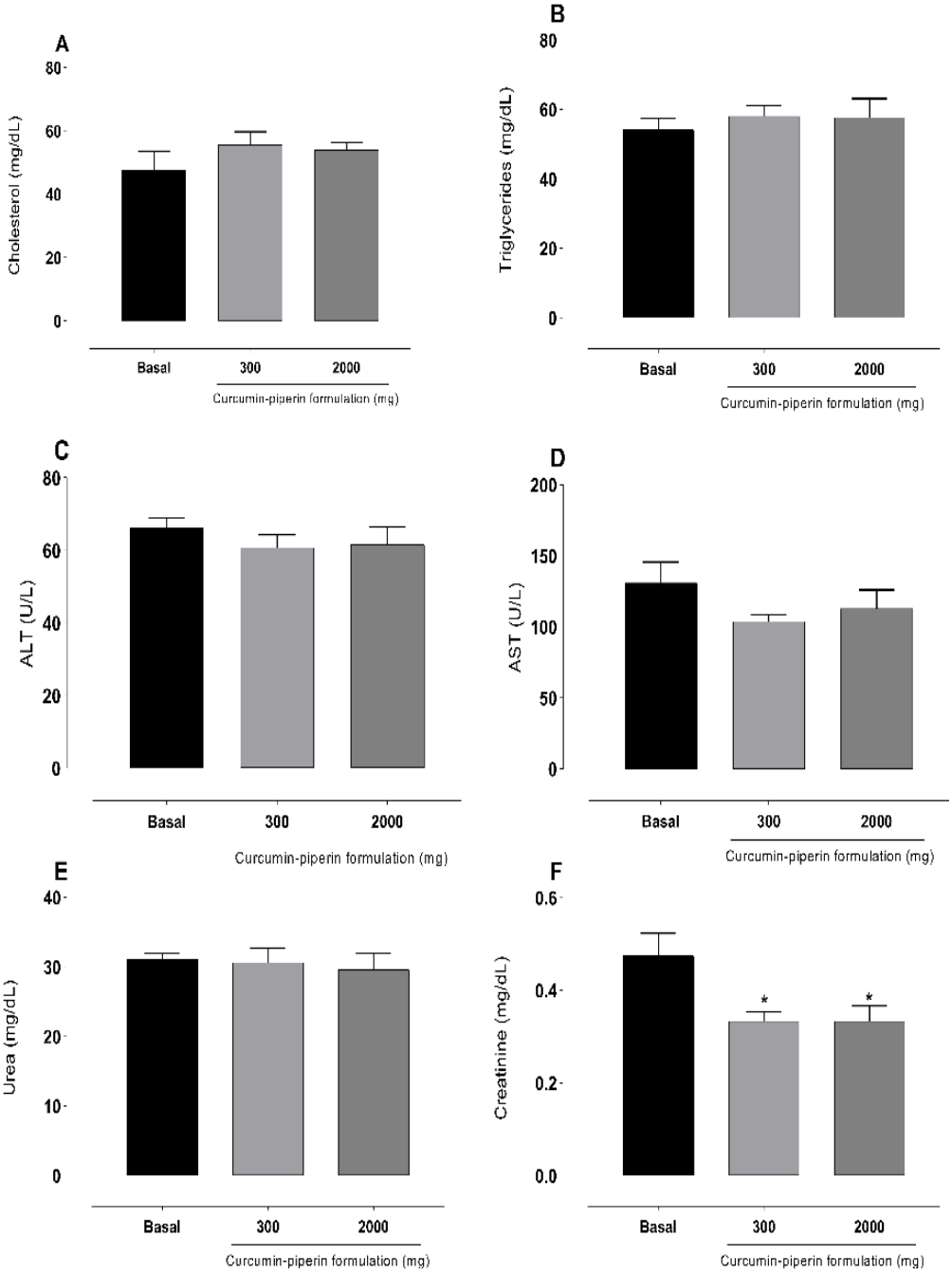

FIGURE 7. Serum biochemical parameters of Wistar rats treated orally with a single dose of submicrometric polymeric particles CUR/PIP (300 or 2000 mg/kg) or vehicle (filtered water). Measured parameters include (A) total cholesterol, (B) triglycerides, (C) alanine aminotransferase (ALT), (D) aspartate aminotransferase (AST), (E) urea and (F) creatinine. Values are presented as mean ± S.E.M. (*n* = 5–6 per group). Data were analyzed using one-way ANOVA followed by Tukey's post hoc test. *p < 0.05 *vs.* Basal

3.4.3. Hematological profile of rats treated with curcumin–piperine submicrometric polymeric particles

Hematological analysis showed that administration of curcumin–piperine **submicrometric polymeric particles** did not provoke systemic hematotoxic effects at any dose tested. Erythrocyte parameters—including total red blood cell count, hemoglobin concentration and hematocrit—remained comparable to controls, indicating preserved erythropoietic function. Total leukocyte counts also showed no significant differences among groups, suggesting that treatment did not trigger inflammatory or immunosuppressive responses. Likewise, differential leukocyte profiles remained consistent, with neutrophils, lymphocytes, monocytes, eosinophils and basophils showing no dose-dependent changes. Platelet counts and mean platelet volume were also unaffected, reinforcing hematological safety of the **submicrometric polymeric particles**.

3.4.4. Curcumin–piperine submicrometric polymeric particles do not induce hepatic, cardiac, or renal cellular changes

Histopathological examination of liver, spleen, heart and kidneys from rats treated with curcumin–piperine submicrometric polymeric particles at 300 mg/kg and 2000 mg/kg revealed preserved tissue architecture comparable to controls (Figure 8). Splenic architecture was maintained, with well-defined white and red pulp regions, with no evidence of lymphocyte depletion or structural disorganization. Hepatic sections exhibited hepatocytes organized in typical cords with intact cytoplasm and nuclei, without signs of steatosis, inflammatory infiltration, cellular swelling, or necrosis. Cardiac tissue presented normal myocardial fibers, without structural disorganization, inflammatory infiltration, or fibrosis. Renal histology showed intact glomerular and tubular structures, with no indications of necrosis, edema, or inflammatory cells.

The observed results indicate that curcumin–piperine submicrometric polymeric particles present low acute toxicity, as no relevant clinical, hematological, biochemical, or histopathological changes were detected, reinforcing the potential of the formulation as a safe alternative for oral administration.

This is one of the first reports to associate detailed physicochemical characterization and *in vitro* dissolution evaluation with *in vivo* toxicity assays for the curcumin–piperine combination, consolidating the translational potential of the system for pharmaceutical and nutraceutical applications. Comparable polymeric nanoencapsulated systems have already demonstrated

clinical safety and efficacy, further supporting the biocompatibility and translational relevance of polymer-based delivery technologies (Vilela et al., 2021).

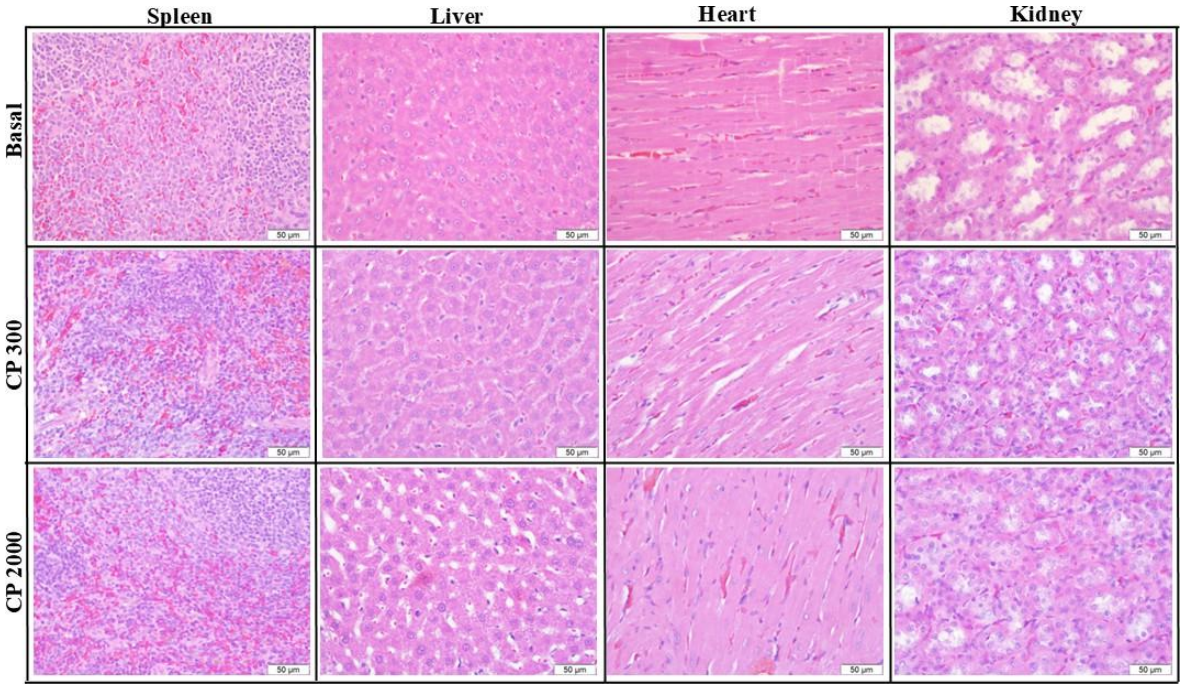

Figure 8. Representative H&E-stained histological sections of spleen, liver, heart and kidney from Wistar rats treated orally with curcumin–piperine submicrometric polymeric particles (300 or 2000 mg/kg) or vehicle (control). Tissues exhibit preserved morphology comparable to controls. Magnification: 20×. CP: submicrometric polymeric particles containing CUR/PIP.

Despite the promising results, further studies are necessary to confirm system applicability. *In vivo* bioavailability and subchronic toxicity assays should be conducted to elucidate the real impact of sustained release on intestinal absorption and on the safety of prolonged use. Such investigations will validate system performance under conditions closer to human consumption. In addition, incorporation of microparticles into different food matrices and pharmaceutical formulations represents a practical avenue to explore their versatility, reinforcing the safety and translational potential of the technology for both nutraceutical products and functional applications.

4. CONCLUSION

In the present study, submicrometric polymeric particles based on Eudragit S100 containing curcumin and piperine were successfully produced, demonstrating the technological feasibility

of the proposed formulation. Encapsulation efficiencies close to 100% confirmed the suitability of the polymeric system for the effective incorporation of these bioactive compounds.

Safety-related assessments indicated an adequate degree of biocompatibility, primarily evidenced by the absence of adverse outcomes in the acute oral toxicity evaluation, while the hemolysis assay served as a complementary *in vitro* safety screening. In addition, the *in vitro* dissolution studies revealed a sustained release profile for both curcumin and piperine, supporting the ability of the Eudragit S100 matrix to modulate and modulate intestinal release of encapsulated bioactives.

From a technological perspective, the spray drying process yielded submicrometric polymeric particles with favorable characteristics, including low production cost and scalability, which are essential attributes for industrial application. Taken together, these findings support the developed system as a versatile delivery platform capable of modulating intestinal release and supporting a favorable preliminary safety profile, while further *in vivo* absorption behavior studies are required to confirm its impact on systemic bioavailability.

REFERENCES

1. Abdul Rasool, B. K., Mohammed, A. A., & Salem, Y. Y. (2021). The optimization of a dimenhydrinate transdermal patch formulation based on the quantitative analysis of in vitro release data by DDSolver through skin penetration studies. *Scientia Pharmaceutica, 89*(3), 33.
2. Al Khatib, A. O., Yousfan, A., Abed, A., El-Tanani, M., & Al-Obaidi, H. (2025). Development of pimozide spray dried lipid nanoparticles with enhanced targeting of non-small cell lung cancer. *Journal of Drug Delivery Science and Technology*, 106969, 1–25.
3. Almeida, R. L., Fernandes, J., Silva, A., et al. (2014). Fourier transform infrared spectroscopy (FTIR) and near infrared spectroscopy (NIR) applied to pharmaceutical analysis. *Journal of Analytical Chemistry, 69*(9), 883–890. https://doi.org/10.1134/S1061934814090023
4. Alshehri, S., Haq, N., & Shakeel, F. (2018). Solubility, molecular interactions and mixing thermodynamic properties of piperine in various pure solvents at different temperatures. *Journal of Molecular Liquids, 250*, 63–70.
5. Ansari, K. A., Vavia, P. R., Trotta, F., & Cavalli, R. (2011). Cyclodextrin-based nanosponges for delivery of resveratrol: In vitro characterisation, stability, cytotoxicity and permeation study. *AAPS PharmSciTech, 12*(1), 279–286.
6. ASTM International. (2017). *ASTM F756-17: Standard practice for assessment of hemolytic properties of materials*. West Conshohocken, PA: ASTM International. https://doi.org/10.1520/F0756-17
7. Azad, A. K., Lai, J., Sulaiman, W. M. A. W., Almoustafa, H., Alshehade, S. A., Kumarasamy, V., & Subramaniyan, V. (2024). The fabrication of polymer-based curcumin-loaded formulation as a drug delivery system: An updated review from 2017 to the present. *Pharmaceutics, 16*(2), 160. https://doi.org/10.3390/pharmaceutics16020160
8. Azkia, A., Baihaqi, A. I., Prabowo, H. A., Hendri, H., Handayani, S., & Agustiany, T. (2020). A preliminary study on modified chitosan–curcuminoids as active material for food packaging with antioxidant and antibacterial activities [In Portuguese]. *IOP Conference Series: Materials Science and Engineering, 902*, 012040. https://doi.org/10.1088/1757-899X/902/1/012040
9. Baranska-Dołomisiewicz, A., Jedlinska, A., & Samborska, K. (2025). Investigation on the role of drying air humidity and process parameters in shaping the conditions of spray drying using model feed materials. *Applied Sciences, 15*, 5761. https://doi.org/10.3390/app15105761

10. Biscaia, P. B., Gomes, T., Ferreira, A., et al. (2023). Meth(acrylic) microparticles containing piperine: Development and validation of an RP-UHPLC-DAD method for assessing the drug-loading efficiency and the in vitro drug release. *Latin American Journal of Pharmacy, 42*(9), 1–12.
11. Bobek, V. B., Heiden, G., Oliveira, C. F., Almeida, V. P., Paula, J. P., Farago, P. V., Nakashima, T., & Budel, J. M. (2016). Comparative analytical micrographs of “vassouras” (Baccharis, Asteraceae). *Revista Brasileira de Farmacognosia, 26*(6), 665–672. https://doi.org/10.1016/j.bjp.2016.05.001
12. Brown, C. K., Friedel, H. D., Barker, A. R., Buhse, L. F., Keitel, S., Cecil, T. L., Kraemer, J., Morris, J. M., Reppas, C., Stickelmeyer, M. P., Yomota, C., & Shah, V. P. (2011). FIP/AAPS joint workshop report: Dissolution/in vitro release testing of novel/special dosage forms. *AAPS PharmSciTech, 12*(2), 782–794.
13. Bunhak, E. J., Silva, L., Prado, M., et al. (2015). Physicochemical analyses of modified chondroitin sulfate biofilms [In Portuguese]. *Química Nova, 38*(3), 316–320.
14. Camargo, G. d. A., Ferreira, L., Schebelski, D. J., Lyra, A. M., Barboza, F. M., Carletto, B., Koga, A. Y., Semianko, B. C., Dias, D. T., Lipinski, L. C., Novatski, A., Raman, V., Manfron, J., Nadal, J. M., & Farago, P. V. (2021). Characterization and In Vitro and In Vivo Evaluation of Tacrolimus-Loaded Poly(ε-Caprolactone) Nanocapsules for the Management of Atopic Dermatitis. *Pharmaceutics, 13*(12), 2013. https://doi.org/10.3390/pharmaceutics13122013
15. Chassot, J. M., Ribas, D., Silveira, E. F., Grünspan, L. D., Pires, C. C., Farago, P. V., Braganhol, E., Tasso, L., & Cruz, L. (2015). Beclomethasone dipropionate-loaded polymeric nanocapsules: Development, in vitro cytotoxicity and in vivo evaluation of acute lung injury. *Journal of Nanoscience and Nanotechnology, 15*(1), 855–864. https://doi.org/10.1166/jnn.2015.9178
16. Chen, S., McClements, D. J., Jian, L., Han, Y., Dai, L., Mao, L., & Gao, Y. (2019). Core–shell biopolymer nanoparticles for co-delivery of curcumin and piperine: Sequential electrostatic deposition of hyaluronic acid and chitosan shells on the zein core. *ACS Applied Materials & Interfaces, 11*(41), 38103–38115. https://doi.org/10.1021/acsami.9b11782
17. Chopra, B., Dhingra, A. K., Kapoor, R. P., & Prasad, D. N. (2017). Piperine and its various physicochemical and biological aspects: A review. *Open Chemistry Journal, 3*(1), 75–96.
18. Costa, P., & Sousa Lobo, J. M. (2001). Modeling and comparison of dissolution profiles. *European Journal of Pharmaceutical Sciences, 13*(2), 123–133. https://doi.org/10.1016/S0928-0987(01)00095-1
19. Cruz, L., Oliveira, M., Santos, F., et al. (2010). Gastroresistant microparticles containing sodium alendronate prevent the bone loss in ovariectomized rats. *European Journal of Pharmaceutical Sciences, 40*(5), 441–447.
20. da Silva, K. L., Hortkoff, D., Favoreto, M. W., Rezende, M., Nadal, J. M., Armas-Vega, A., Loguercio, A. D., & Farago, P. V. (2024). Preparation and characterization of a novel hydroxyapatite-capsaicin composite intended for the in-office dental bleaching use. *Journal of Composites Science, 8*(12), 496. https://doi.org/10.3390/jcs8120496
21. Dahiya, S., Rani, R., Dhingra, D., Kumar, S., & Dilbaghi, N. (2018). Conjugation of epigallocatechin gallate and piperine into a zein nanocarrier: Implication on antioxidant and anticancer potential. *Advances in Natural Sciences: Nanoscience and Nanotechnology*.
22. Dewi, M. O. T., & Setyaningsih, D. (2023). Effects of drying temperature on curcumin and piperine dissolution and the release kinetics of solid dispersion-based microparticles: A preliminary study. *Journal of Faculty of Pharmacy of Ankara University, 47*(3), 853–863. https://doi.org/10.33483/jfpau.1253561
23. EFSA (European Food Safety Authority). (2010a). Scientific opinion on the safety of basic methacrylate copolymer (E 1205) for use as a food additive. *EFSA Journal, 8*(10), 1–25.
24. EFSA (European Food Safety Authority). (2010b). Scientific opinion on the safety of anionic methacrylate copolymer for use as a food additive. *EFSA Journal, 8*(10), 1–18.
25. El-Saadony, M. T., Saad, A. M., Taha, A. E., Najjar, A. A., Zabermawi, N. M., et al. (2023). Curcumin and piperine as bioactive dietary compounds: Antioxidant, anti-inflammatory and nephroprotective mechanisms. *Food Chemistry, 402*, 134205. https://doi.org/10.1016/j.foodchem.2022.134205
26. European Commission. (2013). Commission Regulation (EU) No 816/2013 amending Regulation (EU) No 231/2012 as regards certain food additives. *Official Journal of the European Union*, L 223, 14–26.
27. Evonik Rohm GmbH. (2018). *Technical report* (Darmstadt, Germany). http://www.rofarma.com/allegati/97.pdf

28. Ferreira, L. M., Sari, M. H. M., Cervi, V. F., Prado, V. C., Nadal, J. M., Azambuja, J. H., Silveira, E. F., Nogueira, C. W., Farago, P. V., Braganhol, E., & Cruz, L. (2020). *Design of pegylated-nanocapsules to diphenyl diselenide administration: In vitro evidence of hemocompatible and selective antiglioma formulation*. AAPS PharmSciTech,, Article 307.
29. Food and Drug Administration (FDA). (2017). *GRAS Notice No. 710: Basic methacrylate copolymer*. Washington, DC: U.S. FDA.
30. Food and Drug Administration (FDA). (2021). *Indirect food additives: Polymers (21 CFR Part 177)*. Washington, DC: U.S. Government Printing Office.
31. Fortunato, K. A., Doile, M. M., Schmücker, I. C., Schucko, S. K., Silva, M. A. S., & Rodrigues, P. O. (2007). Influence of β-cyclodextrin complexation on dexamethasone acetate release from HPMC and PEO hydrophilic matrices [In Portuguese]. *Latin American Journal of Pharmacy, 26*, 513–521.
32. Gadade, D. D., & Pekamwar, S. S. (2016). Pharmaceutical cocrystals: Regulatory and strategic aspects, design and development. *Advanced Pharmaceutical Bulletin, 6*(4), 479–494.
33. Goëlo, V., Chaumun, M., Gonçalves, A., Estevinho, B. N., & Rocha, F. (2020). Polysaccharide-based delivery systems for curcumin and turmeric powder encapsulation using a spray-drying process. *Powder Technology, 370*, 137–146. https://doi.org/10.1016/j.powtec.2020.06.045
34. Gupta, S. C., Patchva, S., Koh, W., & Aggarwal, B. B. (2020). Discovery of curcumin, a component of golden spice and its miraculous biological activities. *Clinical and Experimental Pharmacology and Physiology, 47*(5), 705–722. https://doi.org/10.1111/1440-1681.13255
35. Gupta, T., Kumar, S., Kaur, A., Singh, P., Sharma, R., Mehta, N., et al. (2020). Enhancing bioavailability and stability of curcumin using solid lipid nanoparticles (CLEN): A covenant for its effectiveness. *Frontiers in Bioengineering and Biotechnology, 8*, 879. https://doi.org/10.3389/fbioe.2020.00879
36. Hassan, A. S., El-Mahdy, M. M., El-Badry, M., & El-Gindy, G. E.-D. A. (2019). Different approaches for enhancement of curcumin aqueous solubility and dissolution rate. *Journal of Advanced Biomedical and Pharmaceutical Sciences, 2*, 152–361.
37. Hegde, M., Girisa, S., Chetty, B. B., Vishwa, R., & Kunnumakkara, A. B. (2023). Curcumin formulations for better bioavailability: What we learned from clinical trials thus far? *ACS Omega, 8*(12), 10713–10746. https://doi.org/10.1021/acsomega.3c00123
38. Heredia, N. S., Vizuete, K., Flores-Calero, M., Pazmiño, V. K., Pilaquinga, F., Kumar, B., & Debut, A. (2022). Comparative statistical analysis of the release kinetics models for nanoprecipitated PLGA nanoparticles. *PLOS ONE, 17*(3), e0264825. https://doi.org/10.1371/journal.pone.0264825
39. Higashi, K., Okamoto, A., Masuda, T., et al. (2015). The effect of drug and Eudragit® S100 miscibility in solid dispersions on the drug and polymer dissolution rate. *International Journal of Pharmaceutics, 494*(1), 9–16.
40. Huang, W., Lee, S. L., & Yu, L. X. (2009). Mechanistic approaches to predicting oral drug absorption. *The AAPS Journal, 11*, 217–224.
41. International Organization for Standardization (ISO). (2017). *ISO 10993-4: Biological evaluation of medical devices—Part 4: Selection of tests for interactions with blood*. Geneva: ISO. https://www.iso.org/standard/63448.html
42. Junqueira, V. B. C., Simões, M. R., & Ribeiro, D. A. (2021). Interpretation of serum creatinine variations in toxicological studies: Physiological versus adverse responses. *Toxicology Letters, 337*, 1–8. https://doi.org/10.1016/j.toxlet.2020.11.013
43. Justus, B., Kanunfre, C. C., Budel, J. M., Faria, M. F., Raman, V., Paula, J. P., & Farago, P. V. (2019). New insights into the mechanisms of French lavender essential oil on non-small-cell lung cancer cell growth. *Industrial Crops and Products, 136*, 28–36. https://doi.org/10.1016/j.indcrop.2019.04.054
44. Kawabata, Y., Wada, K., Nakatani, M., Yamada, S., & Onoue, S. (2011). Formulation design for poorly water-soluble drugs based on biopharmaceutics classification system: Basic approaches and practical applications. *International Journal of Pharmaceutics, 420*(1), 1–10.
45. Li, M., Rouaud, O., & Poncelet, D. (2008). Microencapsulation by solvent evaporation: State of the art for process engineering approaches. *International Journal of Pharmaceutics, 363*(1–2), 26–39. https://doi.org/10.1016/j.ijpharm.2008.07.018
46. Lu, W., Yang, X., Shen, J., Li, Z., Tan, S., Liu, W., & Cheng, Z. (2021). Choosing the appropriate wall materials for spray-drying microencapsulation of natural bioactive ingredients: Taking phenolic compounds as examples. *Powder Technology, 394*, 562–574. https://doi.org/10.1016/j.powtec.2021.09.035

47. Machado, C. D., Farago, P. V., Costa, C. M., Farias, K. S., Silva, D. B., Marques, A. A. M., Moreno, K. G. T., Pael, L. A. B., Silva, M. L. F. da, Gasparotto Júnior, A., & Manfron, J. (2024). *Acute toxicity and genotoxicity of Schinus molle L. aqueous extract/ethanol-soluble fraction in rats*. Journal of Ethnopharmacology, 118499. https://doi.org/10.1016/j.jep.2024.118499
48. Marcon, M. V., Schafka, V. M., Justus, B., Nadal, J. M., Schnekenberg, C. M., Shirabayashi, J. de B., Lívero, F. A. dos R., & Farago, P. V. (2025). Co-quantification of curcuminoids and piperine by RP-HPLC/DAD from spray-dried microparticles for routine quality control. *Brazilian Archives of Biology and Technology, 68*, e250760. https://doi.org/10.1590/1678-4324-2025250760
49. Martín-Camacho, U. de J., Alías, M., & Rodríguez, A. (2023). Weibull β value for the discernment of drug release mechanisms. *Journal of Controlled Release, 354*, 118–129. https://doi.org/10.1016/j.jconrel.2023.05.017
50. Mithu, S. H., Rani, R., Dhingra, D., Kumar, S., & Dilbaghi, N. (2017). Evaluation of the surface chemistry and drug–polymer interaction of semi-crystalline microparticles for the development of controlled release formulations. *Materials Science and Engineering: C, 76*, 559–567.
51. Mohylyuk, V., Simões, S., Veiga, F., & Cabral-Marques, H. (2020). Wurster fluidized bed coating of microparticles: Towards scalable production of oral sustained-release liquid medicines for patients with swallowing difficulties. *AAPS PharmSciTech, 21*(3).
52. Neves, A. R., Lucena, C., Lima, F., et al. (2013). Novel resveratrol nanodelivery systems based on lipid nanoparticles to enhance its oral bioavailability. *International Journal of Nanomedicine, 8*, 177–187.
53. Octavia, M. D., Munandar, A., Sari, Y. N., Yudha, R. P., Wahdini, D., Wahyuni, R., Makmur, I., Azizah, Z., & Zafrul, A. (2024). Characterization of physicochemical properties and dissolution studies of multicomponent crystals of piperine and glutamic acid. *Tropical Journal of Natural Product Research, 8*(12), 9643–9647. https://doi.org/10.26538/tjnpr/v8i12.43
54. Oliveira, M. A., Yoshida, M. I., & Gomes, E. C. L. (2011). Thermal analysis applied to drugs and pharmaceutical formulations in the pharmaceutical industry [In Portuguese]. *Química Nova, 34*(7), 1224–1230.
55. Organisation for Economic Co-operation and Development (OECD). (2001). *Guideline 423: Acute oral toxicity—Acute toxic class method*. https://doi.org/10.1787/9789264071001-en
56. Ozawa, H., Tanaka, K., Yamada, H., et al. (2017). Curcumin β-D-glucuronide plays an important role to keep high levels of free-form curcumin in the blood. *Biological and Pharmaceutical Bulletin, 40*(9), 1515–1524.
57. Panahi, Y., Ahmadi, Y., Teymouri, M., Johnston, T. P., & Sahebkar, A. (2020). Effects of curcumin on serum creatinine, uric acid and oxidative stress in patients with chronic inflammatory conditions: A randomized controlled trial. *Phytotherapy Research, 34*(6), 1351–1359. https://doi.org/10.1002/ptr.6613
58. Patel, B. B., Sharma, N., Mehra, R., et al. (2015). Revealing facts behind spray dried solid dispersion technology used for solubility enhancement. *Saudi Pharmaceutical Journal, 23*(4), 352–365.
59. Patra, J. K., Das, G., Fraceto, L. F., Campos, E. V. R., Rodriguez-Torres, M. D. P., Acosta-Torres, L. S., et al. (2018). Nano based drug delivery systems: Recent developments and future prospects. *Journal of Nanobiotechnology, 16*, 71. https://doi.org/10.1186/s12951-018-0392-8
60. Percie du Sert, N., Hurst, V., Ahluwalia, A., Alam, S., Avey, M. T., Baker, M., Browne, W. J., et al. (2020). The ARRIVE guidelines 2.0: Updated guidelines for reporting animal research. *Journal of Cerebral Blood Flow & Metabolism, 40*(9), 1769–1777. https://doi.org/10.1177/0271678X20943823
61. Porras-Saavedra, J., López, E., García, A., et al. (2015). Microstructural properties and distribution of components in microparticles obtained by spray-drying. *Journal of Food Engineering, 152*, 105–112.
62. Pupo, Y. M., Farago, P. V., Nadal, J. M., Esmerino, L. A., Maluf, D. F., Zawadzki, S. F., Michél, M. D., Santos, F. A., Gomes, O. M. M., & Gomes, J. C. (2013). An innovative quaternary ammonium methacrylate polymer can provide improved antimicrobial properties for a dental adhesive system. *Journal of Biomaterials Science, Polymer Edition, 24*(12), 1443–1458. https://doi.org/10.1080/09205063.2013.766784
63. Purnamasari, L., Handayani, I., & Budiman, A. (2023). Advances in curcumin delivery systems for functional foods: A review. *Foods, 12*(7), 1505. https://doi.org/10.3390/foods12071505
64. Ribeiro, J. P. M., Schebelski, D. J., Lyra, A. M., Camargo, G. dos A., Nadal, J. M., Novatski, A., Manfron, J., & Farago, P. V. (2023). Physicochemical characterization, quantitative drug analysis, and stability testing of hydroxytyrosol-loaded poly(ε-caprolactone) nanocapsules.

Brazilian Archives of Biology and Technology, 66, e23230081. https://doi.org/10.1590/1678-4324-2023230081

65. Roland, F., & Bhawani, S. A. (2016). Applications of infrared spectroscopy in food analysis. *Food Research International, 76*, 646–652. https://doi.org/10.1016/j.foodres.2015.08.003
66. Rudnik, L. A. C. (2022). *Microparticulate inhalable powder with polymeric nanoparticles containing curcumin and piperine: Development, physicochemical characterization and cytotoxicity in lung tumor cell lines* [Doctoral thesis, Universidade Estadual de Ponta Grossa]. [In Portuguese].
67. Schneider, A. C., Brener, C. E. S., Daudt, N. F., Cruz, L., & Silva, C. B. (2023). Development of microparticles and microparticulated tablets containing piperine. *Brazilian Journal of Pharmaceutical Sciences*. https://doi.org/10.1590/s2175-97902023e21265
68. Schneider, L. F., Müller, F., & Yildiz, S. (2023). Controlled release of nutraceuticals: Design, evaluation and regulatory aspects. *Food & Function, 14*(2), 765–781. https://doi.org/10.1039/d2fo03242g
69. Setyaningsih, D., Santoso, Y. A., Hartini, Y. S., Murti, Y. B., Hinrichs, W. L. J., & Patramurti, C. (2021). Isocratic high-performance liquid chromatography (HPLC) for simultaneous quantification of curcumin and piperine in a microparticle formulation containing *Curcuma longa* and *Piper nigrum*. *Heliyon, 7*(3), e06541.
70. Sharma, V., & Pathak, K. (2016). Effect of hydrogen bond formation/replacement on solubility characteristics, gastric permeation and pharmacokinetics of curcumin by application of powder solution technology. *Acta Pharmaceutica Sinica B, 6*(6), 600–613.
71. Siepmann, J., & Peppas, N. A. (2001). Modeling of drug release from delivery systems based on hydroxypropyl methylcellulose (HPMC). *Advanced Drug Delivery Reviews, 48*(2–3), 139–157.
72. Silva, G. R. D., Amaral, E. C., Silva, M. L. M., Silva, A. O., da Silva, L. I., Froehlich, D. L., Faria, M. G. I., Linde, G. A., Colauto, N. B., Lovato, E. C. W., & Lívero, F. A. R. (2022). Acute safety assessment of lithium bioaccumulated in mycelial biomass of *Ganoderma lucidum*. *Conjecturas, 22*(2), 322–337. https://doi.org/10.53660/CONJ-644-611
73. Stevens, P. E., & Levin, A. (2019). Evaluation and management of chronic kidney disease: Synopsis of the kidney disease: Improving global outcomes 2012 clinical practice guideline. *Annals of Internal Medicine, 158*(11), 825–830. https://doi.org/10.7326/0003-4819-158-11-201306040-00007
74. Sundararajan, P., Moser, J., Williams, L., Chiang, T., Riordan, C., Metzger, M., Zhang-Plasket, F., Wang, F., Collins, J., & Williams, J. (2023). Driving spray drying towards better yield: Tackling a problem that sticks around. *Pharmaceutics, 15*, 2137. https://doi.org/10.3390/pharmaceutics15082137
75. Tabanelli, R., Manfrini, E., & Verardo, V. (2021). Improving curcumin bioavailability: Current strategies and perspectives. *International Journal of Molecular Sciences, 22*(20), 10878. https://doi.org/10.3390/ijms222010878
76. Tagde, P., Tagde, P., Islam, F., Tagde, S., Shah, M., Hussain, Z. D., et al. (2021). The multifaceted role of curcumin in advanced nanocurcumin form in the treatment and management of chronic disorders. *Molecules, 26*(23), 7109. https://doi.org/10.3390/molecules26237109
77. Taghadosi, M., Mohammadi, M., Zare, M., et al. (2024). Encapsulation of curcumin with Persian gum and its stability enhancement in dairy products. *Food Science & Nutrition, 12*(11), 9379–9390. https://doi.org/10.1002/fsn3.4499
78. Teixeira, C. C. C., Mendonça, L. M., Bergamaschi, M. M., Queiroz, R. H. C., Souza, G. E. P., Antunes, L. M. G., & Freitas, L. A. P. (2016). Microparticles containing curcumin solid dispersion: Stability, bioavailability and anti-inflammatory activity. *AAPS PharmSciTech, 17*(2), 376–384. https://doi.org/10.1208/s12249-015-0337-6
79. Trujillo, J., Chirino, Y. I., Molina-Jijón, E., Andérica-Romero, A. C., Tapia, E., & Pedraza-Chaverri, J. (2021). Renoprotective effect of the antioxidant curcumin: Recent findings. *Redox Biology, 38*, 101788. https://doi.org/10.1016/j.redox.2020.101788
80. Umerska, A., Gaucher, C., Oyarzun-Ampuero, F., Fries-Raeth, I., Colin, F., Villamizar-Sarmiento, M. G., Maincent, P., & Sapin-Minet, A. (2018). Polymeric nanoparticles for increasing oral bioavailability of curcumin. *Antioxidants, 7*(4), 46. https://doi.org/10.3390/antiox7040046
81. Umerska, A., Paluch, K. J., Inkielewicz-Stepniak, I., & Tajber, L. (2018). Exploring the release mechanisms of curcumin from polymeric carriers—A Weibull model approach. *European Journal of Pharmaceutics and Biopharmaceutics, 132*, 180–190. https://doi.org/10.1016/j.ejpb.2018.09.001

82. van Duong, T., & van den Mooter, G. (2016). The role of the carrier in the formulation of pharmaceutical solid dispersions. Part I: Crystalline and semi-crystalline carriers. *Expert Opinion on Drug Delivery, 13*(11), 1583–1594.
83. Vilela, A. P., Rezende, M., Terra, R. M. O., Silva, K. L., Sutil, E., Calixto, A. L., Reis, A., Loguercio, A. D., & Farago, P. V. (2021). Effect of topical application of nanoencapsulated eugenol on dental sensitivity reduction after in-office dental bleaching: A randomized, triple-blind clinical trial. *Journal of Esthetic and Restorative Dentistry, 33*(5), 692–700. https://doi.org/10.1111/jerd.12728
84. Yupangui, K., Oliveira, R., Santos, J., & Silva, T. (2024). Chitosan–mannitol microparticles for gastroresistant delivery of turmeric extract. *Food Hydrocolloids, 152*, 108021. https://doi.org/10.1016/j.foodhyd.2024.108021
85. Yupanqui, C. T., Suksanga, A., Ardhanwanich, S., & Ungphaiboon, S. (2024). Spray-dried microparticles of turmeric extract for improved delivery and low toxicity. *Pharmacia, 71*, 1–10. https://doi.org/10.3897/pharmacia.71.e126108
86. Yusuf, H., Rahmawati, R. A., Rijal, M. A. S., & Isadiartuti, D. (2021). Curcumin micelles entrapped in Eudragit S-100 matrix: A synergistic strategy for enhanced oral delivery. *Future Science OA, 7*(4), FSO677. https://doi.org/10.2144/fsoa-2020-0131
87. Zaini, E., Afriyani, L., Fitriani, L., Ismed, F., Horikawa, A., & Uekusa, H. (2020). Improved solubility and dissolution rates in novel multicomponent crystals of piperine with succinic acid. *Scientia Pharmaceutica, 88*(2), 21. https://doi.org/10.3390/scipharm88020021
88. Zhang, Y., Huo, M., Zhou, J., Zou, A., Li, W., Yao, C., & Xie, S. (2010). DDSolver: An add-in program for modeling and comparison of drug dissolution profiles. *The AAPS Journal, 12*(3), 263–271.
89. Zhao, Y., Xu, X., Dai, A., Jia, Y., & Wang, W. (2024). Enhanced dissolution and bioavailability of curcumin nanocrystals prepared by hot-melt extrusion technology. *International Journal of Nanomedicine, 19*, 5721–5737. https://doi.org/10.2147/IJN.S463918

Supplementary Material Article 2

Table S1. Statistical parameters describing curcumin and piperine release from Eudragit S100 submicrometric polymeric particles (SPP) and from free-bioactive mixture (FM), by each kinetic model.

Formulation	Model	Parameters of dissolution model (mean)		
		Adjusted R^2	**AIC**	**MSC**
CUR-FM	Zero Order	0.39465	135.92033	6.79602
	First Order	0.98775	57.91034	2.89552
	Higuchi	0.87469	104.42071	5.22104
	Hopfenberg	0.94933	86.3116	4.31558
	Korsmeyer-Peppas	0.87548	105.15098	5.25755
	Weibull	0.99716	29.53452	1.47673
	Gompertz	0.99033	54.83138	2.74157
	Baker-Lonsdale	0.94933	86.3116	4.31558
	Biexponential	0.99147	53.02978	2.65149
CUR-SPP	Zero Order	0.92602	81.58345	4.07917
	First Order	0.97263	61.69758	3.08488
	Higuchi	0.88083	91.11787	4.55589
	Hopfenberg	0.9902	41.15204	2.0576
	Korsmeyer-Peppas	0.975	60.74225	3.03711
	Weibull	0.99641	21.94327	1.09716
	Gompertz	0.99012	42.95588	2.14779
	Baker-Lonsdale	0.9902	41.15204	2.0576
	Biexponential	0.99973	-28.62647	-1.43132

PIP-FM	Zero Order	0.42141	134.4229	6.72115
	First Order	0.98805	56.82111	2.84106
	Higuchi	0.88238	102.56043	5.12802
	Hopfenberg	0.95961	81.18455	4.05923
	Korsmeyer-Peppas	0.88115	103.62532	5.18127
	Weibull	0.99722	28.54172	1.42709
	Gompertz	0.99066	53.54989	2.67749
	Baker-Lonsdale	0.95961	81.18455	4.05923
	Biexponential	0.99146	52.45431	2.62272
PIP-SPP	Zero Order	0.91348	85.13751	4.25688
	First Order	0.97511	60.21875	3.01094
	Higuchi	0.89029	89.88545	4.49427
	Hopfenberg	0.9916	38.48518	1.92426
	Korsmeyer-Peppas	0.97339	62.41208	3.1206
	Weibull	0.99599	24.53881	1.22694
	Gompertz	0.99002	43.57984	2.17899
	Baker-Lonsdale	0.9916	38.48518	1.92426
	Biexponential	0.99952	-16.41402	-0.8207

Table S2. Assessment of clinical signs in Wistar rats treated with vehicle or curcumin–piperine submicrometric polymeric particles (300 or 2000 mg/kg), orally, in a single dose.

			Time					
3.2.1.31 Clinical sign			30 min	1h	2h	3h	4h	14 days
Basal (vehicle)		*Self-cleaning absence*	0/5	0/5	0/5	0/5	0/5	0/5
		Piloerection	0/5	0/5	0/5	0/5	0/5	0/5
		Dyspnea	0/5	0/5	0/5	0/5	0/5	0/5
		Abdominal constriction	0/5	0/5	0/5	0/5	0/5	0/5
		Diarrhea	0/5	0/5	0/5	0/5	0/5	0/5
		Prostration	0/5	0/5	0/5	0/5	0/5	0/5
		Ataxia	0/5	0/5	0/5	0/5	0/5	0/5
		Sedation	0/5	0/5	0/5	0/5	0/5	0/5
		Coma	0/5	0/5	0/5	0/5	0/5	0/5
		Death	0/5	0/5	0/5	0/5	0/5	0/5
Curcumin –piperine SPP	**300 mg/kg**	*Self-cleaning absence*	0/6	0/6	0/6	0/6	0/6	0/6
		Piloerection	0/6	0/6	0/6	0/6	0/6	0/6
		Dyspnea	0/6	0/6	0/6	0/6	0/6	0/6
		Abdominal constriction	0/6	0/6	0/6	0/6	0/6	0/6
		Diarrhea	0/6	0/6	0/6	0/6	0/6	0/6
		Prostration	0/6	0/6	0/6	0/6	0/6	0/6
		Ataxia	0/6	0/6	0/6	0/6	0/6	0/6
		Sedation	0/6	0/6	0/6	0/6	0/6	0/6
		Coma	0/6	0/6	0/6	0/6	0/6	0/6
		Death	0/6	0/6	0/6	0/6	0/6	0/6

	2000 mg/kg	*Self-cleaning absence*	0/6	0/6	0/6	0/6	0/6	0/6
		Piloerection	0/6	0/6	0/6	0/6	0/6	0/6
		Dyspnea	0/6	0/6	0/6	0/6	0/6	0/6
		Abdominal constriction	0/6	0/6	0/6	0/6	0/6	0/6
		Diarrhea	0/6	0/6	0/6	0/6	0/6	0/6
		Prostration	0/6	0/6	0/6	0/6	0/6	0/6
		Ataxia	0/6	0/6	0/6	0/6	0/6	0/6
		Sedation	0/6	0/6	0/6	0/6	0/6	0/6
		Coma	0/6	0/6	0/6	0/6	0/6	0/6
		Death	0/6	0/6	0/6	0/6	0/6	0/6

6 ARTIGO CIENTÍFICO 3

Gastro-resistant curcumin–piperine microparticles improve cardiometabolic and inflammatory parameters and modulate gut microbiota in an experimental model of metabolic syndrome

Marcia Viviane Marcon[4],

Jaqueline de Bortoli Shirabayashi[1],

Arianne Jung Kluck[2],

Arisa Namie Higashijima[2],

Rafaela Caroline Santa Clara[2],

Mayara Alves Amorim[3],

Camila Silva Bezerra[2],

Nattaly Viana Lowen[2],

Gustavo Ratti da Silva[1],

Barbara Justus[6],

Celso Luiz Borges[6],

Fernando Augusto Lavezzo Dias[7],

Marcelo Cardoso Ferrari[8],

Paulo Vítor Farago[4,5],

Francislaine Aparecida dos Reis Lívero[1,2*]

*Correspondence of address with this author in the Laboratory of Cardiometabolic Pharmacology, Department of Pharmacology, Biological Sciences Sector, Federal University of Paraná – UFPR, PO Box 19031, Curitiba, PR, 81531-980, Brazil. Tel: +55 (43) 3361-1693. E-mail: francislaine@ufpr.br.

[1] Laboratory of Preclinical Research of Natural Products, Paranaense University, Umuarama, Paraná, Brazil; [2] Laboratory of Cardiometabolic Pharmacology, Federal University of Paraná, Curitiba, Paraná, Brazil; [3] Laboratory of TRP Receptors and Inflammatory Diseases, Federal University of Paraná, Curitiba, Paraná, Brazil; [4] Graduate Program in Pharmaceutical Sciences, State University of Ponta Grossa (UEPG), Ponta Grossa, Paraná, Brazil; [5] Graduate Program in Health Sciences, State University of Ponta Grossa (UEPG), Ponta Grossa, Paraná, Brazil; [6] State University of Ponta Grossa (UEPG), Ponta Grossa, Paraná, Brazil; [7] Department of Physiology, Federal University of Paraná (UFPR), Curitiba, Paraná, Brazil; [8] School of Medicine and Life Sciences, Pontifical Catholic University of Paraná (PUC-PR), Curitiba, Paraná, Brazil.

GRAPHICAL ABSTRACT

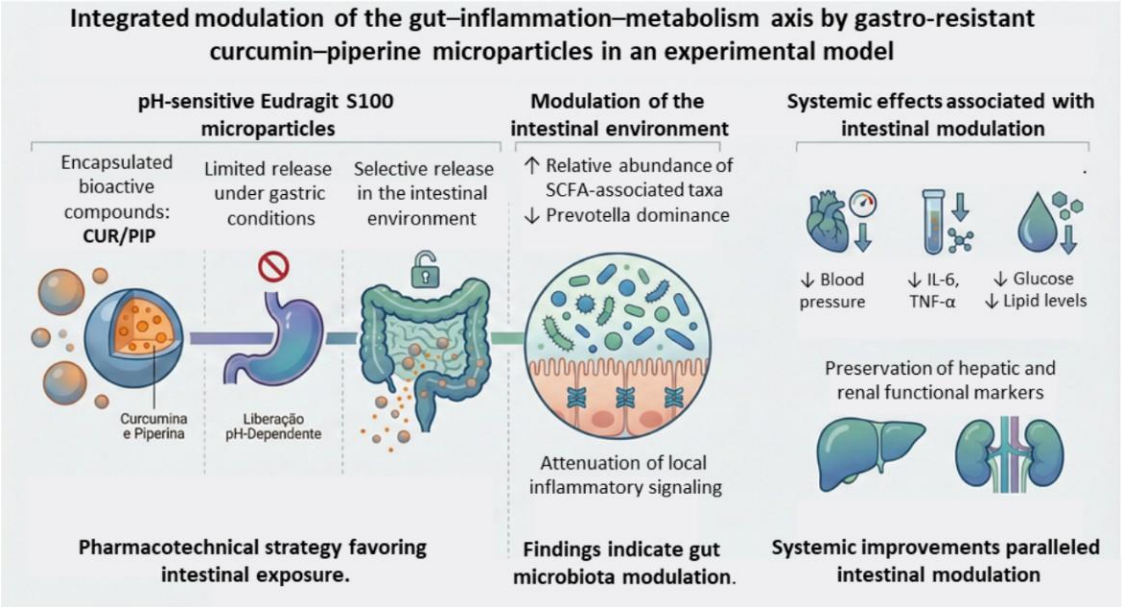

ABSTRACT

Metabolic syndrome (MetS) is a multifactorial condition characterized by metabolic, inflammatory, and cardiovascular disturbances and is frequently associated with gut dysbiosis. Curcumin exhibits relevant pharmacological properties in this context; however, its clinical applicability is limited by poor oral bioavailability. This study evaluated the effects of gastro-resistant curcumin–piperine microparticles on cardiometabolic, inflammatory, and gut microbiota parameters in an experimental model of MetS. Spontaneously hypertensive rats (SHR) subjected to dyslipidemia induction and fructose consumption were treated for four weeks with curcumin–piperine microparticles (25, 75, or 225 mg/kg) or conventional pharmacotherapy based on enalapril and simvastatin. Hemodynamic, anthropometric, metabolic, renal, and hepatic parameters were assessed, along with inflammatory cytokines and gut microbiota composition by 16S rRNA gene sequencing. Treatment with the highest dose of the formulation (225 mg/kg) significantly improved blood pressure, lipid and glycemic profiles, reduced visceral adiposity, and attenuated markers of hepatic and renal dysfunction. A dose-dependent reduction in pro-inflammatory cytokines was also observed, with normalization of IL-6 levels exclusively in the group treated with the highest dose. Gut microbiota analysis revealed that MetS was associated with reduced microbial diversity and dominance of a limited number of taxa, whereas curcumin–piperine treatment promoted a functionally favorable microbial reorganization characterized by enrichment of short-chain fatty acid–producing genera, although without complete restoration of the basal profile. Collectively, these findings indicate that the gastro-resistant curcumin–piperine formulation is capable of modulating multiple pathophysiological components of MetS. Modulation of the gut–inflammation–metabolism axis appears to represent an important component of these effects, highlighting the relevance of pharmacotechnical strategies aimed at improving the bioavailability and systemic activity of curcumin.

Keywords: Metabolic syndrome; Curcumin–piperine; Gastro-resistant microparticles; Inflammation; Gut microbiota modulation.

1. INTRODUCTION

Metabolic syndrome (MetS) represents one of the major contemporary challenges in public health, as it encompasses a cluster of cardiometabolic risk factors, including abdominal obesity, insulin resistance, atherogenic dyslipidemia, hyperglycemia, and systemic arterial hypertension (SAH), which substantially increase cardiovascular and metabolic morbidity and mortality (Hosseini et al., 2023; Qiu et al., 2023). It is estimated that approximately one quarter of the adult population worldwide is affected by MetS, with a growing prevalence driven by population aging, physical inactivity, and unhealthy dietary patterns (Valadares et al., 2022; Mambrini et al., 2023).

The pathophysiology of MetS is complex and multifactorial, involving hemodynamic alterations, metabolic dysfunction, chronic low-grade inflammation, oxidative stress, and changes in body composition, particularly the accumulation of visceral adipose tissue (Dziegielewska-Gesiak, 2021). Among its components, SAH plays a central role not only as a diagnostic criterion but also as a major determinant of cardiovascular risk, frequently showing resistance to pharmacological control when treated in isolation (Verhaar et al., 2020; Ge et al., 2024). This context underscores the need for therapeutic strategies capable of acting in an integrated manner on multiple pathophysiological axes of MetS.

Growing evidence indicates that the gut microbiome actively participates in metabolic, inflammatory, and cardiovascular regulation, interacting with classical mechanisms involved in MetS. Intestinal dysbiosis and increased gut barrier permeability have been associated with obesity, insulin resistance, systemic inflammation, and SAH, accompanied by elevated circulating markers such as lipopolysaccharides (LPS), *D*-lactate, and zonulin (Xiao et al., 2024, de Vos et al., 2022; Cani, 2018). In addition, a reduction in short-chain fatty acid (SCFA)–producing bacteria compromises vascular and metabolic homeostasis, favoring endothelial dysfunction, inflammation, and hemodynamic alterations (Wu et al., 2021; Zuo et al., 2022; Snelson et al., 2024). Recent guidelines from the American Heart Association (2025) recognize that acetate, propionate, and butyrate exert beneficial effects on blood pressure regulation and energy metabolism, highlighting the gut–metabolism–heart axis as a relevant, although not exclusive, component of MetS.

Within this multifactorial framework, increasing attention has been directed toward bioactive compounds capable of simultaneously modulating metabolic, inflammatory, anthropometric, and cardiovascular parameters. Curcumin, the principal polyphenol derived from *Curcuma longa* L., exhibits anti-inflammatory, antioxidant, hypolipidemic, and insulin-sensitizing properties, in addition to modulatory effects on gut microbiota composition (Jabczyk et al., 2024; Panahi et al., 2018; Deng et al., 2023). Recent clinical evidence indicates that optimized

curcumin formulations can reduce blood pressure and improve inflammatory and metabolic markers in individuals at cardiometabolic risk (Funamoto et al., 2022). However, its poor oral bioavailability limits clinical efficacy, prompting the development of pharmacotechnical strategies such as combination with piperine and controlled-release delivery systems, including gastro-resistant microparticles, aimed at enhancing absorption and potentiating biological effects (Ghoran et al., 2022; Hamed et al., 2024).

In this context, the present study investigated whether an innovative curcumin–piperine formulation delivered via gastro-resistant microparticles is capable of modulating multiple components of MetS. To this end, its biological effects were evaluated in an experimental model of MetS in spontaneously hypertensive rats through the assessment of hemodynamic, metabolic, anthropometric, inflammatory, and gut microbiota–related parameters, with the aim of exploring its systemic effects and potential underlying mechanisms.

2. MATERIALS AND METHODS

2.1. Reagents

All chemicals and reagents used in this study were of analytical grade. Ammonium ferric sulfate, dipotassium phosphate, monopotassium phosphate, sodium citrate dihydrate, sulfuric acid, hydrochloric acid, ethanol, methanol, formalin, pyrogallol, eosin, Harris hematoxylin, Hayem's solution, and Turk's solution were obtained from Êxodo Científica® (Sumaré, Brazil). Butylated hydroxytoluene was purchased from Synth® (Diadema, Brazil). Chloroform and isopropanol were supplied by Biotec® (Curitiba, Brazil), while hexane was obtained from Dinâmica® (Indaiatuba, Brazil). Ethylenediaminetetraacetic acid (EDTA) was acquired from Neon Reagentes® (Suzano, Brazil). Doxorubicin, Ellman's reagent (DTNB), reduced glutathione, MTT, saline solution, and xylenol orange were purchased from Sigma-Aldrich® (St. Louis, MO, USA). Isoflurane was obtained from Cristália® (Itapira, Brazil). Paraffin and xylene were supplied by Allkimia® (Campinas, Brazil). Trichloroacetic acid was purchased from Proquímios® (Bangu, Brazil), and Tris buffer was obtained from Invitrogen™ (Carlsbad, CA, USA). Simvastatin was kindly provided by Novartis® (Basel, Switzerland). A *Curcuma longa* L. extract standardized to 95.2% total curcuminoid content was supplied by Tianxu Natural Pigment (China). *Piper nigrum* L. extract was obtained from Xi'an Tian Ben Bio-engineering (China). The polymer poly(methacrylic acid-co-methyl methacrylate) 1:2 (Eudragit® S100) was kindly donated by Evonik (Brazil).

2.2. Preparation of polymeric microparticles containing curcumin and piperine

Polymeric microparticles containing curcumin and piperine were prepared using poly(methacrylic acid–co–methyl methacrylate) (Eudragit® S100), curcumin (CUR), and piperine (PIP), resulting in a total formulation mass of 10 g, with a drug loading of 20% (500 mg of CUR and 20 mg of PIP). An ethanol–water mixture (60:40, v/v) was used as solvent.

CUR and PIP were initially dissolved in 720 mL of ethanol under magnetic stirring (800 rpm; FISATOM, model 754, São Paulo, Brazil), followed by the addition of the polymer under the same conditions. After complete dissolution, 480 mL of distilled water were gradually added, and the mixture was maintained under continuous stirring for 12 h. The resulting solution was dried by spray drying using a laboratory-scale spray dryer (LABMAQ, model MSD 0.5) under the following conditions: atomizer diameter 0.82 mm, atomization pressure 3 kgf·cm^{-2}, airflow rate 25 L·min^{-1}, feed rate 0.40 L·h^{-1}, inlet temperature 135 ± 5 °C, and outlet temperature 60 ± 5 C° (Marcon, et al., 2025).

2.3. Formulation yield

The yield (R) of the spray-dried microparticles containing curcumin and piperine was determined in triplicate and calculated as the ratio between the final mass of the microparticles and the sum of the initial masses of polymer and bioactive compounds, according to Equation 1:

$$R(\%) = \frac{microparticle\ 5ei6ht}{initial\ 5ei6ht\ (polymer<bioactive)} x100 \quad \text{(Equation 1)}$$

2.4. Encapsulation efficiency assessment

2.4.1. Equipment and chromatographic conditions

Analyses were performed using a Shimadzu Nexera-i LC-2040C HPLC system (Japan) equipped with a diode-array detector (DAD), pump, degasser (DGU), autosampler (SIL), and column oven. Separation was achieved on a C18 reverse-phase Shim-pack column (150 × 4.6 mm, 5 µm).

Detection wavelengths were selected based on UV–Vis scanning (190–400 nm), set at 410 nm for CUR and 341 nm for PIP. The previously validated method (Marcon et al. 2025) was performed isocratically at 25 °C using a mobile phase composed of acetonitrile:methanol:water

(55:5:45, v/v/v), with a flow rate of 1.00 mL·min⁻¹, injection volume of 10.0 µL, and total run time of 15.0 min.

2.4.2. Encapsulation efficiency

Encapsulation efficiency (EE, %) was determined according to the method described by Li, Rouaud, and Poncelet (2008), using Equation 2:

$$EE(\%) = \frac{dru6\ \ 5ei6ht\ \ in\ \ microparticle}{initial\ \ 5ei6ht\ \ (theoretical)} x100 \qquad \text{(Equation 2)}$$

Microparticles containing curcumin and piperine were accurately weighed into 10.0 mL volumetric flasks, and 8.00 mL of methanol were added. The suspensions were maintained under magnetic stirring at 1000 rpm for 12 h. The volume was then adjusted to 10.0 mL, and the resulting solutions were filtered through PTFE membrane filters (0.22 µm).

The theoretical concentration was 300.00 µg·mL⁻¹, corresponding to 288.48 µg·mL⁻¹ of CUR and 11.52 µg·mL⁻¹ of PIP. Analyses were performed in triplicate using the validated method within analytical ranges of 200.0–500.0 µg·mL⁻¹ for CUR and 8.00–20.00 µg·mL⁻¹ for PIP, with detection at 410 nm and 341 nm, respectively.

2.5. Pharmacological studies

2.5.1. Animals

A total of 36 male rats (200–250 g) were used in this study, including 30 spontaneously hypertensive rats (SHR) and 6 male Wistar rats obtained from the Animal Facility of the University of Vale do Itajaí (UNIVALI). Animals were randomly allocated into six experimental groups (n = 6 per group). Sample size was determined based on previous studies employing comparable experimental designs (Auth et al., 2022; Albuquerque et al., 2023; Amaral et al., 2023; Silva et al., 2024).

Throughout the experimental period, animals were housed at the Animal Facility of the Cardiometabolic Pharmacology Laboratory, Federal University of Paraná (UFPR). Rats were maintained under controlled environmental conditions (temperature 20 ± 2 °C; relative humidity

50 ± 10%; 12 h light/dark cycle, with lights on at 7:00 a.m.) and had ad libitum access to solid and liquid diets, with environmental enrichment provided.

Animal handling, monitoring, and welfare assessment were conducted in accordance with the Animal Research: Reporting of *In Vivo* Experiments (ARRIVE) guidelines (Percie du Sert et al., 2020). The experimental protocol was approved by the Ethics Committee on the Use of Animals of UFPR (CEUA/UFPR no. 1656). All procedures were performed in strict compliance with the regulations and recommendations of the Brazilian National Council for the Control of Animal Experimentation (CONCEA), prioritizing animal welfare and adhering to the principles of Replacement, Reduction, and Refinement (3Rs).

2.5.2. Experimental design and treatments

The experimental protocol (Figure 1) was conducted over a total period of seven weeks. Throughout the study, animals were exposed to cardiometabolic risk factors, including hypertension and dyslipidemia. Dyslipidemia was induced by *ad libitum* access to a standard commercial diet supplemented with 0.5% cholesterol, following the protocol previously described by Silva et al. (2024). Alterations in glucose metabolism were induced by continuous intake of fructose at a concentration of 10% (w/v) in the drinking water during the experimental period, according to the protocol proposed by Mamikutty et al. (2014).

After the induction phase, animals were randomized into experimental groups according to exposure to cardiometabolic risk factors and treatment regimen. Treatments were administered during the final four weeks of the experimental protocol and consisted of: (i) a basal group not exposed to cardiometabolic risk factors and treated with vehicle (1 mL/kg); (ii) a negative control group exposed to cardiometabolic risk factors and treated with vehicle (1 mL/kg); (iii) three treatment groups exposed to cardiometabolic risk factors and treated with curcumin–piperine microparticles at doses of 25, 75, or 225 mg/kg (CP 25, 75 or 225); and (iv) a positive control group exposed to cardiometabolic risk factors and treated with reference drugs (enalapril 15 mg/kg and simvastatin 2.5 mg/kg).

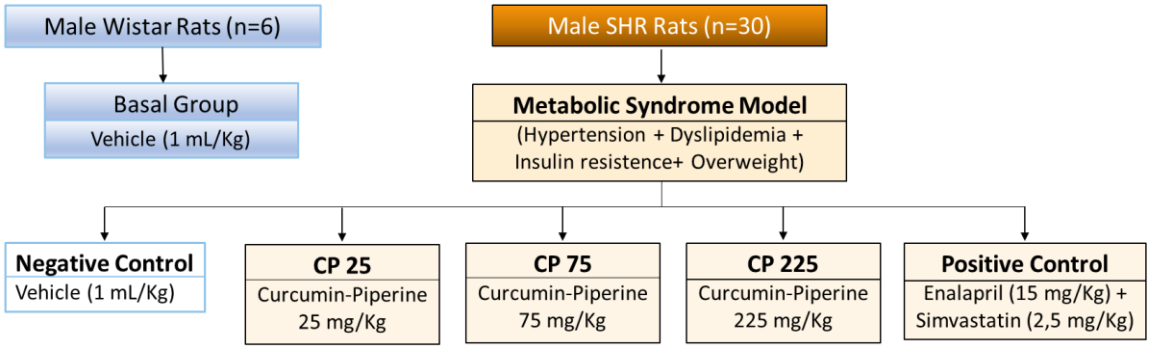

Figure 1. Experimental design and group allocation. Basal: healthy rats not subjected to the disease model and treated with vehicle. C–: rats subjected to hypertension, dyslipidemia, and fructose consumption, treated with vehicle. 25, 75, and 225: rats subjected to the disease model and treated with the curcumin–piperine microparticles at doses of 25, 75, or 225 mg/kg, respectively. C+: rats subjected to the disease model and treated with enalapril plus simvastatin. *n* = 6 animals per group.

All treatments were administered orally by gavage once daily. Both the curcumin–piperine microparticles and the reference drugs were freshly prepared immediately prior to administration. Dose selection was based on previous experimental studies conducted by the research group and supported by the available literature (Barbosa et al., 2020; Zago et al., 2021; Auth et al., 2022).

2.5.3. Assessment of hemodynamic and electrocardiographic parameters

2.5.3.1. Electrocardiographic recording and analysis

Electrocardiographic activity was recorded in slightly sedated animals using ketamine (30 mg/kg) and xylazine (2.5 mg/kg). Experiments were performed in a silent and reserved room at a temperature of 25 °C. Frontal plane electrocardiographic activity was collected using a PowerLab acquisition system, model 26T (ADInstrument, Australia) and later analyzed using LabChart version 8.0 software (ADInstrument) as previously described (Souza Neto et al, 2023). Electrodes were mounted on an acrylic plate allowing positioning of the animal's front and rear paws using a small amount of contact gel. Noninvasive blood pressure measurements were collected simultaneously, as described below. Data was pooled and calculated between the third and fourth minutes after stable EKG signal acquisition. For data calculation we used measurements obtained from DII (Souza Neto et al., 2023).

2.5.3.2. Noninvasive blood pressure measurements

Noninvasive Blood Pressure was assessed using a tail-cuff system and pulse transducer connect to a controller (Controller ML125, ADInstruments) coupled to a biopotential acquisition system hardware (PowerLab ML856, ADInstruments) in non-restrained, slightly sedated animals. Data was collected and analyzed in LabChart 8 software. A series of 5 consecutive measurements were performed 1 minute apart using constricting pressure up to 280 mm Hg. Systolic blood pressure was calculated as the corresponding pressure of the first identifiable peak in pulse pressure during cuff deflation, associated with the identification of heart rate returning to be recorded in a channel derived from the pulse pressure data. We averaged the pressure from the first 3 measurements and in case of problems with the acquisition of the first measurements they were substituted by the fourth and fifth measurements consecutively. Diastolic blood pressure was estimated based on the minimum amplitude of the pulse pressure signal during cuff deflation, as automatically calculated by the LabChart software (Souza Neto et al., 2023).

2.5.4. Anthropometric measurements and abdominal obesity index

Anthropometric measurements were performed to assess body fat distribution and abdominal obesity. All measurements were obtained with animals under light sedation with isoflurane to minimize stress and movement. Abdominal circumference, thoracic circumference, and naso-anal length were measured at the end of the experimental period using a flexible, non-elastic measuring tape commonly employed for anthropometric assessments.

Abdominal circumference was measured at the midpoint between the last rib and the iliac crest, while thoracic circumference was measured at the level of the xiphoid process. Naso- anal length was determined as the linear distance from the tip of the nose to the anus, with the animal positioned in standardized dorsal recumbency. An abdominal obesity index was calculated as the ratio between abdominal circumference and naso-anal length, providing an indirect estimate of central adiposity.

2.5.5. Euthanasia, sample collection, and biochemical analyses

At the end of the treatment period, after a 12 h fasting period, animals were euthanized by anesthetic overdose using isoflurane (20%) in a saturated chamber. Blood samples were collected by decapitation. Serum glucose levels were measured using a portable glucometer (Accu-Chek Active®, Roche, Mannheim, Germany).

Plasma concentrations of γ-glutamyl transferase (γ-GT), alanine aminotransferase (ALT), aspartate aminotransferase (AST), total cholesterol, triglycerides, very-low-density lipoprotein cholesterol (VLDL-C), low-density lipoprotein cholesterol (LDL-C), high-density lipoprotein cholesterol (HDL-C), urea, and creatinine were determined using enzymatic colorimetric assays in a semi-automated analyzer (Global Analyzer®, model GTA-300, Calgary, AB, Canada).

Tumor necrosis factor-alpha (TNF-α) and interleukin-6 (IL-6) were quantified by enzyme-linked immunosorbent assay (ELISA). Immediately after euthanasia, fecal content was collected directly from the intestinal lumen under sterile conditions and stored at 8 °C for subsequent gut microbiota analysis.

Selection of the experimental group for microbiota analysis was performed at the time of euthanasia based on macroscopic evaluation of tissues and organs, as well as previously obtained hemodynamic and anthropometric data. This decision preceded biochemical, inflammatory, and microbiome analyses, ensuring independence of CP225 group selection from subsequent analytical outcomes.
Epididymal adipose tissue, liver, heart, kidneys, and spleen were excised, weighed using an analytical balance, and dissected. Representative portions of each organ were fixed for histopathological evaluation, while remaining tissue samples were stored at −20 °C for subsequent analyses of oxidative stress markers and lipid content.

2.5.6. Determination of inflammatory cytokines TNF-α and IL-6

Plasma concentrations of TNF-α and IL-6 were determined by enzyme-linked immunosorbent assay (ELISA) using rat-specific commercial kits: TNF-α (Kit ELK1396 – Rat TNF-α, ELK Biotechnology Co., Ltd., Sugar Land, TX, USA) and IL-6 (Kit ELK1158 – Rat IL-6, ELK Biotechnology Co., Ltd., Sugar Land, TX, USA), according to the manufacturers' instructions.

Absorbance readings were obtained at 450 nm using a microplate washer (PR 4100) and reader (PW 40), both from Bio-Rad Laboratories, Inc. (Hercules, CA, USA). Cytokine concentrations were calculated from seven-point standard curves using appropriate regression models. Results were expressed as picograms per milliliter (pg/mL) for each animal, and 95% confidence intervals were determined for each experimental group.

2.5.7. Gut microbiome analysis

2.5.7.1. Sample collection

Fecal samples were collected directly from the large intestine of each animal into sterile, RNase-free tubes previously identified. Samples were homogenized in SEMol medium at a ratio of 1:2 (feces:medium) and stored at −80 °C until analysis.

2.5.7.2. DNA extraction

Microbial DNA was extracted using a commercial kit specific for fecal samples (QIAamp® Fast DNA Stool Mini Kit, QIAGEN), according to the manufacturer's instructions. DNA concentration and purity were assessed by spectrophotometry using a NanoDrop™ system (Thermo Scientific™, Waltham, MA, USA).

2.5.7.3. Amplification and sequencing

The V3–V4 hypervariable region of the 16S rRNA gene (~460 bp) was amplified using primers 375F and 805R. PCR conditions consisted of an initial denaturation at 95 °C for 3 min, followed by 25 cycles of 95 °C for 30 s, 55 °C for 30 s, and 72 °C for 30 s, with a final extension at 72 °C for 5 min. Amplicons were indexed with Illumina® Nextera adapters and barcodes, purified, normalized, and sequenced on an Illumina NextSeq platform using paired-end mode (2 × 300 bp). Raw reads were processed using QIIME2 software (Degnan & Ochman, 2012; Caporaso et al., 2010; 2011), including truncation at 200 bp, low-quality filtering, chimera removal, and generation of amplicon sequence variants (ASVs). Taxonomic assignment was performed using the Genome Taxonomy Database (GTDB), version 226 (2024) (Parks et al., 2022).

2.5.7.4. Diversity analyses and microbiological outcomes

Microbiota diversity analyses included assessment of alpha diversity using Chao1, Fisher, Shannon, and Pielou Evenness índices. ASVs with ≤10 reads were excluded to reduce statistical noise. Analyses were conducted in the R environment using the phyloseq (McMurdie & Holmes, 2013), vegan (Oksanen et al., 2007), and microbiome (Lahti & Shetty, 2018) packages. Microbiological outcomes included: (i) alpha diversity, (ii) taxonomic composition at different hierarchical levels, (iii) differential taxon abundance, and (iv) the Firmicutes/Bacteroidota ratio as an additional marker of intestinal dysbiosis.

2.6. Statistical analysis

Statistical analyses were preceded by assessment of data normality and homogeneity of variances. Comparisons among experimental groups were performed using one-way analysis of variance (ANOVA), followed by Tukey's post hoc test for multiple comparisons. Statistical significance was defined as $p < 0.05$. Results are expressed as mean ± standard error of the

mean (SEM). All statistical analyses were conducted using GraphPad Prism software (version 9.0; GraphPad Software, San Diego, CA, USA).

3. RESULTS AND DISCUSSION

3.1. Preparation, yield, and encapsulation efficiency of curcumin–piperine polymeric microparticles

Polymeric microparticles based on Eudragit® S100 containing curcumin and piperine (CP–SPPs) were successfully obtained by spray-drying, yielding free-flowing powders with a characteristic orange coloration, comparable to that of non-encapsulated curcumin. The process resulted in a mean yield of 53.34 ± 0.71% (n = 3) and was associated with high encapsulation rates for both bioactive compounds, as determined by high-performance liquid chromatography (HPLC).

The experimentally incorporated amounts of curcumin (289.01 ± 6.97 µg/mL) and piperine (11.47 ± 0.24 µg/mL) were virtually identical to the theoretical concentrations (288.48 and 11.52 µg/mL, respectively), corresponding to encapsulation efficiencies of 100.18% for curcumin and 99.56% for piperine. These values are consistent with, although slightly higher than, those previously reported for curcumin-based formulations (Yupangui et al., 2024; Dewi & Setyaningsih et al., 2021) and piperine-containing systems (Schneider et al., 2023; Biscaia et al., 2023).

Taken together, these findings demonstrate the high incorporation capacity of the polymeric matrix, confirm the reproducibility of the spray-drying method, and support the suitability of Eudragit® S100 as an efficient carrier system for poorly soluble bioactive compounds such as curcumin.

3.2. Hemodynamic and electrocardiographic alterations induced by the disease model and their modulation by curcumin–piperine microparticles

Rats subjected to the cardiometabolic disease model (C–) exhibited marked hemodynamic disturbances compared with the basal group, characterized by significant increases in systolic and diastolic blood pressure (Table 1). Treatment with curcumin–piperine microparticles at doses of 25 and 75 mg/kg did not prevent the elevation of blood pressure. In contrast, administration of the highest dose (225 mg/kg) significantly reduced both systolic and diastolic

blood pressure, restoring values comparable to those observed in basal animals. A similar normalization of blood pressure was observed in the C+ group.

Heart rate was not significantly altered in the C– group compared with basal animals. Among treated groups, a significant reduction in heart rate was observed exclusively in animals receiving the highest dose of curcumin–piperine microparticles (225 mg/kg), whereas the remaining treatment groups and the C+ did not differ from either the basal or C– groups. These findings suggest that, at higher concentrations, the curcumin–piperine formulation may exert additional cardiovascular effects, potentially related to reduced hemodynamic load and improved vascular function, as previously reported in experimental models and clinical studies (Du Preez et al., 2019; Funamoto et al., 2022; Yadav et al., 2025).

Electrocardiographic analysis revealed a significant prolongation of QRS and QT intervals in the C– group compared with basal animals. This prolongation persisted in rats treated with curcumin–piperine microparticles at doses of 25, 75, and 225 mg/kg, whereas the C+ group exhibited values comparable to those of the basal group. Regarding the corrected QT interval (QTc), significant prolongation was observed in the C– group and in animals treated with 25 mg/kg, while no significant differences were detected in the groups treated with 75 or 225 mg/kg or in the C+ group relative to basal animals.

Table 1. Hemodynamic and electrocardiographic parameters of rats subjected to hypertension, dyslipidemia, and fructose consumption and treated with a curcumin–piperine microparticles.

	Basal	**C-**	**25**	**75**	**225**	C+
			Curcumin–piperine microparticles			
HR (bpm)	269.20±8.70	253.7±7.90	260.1±9.10	245.10±3.80	226.30±6.10^{ac}	260.70±7.10
SBP (mmHg)	113.60±3.90	154.1±6.30^{a}	146.0±8.80^{ac}	144.60±6.60^{ac}	116.90±4.70^{b}	96.10±7.60^{b}
DBP (mmHg)	74.20±4.10	113.6±3.50^{a}	110.6±6.90^{ac}	102.30±2.50^{ac}	88.30±5.40^{b}	68.50±5.60^{b}
QRS (ms)	21.69±0.71	27.14±0.70^{a}	27.94±1.11^{a}	28.00±1.43^{a}	27.48±1.18^{a}	27.29±2.69
QT (ms)	73.57±5.03	96.49±3.68^{a}	94.91±3.21^{a}	91.29±3.74^{a}	96.30±3.50^{a}	86.97±2.52
QTC (ms)	161.80±11.50	198.60±8.90^{a}	197.20±5.90^{a}	183.70±5.80	192.40±5.40	181.50±4.50

Abbreviations: HR, heart rate; bpm, beats per minute; SBP, systolic blood pressure; DBP, diastolic blood pressure; mmHg, millimeters of mercury; QRS, QRS complex duration; QT, QT interval; QTc, corrected QT interval. Basal: healthy rats not subjected to the disease model and treated with vehicle. C–: rats subjected to hypertension, dyslipidemia, and fructose

consumption, treated with vehicle. 25, 75, and 225: rats subjected to the disease model and treated with the curcumin–piperine microparticles at doses of 25, 75, or 225 mg/kg, respectively. C+: rats subjected to the disease model and treated with enalapril plus simvastatin. *n* = 6-7 animals per group. Data are expressed as mean ± SEM. [a]p < 0.05 *vs*. Basal; [b]p < 0.05 *vs*. C–; [c]p<0.05 *vs*. C+ (one-way ANOVA followed by Tukey's post hoc test).

Overall, these findings demonstrate that the gastro-resistant curcumin–piperine microparticle formulation effectively reversed the core hemodynamic alterations associated with MetS, particularly at higher doses, although its effects on electrocardiographic parameters were more limited. This dissociation suggests that the observed cardiovascular benefits are primarily related to reductions in peripheral vascular resistance and arterial pressure rather than to a direct modulation of cardiac electrical conduction.

Experimental and clinical evidence supports the hypotensive effects of curcumin, particularly when formulation strategies are employed to overcome its low oral bioavailability. In an experimental model of diet-induced metabolic syndrome in rats, Du Preez et al. (2019) demonstrated normalization of systolic blood pressure after eight weeks of treatment with either high-dose curcumin (100 mg/kg/day) or low-dose curcumin nanoparticles (5 mg/kg/day), highlighting the relevance of improved bioavailability for achieving cardiovascular effects. Consistent with these findings, other preclinical studies have shown that curcumin can attenuate hypertension and vascular dysfunction in experimental models of cardiometabolic disease following chronic administration for 6–8 weeks at doses ranging from 50 to 100 mg/kg/day (Wang et al., 2020). In addition to vascular effects, curcumin has also been reported to improve several metabolic alterations associated with high-fat diet–induced metabolic syndrome after long-term supplementation in animal models (Zhang et al., 2021).

Evidence from clinical studies further supports the potential cardiometabolic benefits of curcumin supplementation. In a randomized clinical trial, Funamoto et al. (2022) evaluated a highly bioavailable curcumin formulation (90 mg twice daily for 24 weeks) in patients with hypertensive heart disease and reported improvements in circulating BNP levels, suggesting cardioprotective effects without significant changes in blood pressure. Similarly, El-Rakabawy et al. (2025) reported significant reductions in both systolic and diastolic blood pressure in patients with type 2 diabetes and elevated cardiovascular risk treated with curcumin supplementation (1500 mg/day for 14 weeks), without concomitant changes in body weight, body mass index, or glycemic parameters, indicating a relatively direct hemodynamic effect independent of global metabolic changes.

3.3. Anthropometric and glycemic characterization of the cardiometabolic model

Anthropometric and glycemic parameters are summarized in Table 2. The combination of hypertension, dyslipidemia, and fructose consumption resulted in a significant increase in epididymal fat mass, abdominal obesity index, and fasting glucose levels in the untreated disease model group (C–) compared with basal animals, confirming the successful establishment of a cardiometabolic phenotype.

Treatment with curcumin–piperine microparticles significantly reduced epididymal fat mass at doses of 75 and 225 mg/kg, as well as in the C+, whereas no significant effect was observed at the 25 mg/kg dose. Regarding central adiposity, the abdominal obesity index was partially reduced at doses of 25 and 75 mg/kg, while treatment with the highest dose (225 mg/kg) and the C+ resulted in a significant reduction, restoring values close to those observed in the basal group.

With respect to glycemic control, fasting glucose levels were partially reduced at the 25 mg/kg dose, whereas significant reductions were observed at doses of 75 and 225 mg/kg and in the C+ group, indicating a clear dose-dependent improvement in glycemic homeostasis.

Table 2. Anthropometric and glycemic characterization of rats subjected to hypertension, dyslipidemia, and fructose consumption and treated with a curcumin–piperine microparticles.

	Basal	**C-**	**25**	**75**	**225**	C+
			Curcumin–piperine microparticles			
Epididymal fat (g)	1.14±0.06	1.44±0.04[a]	1.21±0.04	1.11±0.09[b]	1.13±0.05[b]	1.23±0.03[b]
Abdominal obesity index	0.62±0.01	0.80±0.01[a]	0.72±0.01[ab]	0.70±0.01[ab]	0.63±0.01[b]	0.65±0.02[b]
Glucose (mg/dL)	88.43±6.22	154.30± .64[a]	129.20±0.59[abc]	107.70±3.8[b]	94.83±4.01[b]	102.70±4.63[b]

Abbreviations: Basal: healthy rats not subjected to the disease model and treated with vehicle. C–: rats subjected to hypertension, dyslipidemia, and fructose consumption, treated with vehicle. 25, 75, and 225: rats subjected to the disease model and treated with the curcumin–piperine microparticles at doses of 25, 75, or 225 mg/kg, respectively. C+: rats subjected to the disease model and treated with enalapril plus simvastatin. *n* = 6-7 animals per group. Data are expressed as mean ± SEM. [a]$p < 0.05$ *vs*. Basal; [b]$p < 0.05$ *vs*. C–; [c]$p<0.05$ *vs*. C+ (one-way ANOVA followed by Tukey's post hoc test).

The observed effects on visceral adiposity and fasting glycemia are consistent with experimental studies demonstrating the ability of curcumin to reduce adipose tissue accumulation and improve glycemic homeostasis in models of obesity and metabolic dysfunction (Pan et al., 2017). Increasing evidence suggests that these effects are mediated, at least in part, by modulation of gut dysbiosis and attenuation of low-grade systemic inflammation, both hallmarks of MetS, thereby contributing to reduced insulin resistance and central adiposity (Lamichhane et al., 2024). The lack of significant glycemic improvement reported in some clinical studies, such as those by Funamoto et al. (2022) and El-Rakabawy et al. (2025), has been attributed to short intervention periods, differences in baseline metabolic status, and the use of curcumin formulations with limited bioavailability.

3.4. Curcumin–piperine microparticles improve lipid homeostasis

The combined induction of hypertension, dyslipidemia, and fructose consumption produced a pronounced disruption of plasma lipid homeostasis in the present model. Accordingly, animals in the untreated disease model group (C–) exhibited marked elevations in plasma lipid parameters compared with basal animals. Treatment with curcumin–piperine microparticles resulted in a clear dose-dependent correction of these alterations.

Animals in the untreated disease model group (C–) exhibited a marked increase in total cholesterol levels (273.7 ± 5.7 mg/dL) compared with the basal group (59.0 ± 2.6 mg/dL). Treatment with curcumin–piperine microparticles produced a dose-dependent reduction in cholesterol levels. Partial reductions were observed at doses of 25 and 75 mg/kg, with concentrations decreasing to 172.0 ± 4.4 mg/dL and 124.7 ± 3.8 mg/dL, respectively. In contrast, administration of the highest dose (225 mg/kg) resulted in a robust reduction in total cholesterol (74.5 ± 4.3 mg/dL), restoring levels to values comparable to those of the basal group. A similar normalization was observed in animals treated with the reference therapy (enalapril plus simvastatin; 71.3 ± 5.4 mg/dL) (Figure 2A).

A comparable pattern was observed for plasma triglyceride levels. The C– group exhibited a significant increase (261.7 ± 13.5 mg/dL) relative to basal animals (73.3 ± 5.1 mg/dL). Treatment with curcumin–piperine microparticles at doses of 25 and 75 mg/kg led to partial reductions, reaching 140.7 ± 8.9 mg/dL and 102.7 ± 5.2 mg/dL, respectively. Complete reversal of hypertriglyceridemia was observed at the 225 mg/kg dose (67.5 ± 6.6 mg/dL), as well as in the C+ group (52.7 ± 4.9 mg/dL), with values comparable to or lower than those of healthy animals (Figure 2B).

Consistent with these findings, VLDL-C levels were significantly elevated in the C– group (32.0 ± 2.7 mg/dL) compared with the basal group (14.9 ± 1.1 mg/dL). Partial attenuation

was observed following treatment with 25 and 75 mg/kg of the microparticles (21.9 ± 1.4 and 16.5 ± 1.5 mg/dL, respectively). In contrast, the 225 mg/kg dose (10.5 ± 1.0 mg/dL) and the reference therapy (11.3 ± 1.2 mg/dL) completely reversed VLDL-C elevation, yielding values comparable to those of the basal group (Figure 2C).

LDL-C levels followed a similar trend. A significant increase was observed in the C– group (19.2 ± 1.6 mg/dL) relative to basal animals (6.1 ± 0.8 mg/dL). Treatment with the lowest microparticle dose (25 mg/kg) did not significantly modify LDL-C levels (15.3 ± 1.1 mg/dL), whereas a partial reduction was observed at 75 mg/kg (11.0 ± 0.7 mg/dL). Complete normalization was achieved with the 225 mg/kg dose (8.3 ± 0.9 mg/dL) and in the C+ group (7.3 ± 0.7 mg/dL) (Figure 2D).

In contrast to the other lipid parameters, HDL-C levels were significantly reduced in the C– group (15.6 ± 1.2 mg/dL) compared with the basal group (32.7 ± 1.4 mg/dL). Administration of curcumin–piperine microparticles at 25 mg/kg did not significantly affect HDL-C concentrations (19.0 ± 1.2 mg/dL), whereas partial recovery was observed at 75 mg/kg (23.2 ± 1.4 mg/dL). Complete restoration of HDL-C levels was achieved at the 225 mg/kg dose (30.8 ± 1.4 mg/dL) and in the reference therapy group (30.7 ± 1.7 mg/dL), reaching values comparable to those of healthy controls (Figure 2E).

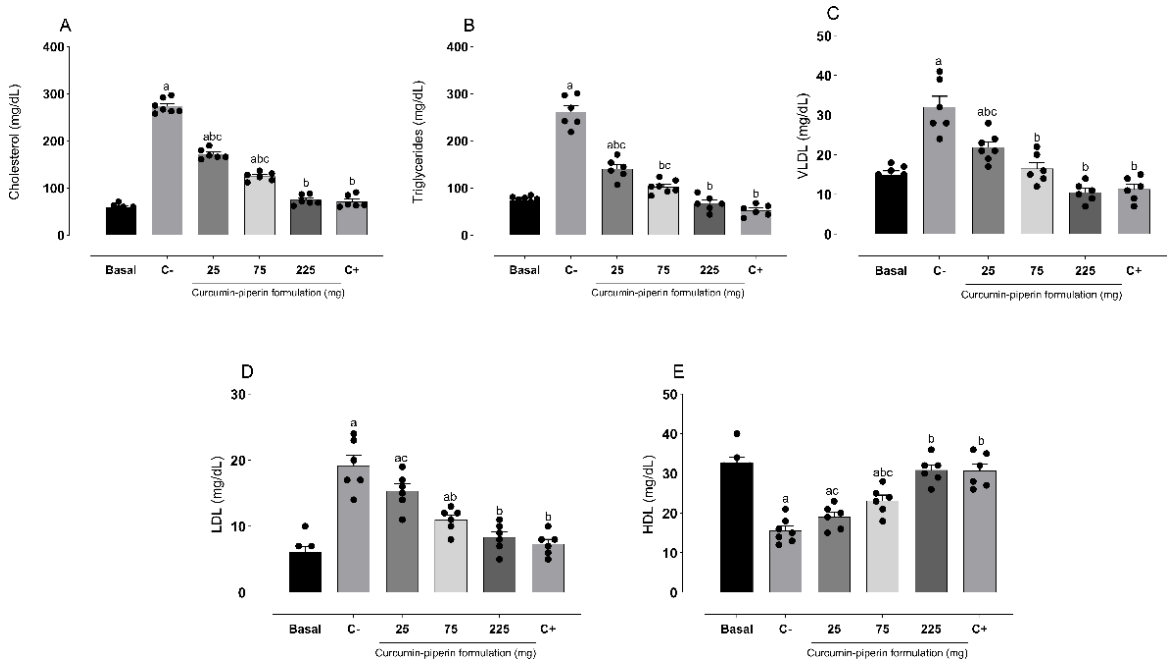

Figure 2. Serum lipid profile. Serum levels of (**A**) total cholesterol, (**B**) triglycerides, (**C**) very-low-density lipoprotein cholesterol (VLDL-c), (**D**) low-density lipoprotein cholesterol (LDL-c), and (**E**) high-density lipoprotein cholesterol (HDL-c). Basal: healthy rats not subjected to the disease model and treated with vehicle. C–: rats subjected to hypertension, dyslipidemia, and

fructose consumption, treated with vehicle. 25, 75, and 225: rats subjected to the disease model and treated with the curcumin–piperine microparticles at doses of 25, 75, or 225 mg/kg, respectively. C+: rats subjected to the disease model and treated with enalapril plus simvastatin. *n* = 6-7 animals per group. Data are expressed as mean ± SEM. [a]p < 0.05 *vs*. Basal; [b]p < 0.05 *vs*. C–; [c]p<0.05 *vs*. C+ (one-way ANOVA followed by Tukey's post hoc test).

The improvement in lipid profile observed in the present study, characterized by reductions in total cholesterol, triglycerides, VLDL-C, and LDL-C together with increased HDL-C levels, particularly at the highest curcumin dose, is consistent with both experimental and clinical evidence. In the present model, the combined induction of hypertension, dyslipidemia, and fructose consumption produced a marked disruption of lipid homeostasis, with pronounced elevations in total cholesterol and triglycerides in untreated animals. Treatment with curcumin–piperine microparticles resulted in a clear dose-dependent improvement in lipid parameters, with partial attenuation at 25 and 75 mg/kg and near-complete normalization at the highest dose (225 mg/kg), restoring several parameters to levels comparable to those observed in basal animals and in the group receiving reference pharmacotherapy.

These findings are consistent with previous reports demonstrating the lipid-modulating effects of curcumin. In a randomized, double-blind clinical trial conducted in individuals with metabolic syndrome, Sangouni et al. (2022) demonstrated that supplementation with isolated curcumin (200 mg/day) for 12 weeks significantly improved lipid parameters, including reductions in total cholesterol and triglycerides. Similarly, in a preclinical study using rats with diet-induced dyslipidemia, Abuelezz et al. (2020) reported dose-dependent lipid-lowering effects following treatment with nanocurcumin administered at doses ranging from 100 to 200 mg/kg/day for four weeks, with greater efficacy observed at the higher dose. These observations are further supported by a meta-analysis of randomized controlled trials conducted by Panahi et al. (2022), which reported consistent reductions in triglycerides, total cholesterol, and LDL-C following curcuminoid supplementation across multiple experimental and clinical studies.

Taken together, these data provide translational support for the present findings and suggest that the normalization of lipid parameters observed at the highest curcumin–piperine dose reflects a robust biological effect. The lipid-lowering response to curcumin has been attributed to multiple mechanisms, including modulation of hepatic lipogenesis, increased fatty-acid oxidation, improved lipoprotein metabolism, and attenuation of systemic inflammation.

Interestingly, emerging evidence also indicates that part of the metabolic benefits associated with curcumin supplementation may involve modulation of the gut microbiota. In experimental models, curcumin has been shown to reshape gut microbial composition and associated

metabolic pathways, contributing to improved metabolic homeostasis and reduced inflammatory signaling (Cui et al., 2022). These observations suggest that the beneficial cardiometabolic effects observed in the present study may also be partly mediated through interactions within the gut–microbiota–metabolism axis.

3.5. Curcumin–piperine microparticles attenuate hepatic enzyme alterations

Induction of the cardiometabolic disease model resulted in a marked elevation of serum γGT levels in the untreated group (C–), which increased from 1.14 ± 0.40 U/L in basal animals to 6.00 ± 0.49 U/L, indicating significant hepatic dysfunction (Figure 3A). Treatment with curcumin–piperine microparticles produced dose-dependent reductions in γGT levels. While the lowest dose (25 mg/kg) did not significantly alter γGT compared with the C– group (4.17 ± 0.60 U/L), administration of 75 mg/kg fully restored γGT levels to values comparable to those of the basal group (2.67 ± 0.33 U/L). Notably, treatment with the highest dose (225 mg/kg) resulted in complete normalization of γGT levels (1.50 ± 0.22 U/L). In contrast, animals treated with the reference therapy (C+ group) exhibited only partial improvement, with γGT levels reduced to 3.50 ± 0.43 U/L, remaining significantly higher than those observed in basal animals.

A similar pattern was observed for AST levels (Figure 3B). The C– group showed a pronounced increase in AST compared with basal animals (333.4 ± 13.22 vs. 102.0 ± 7.26 U/L). Treatment with the lowest microparticle dose (25 mg/kg) resulted in partial AST reduction (271.5 ± 13.39 U/L), whereas the 75 mg/kg dose further decreased AST levels (201.7 ± 9.67 U/L), although values remained elevated relative to the basal group. Administration of the highest dose (225 mg/kg) completely reversed AST elevation, restoring enzyme levels to those observed in healthy controls (105.8 ± 8.49 U/L). In contrast, the C+ group exhibited only partial AST reduction (283.0 ± 9.43 U/L), indicating incomplete recovery of this parameter.

Regarding ALT, disease induction significantly increased serum levels in the C– group compared with basal animals (90.50 ± 5.58 vs. 47.71 ± 4.25 U/L; Figure 3C). Treatment with 25 mg/kg did not significantly modify ALT levels relative to the C– group (75.00 ± 3.89 U/L). In contrast, administration of the 75 mg/kg dose resulted in complete normalization of ALT levels (64.50 ± 1.75 U/L). Consistent with the effects observed for γGT and AST, the highest dose (225 mg/kg) fully reversed ALT elevations, restoring values to those of the basal group (49.83 ± 3.95 U/L). Animals treated with the reference therapy (C+ group) exhibited only partial ALT reduction (71.00 ± 4.35 U/L), with levels remaining significantly higher than those of healthy controls.

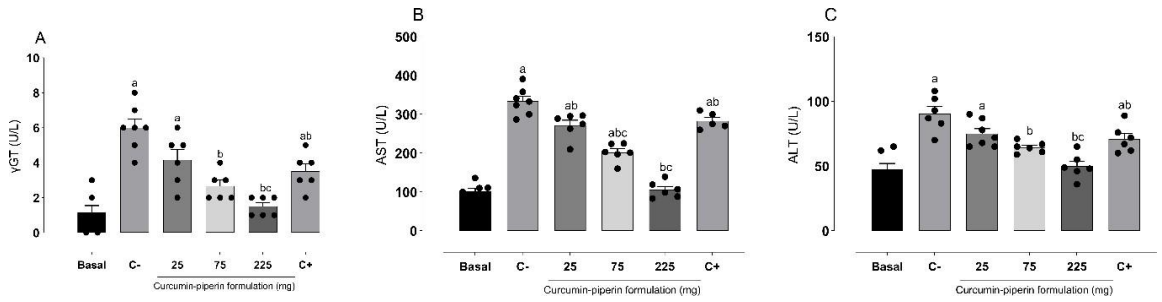

Figure 3. Serum levels of (**A**) γ-glutamyl transferase (γGT), (**B**) aspartate aminotransferase (AST), and (**C**) alanine aminotransferase (ALT). Basal: healthy rats not subjected to the disease model and treated with vehicle. C–: rats subjected to hypertension, dyslipidemia, and fructose consumption, treated with vehicle. 25, 75, and 225: rats subjected to the disease model and treated with the curcumin–piperine microparticles at doses of 25, 75, or 225 mg/kg, respectively. C+: rats subjected to the disease model and treated with enalapril plus simvastatin. *n* = 6-7 animals per group. Data are expressed as mean ± SEM. $^{a}p < 0.05$ *vs*. Basal; $^{b}p < 0.05$ *vs*. C–; $^{c}p<0.05$ *vs*. C+ (one-way ANOVA followed by Tukey's post hoc test).

The marked reductions in AST, ALT, and γ-GT observed in the present preclinical study following treatment with curcumin–piperine microparticles indicate a significant hepatoprotective effect in this cardiometabolic model. In the experimental design adopted, animals were treated for four weeks with curcumin–piperine microparticles at doses ranging from 25 to 225 mg/kg/day. The highest dose produced reductions in hepatic enzyme levels that exceeded those observed with conventional pharmacological therapy, suggesting that enhanced bioavailability and dose-dependent exposure may contribute to the restoration of hepatic biochemical homeostasis under cardiometabolic stress conditions.

Clinical evidence provides partial support for these findings. In a randomized, double-blind, placebo-controlled clinical trial conducted in patients with non-alcoholic fatty liver disease (NAFLD), Panahi et al. (2017) demonstrated that supplementation with curcumin (1000 mg/day) for eight weeks significantly reduced serum ALT and AST levels and improved several metabolic parameters associated with hepatic steatosis. Similarly, Safari et al. (2023), in a randomized clinical trial involving NAFLD patients treated with curcumin (250 mg/day) for eight weeks, reported improvements in liver enzyme activity and metabolic markers. These findings support the hepatoprotective potential of curcumin in clinical settings, although the magnitude of enzyme reductions observed in human studies is generally more moderate than those reported in controlled experimental models.

Additional evidence is provided by a meta-analysis of randomized controlled trials conducted by Jalali et al. (2020), which evaluated the effects of curcumin supplementation in patients with NAFLD. Across studies lasting approximately 8–12 weeks and using curcumin doses ranging from about 80 to 1500 mg/day, the authors reported significant reductions in ALT and AST levels, confirming a consistent beneficial effect of curcumin on markers of hepatocellular injury. However, reductions in γ-GT were less consistently observed across clinical trials, possibly reflecting differences in disease severity, baseline hepatic dysfunction, or the bioavailability of the formulations used.

Collectively, these findings indicate that curcumin supplementation may contribute to the improvement of biochemical markers of hepatic injury across different cardiometabolic contexts, particularly when administered in formulations designed to enhance systemic bioavailability. Considering that hepatic dysfunction frequently coexists with systemic metabolic disturbances and impairment of other target organs, including the kidney, these results reinforce the potential of curcumin to modulate multiple components of cardiometabolic syndrome.

3.6. Renoprotective effects of curcumin–piperine microparticles

The combined induction of hypertension, dyslipidemia, and fructose consumption resulted in pronounced renal dysfunction, as evidenced by a significant increase in plasma urea levels. The untreated disease model group (C–) exhibited urea concentrations of 62.00 ± 3.70 mg/dL, significantly higher than those observed in basal animals (27.86 ± 2.32 mg/dL). Treatment with curcumin–piperine microparticles at doses of 25 and 75 mg/kg produced partial reductions in urea levels, reaching 47.67 ± 1.96 and 35.67 ± 2.69 mg/dL, respectively. Administration of the highest dose (225 mg/kg) resulted in complete normalization of urea concentrations (26.50 ± 1.67 mg/dL), with values comparable to those of healthy controls. In contrast, the C+ group, treated with enalapril and simvastatin, exhibited only partial reduction in urea levels (43.00 ± 2.76 mg/dL), indicating incomplete reversal of renal impairment (Figure 4B).

A similar pattern was observed for plasma creatinine levels. Animals in the C– group showed a significant elevation in creatinine concentrations (47.33 ± 2.28 µmol/L) compared with basal animals (31.86 ± 1.46 µmol/L), confirming renal dysfunction induced by cardiometabolic risk factors. Treatment with curcumin–piperine microparticles at doses of 25 and 75 mg/kg resulted in partial reductions in creatinine levels, reaching 40.33 ± 2.28 and 33.17 ± 2.14 µmol/L, respectively. Notably, administration of the 225 mg/kg dose fully restored creatinine concentrations to values comparable to those of the basal group (28.00 ± 1.89 µmol/L). In contrast, the C+ group did not exhibit significant improvement in creatinine levels (45.43 ± 2.09

µmol/L), indicating the absence of a renoprotective effect on this parameter under the experimental conditions employed (Figure 4C). In addition to biochemical markers of renal function, macroscopic analysis demonstrated a significant increase in kidney weight relative to body weight in the untreated disease model group (C–), consistent with renal hypertrophy associated with cardiometabolic injury. Treatment with curcumin–piperine microparticles, particularly at the 225 mg/kg dose, attenuated this increase, restoring relative kidney weight to values comparable to those observed in basal animals, whereas only partial normalization was observed in the C+ group (Figure 4A). These findings indicate that the improvements in renal biochemical markers were accompanied by preservation of renal morphology.

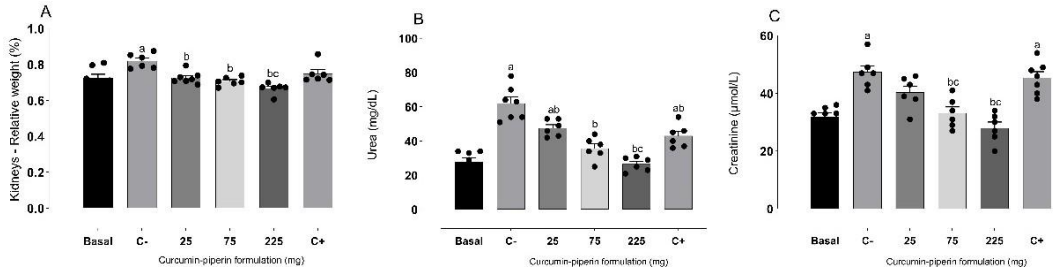

Figure 4. Renal parameters in rats exposed to the cardiometabolic disease model and treated with curcumin–piperine microparticles. Relative kidney weight (A) and plasma levels of (B) urea and (C) creatinine. Basal: healthy rats not exposed to the disease model and treated with vehicle. C–: rats exposed to hypertension, dyslipidemia, and fructose consumption and treated with vehicle. 25, 75, and 225: rats exposed to the disease model and treated with the curcumin–piperine formulation at doses of 25, 75, or 225 mg/kg, respectively. C+: rats exposed to the disease model and treated with enalapril plus simvastatin. Data are expressed as mean ± SEM (n = 6–7 animals per group). Different letters indicate statistically significant differences ($p < 0.05$): a vs. Basal; b vs. C–; c vs. C+ (one-way ANOVA followed by Tukey's post hoc test).

Previous studies consistently demonstrate the renoprotective potential of curcumin, primarily evidenced by reductions in urea and creatinine levels across different models of renal injury. The seminal review by Trujillo et al. (2013) described that curcumin attenuates elevations in these markers in models of drug-induced nephrotoxicity, ischemia–reperfusion injury, and partial nephrectomy. These effects are largely attributed to its antioxidant and anti-inflammatory actions within renal tissue, including attenuation of oxidative stress, inflammation, and apoptosis.

Similar renoprotective effects have been reported in experimental models of metabolic and oxidative renal injury. In streptozotocin-induced diabetic rats, curcumin administration

attenuated renal dysfunction and fibrosis through inhibition of protein kinase C signaling and inflammatory pathways (Soetikno et al., 2013). Experimental studies have also demonstrated that curcumin activates the Nrf2 antioxidant pathway and reduces apoptosis and oxidative stress in renal tissue, contributing to improvements in serum urea and creatinine levels (Cui et al., 2014). More recent evidence further indicates that curcumin improves renal function through modulation of redox and inflammatory pathways, including Nrf2 and NF-κB signaling, while attenuating structural alterations in renal tissue (Saberian et al., 2022).

Contemporary literature indicates that the pleiotropic antioxidant and anti-inflammatory actions of curcumin may distinguish it from conventional pharmacological therapies that primarily target individual cardiometabolic risk factors. In the present study, the reference therapy consisted of enalapril, an angiotensin-converting enzyme inhibitor widely used for blood pressure control and reduction of glomerular hemodynamic stress, and simvastatin, a lipid-lowering statin commonly prescribed to manage dyslipidemia and reduce cardiovascular risk. Although these agents are effective in addressing major cardiometabolic abnormalities, their direct effects on renal biochemical markers may vary depending on disease severity, baseline renal function, and treatment duration.

ACE inhibitors such as enalapril reduce intraglomerular pressure by dilating the efferent arteriole, thereby decreasing glomerular hyperfiltration and providing long-term renoprotective benefits in several cardiometabolic conditions. However, this mechanism can transiently reduce glomerular filtration rate and increase serum creatinine in susceptible individuals, reflecting the hemodynamic adjustments induced by these agents. More broadly, cardiovascular drugs may exert heterogeneous renal effects because the kidneys are continuously exposed to circulating xenobiotics and their metabolites, making renal tissues particularly susceptible to functional alterations depending on drug class, dosage, and duration of exposure (Caiati et al., 2025).

Similarly, statins primarily exert their therapeutic effects through lipid lowering and cardiovascular risk reduction. Evidence regarding their direct impact on renal function remains heterogeneous. Some clinical studies and meta-analyses suggest modest improvements in renal parameters such as albuminuria or creatinine clearance, whereas others report limited effects on estimated glomerular filtration rate or serum creatinine levels during long-term treatment (Zhao et al., 2021).

Accumulating experimental and translational evidence indicates that curcumin exerts multifaceted nephroprotective actions. These include attenuation of oxidative stress, suppression of inflammatory signaling pathways, and modulation of metabolic processes involved in renal injury. In particular, curcumin has been shown to inhibit pro-inflammatory

transcription factors such as NF-κB, enhance endogenous antioxidant defenses, and reduce fibrotic signaling pathways associated with renal tissue damage (Ofori-Attah et al., 2025).

Taken together, these findings indicate that the curcumin–piperine microparticle formulation effectively attenuated renal dysfunction associated with the cardiometabolic disease model, restoring plasma urea and creatinine levels toward values observed in healthy animals. The pronounced normalization observed at the highest dose suggests that improved curcumin bioavailability may enhance its systemic biological activity, particularly when pharmacotechnical strategies are used to increase intestinal absorption and metabolic stability of the compound (Bertoncini-Silva et al., 2024).

The pronounced normalization observed at the highest dose suggests that improved curcumin bioavailability may enhance its systemic biological activity, particularly when pharmacotechnical strategies are used to increase intestinal absorption and metabolic stability of the compound (Bertoncini-Silva et al., 2024).

Renal dysfunction in cardiometabolic disorders results from the interaction of multiple pathophysiological mechanisms, including hemodynamic alterations, metabolic disturbances, oxidative stress, and systemic inflammation. Therefore, the renoprotective effects observed in the present study likely reflect the integrated cardiometabolic improvements induced by curcumin treatment. Among these mechanisms, chronic low-grade inflammation plays a central role in the progression of renal injury, which makes the modulation of inflammatory mediators particularly relevant. The effects of the curcumin–piperine formulation on systemic inflammatory markers are therefore described in the following section.

3.7. Curcumin–piperine microparticles reduce TNF-α and IL-6 levels

Induction of the disease model resulted in a pronounced systemic inflammatory response, as evidenced by a significant increase in plasma TNF-α levels. The untreated disease model group (C–) exhibited TNF-α concentrations of 60.66 ± 2.02 pg/mL, markedly higher than those observed in the basal group (22.12 ± 0.63 pg/mL), confirming inflammatory activation driven by cardiometabolic risk factors. Treatment with curcumin–piperine microparticles at doses of 25 and 75 mg/kg significantly reduced TNF-α levels to 41.30 ± 1.79 and 40.03 ± 1.46 pg/mL, respectively, although values remained above basal levels. Administration of the highest dose (225 mg/kg) produced a more pronounced reduction, yielding TNF-α concentrations of 25.26 ± 0.63 pg/mL, statistically comparable to both the basal group and the C+ (26.27 ± 1.37 pg/mL). These findings indicate that the higher dose of the microparticle formulation effectively normalized TNF-α-mediated inflammatory responses (Figure 5A).

A similar pattern was observed for plasma IL-6 levels. Animals in the C– group showed a marked elevation in IL-6 concentrations (42.26 ± 2.92 pg/mL) compared with the basal group (16.56 ± 0.47 pg/mL), confirming the establishment of a systemic inflammatory state in the experimental model. Treatment with curcumin–piperine microparticles at doses of 25 and 75 mg/kg resulted in partial reductions in IL-6 levels, reaching 26.35 ± 0.52 and 22.78 ± 0.34 pg/mL, respectively, with values still higher than those observed in healthy controls. The C+ group exhibited intermediate IL-6 concentrations (21.51 ± 0.84 pg/mL), similar to those observed in animals treated with intermediate doses of the microparticles. Notably, administration of the 225 mg/kg dose reduced IL-6 levels to 18.78 ± 0.63 pg/mL, statistically indistinguishable from basal values, indicating normalization of the induced inflammatory response (Figure 5B).

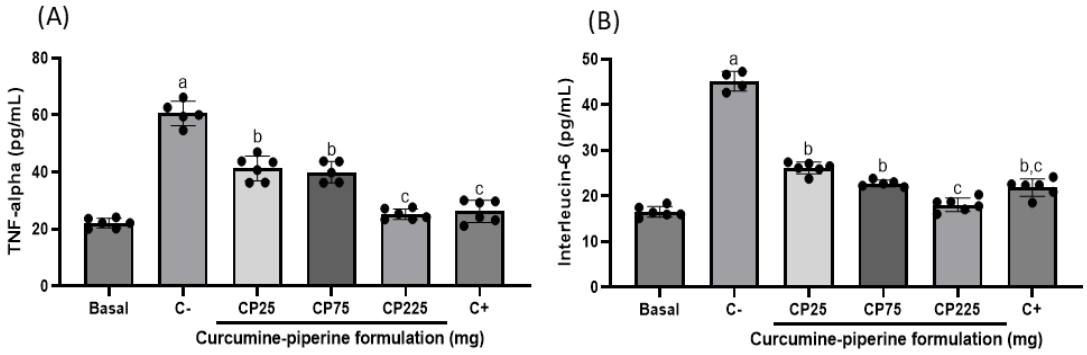

Figure 5. Plasma levels of inflammatory cytokines in rats exposed to the cardiometabolic disease model and treated with curcumin–piperine microparticles. Plasma levels of (A) TNF-α and (B) IL-6. Basal: healthy rats not exposed to the disease model and treated with vehicle. C–: rats exposed to hypertension, dyslipidemia, and fructose consumption and treated with vehicle. 25, 75, and 225: rats exposed to the disease model and treated with the curcumin–piperine formulation at doses of 25, 75, or 225 mg/kg, respectively. C+: rats exposed to the disease model and treated with enalapril plus simvastatin. Data are expressed as mean ± SEM (n = 6–7 animals per group). Different letters indicate statistically significant differences ($p < 0.05$): a vs. Basal; b vs. C–; c vs. C+ (one-way ANOVA followed by Tukey's post hoc test).

The results reinforce MetS as a state of chronic low-grade systemic inflammation, in which pro-inflammatory cytokines, particularly TNF-α and IL-6, play a central role in metabolic dysfunction, insulin resistance, and progression of cardiovascular risk (Lopez-Candales et al., 2017; Wozniak et al., 2010). The marked elevation of these mediators in the untreated disease model group confirms the effectiveness of the inflammatory phenotype induction, in line with evidence linking visceral adiposity and metabolic dysfunction to sustained increases in IL-6

and TNF-α. Treatment with curcumin–piperine microparticles promoted a dose-dependent reduction in these cytokines, consistent with studies demonstrating enhanced anti-inflammatory efficacy of formulations with improved bioavailability compared with free curcumin (Bulboacă et al., 2019; Rinkunaite et al., 2021).

Particular attention should be given to the behavior of IL-6, a cytokine known to be more resistant to complete normalization in chronic metabolic inflammation, even under standard pharmacological therapy (Lopez-Candales et al., 2017). In this regard, the intermediate IL-6 levels observed in the C+ group treated with enalapril, and simvastatin suggest the persistence of residual inflammation, a phenomenon frequently described in the literature. In contrast, normalization of this marker observed exclusively with the highest dose of the microparticle formulation indicates a more comprehensive anti-inflammatory effect. This finding suggests that the curcumin–piperine formulation may more effectively modulate inflammatory pathways directly involved in IL-6 regulation, such as NF-κB and JAK/STAT-3 signaling, partially overcoming the limitations of conventional pharmacotherapy in controlling systemic inflammation associated with MetS (Zhong et al., 2020; Dokumacioglu et al., 2025).

3.8. Curcumin–piperine microparticles modulate the gut microbiota

3.8.1 Alpha diversity and global structure of the gut microbiota

The diversity analysis revealed consistent differences among the experimental groups, reflecting changes in the richness, diversity, and evenness of the intestinal microbiota. Taxonomic richness was estimated using the number of observed ASVs (Amplicon Sequence Variants) and the Chao1 index, whereas diversity was assessed using the Shannon index, which integrates richness and the distribution of abundances. Evenness was evaluated using the Pielou index (Figures 6A–6C).

The basal group exhibited the highest values of observed ASVs and Chao1, accompanied by elevated Shannon and Pielou indices, characterizing a more diverse and ecologically balanced microbial community (Figure 6). In contrast, the negative and positive control groups showed a consistent reduction in these parameters, indicating a loss of taxonomic richness and increased dominance by a limited number of taxa, a pattern commonly associated with dysbiosis in cardiometabolic contexts (Gurung et al., 2020; Wang et al., 2020). This finding is consistent with the literature describing reduced microbial diversity in obesity, type 2 diabetes, and metabolic

syndrome, conditions frequently associated with metabolic inflammation and decreased functional redundancy of the microbiome (Fan & Pedersen, 2021).

High microbial diversity is considered one of the main indicators of ecological stability in the intestinal ecosystem. More diverse microbial communities tend to exhibit greater functional redundancy and an enhanced capacity to withstand metabolic and environmental perturbations (Tilg & Adolph, 2021). Therefore, the reduction in diversity observed in the control groups may reflect impairment of the ecological stability of the intestinal microbiota and a potential decrease in the functional diversity of microbial metabolic pathways.

Animals treated with curcumin–piperine microparticles (225 mg/kg) also showed lower diversity indices relative to the basal group; however, they exhibited greater diversity and evenness compared with the control groups (C− and C+), with higher Shannon and Pielou values. Although these levels were not fully restored, the observed profile suggests a partial reorganization of the bacterial community and attenuation of dysbiosis.

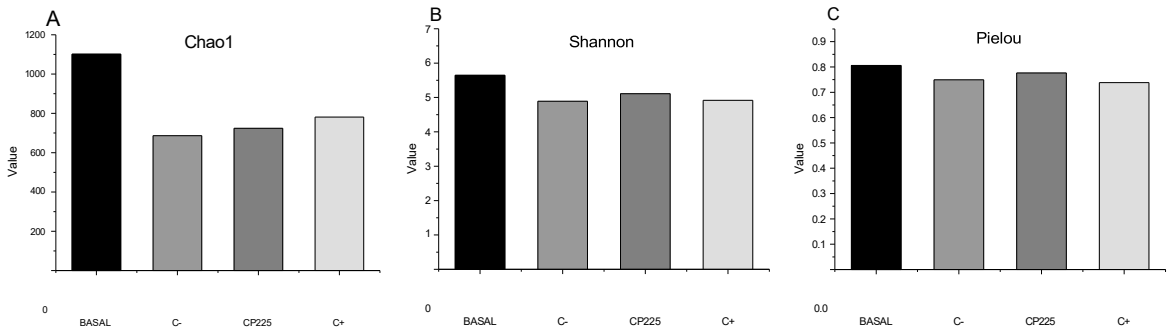

Figure 6. Alpha-diversity of the gut microbiota in rats exposed to the cardiometabolic disease model and treated with curcumin–piperine microparticles. Alpha-diversity was assessed using richness (Chao1), diversity (Shannon), and evenness (Pielou) indices. Basal: healthy rats not exposed to the disease model and treated with vehicle. C–: rats exposed to hypertension, dyslipidemia, and fructose consumption and treated with vehicle. 225: rats exposed to the disease model and treated with the curcumin–piperine formulation at a dose of 225 mg/kg. C+: rats exposed to the disease model and treated with enalapril plus simvastatin.

This pattern is consistent with the modulatory effect attributed to curcumin, which has been described as capable of altering intestinal microbial composition and promoting the expansion of metabolically favorable bacterial communities (Li et al., 2020; Zhang et al., 2022). The

interaction between plant-derived bioactive compounds and the intestinal microbiota has been recognized as an important mechanism of metabolic modulation, as these compounds may act both as substrates and as modulators of bacterial growth.

3.8.2 Taxonomic composition of the gut microbiota at phylum and class levels

The overall taxonomic composition revealed a predominance of the phyla Bacteroidota and Firmicutes (Bacillota) across all experimental groups (Figure 7A), a pattern commonly observed in the mammalian intestinal microbiota (Wang et al., 2020). The basal group showed a higher relative contribution of Firmicutes (52.3%), whereas the negative and positive control groups exhibited a greater abundance of Bacteroidota (63.6% and 63.2%, respectively). The CP225-treated group displayed an intermediate profile, with 37.7% Firmicutes and 51.0% Bacteroidota, suggesting a moderate redistribution of the dominant phyla.

At the class level, Clostridia and Bacteroidia were the most abundant groups (Figure 7B). While the basal group showed a predominance of Clostridia (49%), the C− and C+ groups presented a relative increase in Bacteroidia, reinforcing a pattern of microbial reorganization associated with an altered metabolic state. Treatment with CP225 also resulted in an intermediate composition, characterized by the maintenance of Clostridia at moderate levels (27.2%) and an increase in Bacilli (7.7%), suggesting structural modulation of the intestinal microbiota.

These changes are particularly relevant because the class Clostridia includes several bacterial groups capable of producing short-chain fatty acids (SCFAs), especially butyrate, propionate, and acetate, metabolites that play a central role in the metabolic communication between the microbiota and the host (Louis & Flint, 2017). SCFAs are primarily generated through the bacterial fermentation of non-digestible complex carbohydrates, such as dietary fibers and resistant starch.

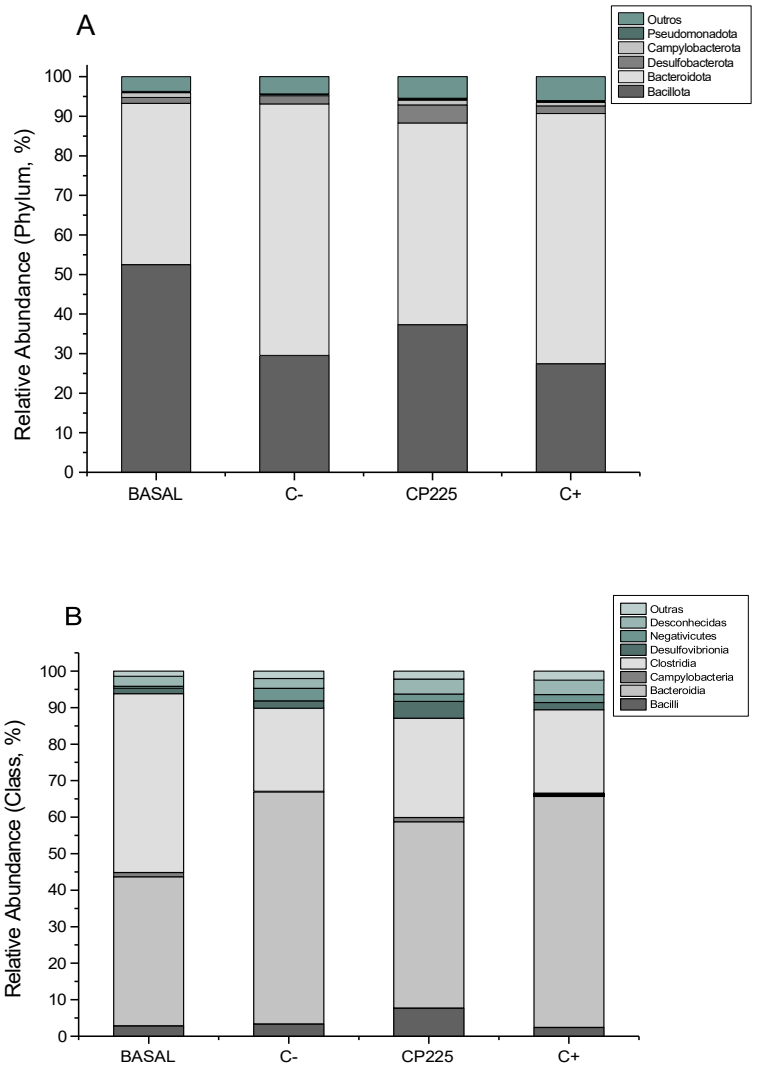

Figure 7. Global taxonomic composition of the gut microbiota in rats exposed to the cardiometabolic disease model and treated with curcumin–piperine microparticles**.** Relative abundance of bacterial taxa at the phylum (A) and class (B) levels across experimental groups. Stacked bar plots represent taxa with a relative abundance ≥ 2% in at least one experimental group. Basal: healthy rats not exposed to the disease model and treated with vehicle. C–: rats exposed to hypertension, dyslipidemia, and fructose consumption and treated with vehicle. 225: rats exposed to the disease model and treated with the curcumin–piperine formulation at a dose of 225 mg/kg. C+: rats exposed to the disease model and treated with enalapril plus simvastatin.

The production of these metabolites occurs predominantly in the large intestine, where microbial density is highest and the availability of fermentable substrates is greater. In rodents,

the cecum represents the main site of bacterial fermentation, accounting for a substantial proportion of SCFA production due to its highly developed anatomy and the intense metabolic activity of the microbiota inhabiting this region (den Besten et al., 2013; Koh et al., 2016).

SCFAs exert several important physiological effects, including maintenance of intestinal barrier integrity, modulation of inflammatory responses, and regulation of host energy metabolism (Koh et al., 2016). Experimental evidence also indicates that microbiota-derived metabolites can contribute to the regulation of intestinal barrier integrity through modulation of epithelial junction proteins. In a model of spontaneously hypertensive rats, for example, administration of Ligilactobacillus murinus restored the expression of tight junction proteins, reduced intestinal permeability, and decreased circulating endotoxin levels, demonstrating the direct influence of the microbiota on intestinal barrier integrity and cardiovascular pathophysiology (Mukohda et al., 2023).

Therefore, the relative reduction of Clostridia observed in the C− and C+ groups may reflect a loss of microbial metabolic functions associated with fiber fermentation and the production of these beneficial metabolites.

3.8.4 Intermediate structure of the gut microbiota: orders and families

The analysis at intermediate taxonomic levels reinforced the patterns observed at higher levels of intestinal microbiota organization. The negative control (C−) and positive control (C+) groups showed a higher abundance of orders associated with Bacteroidales (63.6% and 64.2%, respectively), whereas the basal group exhibited a greater relative contribution of Clostridiales, indicating a microbial structure more closely associated with metabolically balanced physiological profiles.

The CP225-treated group displayed intermediate values of Bacteroidales (50.1%), lower than those observed in the control groups, along with a relative increase in orders belonging to Clostridiales, including Erysipelotrichales, Desulfovibrionales, and Selenomonadales. This redistribution suggests a partial reorganization of the bacterial community toward a functionally more diverse profile.

Among the orders that increased following treatment, Erysipelotrichales has been associated with bacterial fermentation processes and the metabolism of diet-derived compounds, whereas Selenomonadales includes fermentative bacteria capable of participating in the production of intermediate organic metabolites used in microbial metabolic networks. Members of the order Desulfovibrionales, in turn, belong to the group of sulfate-reducing bacteria and participate in the metabolism of sulfur-containing compounds, producing hydrogen sulfide (H_2S), a

metabolite that may exert regulatory effects on the intestinal mucosa depending on its concentration and on the ecological context of the microbiota (Carbonero et al., 2012).

A similar pattern was observed at the family taxonomic level. At the family level, *Lachnospiraceae*, *Ruminococcaceae*, *Oscillospiraceae*, and *Bacteroidaceae* were the most prominent taxa. The C- and C+ groups exhibited predominance of families associated with the class *Bacteroidia*, whereas the basal group showed greater diversity of families belonging to *Clostridia*. Treatment with CP225 promoted a relative increase in families associated with the fermentation of complex carbohydrates and SCFA production, particularly those belonging to *Clostridia*, concomitant with a reduction in families frequently associated with dysbiotic profiles described in experimental models of metabolic syndrome.

Bacterial families belonging to Clostridia include numerous fermentative microorganisms capable of converting non-digestible dietary substrates into bioactive metabolites such as butyrate and propionate, thereby playing a central role in metabolic homeostasis and the maintenance of intestinal barrier integrity (Louis & Flint, 2017; Koh et al., 2016). In addition, SCFAs produced by these bacteria may participate in the regulation of intestinal gluconeogenesis, a metabolic process in which the small intestine synthesizes glucose from non-carbohydrate precursors. This mechanism, particularly stimulated by propionate and butyrate, can activate metabolic circuits along the gut–brain axis and contribute to improved insulin sensitivity and glycemic homeostasis (De Vadder et al., 2014).

Thus, the relative increase in groups belonging to Clostridia observed after treatment suggests a partial recovery of the metabolic functionality of the intestinal microbiota, reflecting a possible enhancement of the fermentative capacity of the microbial ecosystem and increased production of metabolites with beneficial metabolic effects.

3.8.4 Modulation of the gut microbiota at the genus level

Samples were arranged according to biological grouping (Basal, C-, CP225, C+) to facilitate interpretation of microbiome shifts across experimental conditions. Hierarchical clustering of genus-level relative abundance (Figure 8) highlighted that the CP225-treated group displayed a distinct compositional profile compared to control groups (C- and C+), occupying an intermediate position between the basal and metabolic syndrome groups. This pattern suggests that the intervention promoted a partial reorganization of the intestinal microbial community, without fully restoring the profile observed in the basal group. This behavior reinforces the modulatory, rather than fully normalizing, effect of the treatment on intestinal microbiota composition, in agreement with the results observed for alpha diversity indices and for the overall taxonomic structure of the microbiota.

At the genus level, differences among groups were even more evident. The C− and C+ groups exhibited a high relative abundance of *Prevotella* (43.4% and 48.1%, respectively), which constituted the dominant genus, along with the presence of *Alloprevotella*, forming a profile frequently observed in less balanced microbiotas.

The predominance of *Prevotella* observed in the control groups may reflect alterations in the ecological structure of the intestinal microbiota associated with altered metabolic states. Although species within this genus play important roles in the fermentation of complex carbohydrates, excessive dominance of *Prevotella* has often been reported in microbiotas characterized by lower diversity and greater metabolic specialization (Gurung et al., 2020; Wang et al., 2020). From an ecological perspective, this pattern may indicate a reduction in the functional diversity of the microbial ecosystem, favoring simplified communities dominated by a limited number of bacterial groups. In contrast, metabolically healthy microbiotas tend to exhibit greater diversity of fermentative genera and producers of beneficial metabolites, reflecting higher ecological complexity and greater functional redundancy (Fan & Pedersen, 2021).

In contrast, the basal group displayed a more diverse configuration, with lower abundance of *Prevotella* (23.8%) and greater representation of genera such as *Lepagella*, *Dysosmobacter*, *Roseburia*, and *Ligilactobacillus*.

Treatment with CP225 reduced the dominance of *Prevotella* and promoted an increase in genera potentially involved in short-chain fatty acid (SCFA) production, including *Roseburia*, *Faecousia*, and *Dysosmobacter*, as well as an increase in *Dubosiella*, *Taurinivorans*, and *Bacteroides*. This rearrangement suggests a transition toward a functionally more diverse microbial profile.

Genera such as *Roseburia* are recognized butyrate producers and have been associated with improved insulin sensitivity, reduced metabolic inflammation, and maintenance of intestinal barrier integrity (Louis & Flint, 2017; Gurung et al., 2020). The increase in *Dubosiella* observed in the treated group has also been associated with improved intestinal barrier function and modulation of metabolic inflammation in experimental models (Yang et al., 2019).

In addition, two genera that increased exclusively in the CP225 group, *Desulfovibrio* and *Taurinivorans*, point to potential shifts in metabolic pathways associated with sulfur compound metabolism. In line with their established role as sulfate-reducing bacteria, *Desulfovibrio* spp. are linked to the production of hydrogen sulfide (H_2S), a metabolite whose effects on the intestinal mucosa are context-dependent, varying according to its concentration and the ecological configuration of the microbiota (Carbonero et al., 2012).

Taurinivorans, in turn, is associated with the metabolism of taurine and bile acid–derived compounds, potentially participating in metabolic interactions between the intestinal microbiota and host lipid metabolism (Ridlon et al., 2016; Kozakia et al., 2022). Alterations in these metabolic pathways have been linked to modulation of intestinal metabolic signaling and host energy metabolism.

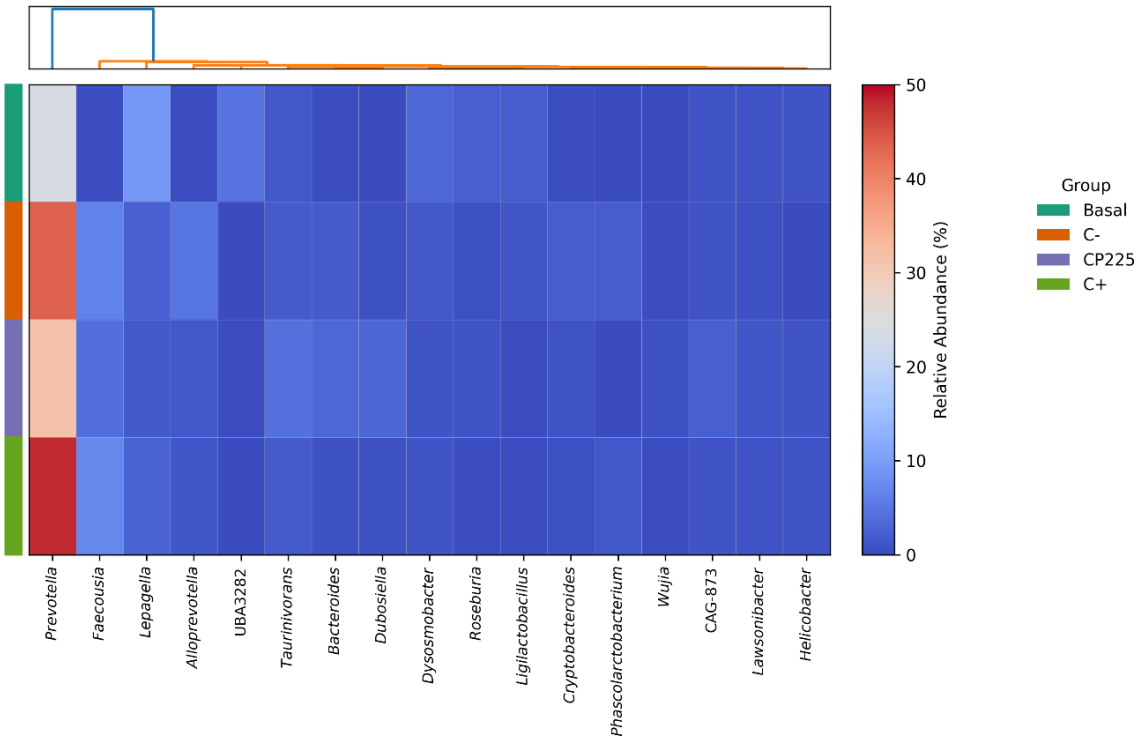

Figure 8. Heatmap of the relative abundance of the main bacterial genera of the gut microbiota in rats exposed to the cardiometabolic disease model and treated with curcumin–piperine microparticles. Heatmap representing the relative abundance (%) of the predominant bacterial genera across experimental groups. Hierarchical clustering based on relative abundance was applied to both genera (horizontal axis) and experimental groups (vertical axis). Color intensity represents relative abundance, ranging from blue (low abundance) to red (high abundance). Basal: healthy rats not exposed to the disease model and treated with vehicle. C–: rats exposed to hypertension, dyslipidemia, and fructose consumption and treated with vehicle. 225: rats exposed to the disease model and treated with the curcumin–piperine formulation at a dose of 225 mg/kg. C+: rats exposed to the disease model and treated with enalapril plus simvastatin.

The reorganization of the gut microbiota at the genus level, characterized by reduced dominance of a limited number of taxa and increased relative abundance of functionally

relevant genera, is further illustrated by the log-transformed (log10) relative abundance heatmap presented in Supplementary Figure S1

3.8.5 Species-level profile and functional redistribution of the gut microbiota

At the species level, a pattern consistent with the alterations described at higher taxonomic levels was observed. The control groups (C- and C+) (C- and C+) exhibited a marked predominance of species belonging to the genus *Prevotella*, consistent with a microbial profile enriched in carbohydrate-fermenting bacteria that are frequently associated with altered metabolic states.

The basal group showed a higher relative abundance of species belonging to the genus *Lepagella*, reflecting a more diverse microbial composition with lower dominance of a single taxon.

In animals treated with CP225, a reduction in the dominance of *Prevotella* species was observed, accompanied by a relative increase in multiple species associated with genera potentially involved in the production of short-chain fatty acids (SCFAs) and related to the maintenance of intestinal barrier integrity, including *Dubosiella*. This redistribution resulted in greater relative diversity among the dominant species, with reduced predominance of a single taxon and a greater contribution of functionally relevant species, suggesting partial reorganization of the ecological balance of the intestinal microbiota.

This pattern is consistent with the hypothesis that interventions capable of modulating the intestinal microbiota may promote redistribution of dominant bacterial populations, favoring microbial communities that are functionally more diverse and metabolically more stable.

To facilitate the visualization of these alterations, the relative abundance of selected bacterial species is presented in a supplementary figure (S2). Taxa were prioritized based on their direct relevance to the central biological axis identified in this study, including species belonging to the genera *Prevotella*, *Faecousia*, *Taurinivorans*, and *Dubosiella* (Supplementary Table S1). Overall, the CP225 group exhibits a more uniform distribution of the selected species, in contrast to the C- e C+ groups, which are characterized by a greater predominance of specific taxa.

To facilitate visualization of these alterations, the relative abundance of selected bacterial species is presented in a supplementary figure (S2). Taxa directly related to the central biological axis identified in this study were prioritized, including species belonging to the genera *Prevotella*, *Faecousia*, *Taurinivorans*, and *Dubosiella* (Supplementary Table S1).

It is important to consider that taxonomic identification at the species level based on 16S rRNA gene sequencing has inherent limitations related to the taxonomic resolution of this approach. In many cases, the amplified regions of the 16S gene do not allow precise discrimination between closely related species, and thus species-level classification should be interpreted with caution. Accordingly, although the patterns observed in this study provide relevant insights into the redistribution of dominant bacterial populations, the functional interpretation of the gut microbiota was primarily conducted at higher taxonomic levels, such as genus and family, where classification reliability is generally more robust (Johnson et al., 2019).

3.8.6 Firmicutes/Bacteroidetes (F/B) ratio

The Firmicutes/Bacteroidetes (F/B) ratio was calculated based on the relative abundance of the major bacterial phyla. The basal group exhibited higher values of this ratio, whereas the control groups showed reduced ratios, reflecting a greater relative proportion of Bacteroidota. The CP225-treated group displayed intermediate values, indicating partial modulation of the intestinal microbiota compared with the control groups (Supplementary Figure S3).

The F/B ratio has been widely investigated as a potential marker of intestinal microbiota alterations associated with obesity and metabolic syndrome. Early studies suggested that shifts in this index could reflect changes in the metabolic capacity of the microbiota, particularly regarding the efficiency of dietary energy extraction. However, more recent evidence indicates that this ratio shows substantial variability across individuals, populations, and experimental models and may be influenced by factors such as diet, age, host characteristics, and analytical methodology (Magne et al., 2020).

Therefore, although the F/B ratio can provide a general overview of the structural organization of the intestinal microbiota, its interpretative value is limited when considered in isolation. In the present study, this parameter was used primarily as a complementary descriptive indicator, whereas the biological interpretation of microbial modulation relied mainly on the alterations observed at lower taxonomic levels, including order, family, and genus, which provide greater functional resolution of the microbial community.

3.8.7 Interplay between intestinal microbiota dysbiosis, metabolic inflammation, and curcumin–piperine intervention

The results indicate that metabolic syndrome is associated with profound reorganization of the intestinal microbiota, characterized by reduced microbial diversity and alterations in bacterial

community structure. This pattern is consistent with the literature describing intestinal dysbiosis as a central component of cardiometabolic pathophysiology (Gurung et al., 2020; Tilg & Adolph, 2021), as showed in Figure 9.

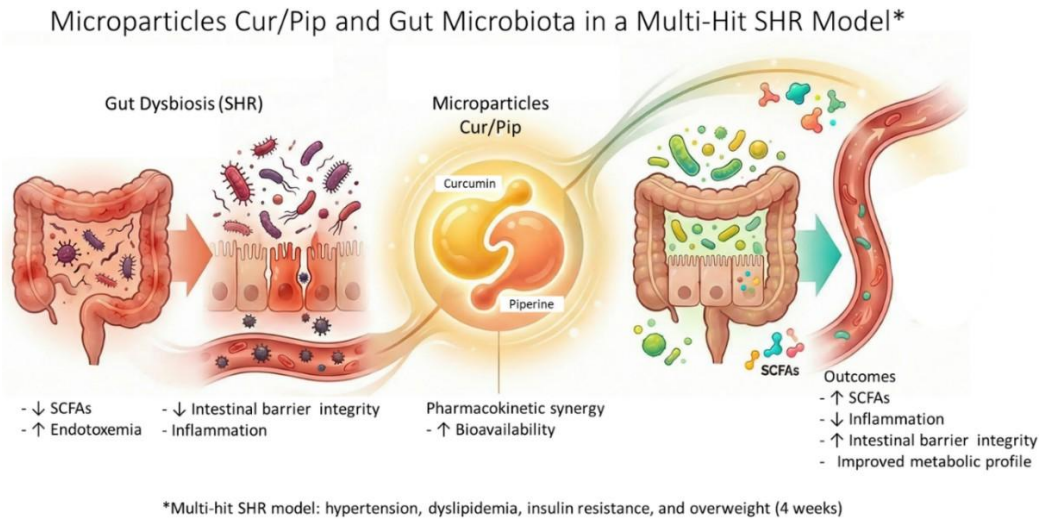

Figure 9. Mechanistic interplay between intestinal dysbiosis and curcumin–piperine microparticle intervention in a multi-hit SHR model. Metabolic syndrome in spontaneously hypertensive rats (SHR) is associated with intestinal dysbiosis and related metabolic disturbances, including alterations in microbial-derived metabolites, barrier dysfunction, endotoxemia, and low-grade inflammation. Administration of curcumin–piperine (Cur/Pip) microparticles enhances curcumin bioavailability through pharmacokinetic synergy, promoting prolonged intestinal exposure. This intervention modulates gut microbiota composition and function, contributing to increased SCFA production, improved barrier integrity, reduced inflammation and endotoxemia, and overall improvement in metabolic profile. The multi-hit SHR model includes hypertension, dyslipidemia, insulin resistance, and overweight.

In this context, short-chain fatty acids (SCFAs) represent key mediators of the interaction between the intestinal microbiota and host metabolism, contributing to immune modulation, maintenance of intestinal barrier function, and regulation of energy homeostasis (Koh et al., 2016; Louis & Flint, 2017).

The reorganization observed in the intestinal microbiota following curcumin–piperine treatment suggests not only structural changes in bacterial composition but also functional adaptations within the microbial ecosystem. The enrichment of SCFA-producing bacteria, along with microorganisms involved in sulfur compound and bile acid metabolism, indicates diversification

of microbial metabolic pathways. Such changes may expand host–microbiota interactions and contribute to the regulation of metabolic and inflammatory processes, as well as intestinal barrier integrity.

These findings support the hypothesis that intestinal dysbiosis contributes to cardiovascular pathophysiology through mechanisms involving barrier dysfunction and metabolic endotoxemia. Indeed, studies in spontaneously hypertensive models have demonstrated that modulation of the intestinal microbiota can restore mucosal integrity, reduce circulating endotoxin levels, and improve hemodynamic parameters, including blood pressure and endothelial function (Mukohda et al., 2023).

Thus, modulation of the intestinal microbiota may represent one of the mechanisms through which bioactive compounds such as curcumin exert systemic metabolic effects.

In addition, the presence of piperine in the formulation may potentiate the biological effects of curcumin. Piperine is recognized as a natural bioenhancer capable of significantly increasing curcumin bioavailability by inhibiting enzymes involved in its intestinal and hepatic metabolism and conjugation, including enzymes of the UDP-glucuronosyltransferase family (Shoba et al., 1998). This effect may prolong curcumin persistence in the intestinal lumen, enhancing its interaction with the intestinal microbiota. Consequently, the curcumin–piperine association may promote microbiome modulation both through direct microbial effects and through changes in the availability and metabolism of these bioactive compounds within the intestinal environment (Lopresti, 2018; Zhang et al., 2022).

Taken together, these results suggest that intervention with curcumin–piperine microparticles promotes partial reorganization of the intestinal microbiota, favoring bacterial communities associated with beneficial metabolite production and the maintenance of metabolic homeostasis.

3.2.1.32 Scientific, technological, and societal implications

Beyond the limitations discussed above, the present findings highlight the potential scientific, technological, and societal relevance of developing innovative delivery systems for bioactive compounds targeting cardiometabolic disorders. The gastro-resistant curcumin–piperine microparticle formulation investigated in this study demonstrated the capacity to modulate metabolic, inflammatory, and microbial parameters simultaneously, suggesting a multi-target mechanism of action involving both host physiology and gut microbial ecology.

From a scientific perspective, these results contribute to the growing body of evidence supporting the role of the gut microbiota as an important mediator of the systemic effects of dietary bioactive compounds. The observed partial reorganization of the microbial community toward taxa associated with short-chain fatty acid production suggests that microbiota modulation may represent one of the pathways through which curcumin-based interventions exert beneficial metabolic effects.

From a technological standpoint, the development of gastro-resistant microparticles represents an important strategy to improve the stability and intestinal delivery of curcumin, a compound known to exhibit low oral bioavailability. The protection of the bioactive compound from gastric degradation and its targeted release in the intestinal environment may enhance both host absorption and direct interactions with the intestinal microbiota. Such technological approaches may expand the potential therapeutic applications of plant-derived bioactive compounds by improving their pharmacokinetic and pharmacodynamic profiles.

From a societal and public health perspective, strategies capable of modulating the intestinal microbiota and reducing metabolic inflammation may contribute to the development of complementary approaches for the prevention and management of cardiometabolic diseases, which represent a major global health burden. The integration of nutraceutical formulations with microbiome-targeted interventions may therefore represent a promising avenue for the development of more holistic and personalized strategies for metabolic health.

3.2.1.33 Additional limitations and future research directions

Additional limitations should also be acknowledged. The experimental design employed independent treatment groups, which limits the ability to evaluate longitudinal microbiota dynamics within the same individuals. Future studies incorporating longitudinal sampling could provide deeper insight into temporal changes in microbial community structure during treatment.

Moreover, the present study evaluated the effects of the curcumin–piperine formulation as a standalone intervention. Future investigations should explore its potential synergistic effects when combined with conventional pharmacological treatments commonly used in the management of cardiometabolic disorders.

Finally, although the results suggest that microbiota modulation may contribute to the observed metabolic and inflammatory improvements, the underlying mechanisms of action remain to be fully elucidated. Further studies integrating metagenomics, metabolomics, and targeted quantification of microbial metabolites will be important to clarify the mechanistic pathways

linking the curcumin–piperine formulation, microbiota modulation, and host metabolic regulation.

4. CONCLUSIONS

This study demonstrates that gastro-resistant curcumin–piperine microparticles exert integrated beneficial effects on multiple components of metabolic syndrome in an experimental model. Treatment, particularly at 225 mg/kg, improved hemodynamic, metabolic, anthropometric, and inflammatory parameters, while also promoting hepatoprotective and renoprotective effects, indicating a broad systemic response.

These effects were accompanied by improvements in inflammatory status, including normalization of IL-6 levels, together with favorable changes in lipid metabolism, glycemic homeostasis, and hepatorenal function. In parallel, metabolic syndrome was associated with reduced gut microbial diversity and taxonomic dominance, whereas treatment promoted partial microbial reorganization characterized by increased representation of genera associated with short-chain fatty acid production.

Collectively, these findings indicate that the gastro-resistant curcumin–piperine formulation improves cardiometabolic parameters while modulating the gut microbiota–inflammation–metabolism axis. Importantly, this study provides experimental evidence that an optimized delivery system for curcumin can substantially enhance its systemic biological effects, highlighting the potential of microbiota-targeted nutraceutical formulations as complementary strategies for the integrated management of metabolic syndrome.

5. Supplementary Material – Article 3

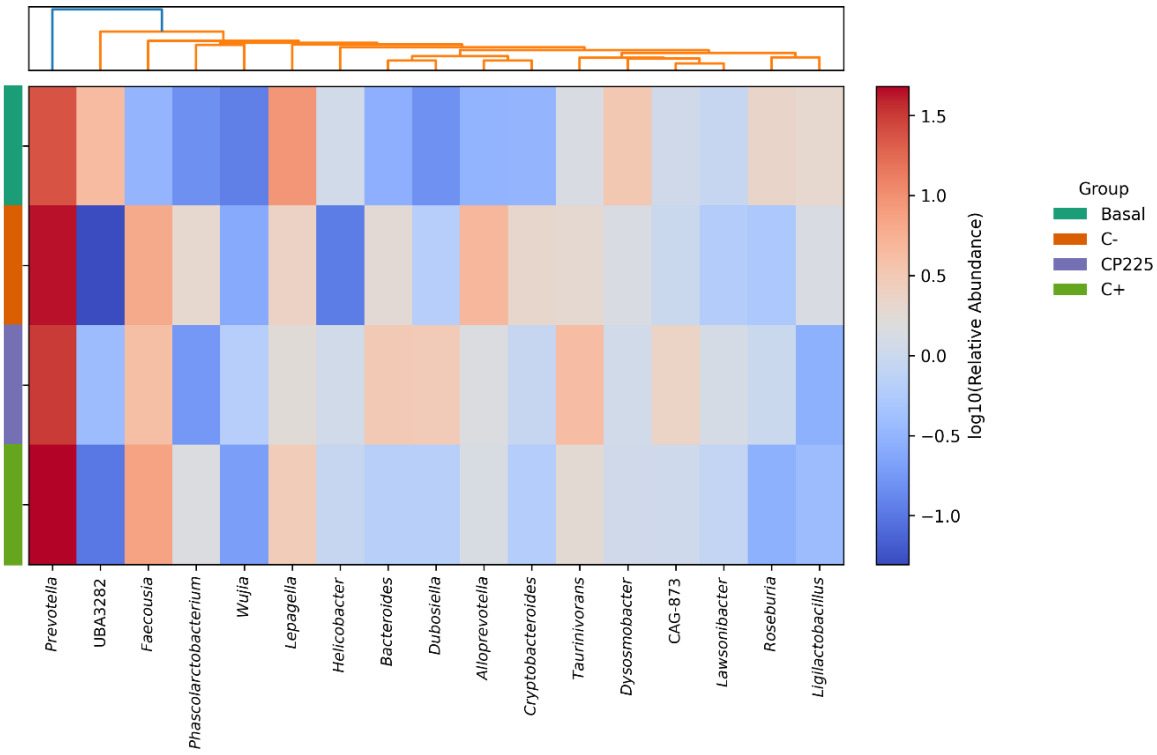

Figure S1. Heatmap of the relative abundance of the main bacterial genera of the gut microbiota in rats exposed to the cardiometabolic disease model and treated with curcumin–piperine microparticles after logarithmic transformation. Heatmap representing the relative abundance (%) of the predominant bacterial genera across experimental groups after log10 transformation to enhance the visualization of low-abundance taxa. Hierarchical clustering was applied to both bacterial genera (horizontal axis) and experimental groups (vertical axis). Color intensity represents log10-transformed relative abundance, with warmer colors indicating higher values. Basal: healthy rats not exposed to the disease model and treated with vehicle. C–: rats exposed to hypertension, dyslipidemia, and fructose consumption and treated with vehicle. 225: rats exposed to the disease model and treated with the curcumin–piperine formulation at a dose of 225 mg/kg. C+: rats exposed to the disease model and treated with enalapril plus simvastatin.

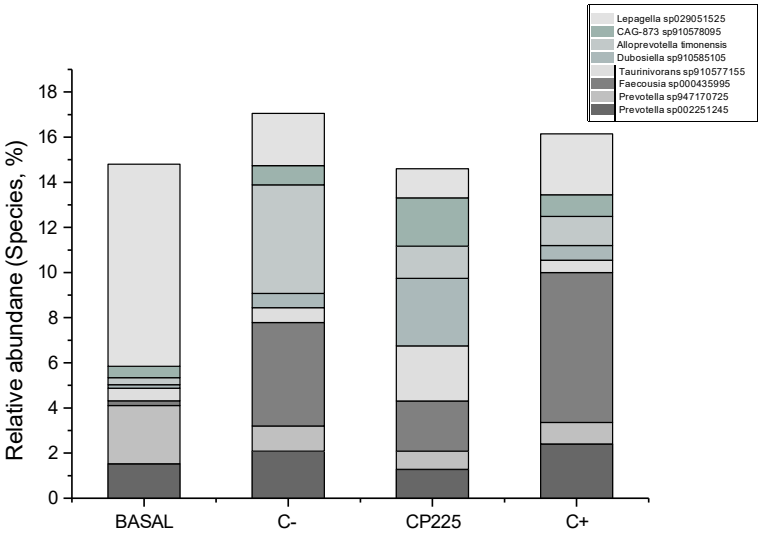

Figure S2. Relative abundance of selected bacterial species of the gut microbiota in rats exposed to the cardiometabolic disease model and treated with curcumin–piperine microparticles. Relative abundance (%) of representative bacterial species selected based on their biological relevance to the gut–inflammation–metabolism axis investigated in this study. Data were log10-transformed to enhance the visualization of low-abundance taxa. The selected taxa include species associated with Prevotella dominance in control groups and species linked to the microbial changes observed following treatment with curcumin–piperine microparticles. Basal: healthy rats not exposed to the disease model and treated with vehicle. C–: rats exposed to hypertension, dyslipidemia, and fructose consumption and treated with vehicle. 225: rats exposed to the disease model and treated with the curcumin–piperine formulation at a dose of 225 mg/kg. C+: rats exposed to the disease model and treated with enalapril plus simvastatin. Data are shown for illustrative and comparative purposes and do not represent the full taxonomic composition of the gut microbiota.

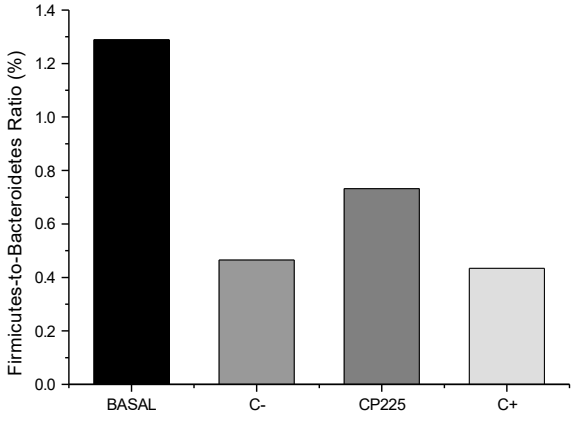

Figure S3. Firmicutes/Bacteroidetes (F/B) ratio in rats exposed to the cardiometabolic disease model and treated with curcumin–piperine microparticles. The F/B ratio was calculated from

the relative abundance of the dominant bacterial phyla across experimental groups and is presented as a complementary descriptive parameter. Basal: healthy rats not exposed to the disease model and treated with vehicle. C–: rats exposed to hypertension, dyslipidemia, and fructose consumption and treated with vehicle. 225: rats exposed to the disease model and treated with the curcumin–piperine formulation at a dose of 225 mg/kg. C+: rats exposed to the disease model and treated with enalapril plus simvastatin. The F/B ratio should be interpreted in conjunction with taxonomic changes observed at lower hierarchical levels.

Table S1. Relative abundance of selected bacterial genera associated with short-chain fatty acid production and intestinal barrier integrity in rats exposed to the cardiometabolic disease model and treated with curcumin–piperine microparticles**.** Relative abundance (%) of representative bacterial genera with functional relevance to the gut–inflammation–metabolism axis across experimental groups. Genera are grouped according to their predominant metabolic functions, including lactate production, butyrate production, and propionate production. Basal: healthy rats not exposed to the disease model and treated with vehicle. C– : rats exposed to hypertension, dyslipidemia, and fructose consumption and treated with vehicle. 225: rats exposed to the disease model and treated with the curcumin–piperine formulation at a dose of 225 mg/kg. C+: rats exposed to the disease model and treated with enalapril plus simvastatin. The taxa listed represent selected genera of functional interest and do not reflect the complete taxonomic composition of the gut microbiota.

3.2.1.34 Functional group	**Genus**	**Basal**	**C–**	**CP225**	**C+**
Lactate producers and barrier-supporting bacteria	Bifidobacterium	0.03	0.02	0.04	0.01
	Lactobacillus	0.12	0.06	0.08	0.07
	Ligilactobacillus	0.85	0.72	0.11	0.19
	Limosilactobacillus	0.04	0.07	0.02	0.04
	Lactiplantibacillus	0.00	0.00	0.00	0.00

Functional group	Genus	Basal	C–	CP225	C+
Butyrate-producing bacteria	Faecalibacterium	0.02	0.00	0.01	0.01
	Roseburia	0.30	0.09	0.14	0.05
	Butyricicoccus	0.01	0.02	0.01	0.02
	Butyrivibrio	0.06	0.00	0.00	0.00
Propionate-producing bacteria	Phascolarctobacterium	0.01	0.18	0.01	0.13

3.2.1.35 6 References

Abuelezz, N. Z., Shabana, M. E., Abdel-Mageed, H. M., Rashed, L., & Morcos, G. N. B. (2020). Nanocurcumin alleviates insulin resistance and pancreatic deficits in polycystic ovary syndrome rats: Insights into PI3K/Akt/mTOR and TNF-α modulations. *Life Sciences, 256*, 118003. https://doi.org/10.1016/j.lfs.2020.118003

Albuquerque, E. R., Silva, G. R., Braga, F. A., Silva, E. P., Negrini, K. S., Fracasso, J. A. R., Guarnier, L. P., Jacomassi, E., Ribeiro-Paes, J. T., Gomes, R. S., Gasparotto Junior, A., & Lívero, F. A. D. R. (2023). Bridging the gap: Exploring the preclinical potential of *Pereskia grandifolia* in metabolic-associated fatty liver disease. *Evidence-Based Complementary and Alternative Medicine, 2023*, 8840427. https://doi.org/10.1155/2023/8840427

Amaral, E. C., da Silva, G. R., Braga, F. A., Palozi, R. A. C., Lorençone, B. R., Marques, A. A. M., Moreno, K. G. T., Leite, P. R. T., Barboza, L. N., Souza, R. I. C., dos Santos, A. C., Lovato, E. C. W., Ribeiro-Paes, J. T., Gasparotto Junior, A., & Lívero, F. A. R. (2023). Cardioprotective effects of *Baccharis trimera* (Less.) DC in a rodent model of hookah, alcohol, and energy drink exposure. *Boletín Latinoamericano y del Caribe de Plantas Medicinales y Aromáticas, 22*(3), 377–392. https://doi.org/10.37360/blacpma.23.22.3.28

American Heart Association. (2025). Gut microbiota–derived metabolites and cardiovascular health: A scientific statement from the American Heart Association. *Circulation*. Advance online publication.

Auth, P. A., da Silva, G. R., Amaral, E. C., Bortoli, V. F., Manzano, M. I., de Souza, L. M., Lovato, E. C. W., Ribeiro-Paes, J. T., Gasparotto Junior, A., & Lívero, F. A. D. R. (2022). *Croton urucurana* Baill. ameliorates metabolic associated fatty liver disease in rats. *Frontiers in Pharmacology, 13*, 886122. https://doi.org/10.3389/fphar.2022.886122

Barbosa, R. J., Ratti da Silva, G., Bortoli, V. F., ... & Lívero, F. A. D. R. (2020). Promising therapeutic use of Baccharis trimera (Less.) DC as a natural hepatoprotective agent against hepatic lesions caused by multiple risk factors. Journal of Ethnopharmacology, 254, 112729. https://doi.org/10.1016/j.jep.2020.112729

Bertoncini-Silva, C., Pedrosa, A. M., Rodrigues, C. E., & Pimenta, F. C. (2024). Drug-induced nephrotoxicity in cardiometabolic diseases: Mechanisms, clinical implications, and protective strategies. Frontiers in Pharmacology, 14, 1178452. https://doi.org/10.3389/fphar.2023.1178452

Biscaia, P. B., Gomes, T., Ferreira, A., et al. (2023). Meth(acrylic) microparticles containing piperine: Development and validation of an RP-UHPLC-DAD method for assessing drug-loading efficiency and in vitro drug release. Latin American Journal of Pharmacy, 42(9), 1809–1818.

Brandão, A. A., Rodrigues, C. I. S., Bortolotto, L. A., Nadruz, W., et al. (2025). Brazilian guideline of arterial hypertension – 2025. Arquivos Brasileiros de Cardiologia, 122(3), e20240761. https://doi.org/10.36660/abc.20240761

Bulboacă, A. E., et al. (2019). Comparative effect of curcumin versus liposomal curcumin on systemic pro-inflammatory cytokines in experimental diabetes mellitus. International Journal of Nanomedicine, 14, 8961–8972. https://doi.org/10.2147/IJN.S226790

Caiati, C., Arrigoni, R., Stanca, A., & Lepera, M. E. (2025). Kidney toxicity of drugs for the heart: An updated perspective. Metabolites, 15(3), 191. https://doi.org/10.3390/metabo15030191

Cani, P. D. (2018). Human gut microbiome: Hopes, threats and promises. Gut, 67(9), 1716–1725. https://doi.org/10.1136/gutjnl-2018-316723

Cani, P. D., Amar, J., Iglesias, M. A., Poggi, M., Knauf, C., Bastelica, D., et al. (2007). Metabolic endotoxemia initiates obesity and insulin resistance. Diabetes, 56(7), 1761–1772. https://doi.org/10.2337/db06-1491

Caporaso, J. G., et al. (2010). QIIME allows analysis of high-throughput community sequencing data. Nature Methods, 7(5), 335–336. https://doi.org/10.1038/nmeth.f.303

Caporaso, J. G., et al. (2011). Global patterns of 16S rRNA diversity at a depth of millions of sequences per sample. Proceedings of the National Academy of Sciences of the United States of America, 108(Suppl. 1), 4516–4522. https://doi.org/10.1073/pnas.1000080107

Carbonero, F., Benefiel, A. C., & Gaskins, H. R. (2012). Contributions of the microbial hydrogen economy to colonic homeostasis. Frontiers in Microbiology, 3, 1–15. https://doi.org/10.3389/fmicb.2012.00387

Cerletti, C., Colucci, M., Storto, M., Semeraro, F., Ammollo, C. T., Incampo, F., et al. (2020). Randomised trial of chronic supplementation with a nutraceutical mixture in subjects with non-alcoholic fatty liver disease. British Journal of Nutrition, 123(2), 190–197. https://doi.org/10.1017/S0007114519002484

Cui, C., Wang, Y., Liu, H., et al. (2022). Curcumin-driven reprogramming of the gut microbiota and metabolome ameliorates motor deficits in a Parkinson's disease mouse model. *Frontiers in Cellular and Infection Microbiology, 12*, 887407. https://doi.org/10.3389/fcimb.2022.887407

De Vadder, F., Kovatcheva-Datchary, P., Zitoun, C., Duchamps, S., Bäckhed, F., & Mithieux, G. (2014). Microbiota-generated metabolites promote metabolic benefits via gut–brain neural circuits. *Cell, 156*(1–2), 84–96. https://doi.org/10.1016/j.cell.2013.12.016

De Vos, W. M., Tilg, H., Van Hul, M., et al. (2022). Gut microbiome and health: Mechanistic insights. *Gut, 71*(5), 1020–1032. https://doi.org/10.1136/gutjnl-2021-326789

Degnan, P. H., & Ochman, H. (2012). Illumina-based analysis of microbial community diversity. *The ISME Journal, 6*(1), 183–194. https://doi.org/10.1038/ismej.2011.74

Den Besten, G., Van Eunen, K., Groen, A. K., Venema, K., Reijngoud, D. J., & Bakker, B. M. (2013). The role of short-chain fatty acids in the interplay between diet, gut microbiota and host energy metabolism. *Journal of Lipid Research, 54*(9), 2325–2340. https://doi.org/10.1194/jlr.R036012

Deng, Y., Wang, Y., Li, S., & Zhang, Y. (2023). Curcumin supplementation improves metabolic and inflammatory markers in metabolic syndrome: A systematic review and meta-analysis. *Nutrients, 15*(4), 912. https://doi.org/10.3390/nu15040912

Dewi, M. O. T., & Setyaningsih, D. (2023). Effects of drying temperature on curcumin and piperine dissolution and the release kinetics of solid dispersion-based microparticles: A preliminary study. *Ankara Üniversitesi Eczacılık Fakültesi Dergisi, 47*(3), 853–863. https://doi.org/10.33483/jfpau.1253561

Dokumacioglu, E., Iskender, H., Bolat, I., Kapakin, K. A. T., Mokhtare, B., Omur, A. D., & Hayirli, A. (2025). Curcumin exerts protective effects against valproic acid-induced testicular damage through modulation of the JAK1/STAT-3/IL-6 signaling pathway in rats. *Iranian Journal of Basic Medical Sciences, 28*(2), 230–236. https://doi.org/10.22038/ijbms.2024.76948.16659

Du Preez, R., et al. (2019). Low-dose curcumin nanoparticles normalise blood pressure in rats with metabolic syndrome. *Nutrients, 11*(7), 1542. https://doi.org/10.3390/nu11071542

Dziegielewska-Gesiak, S. (2021). Metabolic syndrome in an aging society. *Clinical Interventions in Aging, 16*, 1057–1070. https://doi.org/10.2147/CIA.S308861

El-Rakabawy, O. M., Elkholy, A. A., Mahfouz, A. A., Abdelsalam, M. M., & El Wakeel, L. M. (2025). Curcumin supplementation improves the clinical outcomes of patients with diabetes and atherosclerotic cardiovascular risk. *Scientific Reports, 15*, 28358. https://doi.org/10.1038/s41598-025-09783-5

Fan, Y., & Pedersen, O. (2021). Gut microbiota in human metabolic health and disease. *Nature Reviews Microbiology, 19*, 55–71. https://doi.org/10.1038/s41579-020-0433-9

Flint, H. J., Scott, K. P., Louis, P., & Duncan, S. H. (2012). Microbial degradation of complex carbohydrates in the gut. *Gut Microbes, 3*(4), 289–306. https://doi.org/10.4161/gmic.19897

Funamoto, M., et al. (2022). High-absorption curcumin prevents hypertensive heart disease. *European Heart Journal Open, 2*(1), oeac057. https://doi.org/10.1093/ehjopen/oeac057

Ge, S., He, J., Chen, Y., Dong, B., & Li, Y. (2024). Global burden of hypertension and challenges in blood pressure control. *The Lancet Global Health, 12*(1), e45–e56. https://doi.org/10.1016/S2214-109X(23)00412-6

Ghoran, S. H., et al. (2022). Curcumin–piperine co-delivery systems: Enhancing bioavailability. *Journal of Functional Foods, 92*, 105054. https://doi.org/10.1016/j.jff.2022.105054

Gurung, M., Li, Z., You, H., Rodrigues, R., Jump, D. B., Morgun, A., et al. (2020). Role of gut microbiota in type 2 diabetes pathophysiology. *EBioMedicine, 51*, 102590. https://doi.org/10.1016/j.ebiom.2019.11.051

Hamed, S., Alavi, S., & Rezaei, M. (2024). Gastro-resistant microparticles for polyphenol delivery. *Pharmaceutics, 16*(1), 88. https://doi.org/10.3390/pharmaceutics16010088

Hosseini, Z., Whiting, S. J., & Vatanparast, H. (2023). Metabolic syndrome: Risk factors and emerging therapies. *Nutrition Reviews, 81*(5), 529–546. https://doi.org/10.1093/nutrit/nuad004

Jabczyk, M., et al. (2021). Curcumin and its potential impact on the gut microbiota. *Nutrients, 13*(6), 2004. https://doi.org/10.3390/nu13062004

Jalali, M., et al. (2020). Effects of curcumin supplementation in non-alcoholic fatty liver disease: A meta-analysis. *Complementary Therapies in Medicine, 48*, 102283. https://doi.org/10.1016/j.ctim.2020.102283

Johnson, J. S., Spakowicz, D. J., Hong, B. Y., Petersen, L. M., Demkowicz, P., Chen, L., Leopold, S. R., Hanson, B. M., Agresta, H. O., Gerstein, M., Sodergren, E., Weinstock, G. M., & Dupont, C. L. (2019). Evaluation of 16S rRNA gene sequencing for species and strain-level microbiome analysis. *Nature Communications, 10*, 5029. https://doi.org/10.1038/s41467-019-13036-1

Koh, A., De Vadder, F., Kovatcheva-Datchary, P., & Bäckhed, F. (2016). From dietary fiber to host physiology: Short-chain fatty acids as key bacterial metabolites. *Cell, 165*(6), 1332–1345. https://doi.org/10.1016/j.cell.2016.05.041

Lahti, L., & Shetty, S. (2018). *microbiome R package*. https://microbiome.github.io Esse formato fica mais limpo do que “Introduction to the microbiome R package”.

Lamichhane, G., et al. (2024). Curcumin mitigates gut dysbiosis in obese aged mice. *Biology, 13*, 955. https://doi.org/10.3390/biology13060955

Ley, R. E., Turnbaugh, P. J., Klein, S., & Gordon, J. I. (2005). Obesity alters gut microbial ecology. *Proceedings of the National Academy of Sciences of the United States of America, 102*(31), 11070–11075. https://doi.org/10.1073/pnas.0504978102

Li, H., Sureda, A., Devkota, H. P., Pittalà, V., Barreca, D., Silva, A. S., Tufano, V., & Nabavi, S. M. (2020). Curcumin and cardiovascular diseases: A review of the pharmacological effects. *Biotechnology Advances, 38*, 107343. https://doi.org/10.1016/j.biotechadv.2019.107343

Li, M., Rouaud, O., & Poncelet, D. (2008). Microencapsulation by solvent evaporation: State of the art for process engineering approaches. *International Journal of Pharmaceutics, 363*(1–2), 26–39. https://doi.org/10.1016/j.ijpharm.2008.04.024

Liu, Y., et al. (2024). Nano-curcumin attenuates renal dysfunction in cardiometabolic disease. *Phytomedicine, 124*, 155245. https://doi.org/10.1016/j.phymed.2024.155245

Lívero, F. A. R., Martins, G. G., Queiroz Telles, J. E., Beltrame, O. C., Petris Biscaia, S. M., Cavicchiolo Franco, C. R., Oude Elferink, R. P., & Acco, A. (2016). Hydroethanolic extract of *Baccharis trimera* ameliorates alcoholic fatty liver disease in mice. *Chemico-Biological Interactions, 260*, 22–32. https://doi.org/10.1016/j.cbi.2016.10.003

Lopez-Candales, A., Hernández Burgos, P. M., Hernandez-Suarez, D. F., & Harris, D. (2017). Linking chronic inflammation with cardiovascular disease: From normal aging to the metabolic syndrome. *Journal of Natural Science, 3*(4), e341.

Lopresti, A. L. (2018). The problem of curcumin and its bioavailability: Could its gastrointestinal influence contribute to its overall health-enhancing effects? *Advances in Nutrition, 9*(1), 41–50. https://doi.org/10.1093/advances/nmx011

Louis, P., & Flint, H. J. (2017). Formation of propionate and butyrate by the human colonic microbiota. *Environmental Microbiology, 19*(1), 29–41. https://doi.org/10.1111/1462-2920.13589

Magne, F., Gotteland, M., Gauthier, L., Zazueta, A., Pesoa, S., Navarrete, P., et al. (2020). The Firmicutes/Bacteroidetes ratio: A relevant marker of gut dysbiosis in obese patients? *Nutrients, 12*(5), 1474. https://doi.org/10.3390/nu12051474

Mambrini, J. V. M., Malta, D. C., Lima-Costa, M. F., & Peixoto, S. V. (2023). Lifestyle changes and metabolic syndrome in Brazilian adults. *Revista de Saúde Pública, 57*, 18. https://doi.org/10.11606/s1518-8787.2023057004664

Mamikutty, N., et al. (2014). Establishment of metabolic syndrome in rats. *BioMed Research International, 2014*, 349548. https://doi.org/10.1155/2014/349548

Marcon, M. V., Schafka, V. M., Justus, B., Nadal, J. M., Schnekenberg, C. M., Shirabayashi, J. B., Lívero, F. A. R., & Farago, P. V. (2025). Co-quantification of curcuminoids and piperine by RP-HPLC/DAD from spray-dried microparticles for routine quality control. *Brazilian Archives of Biology and Technology, 68*, e250760. https://doi.org/10.1590/1678-4324-2025250760

McMurdie, P. J., & Holmes, S. (2013). phyloseq: An R package for reproducible interactive analysis and graphics of microbiome census data. *PLoS ONE, 8*, e61217. https://doi.org/10.1371/journal.pone.0061217

Moradi, B., Rahmati-Ahmadabad, S., Farzanegi, P., Helalizadeh, M., & Azarbayjani, M. A. (2020). Effects of non-linear resistance training and curcumin supplementation on liver biochemical markers and structure in older women with non-alcoholic fatty liver disease. *Journal of Bodywork and Movement Therapies, 24*, 154–160. https://doi.org/10.1016/j.jbmt.2020.02.021

Mukohda, M., Yano, T., Matsui, T., Nakamura, S., Miyamae, J., Toyama, K., Mitsui, R., Mizuno, R., & Ozaki, H. (2023). Treatment with *Ligilactobacillus murinus* lowers blood pressure and intestinal permeability in spontaneously hypertensive rats. *Scientific Reports, 13*, 15197. https://doi.org/10.1038/s41598-023-42377-7

Nguyen, T. L. A., et al. (2015). How informative is the mouse for human gut microbiota research? *Disease Models & Mechanisms, 8*(1), 1–16. https://doi.org/10.1242/dmm.017400

Ofori-Attah, E., Aning, A., & Simón, L. (2025). Curcumin in the treatment of kidney disease: A systematic review with a focus on drug interactions. *Antioxidants, 14*(11), 1369. https://doi.org/10.3390/antiox14111369

Oksanen, J., et al. (2007). *vegan: Community ecology package* (R package). https://cran.r-project.org/package=vegan

Pan, Y., Zhao, D., Yu, N., An, T., Miao, J., Mo, F., Gu, Y., Zhang, D., Gao, S., & Jiang, G. (2017). Curcumin improves glycolipid metabolism through regulating peroxisome proliferator activated receptor γ signalling pathway in high-fat diet-induced obese mice and 3T3-L1 adipocytes. *Royal Society Open Science, 4*(10), 170917. https://doi.org/10.1098/rsos.170917

Panahi, Y., Kianpour, P., Mohammadi, E., et al. (2017). Efficacy and safety of phytosomal curcumin in non-alcoholic fatty liver disease: A randomized controlled trial. *Drug Research, 67*(4), 244–251. https://doi.org/10.1055/s-0043-100019

Panahi, Y., et al. (2018). Curcumin and piperine supplementation in patients with metabolic syndrome: A randomized controlled trial. *Clinical Nutrition, 37*(1), 215–222. https://doi.org/10.1016/j.clnu.2016.12.019

Pandey, P., et al. (2024). Gut microbiota in inflammatory diseases. *World Journal of Gastroenterology, 30*(4), 353–371. https://doi.org/10.3748/wjg.v30.i4.353

Parks, D. H., et al. (2022). GTDB: An ongoing census of bacterial and archaeal diversity through a phylogenetically consistent, rank-normalized taxonomy. *Nucleic Acids Research, 50*(D1), D785–D794. https://doi.org/10.1093/nar/gkab776

Percie du Sert, N., et al. (2020). The ARRIVE guidelines 2.0: Updated guidelines for reporting animal research. *Journal of Cerebral Blood Flow & Metabolism, 40*(9), 1769–1777. https://doi.org/10.1177/0271678X20943823

Qiu, S., et al. (2023). Metabolic syndrome and cardiovascular disease. *Frontiers in Cardiovascular Medicine, 10*, 1189456. https://doi.org/10.3389/fcvm.2023.1189456

Ridlon, J. M., Harris, S. C., Bhowmik, S., Kang, D. J., & Hylemon, P. B. (2016). Consequences of bile salt biotransformations by intestinal bacteria. *Gut Microbes, 7*(1), 22–39. https://doi.org/10.1080/19490976.2015.1127483

Rinkunaite, I., et al. (2021). Anti-inflammatory effects of different curcumin preparations. *BMC Complementary Medicine and Therapies, 21*, 39. https://doi.org/10.1186/s12906-021-03214-2

Saberian, L., Alimohammadi, N., Koosha, F., Rahvard, H. V., Ahmadi, K., Jahantigh, H. R., & Sadighpur, T. (2022). Therapeutic effects of curcumin on kidney disease: An updated review of the current knowledge. *Journal of Renal Endocrinology, 8*, e23063.

Safari, S., Rahimi, R., Mahdavi, A., et al. (2023). Curcumin supplementation improves metabolic parameters and liver enzyme activity in patients with non-alcoholic fatty liver disease: A randomized clinical trial. *Frontiers in Nutrition, 10*, 1163950. https://doi.org/10.3389/fnut.2023.1163950

Sangouni, A. A., Taghdir, M., Mirahmadi, J., Sepandi, M., & Parastouei, K. (2022). Effects of curcumin and/or coenzyme Q10 supplementation on metabolic control in subjects with metabolic syndrome: A randomized clinical trial. *Nutrition Journal, 21*, 62. https://doi.org/10.1186/s12937-022-00816-7

Scazzocchio, B., Minghetti, L., & D'Archivio, M. (2020). Interaction between gut microbiota and curcumin: A new key of understanding for the health effects of curcumin. *Nutrients, 12*, 2499. https://doi.org/10.3390/nu12082499

Schneider, A. C., Brener, C. E. S., Daudt, N. F., Cruz, L., & Silva, C. B. (2023). Development of microparticles and microparticulated tablets containing piperine. *Brazilian Journal of Pharmaceutical Sciences*.

Silva, G. R. D., Kluck, A. J., Albuquerque, E. R., Guarnier, L. P., Braga, F. A., Silva, E. P., Negrini, K. S., Mendonça, J. A., Gazim, Z. C., Gasparotto Junior, A., Ribeiro-Paes, J. T., & Lívero, F. A. D. R. (2024). Effects of *Baccharis dracunculifolia* DC on an innovative animal model of cardiometabolic syndrome. *Pharmaceutics, 16*, 1446. https://doi.org/10.3390/pharmaceutics16111446

Snelson, M., et al. (2024). Short-chain fatty acids and blood pressure regulation. *Hypertension, 81*(2), 245–254. https://doi.org/10.1161/HYPERTENSIONAHA.123.20734

Soetikno, V., Sari, F. R., Lakshmanan, A. P., Arumugam, S., Harima, M., Suzuki, K., & Watanabe, K. (2013). Curcumin improves diabetic nephropathy by inhibiting PKC signaling pathways in experimental diabetes. *Molecular Nutrition & Food Research, 57*(7), 1310–1321. https://doi.org/10.1002/mnfr.201200540

Souza Neto, E. G. D., Peixoto, J. V. C., Rank Filho, C., Petterle, R. R., Fogaça, R. T. H., Wolska, B. M., & Dias, F. A. L. (2023). Effects of high-intensity interval training and continuous training on exercise capacity, heart rate variability and isolated hearts in diabetic rats. *Arquivos Brasileiros de Cardiologia, 120*(1), e20220396. https://doi.org/10.36660/abc.20220396

Tilg, H., & Adolph, T. E. (2021). Gut microbiota in metabolic disease. *Nature Reviews Gastroenterology & Hepatology, 18*, 159–171. https://doi.org/10.1038/s41575-020-00327-x

Trujillo, J., et al. (2013). Renoprotective effects of curcumin. *Redox Biology, 1*, 448–456. https://doi.org/10.1016/j.redox.2013.08.003

Turnbaugh, P. J., Ley, R. E., Mahowald, M. A., Magrini, V., Mardis, E. R., & Gordon, J. I. (2006). An obesity-associated gut microbiome with increased capacity for energy harvest. *Nature, 444*, 1027–1031. https://doi.org/10.1038/nature05414

Valadares, L. P., Bensenor, I. M., Barreto, S. M., & Lotufo, P. A. (2022). Prevalence of metabolic syndrome and associated factors in Brazilian adults. *Arquivos Brasileiros de Cardiologia, 118*(2), 241–249. https://doi.org/10.36660/abc.20200578

Verhaar, B. J. H., et al. (2020). Gut microbiota in hypertension and atherosclerosis: A review. *Nutrients, 12*(10), 2982. https://doi.org/10.3390/nu12102982

Wahlström, A., Sayin, S. I., Marshall, H. U., & Bäckhed, F. (2016). Intestinal crosstalk between bile acids and microbiota. *Nature Reviews Gastroenterology & Hepatology, 13*, 69–80. https://doi.org/10.1038/nrgastro.2015.211

Wang, P. X., Deng, X., Zhang, C., & Yuan, H. (2020). Gut microbiota and metabolic syndrome. *Chinese Medical Journal, 133*(7), 808–816. https://doi.org/10.1097/CM9.0000000000000696

World Health Organization. (2023). *Noncommunicable diseases*. https://www.who.int/news-room/fact-sheets/detail/noncommunicable-diseases

Wozniak, A., et al. (2010). Inflammatory cytokines in obesity. *European Journal of Medical Research, 15*(Suppl. 2), 347–349. https://doi.org/10.1186/2047-783X-15-S2-347

Wu, Y., Xu, H., Tu, X., & Gao, Z. (2021). The role of short-chain fatty acids of gut microbiota origin in hypertension. *Frontiers in Microbiology, 12*, 730809. https://doi.org/10.3389/fmicb.2021.730809

Yadav, R., Mishra, S., Chaturvedi, R., & Pandey, A. (2025). Therapeutic potential of curcumin in cardiovascular disease: Targeting atherosclerosis pathophysiology. *Biomedicine & Pharmacotherapy, 190*, 118412. https://doi.org/10.1016/j.biopha.2025.118412

Yang, T., Maki, K. A., Marques, F. Z., Cai, J., Joe, B., Pepine, C. J., Pluznick, J. L., Meyer, K. A., Kirabo, A., & Bennett, B. J. (2025). Hypertension and the gut microbiome: A science advisory from the American Heart Association. *Hypertension, 82*(5), e160–e170. https://doi.org/10.1161/HYP.0000000000000247

Yupanqui, C. T., et al. (2024). Spray-dried microparticles of turmeric extract for improved delivery and low toxicity. *Pharmacia, 71*, 1–10. https://doi.org/10.3897/pharmacia 71.e126108

Zago, P. M. J. J., et al. (2021). Multiple risk factors for heart disease: A challenge to the ethnopharmacological use of *Croton urucurana* Baill. *Evidence-Based Complementary and Alternative Medicine, 2021*, 6666017. https://doi.org/10.1155/2021/6666017

Zhang, X., et al. (2020). Simvastatin alters gut microbiota and lipid metabolism. *Frontiers in Microbiology, 11*, 522. https://doi.org/10.3389/fmicb.2020.00522

Zhang, Y., Zhuang, Z., Meng, Q., Jiao, Y., Xu, J., & Fan, H. (2022). Gut microbiota as a prospective therapeutic target for curcumin. *Journal of Nutritional Biochemistry, 103*, 108968. https://doi.org/10.1016/j.jnutbio.2022.108968

Zhao, L., Li, S., & Gao, Y. (2021). Efficacy of statins on renal function in patients with chronic kidney disease: A systematic review and meta-analysis. *Renal Failure, 43*(1), 718–728. https://doi.org/10.1080/0886022X.2021.1915799

Zhong, Y., et al. (2020). Curcumin suppresses IL-6 production via NF-κB signaling pathway. *Experimental and Therapeutic Medicine, 20*, 1856–1870. https://doi.org/10.3892/etm.2020.8849

Zuo, K., et al. (2022). Gut microbiota-derived short-chain fatty acids and hypertension. *Hypertension, 79*(2), 289–300. https://doi.org/10.1161/HYPERTENSIONAHA.121.18244

CONCLUSÕES

As micropartículas poliméricas gastro-resistentes de Eudragit® S100 contendo curcumina e piperina foram obtidas com sucesso, demonstrando elevada viabilidade tecnológica da formulação desenvolvida. O método analítico por HPLC, revalidado para a quantificação simultânea dos dois bioativos, apresentou simplicidade, especificidade, linearidade, precisão e exatidão, atendendo plenamente aos critérios recomendados pela ICH (2005) e pela legislação brasileira vigente (Brasil, 2017). A elevada eficiência de encapsulação confirmou a adequação do sistema polimérico para a incorporação estável de compostos bioativos de baixa solubilidade.

Os ensaios de segurança indicaram um perfil favorável de biocompatibilidade, uma vez que o teste in vitro de hemólise não evidenciou efeitos hemolíticos relevantes, e os estudos de toxicidade aguda não demonstraram alterações clínicas, bioquímicas ou histopatológicas significativas, reforçando a segurança da formulação para administração oral. O perfil de dissolução revelou liberação pH-dependente e sustentada dos compostos encapsulados, corroborando o potencial da matriz polimérica em promover liberação controlada e direcionamento intestinal dos bioativos.

No modelo experimental multifatorial de SM, que integra diferentes determinantes fisiopatológicos da doença, o tratamento com as micropartículas de curcumina–piperina, particularmente na maior dose avaliada, promoveu melhora consistente de parâmetros metabólicos e hemodinâmicos, incluindo redução da dislipidemia, da hiperglicemia, da adiposidade visceral e da pressão arterial. Esses efeitos foram acompanhados por atenuação significativa da inflamação sistêmica, evidenciada pela redução de citocinas pró-inflamatórias, incluindo a normalização dos níveis de IL-6 no grupo tratado com a formulação, superando em alguns desfechos os efeitos observados com a farmacoterapia convencional.

Adicionalmente, a SM associou-se à perda de diversidade e à dominância de poucos táxons da microbiota intestinal, enquanto o tratamento com as micropartículas promoveu uma reorganização microbiana funcionalmente mais favorável, caracterizada pelo enriquecimento de gêneros produtores de ácidos graxos de cadeia curta e pela redução da dominância de perfis disbióticos, embora sem restauração completa do padrão basal. Esses achados sugerem um efeito modulador da formulação sobre o eixo intestino–inflamação–metabolismo, compatível com a integração dos efeitos metabólicos e inflamatórios observados.

Em conjunto, os resultados demonstram que a encapsulação de curcumina e piperina em micropartículas gastro-resistentes constitui uma estratégia farmacotécnica eficaz para potencializar os efeitos sistêmicos desses bioativos. A formulação desenvolvida integra avanços tecnológicos e benefícios biológicos, evidenciando potencial para aplicações farmacêuticas, nutracêuticas e funcionais no contexto de distúrbios cardiometabólicos. Esses achados reforçam a relevância de abordagens baseadas na modulação da microbiota intestinal e justificam investigações futuras voltadas à elucidação de mecanismos funcionais e à validação translacional em estudos clínicos.

REFERÊNCIAS

ABDULGHANI, M. F. et al. Natural products for managing metabolic syndrome. Frontiers in Pharmacology, 2024.

ADEPU, S.; RAMAKRISHNA, S. Controlled drug delivery systems: current status and future directions. Molecules, v. 26, n. 19, p. 5905, 2021. Disponível em: https://doi.org/10.3390/molecules26195905. Acesso em: 01 abr. 2026.

AGGARWAL, B. B.; HARIKUMAR, K. B. Potential therapeutic effects of curcumin, the anti-inflammatory agent, against numerous diseases. International Journal of Biochemistry & Cell Biology, 2009.

AGGARWAL, B. B.; SUNG, B. Pharmacological basis for the role of curcumin in chronic diseases. Trends in Pharmacological Sciences, 2009.

AHMAD, N.; FAZAL, H.; ABBASI, B. H. et al. Biological role of Piper nigrum L. Asian Pacific Journal of Tropical Medicine, p. S1945–S1953, 2012.

ALAM, M. S. et al. The dynamic role of curcumin in mitigating human illnesses. Pharmaceuticals, v. 17, n. 12, p. 1674, 2024.

ALBERTI, K. G. et al. Harmonizing the metabolic syndrome. Circulation, v. 120, n. 16, p. 1640–1645, 2009.

ALKHULAIFI, F.; DARKOH, C. Meal timing, meal frequency and metabolic syndrome. Nutrients, v. 14, n. 9, p. 1–12, 2022.

ALMEIDA, M. A. et al. Enhanced gastric tolerability and improved anti-obesity effect. Materials Science & Engineering C, v. 40, p. 345–356, 2014.

AMBROSELLI, D. et al. New advances in metabolic syndrome. Nutrients, v. 15, p. 640, 2023. Disponível em: https://doi.org/10.3390/nu15030640. Acesso em: 01 abr. 2026.

ASGHARI, K. M. et al. Nano-curcumina ± EPA por 12 semanas em diabetes. Nutrients, v. 16, n. 7, 2024.

ASHOUR, E. A. et al. Solid dispersions of poorly water-soluble drugs. Journal of Pharmacy and Pharmacology, v. 68, n. 12, p. 1645–1663, 2016. Disponível em: https://doi.org/10.1111/jphp.12627. Acesso em: 01 abr. 2026.

AZAD, A. K. et al. Polymer-based curcumin-loaded formulation. Pharmaceutics, v. 16, n. 2, art. 160, 2024.

BARBALHO, S. M. et al. Síndrome metabólica, aterosclerose e inflamação. Jornal Vascular Brasileiro, v. 14, n. 4, p. 319–327, 2015.

BISCAIA, P. B. et al. Meth(acrylic) microparticles containing piperine: development and validation of an RP-UHPLC-DAD method for assessing the drug-loading efficiency and the in vitro drug release. Latin American Journal of Pharmacy, v. 42, n. 9, p. 1–12, 2023.

BISCAIA, S. M. Encapsulação de piperina em micropartículas poliméricas por spray drying e avaliação em modelo de obesidade induzida por dieta de cafeteria. 2018. Dissertação (Mestrado em Ciências Farmacêuticas) – Universidade Federal do Paraná, Curitiba, 2018.

BLAYA, R. et al. Low testosterone levels and metabolic syndrome in aging male. Current Pharmaceutical Design, v. 23, n. 30, p. 4448–4455, 2017.

BOULANGÉ, C. L. et al. Impact of the gut microbiota on inflammation, obesity, and metabolic disease. Genome Medicine, London, v. 8, p. 42, 2016. Disponível em: https://doi.org/10.1186/s13073-016-0303-2. Acesso em: 01 abr. 2026.

BRANDÃO, A. A. et al. Diretriz Brasileira de Hipertensão Arterial – 2025. Arquivos Brasileiros de Cardiologia, v. 122, n. 3, e20240761, 2025. Disponível em: https://doi.org/10.36660/abc.20240761. Acesso em: 01 abr. 2026.

BRASIL. Agência Nacional de Vigilância Sanitária (ANVISA). Resolução da Diretoria Colegiada – RDC nº 985, de 21 de julho de 2025. Dispõe sobre a regulamentação de fitofármacos. Diário Oficial da União, Brasília, DF, 2025. Disponível em: https://www.gov.br/anvisa. Acesso em: 21 mar. 2026.

CELLETTI, F. et al. WHO guideline on glucagon-like peptide-1 receptor agonists for obesity in adults. JAMA, Chicago, v. 334, n. 3, p. 233–245, 2025.

CHEN, H. W. et al. Improvement in curcumin's stability and release by encapsulation with liposomes or flexible liposomes. Nanomaterials, v. 14, n. 22, p. 1836, 2024. Disponível em: https://doi.org/10.3390/nano14221836. Acesso em: 01 abr. 2026.

CHOMIUK, T. et al. Physical activity in metabolic syndrome. Frontiers in Physiology, v. 15, p. 1–11, 2024.

CLIFTON, P. Metabolic syndrome—role of dietary fat type and quantity. Nutrients, v. 11, n. 7, p. 1788, 2019.

CODAZZI, V. et al. Mechanisms and risk factors of metabolic syndrome in children and adolescents. Endocrine, v. 84, n. 1, p. 16–28, 2024.

COLHOUN, H. M. et al. Long-term kidney outcomes of semaglutide in obesity and cardiovascular disease in the SELECT trial. Nature Medicine, London, v. 30, p. 1560–1568, 2024.

DA SILVA, R. Y. P. et al. Microparticulate systems in drug delivery: in vitro and in vivo applications over the last decade. Pharmaceutics, 2023. Disponível em: https://doi.org/10.3390/pharmaceutics. Acesso em: 01 abr. 2026.

DAYI, T.; OZGOREN, M. Effects of the Mediterranean diet on the components of metabolic syndrome. Journal of Preventive Medicine and Hygiene, v. 63, n. 2, p. E206–E212, 2022.

DE SIQUEIRA VALADARES, L. T. et al. Prevalence of metabolic syndrome in Brazilian adults in the last 10 years: a systematic review and meta-analysis. BMC Public Health, v. 22, p. 327, 2022. Disponível em: https://doi.org/10.1186/s12889-022-12753-5. Acesso em: 01 abr. 2026.

DEANFIELD, J. et al. Semaglutide and cardiovascular outcomes by baseline glycaemic status in overweight or obesity. The Lancet, London, v. 405, n. 10415, p. 2103–2112, 2025.

DEI CAS, M.; GHIDONI, R. Dietary curcumin: correlation between bioavailability and health potential. Nutrients, v. 11, n. 9, p. 2147, set. 2019. Disponível em: https://doi.org/10.3390/nu11092147. Acesso em: 01 abr. 2026.

DENISENKO, Y. K. et al. Lipid-induced mechanisms of metabolic syndrome. Journal of Obesity, v. 2020, p. 1–10, 2020.

DEVRAJANI, T. et al. Relationship between aging and control of metabolic syndrome with telomere shortening: a cross-sectional study. Scientific Reports, v. 13, n. 1, p. 1–9, 2023.

DEWI, M. O. T.; SETYANINGSIH, D. Effects of drying temperature on curcumin and piperine dissolution and the release kinetics of solid dispersion-based microparticles: a preliminary study. Ankara Üniversitesi Eczacılık Fakültesi Dergisi, v. 47, n. 3, p. 853–863, 2023. Disponível em: https://doi.org/10.33483/jfpau.1253561. Acesso em: 01 abr. 2026.

DOBROWOLSKI, P. et al. Metabolic syndrome — a new definition and management guidelines. Arterial Hypertension, v. 26, n. 3, p. 99–121, 2022.

DOMINGUEZ, L. J.; BARBAGALLO, M. The biology of the metabolic syndrome and aging. Current Opinion in Clinical Nutrition and Metabolic Care, v. 19, n. 1, p. 5–11, 2016.

DU PREEZ, R. et al. Low-dose curcumin nanoparticles normalise blood pressure in male Wistar rats with diet-induced metabolic syndrome. Nutrients, v. 11, n. 7, p. 1542, 2019. Disponível em: https://doi.org/10.3390/nu11071542. Acesso em: 01 abr. 2026.

DZIEGIELEWSKA-GESIAK, S. Metabolic syndrome in an aging society – role of oxidant-antioxidant imbalance and inflammation markers in disentangling atherosclerosis. Clinical Interventions in Aging, v. 16, p. 1057–1070, 2021.

ENGEL, B. et al. Emprego de spray dryer na indústria de alimentos: uma breve revisão. Revista Jovens Pesquisadores, v. 7, n. 2, p. 2–11, 2017.

EVONIK HEALTH CARE. EUDRAGIT® S 100 — liberação acima de pH 7,0: portfólio de polímeros funcionais para via oral. [S. l.], 2024–2025.

EVONIK ROHM GMBH. Informe técnico. Darmstadt, Germany, 2018. Disponível em: https://www.rofarma.com/allegati/97.pdf. Acesso em: 31 maio 2025.

FAHED, G. et al. Metabolic syndrome: updates on pathophysiology and management in 2021. International Journal of Molecular Sciences, v. 23, n. 2, p. 786, 2022. Disponível em: https://doi.org/10.3390/ijms23020786. Acesso em: 01 abr. 2026.

FALUDI, A. A. et al. Atualização da diretriz brasileira de dislipidemias e prevenção da aterosclerose – 2017. Arquivos Brasileiros de Cardiologia, v. 109, n. 2, supl. 1, p. 1–76, 2017.

FARAGO, P. V. Desenvolvimento de sistemas poliméricos para a liberação modificada do cloridrato de metformina. 2007. Tese (Doutorado em Ciências Farmacêuticas) – Universidade Federal do Paraná, Curitiba, 2007. 195 f.

FATHI, D. B. The investigations of genetic determinants of the metabolic syndrome. Diabetes & Metabolic Syndrome: Clinical Research & Reviews, v. 12, n. 5, p. 783–789, 2018.

FU, Z. H. et al. Impact of metabolic syndrome components on clinical outcomes in hypertriglyceridemia-induced acute pancreatitis. World Journal of Gastroenterology, v. 30, p. 3996–4010, 2024.

GAMA, I. R. S. et al. Síndrome metabólica: evidências atuais sindêmicas, diagnóstico, tratamento e dietoterapia. Lumen et Virtus, v. 15, n. 39, p. 1904–1923, 2024. Disponível em: https://doi.org/10.56238/levv15n39-024. Acesso em: 01 abr. 2026.

GE, Y. et al. Gut microbiota: a potential new regulator of hypertension. Frontiers in Cardiovascular Medicine, Lausanne, v. 11, p. 1333005, 2024. Disponível em: https://doi.org/10.3389/fcvm.2024.1333005. Acesso em: 01 abr. 2026.

GHORAN, S. H. et al. Curcumin-based nanoformulations: a promising adjuvant towards cancer treatment. Molecules, v. 27, p. 5236, 2022. Disponível em: https://doi.org/10.3390/molecules27165236. Acesso em: 01 abr. 2026.

GHOSH, A. et al. Role of free fatty acids in endothelial dysfunction. Journal of Biomedical Science, v. 24, p. 50, 2017.

GRUNDY, S. M. et al. Diagnosis and management of the metabolic syndrome: an American Heart Association/National Heart, Lung, and Blood Institute scientific statement. Circulation, v. 112, n. 17, p. 2735–2752, 2017.

GUO, X. L. et al. Perirenal fat thickness as a superior obesity-related marker of subclinical carotid atherosclerosis in type 2 diabetes mellitus. Frontiers in Endocrinology, v. 14, p. 1–9, 2023.

GUPTA, T. et al. Enhancing bioavailability and stability of curcumin using solid lipid nanoparticles (CLEN): a covenant for its effectiveness. Frontiers in Bioengineering and Biotechnology, v. 8, p. 879, 2020. Disponível em: https://doi.org/10.3389/fbioe.2020.00879. Acesso em: 01 abr. 2026.

GURUNG, M. et al. Role of gut microbiota in type 2 diabetes pathophysiology. EBioMedicine, v. 51, p. 102590, 2020. Disponível em: https://doi.org/10.1016/j.ebiom.2019.11.051. Acesso em: 01 abr. 2026.

HAGBERG, C. E.; SPALDING, K. L. White adipocyte dysfunction and obesity-associated pathologies in humans. Nature Reviews Molecular Cell Biology, v. 25, n. 4, p. 270–289, 2024.

HAMED, A. M. et al. Nanocurcumin vs. curcumina convencional em diabetes: superioridade em glicemia, lipídios e estresse oxidativo. Heliyon, v. 10, n. 24, e170740, 2024. Disponível em: https://doi.org/10.1016/j.heliyon.2024.e170740. Acesso em: 01 abr. 2026.

HEGDE, M. et al. Curcumin formulations for better bioavailability: what we learned from clinical trials thus far? ACS Omega, v. 8, n. 12, p. 10713–10746, 2023. Disponível em: https://doi.org/10.1021/acsomega.3c00123. Acesso em: 01 abr. 2026.

HEIKAL, E. J. et al. Eudragit® S-100-coated alginate/chitosan beads for colon-specific delivery of curcumin–mesalazina: pH-triggered release (pH ≥ 7) and gastro-resistance. Gels, v. 9, n. 4, p. 264, 2023. Disponível em: https://doi.org/10.3390/gels9040264. Acesso em: 01 abr. 2026.

HIMES, R. W.; SMITH, C. W. TLR2 is critical for diet-induced metabolic syndrome in a murine model. FASEB Journal, v. 24, p. 731–739, 2010.

HOSSEINI, H. et al. A systematic review and meta-analysis of randomized controlled trials investigating the effect of the curcumin and piperine combination on lipid profile in patients with metabolic syndrome and related disorders. Phytotherapy Research, v. 37, n. 3, p. 1212–1224, 2023. Disponível em: https://doi.org/10.1002/ptr.7730. Acesso em: 01 abr. 2026.

HOTAMISLIGIL, G. S. Inflammation and metabolic disorders. Nature, v. 444, p. 860–867, 2006.

HUDISH, L. I.; REUSCH, J. E. B.; SUSSEL, L. β cell dysfunction during progression of metabolic syndrome to type 2 diabetes. Journal of Clinical Investigation, v. 129, n. 10, p. 4001–4008, 2019.

JASTREBOFF, A. M. et al. Tirzepatide for obesity treatment and diabetes prevention. New England Journal of Medicine, Boston, v. 392, n. 4, p. 345–357, 2025.

JYOTIRMAYEE, B. et al. Bioactive compounds and biological activities of turmeric (Curcuma longa L.). In: MURTHY, H. N. et al. (ed.). Bioactive Compounds in the Storage Organs of Plants. Cham: Springer Nature Switzerland AG, 2023. (Reference Series in Phytochemistry). Disponível em: https://doi.org/10.1007/978-3-031-29006-0_20-1. Acesso em: 01 abr. 2026.

KÁLLAI-SZABÓ, N. et al. Microparticles and multi-unit systems for advanced drug delivery. International Journal of Pharmaceutics, 2024. Disponível em: https://doi.org/10.1016/j.ijpharm.2024.124015. Acesso em: 01 abr. 2026.

KAROLEWICZ, B. A review of polymers as multifunctional excipients in drug dosage form technology. Saudi Pharmaceutical Journal, v. 24, n. 5, p. 525–536, 2016.

KOPP, H. P. et al. Impact of weight loss on inflammatory proteins and their association with the insulin resistance syndrome in morbidly obese patients. Arteriosclerosis, Thrombosis, and Vascular Biology, v. 23, p. 1042–1047, 2003.

LASSEGUE, B. et al. Novel gp91(phox) homologues in vascular smooth muscle cells: Nox1 mediates angiotensin II-induced superoxide formation and redox-sensitive signaling pathways. Circulation Research, v. 88, p. 888–894, 2001.

LEE, M. K. et al. Cumulative exposure to metabolic syndrome in a national population-based cohort of young adults and sex-specific risk for type 2 diabetes. Diabetology & Metabolic Syndrome, v. 15, n. 1, p. 1–10, 2023.

LEMOS, G. O.; TORRINHAS, R. S.; WAITZBERG, D. L. Nutrients, physical activity, and mitochondrial dysfunction in the setting of metabolic syndrome. Nutrients, v. 15, n. 5, p. 1107, 2023.

LIM, S.; ECKEL, R. H. Pharmacological treatment and therapeutic perspectives of metabolic syndrome. Reviews in Endocrine and Metabolic Disorders, v. 15, p. 329–341, 2014.

LIMA, E. et al. Burden of non-communicable diseases in Brazil: updated analysis of mortality and risk factors. Public Health, v. 230, p. 172–180, 2024.

LIN, L. et al. Metabolic syndrome-related kidney injury: a review and update. Frontiers in Endocrinology, v. 13, p. 1–12, 2022.

LIN, Y. H. et al. The association between metabolic syndrome and successful aging: using an extended definition of successful aging. PLoS One, v. 16, n. 11, e0259413, 2021.

LINCOFF, A. M. et al. Semaglutide and cardiovascular outcomes in obesity. New England Journal of Medicine, Boston, v. 389, n. 24, p. 2221–2232, 2023.

LOOMBA, R. et al. Tirzepatide for metabolic dysfunction–associated steatohepatitis. New England Journal of Medicine, Boston, v. 390, n. 12, p. 1103–1115, 2024.

LOPEZ-CANDALES, A. et al. Linking chronic inflammation with cardiovascular disease: from normal aging to the metabolic syndrome. Journal of Natural Science, v. 3, n. 4, p. 1–14, 2017.

LU, W. et al. Choosing the appropriate wall materials for spray-drying microencapsulation of natural bioactive ingredients: taking phenolic compounds as examples. Powder Technology, v. 394, p. 562–574, 2021. Disponível em: https://doi.org/10.1016/j.powtec.2021.09.003. Acesso em: 01 abr. 2026.

LYRA, R. et al. Manejo da terapia antidiabética no DM2. Diretriz oficial da Sociedade Brasileira de Diabetes. São Paulo: Sociedade Brasileira de Diabetes, 2025. Disponível em: https://doi.org/10.29327/5660187.2025-14. Acesso em: 01 abr. 2026.

MADAN, K. et al. Metabolic syndrome: the constellation of co-morbidities, a global threat. Endocrine, Metabolic & Immune Disorders – Drug Targets, v. 23, n. 12, p. 1491–1504, 2023.

MAMBRINI, S. P. et al. Ultra-processed food consumption and incidence of obesity and cardiometabolic risk factors in adults: a systematic review of prospective studies. Nutrients, v. 15, n. 11, p. 2387, 2023.

MANO, E. B.; MENDES, L. C. Introdução a polímeros. 2. ed. rev. e ampl. São Paulo: Edgard Blücher, 2004.

MARTINIAKOVA, M.; MONDOCKOVA, K.; KOCACOVA, M. Interrelationships among metabolic syndrome, bone-derived cytokines, and the most common metabolic syndrome-related diseases negatively affecting bone quality. Diabetology & Metabolic Syndrome, v. 16, p. 217, 2024.

MASENGA, S. K. et al. Mechanisms of oxidative stress in metabolic syndrome. International Journal of Molecular Sciences, v. 24, n. 9, p. 7654, 2023.

MATSUZAWA, Y.; FUNAHASHI, T.; NAKAMURA, T. The concept of metabolic syndrome: contribution of visceral fat accumulation and its molecular mechanism. Journal of Atherosclerosis and Thrombosis, v. 18, p. 629–639, 2011.

MCGOWAN, B. et al. Framework for the pharmacological treatment of obesity and its complications. Nature Medicine, London, v. 31, p. 1020–1032, 2025.

MEHTA, P. K.; GRIENDLING, K. K. Angiotensin II cell signaling: physiological and pathological effects in the cardiovascular system. American Journal of Physiology – Cell Physiology, v. 292, p. C82–C97, 2007.

METTANANDA, K. C. D.; METTANANDA, S. Global burden and strength of evidence for 88 risk factors in 204 countries and 811 subnational locations, 1990–2021: a systematic analysis for the Global Burden of Disease Study 2021. The Lancet, v. 403, p. 123–145, 2024.

MHASKE, D. B.; SREEDHARAN, S.; MAHADIK, K. R. Role of piperine as an effective bioenhancer in drug absorption. Pharmaceutica Analytica Acta, v. 9, n. 7, p. 591, 2018. Disponível em: https://doi.org/10.4172/2153-2435.1000591. Acesso em: 01 abr. 2026.

MIZUNO, T. M. Fat mass and obesity associated (FTO) gene and hepatic glucose and lipid metabolism. Nutrients, v. 10, n. 11, p. 1600, 2018.

MOON, K. W. et al. Cardiovascular risk according to genetic predisposition to gout, lifestyle and metabolic health across prospective European and Korean cohorts. RMD Open, v. 10, e004552, 2024.

MULÈ, G. et al. Metabolic syndrome in hypertensive patients: an unholy alliance. World Journal of Cardiology, v. 6, n. 9, p. 927–935, 2014.

NAGRANI, R. et al. Common genetic variation in obesity, lipid transfer genes and risk of metabolic syndrome: results from IDEFICS/I.Family study and meta-analysis. Scientific Reports, v. 10, p. 1–11, 2020.

NAIR, A. R.; PILLAI, A. J.; NAIR, N. Cardiovascular changes in menopause. Current Cardiology Reviews, v. 17, n. 4, p. 23–30, 2021.

NAKSURIYA, O. et al. Curcumin nanoformulations: a review of pharmaceutical properties and preclinical studies and clinical data related to cancer treatment. Biomaterials, v. 35, n. 10, p. 3365–3383, 2014.

NEELAND, I. J. et al. Metabolic syndrome. Nature Reviews Disease Primers, v. 10, p. 77, 2024.

NICHOLLS, S. J. et al. Tirzepatide and metabolic syndrome: a post hoc analysis from the SURPASS clinical trial program. Cardiovascular Diabetology, London, v. 23, n. 1, p. 45, 2024.

NILSSON, P. M.; TUOMILEHTO, J.; RYDÉN, L. The metabolic syndrome – what is it and how should it be managed? European Journal of Preventive Cardiology, v. 26, n. 2_suppl, p. 33–46, 2019.

NISHIKAWA, H. et al. Metabolic syndrome and sarcopenia. Nutrients, v. 13, n. 10, p. 3519, 2021.

NOUBIAP, J. J. et al. Geographic distribution of metabolic syndrome and its components in the general adult population: a meta-analysis of global data from 28 million individuals. Diabetes Research and Clinical Practice, v. 188, p. 109924, 2022.

NURCAHYANTI, A. D. R. et al. Curcuminoids for metabolic syndrome: meta-analysis update and mechanistic framing (microbiota/metabólitos). Frontiers in Nutrition, v. 9, p. 891339, 2022. Disponível em: https://doi.org/10.3389/fnut.2022.891339. Acesso em: 01 abr. 2026.

OCTAVIA, M. D. et al. Characterization of physicochemical properties and dissolution studies of multicomponent crystals of piperine and glutamic acid. Tropical Journal of Natural Product Research, v. 8, n. 12, p. 9643–9647, 2024. Disponível em: https://doi.org/10.26538/tjnpr/v8i12.43. Acesso em: 01 abr. 2026.

OLIVEIRA, R. G.; ALENCAR-FILHO, E. B.; VASCONCELLOS, M. L. A. A. A influência da piperina na biodisponibilidade de fármacos: uma abordagem molecular. Química Nova, v. 37, n. 1, p. 69–73, 2014.

OSTMAN, C. et al. The effect of exercise training on clinical outcomes in patients with the metabolic syndrome: a systematic review and meta-analysis. Cardiovascular Diabetology, v. 16, p. 110, 2017.

OZAWA, H. et al. Curcumin β-D-glucuronide plays an important role to keep high levels of free-form curcumin in the blood. Biological and Pharmaceutical Bulletin, v. 40, n. 9, p. 1515–1524, 2017.

PAN AMERICAN HEALTH ORGANIZATION (PAHO). The burden of noncommunicable diseases in the Americas. Washington, DC: Pan American Health Organization, 2023. Disponível em: https://www.paho.org/en/enlace/burden-noncommunicable-diseases. Acesso em: 08 set. 2025.

PANAHI, Y. et al. Curcumin as a potential candidate for treating hyperlipidemia: a review of cellular and metabolic mechanisms. Journal of Cellular Physiology, v. 233, n. 1, p. 141–152, 2018.

PATIAL, R. et al. Etiologia, fisiopatologia e estratégias de tratamento na prevenção e gestão da síndrome metabólica. Archives of Internal Medicine Research, v. 7, n. 1, p. 1–10, 2024. Disponível em: https://doi.org/10.26502/aimr.0184. Acesso em: 01 abr. 2026.

PATRA, J. K. et al. Sistemas de administração de fármacos baseados em nanotecnologia: desenvolvimentos recentes e perspectivas futuras. Journal of Nanobiotechnology, v. 16, p. 71, 2018. Disponível em: https://doi.org/10.1186/s12951-018-0392-8. Acesso em: 01 abr. 2026.

PEKGOR, S. et al. The role of visceral adiposity index levels in predicting the presence of metabolic syndrome and insulin resistance in overweight and obese patients. Metabolic Syndrome and Related Disorders, v. 17, p. 296–302, 2019.

PERKOVIC, V. et al. Effects of semaglutide on chronic kidney disease in patients with type 2 diabetes. New England Journal of Medicine, Boston, v. 390, n. 16, p. 1453–1464, 2024.

PIGEOT, I.; AHRENS, W. Epidemiology of metabolic syndrome. Pflügers Archiv – European Journal of Physiology, v. 477, p. 669–680, 2025. Disponível em: https://doi.org/10.1007/s00424-024-03051-7. Acesso em: 01 abr. 2026.

PREZA-RODRÍGUEZ, L. et al. Turmeric plus black pepper for the improvement and remission of metabolic syndrome: a randomized, double-blind, placebo-controlled clinical trial. Journal of Herbal Medicine, v. 44, p. 100845, 2024. Disponível em: https://doi.org/10.1016/j.hermed.2024.100845. Acesso em: 01 abr. 2026.

PRONE-OLAZABAL, D.; DAVIES, I.; GONZÁLEZ-GALARZA, F. F. Metabolic syndrome: an overview on its genetic associations and gene–diet interactions. Metabolic Syndrome and Related Disorders, v. 21, n. 10, p. 545–560, 2023.

PURNAMASARI, S. A. et al. Drying temperature impact on curcumin–piperine dissolution and release kinetics: solid dispersion-based microparticles from Curcuma longa and Piper nigrum extracts. Journal of Research in Pharmacy, v. 27, n. 4, p. 1329–1337, 2023. Disponível em: https://doi.org/10.29228/jrp.420. Acesso em: 01 abr. 2026.

QIU, L. et al. Effects of dietary polyphenol curcumin supplementation on metabolic, inflammatory and oxidative stress indices in metabolic syndrome: systematic review and meta-analysis of RCTs. Frontiers in Endocrinology, v. 14, p. 1216708, 2023. Disponível em: https://doi.org/10.3389/fendo.2023.1216708. Acesso em: 01 abr. 2026.

QUODBACH, J. Novel strategies for the formulation of poorly water-soluble drugs. Pharmaceutics, v. 18, n. 8, art. 1089, 2025. Disponível em: https://doi.org/10.3390/pharmaceutics18081089. Acesso em: 01 abr. 2026.

RACHED, F. H. et al. Diretriz Brasileira de Dislipidemias e Prevenção da Aterosclerose – 2025. Arquivos Brasileiros de Cardiologia, v. 122, n. 9, e20250640, 2025.

RACZ, L. Z. et al. Strategies for improving bioavailability, bioactivity, and physical-chemical behavior of curcumin. Molecules, v. 27, p. 6854, 2022. Disponível em: https://doi.org/10.3390/molecules27206854. Acesso em: 01 abr. 2026.

RADHA, R. et al. Enhancing curcumin's therapeutic potential in cancer: high-frequency ultrasound release from curcumin liposomes. Scientific Reports, 2024. Disponível em: https://doi.org/10.1038/s41598-024-61278-x. Acesso em: 01 abr. 2026.

RAJAGOPALAN, S. et al. Angiotensin II-mediated hypertension in the rat increases vascular superoxide production via membrane NADH/NADPH oxidase activation. Journal of Clinical Investigation, v. 97, p. 1916–1923, 1996.

RANA, S. et al. Metabolic syndrome and underlying genetic determinants: a systematic review. Journal of Diabetes and Metabolic Disorders, v. 21, n. 1, p. 87–98, 2022.

RAUBER, F. et al. Ultra-processed food consumption and chronic non-communicable diseases-related dietary nutrient profile in the UK. Nutrients, v. 10, n. 5, p. 587, 2018.

RESTANI, R. B. Development of functional mesoporous microparticles for controlled drug delivery. Journal of Supercritical Fluids, v. 55, p. 333–339, 2010.

REYES, S. J.; PAK, T.; MOON, T. S. Metabolic syndrome: evidence-based strategies for patient optimization. Best Practice & Research Clinical Anaesthesiology, v. 34, n. 2, p. 131–140, 2020.

RODRIGUES, S. et al. Inhalable spray-dried chondroitin sulphate microparticles: effect of different solvents on particle properties and drug activity. Polymers, v. 12, n. 2, art. 425, 2020. Disponível em: https://doi.org/10.3390/polym12020425. Acesso em: 01 abr. 2026.

ROGER, J. D. P. Plantas mágicas: enciclopédia de plantas medicinais. São Paulo: Planeta do Brasil, 1998.

ROSENDO-SILVA, D. et al. Clinical and molecular profiling of human visceral adipose tissue reveals impairment of vascular architecture and remodeling as an early hallmark of dysfunction. Metabolism, v. 153, p. 155352, 2024.

SAIKI, A. et al. Circulating angiotensin II is associated with body fat accumulation and insulin resistance in obese subjects with type 2 diabetes mellitus. Metabolism, v. 58, n. 5, p. 708–713, 2009.

SANTIAGO, V. S. et al. Curcumina, o pó dourado do açafrão-da-terra: introspecções sobre química e atividades biológicas. Química Nova, v. 38, n. 4, p. 538–552, 2015.

SATISH, M.; SAXENA, S. K.; AGRAWAL, D. K. Adipokine dysregulation and insulin resistance with atherosclerotic vascular disease: metabolic syndrome or independent sequelae? Journal of Cardiovascular Translational Research, v. 12, p. 415–424, 2019.

SATTAR, N. et al. Tirzepatide and cardiometabolic parameters in obesity. The Lancet Diabetes & Endocrinology, London, v. 13, n. 2, p. 101–112, 2025.

SCAZZOCCHIO, B.; MINGHETTI, L.; D'ARCHIVIO, M. Interaction between gut microbiota and curcumin: a new key of understanding for the health effects of curcumin. Nutrients, v. 12, n. 9, p. 2499, 2020. Disponível em: https://doi.org/10.3390/nu12092499. Acesso em: 01 abr. 2026.

SCHAFROTH, N. et al. Nano and microparticle engineering of water insoluble drugs using a novel spray drying process. Colloids and Surfaces B: Biointerfaces, v. 90, p. 8–15, 2012.

SHANG, Y. et al. Metabolic syndrome traits increase the risk of major adverse liver outcomes in type 2 diabetes. Diabetes Care, v. 47, p. 978–985, 2024.

SHISHIR, M. R. I.; CHEN, W. Trends of spray drying: a critical review on drying of fruit and vegetable juices. Trends in Food Science & Technology, v. 60, p. 27–46, 2017. Disponível em: https://doi.org/10.1016/j.tifs.2016.10.014. Acesso em: 01 abr. 2026.

SHIVANI, S. H. Review article on microparticles. International Journal of Pharmacy and Analytical Research, v. 4, n. 3, p. 302–309, 2015.

SHOBA, G. et al. Influence of piperine on the pharmacokinetics of curcumin in animals and human volunteers. Planta Medica, v. 64, n. 4, p. 353–356, 1998.

SOCIEDADE BRASILEIRA DE CARDIOLOGIA. Atualização da diretriz brasileira de dislipidemias e prevenção da aterosclerose. Rio de Janeiro: SBC, 2017. 71 p.

SOLEIMANI, V.; SAHEBKAR, A.; HOSSEINZADEH, H. Curcuma longa and its main constituent (curcumin) as non-toxic and safe substances: review. Phytotherapy Research, v. 32, p. 985–995, 2018. Disponível em: https://doi.org/10.1002/ptr.6054. Acesso em: 01 abr. 2026.

SOSNIK, A.; SEREMETA, K. P. Advantages and challenges of spray-drying technology for the production of pure drug particles and drug-loaded polymeric carriers. Advanced Drug Delivery Reviews, v. 100, p. 65–77, 2015. Disponível em: https://doi.org/10.1016/j.addr.2015.12.009. Acesso em: 01 abr. 2026.

TAGDE, P. et al. Multifaceted role of curcumin and its advanced nanostructured formulations in the treatment and management of chronic diseases. Molecules, v. 26, p. 7109, 2021. Disponível em: https://doi.org/10.3390/molecules26237109. Acesso em: 01 abr. 2026.

TAGHADOSI, M. et al. Encapsulation of curcumin with Persian gum and its stability enhancement in dairy products. Food Science & Nutrition, v. 12, n. 11, p. 9379–9390, 2024. Disponível em: https://doi.org/10.1002/fsn3.4499. Acesso em: 01 abr. 2026.

TCHERNOF, A.; DESPRÉS, J. P. Pathophysiology of human visceral obesity: an update. Physiological Reviews, v. 93, n. 1, p. 359–404, 2013.

THOMAS, M. S.; CALLE, M.; FERNANDEZ, M. L. Healthy plant-based diets improve dyslipidemias, insulin resistance, and inflammation in metabolic syndrome: a narrative review. Advances in Nutrition, v. 14, n. 1, p. 44–54, 2023.

TORAL, M. et al. Critical role of the interaction gut microbiota–sympathetic nervous system in the regulation of blood pressure. Frontiers in Physiology, Lausanne, v. 10, p. 231, 2019. Disponível em: https://doi.org/10.3389/fphys.2019.00231. Acesso em: 01 abr. 2026.

ULLAH, H. et al. Plant extracts for metabolic syndrome: mechanisms, efficacy and safety. Nutrients, 2025.

VALADARES, A. L. R. et al. Prevalence of metabolic syndrome in Brazilian adults: a systematic review and meta-analysis. Public Health Nutrition, v. 25, n. 9, p. 2519–2529, 2022. Disponível em: https://doi.org/10.1017/S1368980022000352. Acesso em: 01 abr. 2026.

WANG, M.; GONG, X.; ZHOU, H. Sustainably derived turmeric nanoparticles enhance gastrointestinal bioavailability of curcumin. Food Research International, v. 219, art. 117122, 2025. Disponível em: https://doi.org/10.1016/j.foodres.2025.117122. Acesso em: 01 abr. 2026.

WORLD HEALTH ORGANIZATION (WHO). Noncommunicable diseases. Geneva: World Health Organization, 2023. Disponível em: https://www.who.int/news-room/fact-sheets/detail/noncommunicable-diseases. Acesso em: 08 set. 2025.

WU, J. et al. Sedentary time and the risk of metabolic syndrome: a systematic review and dose–response meta-analysis. Obesity Reviews, v. 23, n. 12, e13474, 2022.

XIAO, J. H. et al. Intestinal permeability in human cardiovascular diseases: a systematic review and meta-analysis. Frontiers in Nutrition, v. 11, p. 1361126, 2024. Disponível em: https://doi.org/10.3389/fnut.2024.1361126. Acesso em: 01 abr. 2026.

YADAV, R. et al. Therapeutic potential of curcumin in cardiovascular disease: targeting atherosclerosis pathophysiology. Biomedicine & Pharmacotherapy, v. 190, p. 118412, 2025. Disponível em: https://doi.org/10.1016/j.biopha.2025.118412. Acesso em: 01 abr. 2026.

YANG, T. et al. Gut microbiota dysbiosis is linked to hypertension. Hypertension, Dallas, v. 65, n. 6, p. 1331–1340, 2015. Disponível em: https://doi.org/10.1161/HYPERTENSIONAHA.115.05315. Acesso em: 01 abr. 2026.

YOUSEFZADEH, G. et al. Comparing the association of two metabolic syndrome definitions, NCEP ATP III and IDF, with the risk of developing atherosclerotic cardiovascular disease: an analytical cross-sectional study. Endocrinology, Diabetes & Metabolism, v. 7, n. 1, e468, 2024. Disponível em: https://doi.org/10.1002/edm2.468. Acesso em: 01 abr. 2026.

YUAN, H. et al. The traditional medicine and modern medicine from natural products. Molecules, v. 21, n. 5, p. 559, 2016.

YUPANQUI, C. T. et al. Spray-dried microparticles of turmeric extract for improved delivery and low toxicity. Pharmacia, v. 71, p. 1–10, 2024. Disponível em: https://doi.org/10.3897/pharmacia.71.e126108. Acesso em: 01 abr. 2026.

YUSUF, H. et al. Curcumin micelles entrapped in Eudragit S-100 matrix: a synergistic strategy for enhanced oral delivery. Future Science OA, v. 7, n. 4, FSO677, 2021. Disponível em: https://doi.org/10.2144/fsoa-2020-0131. Acesso em: 01 abr. 2026.

ZAINI, E. et al. Improved solubility and dissolution rates in novel multicomponent crystals of piperine with succinic acid. Scientia Pharmaceutica, v. 88, n. 2, p. 21, 2020. Disponível em: https://doi.org/10.3390/scipharm88020021. Acesso em: 01 abr. 2026.

ZAM, W. Gut microbiota as a prospective therapeutic target for curcumin: a review of mutual influence. Journal of Nutrition and Metabolism, v. 2018, art. ID 1367984, p. 1–11, 2018. Disponível em: https://doi.org/10.1155/2018/1367984. Acesso em: 01 abr. 2026.

ZHANG, H. H. et al. Tumor necrosis factor-alpha stimulates lipolysis in differentiated human adipocytes through activation of extracellular signal-related kinase and elevation of intracellular cAMP. Diabetes, v. 51, p. 2929–2935, 2002.

ZHANG, X. et al. Pharmaceutical dispersion techniques for dissolution and bioavailability enhancement of poorly water-soluble drugs. Pharmaceutics, v. 10, n. 74, p. 1–33, 2018.

ANEXO A – APROVAÇÃO COMITÊ DE ÉTICA

MINISTÉRIO DA EDUCAÇÃO
UNIVERSIDADE FEDERAL DO PARANÁ
SETOR DE CIÊNCIAS BIOLÓGICAS
COMISSÃO DE ÉTICA NO USO DE ANIMAIS

Nº 1536

CERTIFICADO

A Comissão de Ética no Uso de Animais do Setor de Ciências Biológicas da Universidade Federal do Paraná (CEUA/BIO – UFPR), instituída pela Resolução Nº 86/11 do Conselho de Ensino Pesquisa e Extensão (CEPE), de 22 de dezembro de 2011, **CERTIFICA** que os procedimentos utilizando animais no projeto de pesquisa abaixo especificado estão de acordo com a Diretriz Brasileira para o Cuidado e a Utilização de Animais para fins Científicos e Didáticos (DBCA) estabelecidas pelo Conselho Nacional de Controle de Experimentação Animal (CONCEA) e com as normas internacionais para a experimentação animal.

STATEMENT

The Ethics Committee for Animal Use from the Biological Sciences Section of the Federal University of Paraná (CEUA/BIO – UFPR), established by the Resolution Nº 86/11 of the Teaching Research and Extension Council (CEPE) on December 22 nd 2011, **CERTIFIES** that the procedures using animals in the research project specified below are in agreement with the Brazilian Guidelines for Care and Use of Animals for Scientific and Teaching purposes established by the National Council for Control of Animal Experimentation (CONCEA) and with the international guidel ines for animal experimentation.

PROCESSO/PROCESS: 23075.026096/2023-62

APROVADO/APPROVAL: 13/06/2023 – R.O. 05/2023.

TÍTULO: Padronização de um modelo de estudo de doença hepática para triagem de compostos bioativos com atividade hepatoprotetora.

TITLE: Standardization of a liver disease study model for screening bioactive compounds with hepatoprotective activity.

AUTORES/AUTHORS: Francislaine Aparecida dos Reis Lívero.

DEPARTAMENTO/DEPARTAMENT: Farmacologia.

Coordenador(a) da CEUA

Documento assinado eletronicamente por **ANGELA CRISTINA DA FONSECA DE OLIVEIRA**, **INSTITUCIONAL**, em 03/07/2023, às 14:22, conforme art. 1º, III, "b", da Lei 11.419/2006.

Documento assinado eletronicamente por **JANAINA MENEZES ZANOVELI**, **PROFESSOR DO MAGISTERIO SUPERIOR**, em 03/07/2023, às 14:46, conforme art. 1º, III, "b", da Lei 11.419/2006.

A autenticidade do documento pode ser conferida aqui informando o código verificador **5723252** e o código CRC **CB948990.**